

UNIVERSITY OF YAOUNDE I
Faculty of Science

UNIVERSITE DE YAOUNDE I
Faculté des Sciences



Department of Physics
Département de Physique

TRANSITION TO CHAOS INDUCING LOST OF ENERGY CONFINEMENT IN PLASMA

Submitted and defended in fulfillment of the degree of Doctorat/PhD in Physics
Option: Mechanics

By
NONO DUEYOU Buckjohn Clémence
Registration number: 99Y225
DEA in Physics

Under the direction of

TCHAWOUA Clément
Associate Professor

KOFANE Timoléon Crépin
Professor

Year 2014



RAPPORT DE JURY DE SOUTENANCE DE LA THESE DE DOCTORAT/PHD DE PHYSIQUE DE
MONSIEUR NONO DUEYOU Buckjohn Clémence, MATRICULE : 99Y225

Le Jury, composé de :

Président : MANGUELLE-DICOU M Eliezer, Professeur, Université de Yaoundé I,
Rapporteurs : TCHAWOUA Clément, Maître de Conférences, Université de Yaoundé I,
KOFANE Timoléon Crépin, Professeur, Université de Yaoundé I,
Membres : NJOMO Donatien, Professeur, Université de Yaoundé I,
NDJAKA Jean-Marie Bienvenu, Professeur, Université de Yaoundé I,
NGUENANG Jean-Pierre, Maître de Conférences, Université de Douala,
BEN-BOLIE Germain Hubert, Maître de Conférences, Université de Yaoundé I,



s'est réuni le Mardi 29 Juillet 2014 à 13h20 mn dans la salle S01/02 du nouveau bloc pédagogique de la Faculté des Sciences de l'Université de Yaoundé I, pour examiner en soutenance publique la thèse de Doctorat/PhD de Monsieur NONO DUEYOU Buckjohn Clémence, Matricule 99Y225, dont le sujet est intitulé :

« TRANSITION TO CHAOS INDUCING LOST OF ENERGY CONFINEMENT IN PLASMA »

La présentation a durée 40 mn.

Monsieur NONO DUEYOU Buckjohn Clémence a fait un exposé clair et fluide de l'essentiel de son travail en se servant des moyens de projection moderne. Pendant 2 h 00 mn, le candidat a ensuite répondu avec maîtrise et méthode aux questions des membres du Jury. Le Jury relève l'originalité du travail et les nombreux résultats intéressants obtenus par le candidat. Le document présenté est bien rédigé, abondamment illustré et organisé de façon équilibrée et aérée. Le candidat a ressorti, par des outils mathématiques et numériques appropriés, la dynamique complexe chaotique des perturbations de densité d'un dispositif à plasma soumis simultanément à une excitation paramétrique et à une force excitatrice externe. Il a également utilisé la méthode des échelles de temps multiples et les techniques d'approximation stochastique pour montrer l'influence des fluctuations aléatoires de la densité électronique sur les résonances et la stabilité d'une colonne de plasma. Enfin, il a montré que les densités de charge peuvent subir des transitions hystéritiques induites par l'excitation bruitée ou non bruitée externes.

Les travaux de Monsieur NONO DUEYOU Buckjohn Clémence constituent une contribution scientifique significative à la compréhension et à la maîtrise de la dynamique des plasmas de confinement. Par ailleurs, ils ont conduit à trois (03) publications dans les revues scientifiques à comité de lecture de haut niveau.

Compte tenu de tout ce qui précède, le Jury après avoir délibéré, a décidé à l'unanimité d'attribuer à Monsieur NONO DUEYOU Buckjohn Clémence, le grade de Docteur/PhD en Physique, Spécialité Mécanique, avec la mention « Très Honorable ».

Le Jury lui a ensuite adressé ses félicitations orales.

Fait à Yaoundé, le 29 Juillet 2014

LE PRESIDENT

Pr. MANGUELLE-DICOU M Eliezer

LES RAPPORTEURS

Pr. TCHAWOUA Clément

Pr. KOFANE Timoléon Crépin

LES MEMBRES DE JURY

Pr. NJOMO Donatien

Pr. NDJAKA Jean Marie

Pr. NGUENANG Jean-Pierre

Pr. BEN-BOLIE Germain Hubert

University of Yaoundé I

Faculty of Science

Department of Physics

**TRANSITION TO CHAOS INDUCING LOST OF ENERGY
CONFINEMENT IN PLASMA**

Submitted and defended in Fulfillment of the Requirements for the Degree of Doctor of
Philosophy/PhD in Physics
Option: Mechanics

By

Nono Dueyou Buckjohn Clémence

Registration number: 99Y225

DEA in Physics

Director

Prof. Clément Tchawoua

Supervisor

Prof. Timolon Crépin Kofane

Laboratory of mechanics

**All rights reserved. No part of this publication may be reproduced in
any form or by any means without the prior permission of the author.**

Copyright ©Nono Dueyou, bucknono@yahoo.fr

Year 2013

Dedications

To Jesus-Christ, whose riches, wisdom and science are so deep; how unreachable are his judgements and his ways past finding out! The one for of who, through who, and to who are all things, to whom be the glory for ever.

Acknowledgements

So this is the time for some personal word. During those years at the University of Yaoundé I, I have met a lot of people outside and inside the research work sphere, that contributed to make this adventure possible and enjoyable. So, the purpose of these pages is to thank all of you.

-A great thanks to the one above all of us, the allmighty God, for answering my prayers; for giving me the strength to plod on, despite my constitution wanting to give up and throw in the towel, thank you so much dear Lord.

- I have furthermore to thank the persons responsible of the Faculty of Science who gave and confirmed the permission and then encouraged me to go ahead with my thesis.

- I want to thank the Department of Physics of the University of Yaoundé I, for giving me permission to start this thesis in the first instance, and to do the necessary research work .

- I would like to express my deep and sincere gratitude to my supervisor and responsible of the laboratory of mechanics, Professor Kofane Timoleon Crépin, Head of the Department of Physics, Faculty of Science, University of Yaoundé I. His wide knowledge and his logical way of thinking have been of great value for me, from bachelor classes to thesis. Thank you for welcoming me in your lab, giving me the opportunity to write this thesis.

- I am deeply indebted to my thesis director, Professor Tchawoua Clément , from the University of Yaoundé I, whose help, stimulating suggestions and encouragement helped me in all the time of research for and writing of this thesis. Your rigor and diligence in the research; and writing skills for the corrections of my manuscript helped relieve many writing blocks. Professor, it was always a pleasure to share with you new results and your constant cheering, interest and enthusiasm allowed me to push through and complete this thesis. In the time spent in your research group, I will also remember the long work-time till night, and discussions from science to philosophy. I also remember your material assistance and others, thank you for all.

- Foremost, I would like to express my sincere gratitude to my mentor Dr Martin Siewe Siewe, for the continuous support of my Ph. D. study and research, for his patience, motivation, enthusiasm, and knowledge. His guidance helped me in all the time of research and writing of this thesis. I could not have imagined having a better mentor for my Ph. D. study. The new boosting energy that you brought to the research team prove itself by its fruits, I thank you for it.

- My sincere thanks are due to the official editors and referees of Physics Letter A, International journal of bifurcation and Chaos, Physica scripta, ASME journal of computational and nonlinear dynamics, for their detailed review, constructive criticism and excellent advice during the preparation of my different publications.

- I would like to express my gratitude to the members of the jury, Professor Manguelle-

Dicoum Eliezer, Professor Njomo Donatien, Professor Ndjaka Jean Marie Bienvenu, Professor Nguenang Jean-Pierre, Professor Ben-Bolie Germain Hubert, for their noteworthy evaluation of this thesis, for the lavished advices and the remarks made for the correction of this thesis.

- Although doing a Ph. D. is somehow a lonely process you need many people to collaborate with, whose skills allow the project to mature. I wish to extend my warmest thanks to all those who have helped me with my work in the Department of physics. Thanks specially the one of the laboratory of mechanics: Dr Fewo Ibraïd, Dr Woulachie Rosalie, for providing me with publications. Thanks to Dr Talla Mbe Jimmy Hervé, Dr Gambo Betchewe, Dr Voundou debertini . Thanks for your time and your considerate attitude.

- I would like to express my gratitude to my colleagues from the Professor Tchawoua research team who supported me in my research work. I want to thank them for all their help, support, interest and valuable hints. Especially I am obliged to Mrs. Alain bertrand Togueu Motcheyo, Joel Tchingang Tchameu, Hubert Malwé and David Tatchim, your help for the publications project (ideas, software, techniques and positive challenging) was greatly appreciated

- I also want to thank my physicians Dr Ouankou Mérimée, Dr Ourthing Clovis, Dr Seukap Elise, Dr Ouankou Christian, Dr Sini Victor, Dr Kissougle aimé, Dr Yondjio Nadine, Dr Mapoko Berthe, whose threat me all the years I spend in sickness and for all their psychological assistance on these hard days.

-Great thanks to my private secretaries Ms. Guepnang Laure and Ms. Dombou Christelle, your work was of great help in difficult times; for looking closely at the final version of the thesis for English style and grammar, correcting both and offering suggestions for improvement.

- I am indebted to Dr Pieumi Cyriaque, Dr Pedjeu Jean Claude, Dr Gottwald Melbourne and to Professor Tchantcho Bertrand, for their stimulating support and providing me with publications.

- I owe my gratitude to my pastors, Tagne Laurent, Houmeni Richard and Yoda Roger, for their counseling and prayers.

- My dear friends and brothers Jibia Eric and family, Gnecheko Armand and family , Yimbou Dejulio, Tchouya Romaric and family, Tagne Rigobert, Faha martin Luther, Tchokodjeu Bernadette, Kamadeu Gibril and family, Yossa fabrice, Panguetna Scherif, Freh Jean Paul, Ngando Djakou Garnier, Kemdep Yanick, Fankam Boris, Dr Takouchop Corine, Mahendje Auguste - Gladys, Essapo Aristide, Tetsuekoue Herman, Petke Louis, Tetsuekoue Irene and others; the time spent in "Bonamoussadi" or anywhere else was an even nice journey. Seeing you all leave this place one by one was really tough and made me realize how much I valued the moments shared with you. Your constant support even after you were gone helped me through rough times.

- I also owe my most sincere gratitude to Jou André family, for their love, prayers and all. Special thanks to Maman Kianpi Jou Therese, for material assistance and prayers.

- I also owe my most sincere gratitude to Djampou Esaie and Pieumi Nganso families, for their love, financial support, prayers and all the things that I couldn't have right words to express. Special thanks to Mrs. Djampou Cesar, Seukap Roger (our godfather in Yaounde), Pieumi Henri, Djoundjio Leopold, Lawo Carlos, for material assistance, psychological counsel-

ing, prayers, motivation enhancement and others...

- Last but not the least, especially, I would like to give my special thanks to the women who marked my live; my wife Celine whose patient and deeply love enabled me to complete this work; "mami", take my loving thanks; my mothers, Tchonang Pauline, Djampou Tatiana, Seukap Elise, Nono Brigitte, Lasso Alice, Tchuitchou Dueyou rose, Jibia Anne, whose feed and protection made me the man I am.

- Thanks to all the unmentioned persons who have contributed even a little to this work. I did not forget you...

List of Abbreviations

MHD: Magneto Hydro Dynamic
MPD: Magnetoplasma Dynamic
NBI: Neutral Beam Injection
ICRH: Ion Cyclotron Resonance Heating
ECRH: Electron Cyclotron Resonance Heating
LH: Lower Hybrid
TOKAMAK: Toroidalnaya Kamera ee Magnitaya Katushka
LHD: Large Helical Device
JFT2M: Jaeri Fusion Torus Remodelled version
ITER: International Tokamak Experimental Reactor
DC: Direct current
SR: Stochastic Resonance
DV: Discharge Voltage
FTU: Frascati Tokamak Upgrade
TCV: Variable Configuration Tokamak
NCSR: National Centre for Scientific Research "DEMOKRITOS"
CS: Central solenoid
NBI: Neutral Beam Injection
ASDEX: Axisymmetrical Divertor Experiment
ICs: Integrated Circuit
JET: Joint European Torus
DIID: Doublet 3-Dimension
TEXTOR: Tokamak Experiment for Technically Oriented Research
CCT: Continuous current Tokamak
TF: Toroidal Field
RWM: Resistive Wall Mode
ELM: Edge Localised Mode
VCO: Virtual Cathode Oscillator
rf: radio frequency
ESR: Electron Serie Resonance
CHS: Compact Helical system

Contents

List of the Permanent Teaching Staff	i
Dedications	xi
Acknowledgements	xii
List of Abbreviations	xv
Table of Contents	xvi
List of Figures	xviii
Abstract	xxiv
Résumé	xxvi
General Introduction	1
Chapter I Literature review on plasma physics and some methods used therein	6
I.1 Plasma physics	6
I.1.1 Historical perspective of plasma	6
I.1.2 Plasma parameters	9
I.1.3 Plasmas in nature and in laboratory	10
I.2 Plasmas and particles	11
I.2.1 Plasma processing	11
I.2.2 Particles heating	14
I.2.3 Plasma classification	15
I.2.4 Principles of particle confinement	19
I.2.5 Plasmas and technological application	26
I.3 Plasma and numerical computation	29
I.4 Plasma instabilities	30
I.5 Chaos as an explanation of plasma collapse	31
I.5.1 Motivation	33
I.6 Fundamental statement of the thesis	35
I.7 Conclusion	35

Chapter II Methodology: Modelling and mathematical methods	37
II.1 Modelling	37
II.1.1 Boltzman equations for species	38
II.1.2 Two fluid equations	41
II.1.3 Reduced nonlinear model for charge density under parametric and external harmonic oscillations	46
II.1.4 Potential configuration	49
II.1.5 Reduced nonlinear model for charge density under external bounded noise excitation	51
II.1.6 Reduced nonlinear model of radial electric field in plasma L-H transition under external bounded noise	55
II.2 Mathematical methods for the control of global bifurcation	60
II.2.1 Chaos control using Melnikov method	60
II.2.2 Random Melnikov process	67
II.2.3 Response of charge density using multiple scales method	71
II.2.4 Response of density perturbation and resonances	75
II.2.5 Stability of equilibrium states and statistic moments	79
II.3 Conclusion	82
Chapter III RESULTS AND DISCUSSION	83
III.1 Transition to chaos in plasma density with asymmetric double-well potential for parametric and external harmonic oscillations	83
III.1.1 Discussion	90
III.2 Effect of external bounded noise on nonlinear dynamics of plasma density	95
III.2.1 Numerical simulation of nonlinear response	103
III.2.2 Numerical simulations	108
III.2.3 Discussion	109
III.3 Global bifurcation of mean electric field in plasma L-H transition under external bounded noise excitation	112
III.3.1 Numerical simulations	113
III.3.2 Discussion	123
General Conclusion	135
Appendix	138
List of Publications	142
Bibliography	143

List of Figures

Figure 1	Free ions and electrons in plasma. (From: Chen F. F. and Chang J. P., <i>Lecture Notes on principles of plasma processing</i> , Plenum/Kluwer Publishers, (2002).)	7
Figure 2	(a) Natural plasmas: A-stellar space, B-Interplanetary space, C-Solar wind, D-Magnetosphere, E-Ionosphere, F-Solar corona, G-Stellar atmosphere, H-Lightning, I-Stellar interior; and (b) industrial plasmas: A-Flames, B-Intense bundles, C-MHD generators, D-Industrial reactors, E-Laser lamps, F-Tokamaks, G-sparks, H-Pinch and mirrors, I-Laser/plasma interaction. (From: Rax J.-M., <i>Physique des plasmas, Cours et applications</i> , Dunod, Paris, (2005), page 4)	8
Figure 3	Examples of plasmas presents in nature: (a) A comet sketching, (b) A gaseous nebulae, (c) A galaxie. (From: Chen F. F. and Chang J. P., <i>Lecture Notes on principles of plasma processing</i> , Plenum/Kluwer Publishers, (2002), pages 1 and 2)	10
Figure 4	Tokamaks: (a) T1 the first (From: http:// alltheworldstokamaks. word-press. com /gallery- of - external - views/) and (b) Cut-away of ITER (From: Ariola M., Pironti A., <i>Magnetic Control of Tokamak Plasmas</i> , Springer, London, (2008), page 11), (the most recent) showing the vacuum vessel, coils and divertor region. Iter wil have a plasma volume of $840 m^3$	11
Figure 5	Use of tokamaks as energy provider.	12
Figure 6	(a) aurora borealis ((From: Chen F. F. and Chang J. P., <i>Lecture Notes on principles of plasma processing</i> , Plenum/Kluwer Publishers, (2002), pages 1 and 2)), (b) Tokamak	16
Figure 7	Plasmas as a function of temperature and density (From: Harry J. E., <i>Introduction to Plasma Technology Science Engineering and Applications</i> , Wiley-VCH, Weinheim, (2010), page 3).	18
Figure 8	(a) Stellarator configuration (From: Piel A., <i>Plasma Physics, An Intro-duction to Laboratory, Space, and Fusion Plasmas</i> , Springer, New York, (2010), page 21) and (b) The Large Helical Device (LHD) at the National Institute for Fusion Science in Toki, Japan is the world’s largest stellarator (from the Fusion Energy Division Oak Ridge National, TN 37831-6169).	22

Figure 9	(a) Cut of ITER tokamak showing location of plasma facing materials and impurity concentration limit in the plasma core for different elements, and (b) JFT2M tokamak (From: http:// alltheworldstokamaks. word-press. com /gallery- of - external - views/).	23
Figure 10	Particles movement in the torus. (From: Piel A., Plasma Physics, An Introduction to Laboratory, Space, and Fusion Plasmas, Springer, New York, (2010), page 63).	24
Figure 11	(a)Energy consumption (From: http:// www.courtfool. info) and (b)population growth (From: http:// www.roperld.com/ science/ energyfuture. htm) curves	27
Figure 12	Plasma sheath.	38
Figure 13	A configuration space volume element dr with the equivalent velocity space element. $dV = drdv$ is the volume element in (\mathbf{r}, \mathbf{v}) phase space. . .	39
Figure 14	Potential configuration: (a) for $\beta = -0.25$ and $\lambda \in [0.05, 0.5]$, (b) for $\beta = 0.25$ and $\lambda \in [0.05, 0.9]$, (c) for $\beta = 0.25$ and $\lambda \in [1.1, 1.9]$	50
Figure 15	(a) Shape of the renormalized potential Eq. (19), (b) corresponding phase portrait for $\beta = 0.25$ and $\lambda \in [1.01, 1.2]$, with $\lambda^2 - 4\beta > 0$	61
Figure 16	Homoclinic orbits Γ_1 , and Γ_2 for the renormalized bounded double well potential.	64
Figure 17	Critical amplitude versus the frequency ω of the right well for $\mu = 1.0, \gamma = 5.0, \beta = 0.25, \lambda = 1.15, \Omega = 0.66114$; and $h = 0.0$ (red); $h = 0.05$ (black); $h = 0.1$ (blue).	83
Figure 18	Critical amplitude versus the frequency ω the left well for $\mu = 1.0, \gamma = 5.0, \beta = 0.25, \lambda = 1.15, \Omega = 0.66114$; and $h = 0.1$ (black), $h = 0.2$ (red), $h = 0.3$ (blue).	84
Figure 19	Bifurcation diagrams of the system (71) for different values of h , with initial condition taken in the left well; $\omega = 1.33$ and $\Omega = 0.66114$. Other parameters are those of Fig. 4.	86
Figure 20	Corresponding maximum Lyapunov curves of the bifurcation diagrams (Fig.(19)). Other parameters are those of Fig. 4.	87
Figure 21	Bifurcation diagrams of the system (71) and the corresponding maximum Lyapunov exponent calculate for h varying, with initial condition taken in the right well, $\Omega = 0.66114$ and $\omega = 1.33$ for (a) $A_0 = 0.224$, (b) $A_0 = 0.9$, (c) $A_0 = 1.3$ and (d) $A_0 = 1.485$. Other parameters are those of Fig. 4. . . .	88
Figure 22	Bifurcation diagrams of the nonlinear system (71) with initial condition taken in the right well for $\Omega = 0.66114, \omega = 1.33$. System parameters as for Figure 4.	89
Figure 23	Bifurcation diagrams of the nonlinear system (71) with initial condition taken in the right well for $\Omega = 0.66114, h = 0.0, \omega = 1.33$. System parameters as for Figure 4.	89

Figure 24 Influence of the external amplitude on the Poincaré maps of the system (a) a non chaotic states for $A_0 = 1.40$ (b) chaotic attractor for $A_0 = 1.480$. System parameters as for Figure 4. 90

Figure 25 Basin of attraction for strong external forcing, $\ddot{z} = -0.25 \{z^3 - \frac{3}{4}(z_1 + z_2)z^2 + \frac{1}{2}(z_1 z_2)z\} + 0.015(-((1+x_0+5.0x_0^2)+(1+2 \times 5.0 \times x_0)z+(5.0)z^2)v) - h(z+x_0) \cos \Omega \tau + A_0 \cos(1.33\tau)$, for $A_0 = 1.30$: (a) $h = 0.1$ (b) $h = 0.115$, (c) $h = 0.29695$, (d) $h = 0.2980$ with $\Omega = 0.66114$ 91

Figure 26 Basin of attraction for strong external forcing, $\ddot{z} = -0.25 \{z^3 - \frac{3}{4}(z_1 + z_2)z^2 + \frac{1}{2}(z_1 z_2)z\} + 0.015(-((1+x_0+5.0x_0^2)+(1+2 \times 5.0 \times x_0)z+(5.0)z^2)v) - 0.3(z+x_0) \cos \Omega \tau + A_0 \cos(1.33\tau)$, with $\Omega = 0.66114$: (a) $A_0 = 0.81$; (b) $A_0 = 0.9$; (c) $A_0 = 1.0$; (d) $A_0 = 1.1$ 92

Figure 27 Stability map of the equilibrium solutions of equation (143) for $\gamma = 5.0$, $\mu = 0.9$. Shaded regions represent asymptotically stable equilibria. 95

Figure 28 Frequency response of system (57) in the (ρ_a, a_0) -plane, for $\mu = 1.1$, $\gamma = 5.0$, $\sigma = -1.5$; and $\eta = 0.5(blue)$, $\eta = 1.5(black)$, $\eta = 3.5(red)$, $\eta = 5.5(green)$ 96

Figure 29 Frequency response of system (57) in the (σ, ρ_a) -plane, for $\mu = 1.1$, $\gamma = 5.0$, $a_0 = 0.3$; and $\eta = 0.5(blue)$, $\eta = 1.5(black)$, $\eta = 3.5(red)$, $\eta = 5.5(green)$. 96

Figure 30 Frequency response of system (57) in the (σ, ρ_a) -plane, for $\mu = 1.1$, $\gamma = 5.0$, $a_0 = 0.6$; and $\eta = 0.5(blue)$, $\eta = 1.5(black)$, $\eta = 3.5(red)$, $\eta = 5.5(green)$. 97

Figure 31 Regions of the existence of the statistic moment ρ_{20} in the (σ, γ) - plane, for $a_0 = 0.8$; $\mu = 1.1$; $A_0 = 0.2$. There is no solution in the white region. . 97

Figure 32 3-D resonance region plotted in the space (a_0, σ, ρ_a) , for $\mu = 1.1, \gamma = 5.0, \eta = 1.8$ 98

Figure 33 Frequency response of system (57) in the (σ, a_0) -plane, for different values of gaussian noise intensity η , for $\mu = 1.1, \gamma = 6.0, A_0 = 0.2, \rho_a = 1.2$; and $\eta = 4.8(blue)$, $\eta = 8.8(red)$, $\eta = 12.8(green)$, $\eta = 16.8(black)$ 98

Figure 34 Resonance curves measured at successively values of complete statistic moment ρ_a , with: (a) $\eta = 6.8$, (b) $\eta = 5.8$; $\rho_a = 0.2(blue)$, $\rho_a = 0.4(yellow)$, $\rho_a = 0.6(green)$, $\rho_a = 0.8(red)$, $\rho_a = 1.0(black)$. Arrows on the highest pair of curves indicate sweep direction. All lower curves are not similar. Note sharp peak and reinforcement of asymmetry and hysteresis phenomena at the highest moment. 99

Figure 35 Effect of varying parameter μ on the frequency response curves and on the stability of solutions; for $A_0 = 1.2, \gamma = 5.0$ 100

Figure 36 Effect of varying the external excitation magnitude A_0 on the frequency response curves; for $\mu = 1.1, \gamma = 5.0$; and $A_0 = 0.2(black)$, $A_0 = 0.5(blue)$, $A_0 = 1.4(red)$, $A_0 = 2.2(green)$ 100

Figure 37 Forced response of density perturbation in the case of the fundamental parametric resonance, for different values of detuning frequency σ ; $\mu = 1.1, \gamma = 5.0$; and $\sigma = -1.4(black)$, $\sigma = -1.0(blue)$, $\sigma = -0.6(red)$, $\sigma = -0.2(green)$ 101

Figure 38 Effect of varying parameter γ on the frequency response curves; for $\mu = 1.1$, $A_0 = 1.2$; and $\gamma = 12.0$ (black), $\gamma = 8.0$ (blue), $\gamma = 4.0$ (red), $\gamma = 1.0$ (green). 101

Figure 39 Forced response of density perturbation in the case of the fundamental parametric resonance, for different values of parameter γ ; $\mu = 1.1$, $\sigma = -1.0$; and $\gamma = 8.0$ (green), $\gamma = 6.0$ (blue), $\gamma = 4.0$ (red), $\gamma = 2.0$ (black). 102

Figure 40 3-D resonance basin plotted in the space (a_0, σ, ρ_a) , for $\mu = 2.1$, $\gamma = 20.0$, $\eta = 16.8$ 102

Figure 41 Resonance curves measured at successively values of complete statistic moment ρ_a . All curves are not similar as in (34). As in (34), we have: $\rho_a = 0.2$ (blue curve); 0.4 (yellow curve); 0.6 (green curve); 0.8 (red curve); 1.0 (black curve). Note right hand and left hand hysteresis phenomena at the highest moment. 103

Figure 42 Regions of stability of the statistic moment ρ_{20} in the (σ, a_0) - plane, from Eqs. (167)-(170), for different values of parameter: (a)- μ for $\gamma = 4.1$; $A_0 = 0.2$, (b)- γ for $\mu = 1.1$; $A_0 = 0.2$. The solutions are stable in the white region. 104

Figure 43 Bifurcation diagrams obtained from (57) for $\eta = 0$ and : (a)- $\sigma = -1.1$; $\gamma = 5.0$; $\epsilon = 0.4$; (b)- $A_0 = 2.0$; $\gamma = 5.0$; $\epsilon = 0.44$ 105

Figure 44 Bifurcation diagrams obtained from (57) for $\eta = 0$ and : (a)- $A_0 = 2.0$; $\gamma = 7.0$; $\epsilon = 0.44$.(b)- $A_0 = 2.2$; $\sigma = -1.1$; $\epsilon = 0.44$ 105

Figure 45 Influence of parameter γ on the Poincaré maps of (57) for $\eta = 0$ and $\mu = 1.1$; $\beta = 0.15$; $\lambda = 1.9$; $A_0 = 2.2$ 106

Figure 46 Influence of the gaussian noise intensity η on the limit cycles maps of (57) for $\mu = 1.1$; $\beta = 0.15$; $\lambda = 1.9$; $A_0 = 2.2$; $\gamma = 8.5$ 107

Figure 47 Influence of the gaussian noise intensity η on the limit cycles maps of (57) for $\mu = 1.1$; $\beta = 0.15$; $\lambda = 1.9$; $A_0 = 2.2$; $\gamma = 6.85$ 107

Figure 48 3D upper threshold bound in (Ω_2, η) plane with the associated threshold amplitude F_2 versus noise intensity η for homoclinic bifurcation; analytic results for differents values of Ω_2 112

Figure 49 3D inverse upper threshold bound in (Ω_2, η) plane with the associated threshold amplitude F_2 versus noise intensity η for homoclinic bifurcation; analytic results for differents values of Ω_2 113

Figure 50 Asymptotic growth rate K_c versus F_2 for Eq. (66); homoclinic orbits. 114

Figure 51 Plot of asymptotic growth rate K_c versus c for system (66) with the associated mean square displacement $M(n)$ as a function of n . We used here $N = 20000$ data points, and 100 equally spaced values for c . $F_2 \approx 1.2$; $\eta = 0.0$ corresponding to regular dynamics. 114

Figure 52 Plot of asymptotic growth rate K_c versus c for system (66) with the associated mean square displacement $M(n)$ as a function of n . We used here $N = 2000$ data points, and 100 equally spaced values for c . $F_2 \approx 1.31$; $\eta = 0.18$ corresponding to chaotic dynamics. 115

Figure 53 Plot of asymptotic growth rate K_c versus c for system (66) with the associated mean square displacement $M(n)$ as a function of n . We used here $N = 20000$ data points, and 100 equally spaced values for c . $F_2 \approx 1.31$; $\eta = 10.0$ corresponding to noise induced chaotic dynamic dynamics. . . . 115

Figure 54 Asymptotic growth rate K_c versus F_2 for Eq.(66); heteroclinic orbits. . . . 116

Figure 55 Plot of asymptotic growth rate K_c versus c for system (66) with the associated mean square displacement $M(n)$ as a function of n . We used here $N = 20000$ data points, and 100 equally spaced values for c . $F_2 \approx 5.0$; $\eta = 1.0$ corresponding to noisy regular dynamics. 117

Figure 56 Plot of asymptotic growth rate K_c versus c for system (66) with the associated mean square displacement $M(n)$ as a function of n . We used here $N = 20000$ data points, and 100 equally spaced values for c . $F_2 \approx 6.1$; $\eta = 10.0$ corresponding to noise induced chaotic dynamics. 117

Figure 57 Time history with the associated autocorrelation functions and fast Fourier transform for time series data from system (66): $F_2 \approx 1.0$; $\eta = 5.0$ corresponding to noisy motion. 119

Figure 58 Percentage of false nearest neighbor for time series data from system (66), with embedding dimension m in $[0..10]$: $F_2 \approx 1.31$; $\eta = 0.18$ corresponding to chaotic motion. 119

Figure 59 Time history with the associated autocorrelation functions and fast Fourier transform for time series data from system (66)-(heteroclinic orbit): $F_2 \approx 5.0$; $\eta = 5.0$ corresponding to noise-induced chaotic motion. 120

Figure 60 Time history with the associated autocorrelation functions and fast Fourier transform for time series data from system (66)-(heteroclinic orbit): $F_2 \approx 6.1$; $\eta = 0.1$ corresponding to chaotic motion. 120

Figure 61 Time history with the associated autocorrelation functions and fast Fourier transform for time series data from system (66)-(heteroclinic orbit): $F_2 \approx 6.1$; $\eta = 1.0$ 121

Figure 62 Time history with the associated autocorrelation functions and fast Fourier transform for time series data from system (66)-(heteroclinic orbit): $F_2 \approx 6.1$; $\eta = 5.0$ 121

Figure 63 Poincaré map for homoclinic orbits with the associated phase portrait and time history (noise-free system, under the critical threshold): $F_2 = 1.1$; $\eta = 0.0$ 122

Figure 64 Poincaré map for homoclinic orbits with different noise amplitude: $F_2 \approx 1.3$ (first row) $\eta = 0.18$; (second row) $\eta = 1.0$; (third row) $\eta = 5.0$ 123

Figure 65 Noisy bifurcation diagram for heteroclinic orbits with the associated zoom for $F_2 \in [0..4.5]$ (noisy system, under the critical threshold): $\eta = 0.18$ 124

Figure 66 Poincaré map for heteroclinic orbits with the associated phase portrait and time history (noise-free system, under the critical threshold): $F_2 = 5.9$; $\eta = 0.0$ 125

Figure 67	Poincaré map for heteroclinic orbits with the associated phase portrait and time history (noisy system, F_2 under the critical threshold): $F_2 = 5.9; \eta = 5.0$	125
Figure 68	(a)-Poincaré map for heteroclinic orbits (noisy system, F_2 at the critical threshold): $F_2 = 6.1; \eta = 0.1$; (b)-Poincaré map for heteroclinic orbits (noisy system, F_2 at the critical threshold): $F_2 = 6.1; \eta = 1.0$	126
Figure 69	(a)-Poincaré map for heteroclinic orbits: $F_2 = 8.0; \eta = 0.0$. ; (b)-Poincaré map for heteroclinic orbits: $F_2 = 8.0; \eta = 1.0$	126
Figure 70	Scaled power spectrum of $u(t)$ oscillations in system (66) -(homoclinic orbits) for: $F_2 = 1.0$ and noise intensity $\eta = 5.0$	127
Figure 71	(a)-Scaled power spectrum of $u(t)$ oscillations in system(66) -(homoclinic orbits) for: $F_2 \approx 1.3$ and noise intensity $\eta = 0.18$. ; (b)-Scaled power spectrum of $u(t)$ oscillations in system(66) -(heteroclinic orbits) for: $F_2 = 5.9$ and noise intensity $\eta = 0.0$	127
Figure 72	(a)-Scaled power spectrum of $u(t)$ oscillations in system(66) -(heteroclinic orbits) for: $F_2 = 6.1$ and noise intensity $\eta = 0.1$. ; (b)-Scaled power spectrum of $u(t)$ oscillations in system(66) -(heteroclinic orbits) for: $F_2 = 6.1$ and noise intensity $\eta = 5.0$	128

Abstract

In this thesis, the first basic structural model adopted is the two fluid model for plasma density. The second one is defined by a set of Ginzburg-Landau type differential equations, modeling mean electric field change in tokamak L-H transition. These models capture the basic nonlinear phenomena in plasma device and their generalization in large plasma devices as tokamaks, with a minimal complexity in the equations of motion, thus providing a balance between simplicity and accuracy.

We first study the chaotic dynamics of one-degree-of-freedom nonlinear oscillator representing a density perturbation in plasma device excited by parametric force coming from sheath oscillation when heating the plasma with a sinusoidal oscillating voltage, and an external driven force coming from the control device. For this first investigation, parameters for the onset of chaotic motions are specified using Melnikov method. The analytical results are confirmed by numerical simulations. The global dynamical changes of the system have been examined by evaluating parametric changes of the bifurcation diagrams, maximum Lyapunov exponent, Poincaré map and the basin boundaries of attraction. The transitions to chaos caused by the cascade bifurcation and intermittency are clearly shown by graphical methods.

Secondly we show that the random fluctuations in the electronic density referring to the above model, can influence considerably the profile of the resonance and stability curves of a column of plasma. The fluctuations affect the resonance in a different way according to the order of the considered resonance. The purpose of this effort is to investigate the effects of bounded noise on the primary resonances of density fluctuation in plasma. Along this second study, the response and stability are considered and analyzed using the method of multiple scales and the technique of stochastic averaging. Further, the statistical moments are calculated and their stability condition established. Through numerical simulations, we show that the density perturbation may undergo hysteretic transitions induced by external noisy excitation. The response of the global system is affected by bounded noise as demonstrated through Poincaré map.

We end our work by studying the Melnikov function associated with a bounded noise perturbation of a differential equation modeling mean electric field change in tokamak L-H transition, having two homoclinic orbits and one heteroclinic orbit. Our main interest is the characterization of perturbations that give rise to vanishing or non-vanishing of the Melnikov function. For the purpose of analyzing this third model, we

use a test of chaos to verify our prediction. The results reveal that noise intensity, modify the attractor size through power spectra, correlation function and Poincare map. We then found that, the criterion from Melnikov's method could be a valid tool for predicting harmful parameters values involved in experiment on Tokamak L-H transition, allowing quantitative predictions and qualitative description of different control operations.

Keywords: Plasma, Two-fluid model, L-H transition, Energy, Melnikov, Bifurcation, Resonance, Chaos.

Résumé

Nous considérons dans cette thèse, des modèles qui illustrent les phénomènes non linéaires de base, avec une complexité réduite, dans les dispositifs à plasma de laboratoire, et leur généralisation dans les machines à plasma de grande taille comme les tokamaks. Le premier modèle est le plasma à double-fluide, généralement utilisé pour étudier la dynamique des perturbations de densité des ions et des électrons. Nous tenons compte de deux cas de figure: le cas où le modèle n'est influencé par aucun bruit, et le cas où il est soumis à un bruit borné. Le second modèle de notre étude, est défini par des équations de diffusion de type Ginzburg-Landau adimensionnées, caractérisant les fluctuations de densité liées à la variation moyenne du champ électrique radial. Ce modèle permet d'expliquer la transition des états de faible énergie de confinement vers les états de grande énergie de confinement dans le tokamak.

Le travail s'ouvre par l'étude de la dynamique chaotique des perturbations de densité d'un dispositif à plasma soumis simultanément à une excitation paramétrique et à une force motrice externe. Cette force et cette excitation proviennent respectivement d'un dispositif de contrôle et de l'oscillation de la gaine, suite au chauffage du plasma avec une tension sinusoïdale. Les paramètres critiques définissant l'apparition des comportements chaotiques dans ce premier modèle sont déterminés et exprimés analytiquement à l'aide de la méthode de Melnikov. Les simulations numériques, qui s'appuient sur l'étude des diagrammes de bifurcation, le calcul des exposants de Lyapunov, l'analyse des sections de Poincaré et des bassins d'attraction, sont effectuées et confirment les résultats analytiques.

Ensuite, se référant au premier modèle sus-évoqué et en utilisant la méthode des échelles de temps multiples et les techniques d'approximation stochastiques, nous montrons que les fluctuations aléatoires de la densité électronique influencent les résonances et la stabilité d'une colonne de plasma. Il apparaît aussi que les effets de ces fluctuations sur la résonance varient d'un ordre à un autre. Les moments statistiques sont également calculés et leurs conditions de stabilité établies. Numériquement, nous montrons par ailleurs que les perturbations de densité peuvent subir des transitions hystérétiques induites par l'excitation bruitée externe. L'analyse des sections de Poincaré indique des réponses du système affectées par ce bruit.

Afin de déterminer les perturbations qui donnent naissance aux fluctuations chaotiques dans le second modèle, nous nous intéressons enfin à l'étude de la fonction de

Melnikov associée à une perturbation de type bruit borné. Ici les équations d'évolution modélisent les variations du champ électrique radial dans le tokamak. A cet effet, un test binaire appelé 0-1-test est utilisé pour vérifier les prédictions analytiques. Les résultats révèlent que l'intensité du bruit peut modifier la taille des attracteurs. Ces résultats sont confirmés par le biais du tracé des spectres de puissance, des fonctions de corrélation et des sections de Poincaré. Il résulte que le critère de la méthode de Melnikov pourrait être un outil valable pour prédire les valeurs nocives des paramètres utilisés dans les expériences sur le Tokamak. Ceci permet des prédictions quantitatives et des descriptions qualitatives de différentes opérations de contrôle servant à l'optimisation du chauffage du plasma, le confinement d'énergie et la diminution du risque d'accidents.

Mots-Clefs: Plasma, modèle double fluide, transition L-H, Energie, Melnikov, Bifurcation, Résonance, Chaos.

General Introduction

Bifurcations and chaos theory started with the intention of investigating the qualitative behavior of nonlinear problems which were difficult to be solved analytically. In the first half of the 1900s, scientists were interested in nonlinear oscillators like the Van der Pol oscillator; with the advent of high speed computers, many different nonlinear problems were solved [1]. Bifurcation diagrams, Lyapunov exponent, correlation dimension, etc., derived on the basis of chaos theory, have been used to characterize chaos and its different routes [2, 3]. Since the development of nonlinear dynamics, most applications have been in the field of fluid dynamics, particularly fluid turbulence; because fluid and plasma are closely related, the concepts of nonlinear dynamics had been successfully utilized in plasmas.

In the late sixties and later, the idea of van der Pol oscillator was applied to explain the growth and saturation of the plasma instabilities which could not be done using conventional linear theories [4, 5] (and references therein). In their work, Abrams et al. [6] first observed the nonlinear phenomena like period pulling, frequency entrainment, etc., in periodically forced self-oscillatory plasmas. Keen et al., showed using a two-fluid model that the ion sound instabilities behaved in a manner similar to a van der Pol oscillator, when subjected to a driving force. The period doubling route to chaos was also reported in the driven pulsed filament discharge plasma and an electrical discharge tube [7, 8]. In 1989, the intermittency route to chaos was observed in the low frequency self-oscillations in the undriven DC discharge system [9, 10]. Homoclinic chaos [11] was reported in the same electrical discharge plasma system in which the deterministic chaos has been observed, quasiperiodic route to chaos was observed in the driven and undriven discharge plasmas [10]. Period adding route to chaos and period subtracting had been observed in ion beam plasma in double plasma device [12]. In many other researches, almost similar phenomena had been observed where different types of gases, geometric configurations and parametric regimes were explored [13]. In all the above

studies, the common feature was that the plasma dynamics goes towards a chaotic state as the discharge current or discharge voltage (DV) was raised. Plasma machines could be also subjected to external and/or internal noise.

Noise is usually considered as a troublesome feature of real physical systems. Moreover, noise as a source of stochastic motion, plays an important role in the formation of structures in states far from thermodynamic equilibrium. An important step toward a better understanding of the interplay between stochastic and organized motion is the concept of stochastic resonance (SR). SR, which has been observed in many physical, chemical and biological systems [14, 15, 16], is a phenomenon in which the response of the nonlinear system to a weak periodic input signal is amplified or optimized by the presence of a particular level of noise [14], i.e., a previously untraceable subthreshold signal applied to a nonlinear system can be detected in the presence of noise. Over the last few years, it has become apparent that, in a system far from thermal equilibrium, even a small noise can also result in a qualitative change in the system's properties, e.g. the transformation of an unstable equilibrium state into a stable one and vice versa; and the occurrence of multistability or multimodality [17]. The mechanism of SR shows that the response of a bistable system to a weak signal can be optimally amplified by the presence of an intermediate level of dynamical noise. Furthermore, it has been proved that noise may play a constructive or destructive role in nonlinear systems, by enhancing coherent or incoherent behavior near bifurcations and phase transitions [18]. Because the ability to construct coherent plasma structures appears to be of great potential value in a variety of practical problems and in the study of the dynamics of engineering structures such as plasma devices, the existence of noise as an external perturbation cannot be ruled out.

It is known that sudden transitions (the transitions can be considered like bifurcations) to improved confinement modes have been a focus of toroidal confinement research for more than a decade since the discovery of the H-mode in 1982 in a divertor tokamak. The great variety of plasma situations in which the transition to improved confinement is observed suggests that there may be some universal mechanism responsible for the formation of a transport barrier and the decrease in the particle outflow [19]. Several theoretical models on the transition from L-mode to H-mode plasmas have

been presented. In 1990, a radial electric field E_r near the plasma periphery has been found both experimentally and theoretically to play an important role in the L-H transition. This radial electric field, in the thermal transport barrier, is found to become more negative at the L-H transition [20].

Homoclinic or heteroclinic bifurcations could be an important sources of structural instabilities in nonlinear dynamical plasmas models. The subsequent occurrences of scattered chaotic dynamics and fractal basin boundaries are usually derived from the homoclinic or heteroclinic transversal intersections between the stable and unstable manifold of the hilltop saddle in the Poincaré map. In general homoclinic and heteroclinic bifurcations are unwanted dynamical behaviors in most cases, consequently their suppression by using several methods, is desirable from a practical point of view [21].

Melnikov's method was used to study the chaotic behavior [22] of a nonlinear damped three-well ϕ^6 -Vander Pol oscillator under external and parametric excitations; resonance and homoclinic bifurcation [23]; the occurrence of chaos in a parametrically driven extended Rayleigh oscillator with three-well potential [24]. In Ref.[25], the chaotic behavior of Duffing oscillator possessing both homoclinic and heteroclinic orbits and subjected to harmonic and bounded noise excitations was investigated. The result based on Lyapounov exponent reveal that for larger noise intensity the threshold amplitude of bounded noise for onset of chaos will move upward as the noise intensity increases. The same behavior was demonstrated in [26, 27].

So, Homoclinic bifurcations are manageable dynamical behaviors in most cases, consequently their monitoring could be helpful from a practical point of view [21]. For example, Rempel et al. [28] have investigated the relevance of chaotic saddles and unstable periodic orbits at the onset of intermittent chaos in plasmas. They focus on the role of non attracting chaotic solutions, known as chaotic saddles, in the transition from weak chaos to strong chaos via an interior crisis and show how two of these unstable chaotic saddles can interact to produce the plasma intermittency observed in the strongly chaotic regimes. Nevertheless, with the advent of the study of chaotic motion by means of strange attractors, Poincaré maps and fractal basin boundaries, it has become necessary to look for a better understanding of these nonlinear systems like

density perturbation in plasma with higher order nonlinear terms.

The Melnikov method [29, 30], is an effective approach to detect chaotic dynamics and to analyze near homoclinic or heteroclinic motion with deterministic or random perturbation. The method was first applied in [31] to study a periodically forced Duffing oscillator with negative linear stiffness, and by [32] to investigate the chaotic behavior of a parametrically excited system such as the transverse vibration of a buckled column under axial periodic excitation.

Chaos and the induced transport are key ingredients to a number of problems in building a working device for nuclear fusion. Thus effectively controlling or influencing chaos is a major issue in fusion research. There are two ways to control plasma: choosing the right parameters and geometry or activate a control mechanism. In this thesis, we will be focus to the first one.

Plasma processing technology, through many applications, is used in many manufacturing industries [34], especially in the surface treatment of components for the automotive, aerospace and biomedical sectors. Plasma technologies offer advantages in terms of environmental impact, through reduced use of toxic liquids, and in terms of engineering scale, through their compatibility with nanoscale fabrication [35].

In this thesis, the concept of bifurcation and chaos associated to plasma is studied. Two example of macroscopic property (charge density and radial electric field) affected by internal and /or external perturbations are considered for illustration with an incidence on energy confinement. We discuss basic concepts of dynamical chaos and then give their connection with chaos in plasmas.

This Thesis also aims at making a bridge between the fundamental nonlinear theories and nonlinear phenomena involving structural formation, chaos and turbulence in plasmas with an incidence on plasma confinement. We make an emphasis on chaos an turbulence as the consequences of intrinsic plasmas phenomena; for example, zonal flows in magnetized plasma drift wave, with the given formulation and derivations of the basic equations. Certainly, we had to omit a number of topics in developing fields. The thesis also omits some basics of fusion plasmas as they are well covered in a number of good textbooks and monographs.

The manuscript consists of three chapters.

1. Chapter I provides basic concepts and fundamental theories necessary to understand contemporary plasma physics, and gives some motivations of our work.
2. Chapter II covers the ideas and methodologies for exploring nonlinear phenomena associated with plasma modelization, structural formation, turbulence and chaos; enough for understanding the rest of the thesis. Chapter II also connects plasma physics to the stochastic theory, needed in real engineering. Two fluid modeling, stochastic methods, nonlinear methods use to detect chaos; and resonance modes are mainly discussed since they are well established concepts.
3. Chapter III is devoted to summarize the findings of this thesis through characterization of irregular behavior (chaos and turbulence), resonances modes and direct numerical simulations, followed by a conclusion with an outlook for future studies.

LITERATURE REVIEW ON PLASMA PHYSICS AND SOME METHODS USED THEREIN

I.1 Plasma physics

Study of the nonlinear processes in plasmas started in the sixties. Usually, nonlinear dynamics plays a central role in plasma heating and confinement, and phenomena that are involved in turbulence and self-organization. Many nonlinear phenomena had been observed and nonlinear dynamics experiments had been performed in different types of laboratory plasmas. Plasma column devices, as a approximation of tokamaks, easily exhibits nonlinear instabilities. This chapter gives a brief review on nonlinear dynamics in plasma physics and propose the motivation that leads to the fundamental statement of the thesis.

I.1.1 Historical perspective of plasma

In the mid-19th century the Czech physiologist Jan Evangelista Purkinje introduced use of the Greek word *plasma*, meaning “formed or molded” (after the Greek word “πλάσμα”, which means “moldable substance” or “jelly”) to denote the clear fluid which remains after removal of all the corpuscular material in blood. Half a century later, the Nobel prize-winning American chemist Irving Langmuir proposed in 1922 that the electrons, ions and neutrals in an ionized gas could similarly be considered as corpuscular material entrained in some kind of fluid medium and called this entraining medium, *plasma* [36]. He called the discovered electromagnetic oscillations in rarefied gases: “*plasma oscillations*” [37].

The electromagnetic force is generally observed to create structure: e.g., stable atoms and molecules, crystalline solids. In fact, the most studied consequences of the electromagnetic force

form the subject matter of Chemistry and Solid-State Physics, both disciplines developed to understand essentially static structures. Structured systems have binding energies larger than the ambient thermal energy. Placed in a sufficiently hot environment, they decompose: e.g., crystals melt, molecules disassociate. At temperatures near or exceeding atomic ionization energies, atoms similarly decompose into negatively charged electrons and positively charged ions. These charged particles are by no means free: in fact, they are strongly affected by each other's electromagnetic fields. Nevertheless, because the charges are no longer bound, their assemblage becomes capable of collective motions [38] of great vigor and complexity. Such an assemblage is termed a plasma [39].

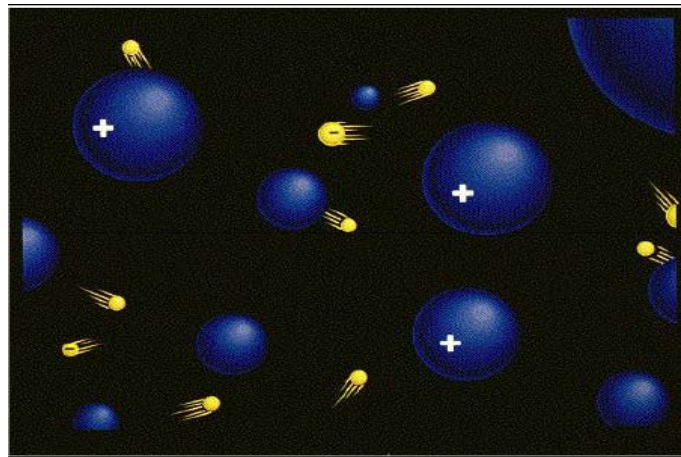


Figure 1: Free ions and electrons in plasma. (From: Chen F. F. and Chang J. P., *Lecture Notes on principles of plasma processing*, Plenum/Kluwer Publishers, (2002).)

A plasma is a hot gas consisting of charged and neutral particles which exhibit collective behaviour [40]. Plasma is matter heated beyond its gaseous state, heated to a temperature so high that atoms are stripped of at least one electron in their outer shells, so that what remains are positive ions in a sea of free electrons. The plasma is often referred to as the fourth state of matter (solid- liquid- gas- plasma) [41]. This concept arises from a thermodynamic description but is not completely rigorous. Ordinary fluids are in thermal equilibrium, meaning that the atoms or molecules have a Maxwellian (Gaussian) velocity distribution. The parameter T , the temperature, determines the width of the distribution. In a plasma, the different species—ions, electrons, and neutrals may have different temperatures: T_i , T_e , and T_n . These three (or more, if there are different kinds of ions or atoms) interpenetrating fluids (even in the case of quantum plasmas [42]) can move through one another, but they may not collide often enough to equalize

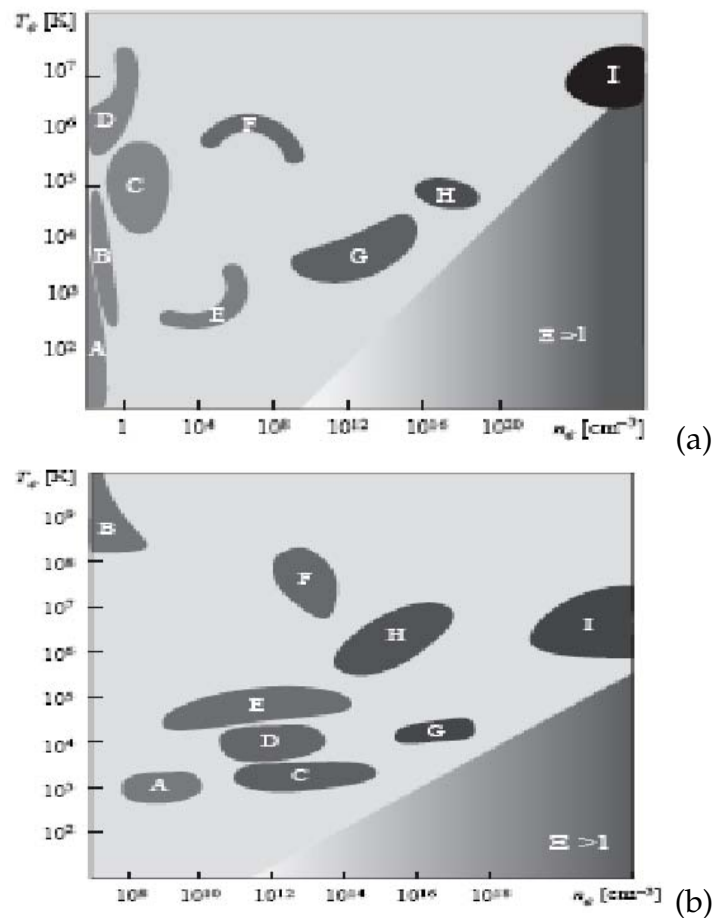


Figure 2: (a) Natural plasmas: A-stellar space, B-Interplanetary space, C-Solar wind, D-Magnetosphere, E-Ionosphere, F-Solar corona, G-Stellar atmosphere, H-Lightning, I-Stellar interior; and (b) industrial plasmas: A-Flames, B-Intense bundles, C-MHD generators, D-Industrial reactors, E-Laser lamps, F-Tokamaks, G-sparks, H-Pinch and mirrors, I-Laser/plasma interaction. (From: Rax J.-M., *Physique des plasmas, Cours et applications*, Dunod, Paris, (2005), page 4)

the temperatures, because the densities are usually much lower than for a gas at atmospheric pressure. However, each species usually collides with itself often enough to have a Maxwellian distribution. The two-fluid model of plasma physics describes the electrons and ions as conducting fluids that are coupled through momentum transfer collisions and Maxwell's equations [43]. Very hot plasmas may be non-Maxwellian and would have to be treated by kinetic theory. The variation of the basic macroscopic physical quantities like density n and temperature T determines the properties of the matter in the plasma state (see Fig. 1). However, the transition from the liquid, gaseous or solid state into the plasma state is not abrupt but continuous. In a gas, for example, more and more of the atoms become ionized with rising temperature and a plasma forms [44].

Langmuir, along with his colleague Lewi Tonks, was investigating the physics and chemistry of tungsten-filament light bulbs, with a view to finding a way to greatly extend the lifetime of the filament (a goal which he eventually achieved). In the process, he developed the theory of plasma sheaths; the boundary layers which form between ionized plasmas and solid surfaces. He also discovered that certain regions of a plasma discharge tube exhibit periodic variations of the electron density, which we nowadays term Langmuir waves. This was the genesis of plasma physics [39].

I.1.2 Plasma parameters

An appropriate way to characterize the plasma is by the Coulomb correlation parameter, Γ defined as follows (in SI units):

$$\Gamma = \frac{q^2}{4\pi\epsilon_0 k_B T a_{WS}} \quad (1)$$

where a_{WS} is the Wigner-Seitz radius defined by $(4\pi/3) n a_{WS}^3 = 1$, n is the particle density, and k_B is Boltzmann's constant. The correlation parameter is simply the ratio of the electrostatic energy of neighboring charges to the thermal energy $k_B T$. It alone determines the thermodynamic equilibrium properties of plasmas in a harmonic trap. The values of Γ encountered in practice range from weakly correlated systems $\Gamma \ll 1$ where the particles execute independent motions, to highly correlated $\Gamma \gg 1$ systems whose dynamics present a many-body problem more akin to condensed matter. More generally, values of $\Gamma > 1$ indicate "strong coupling" with significant correlation between the dynamical variables of the particles, which is manifested as collective behavior.

The basic parameter characterizing collective phenomena in a non-magnetized plasma is the Debye length, it is the natural length scale (or Debye radius, the distance that an electron has to move to screen the plasma from radiation.), and it is defined by

$$\lambda_D = \sqrt{\epsilon_0 k_B T_e / n_e e^2} \quad (2)$$

which is normally very small, and the plasma, or Langmuir frequency

$$\omega_p = \sqrt{n_e e^2 / \epsilon_0 m_e}. \quad (3)$$

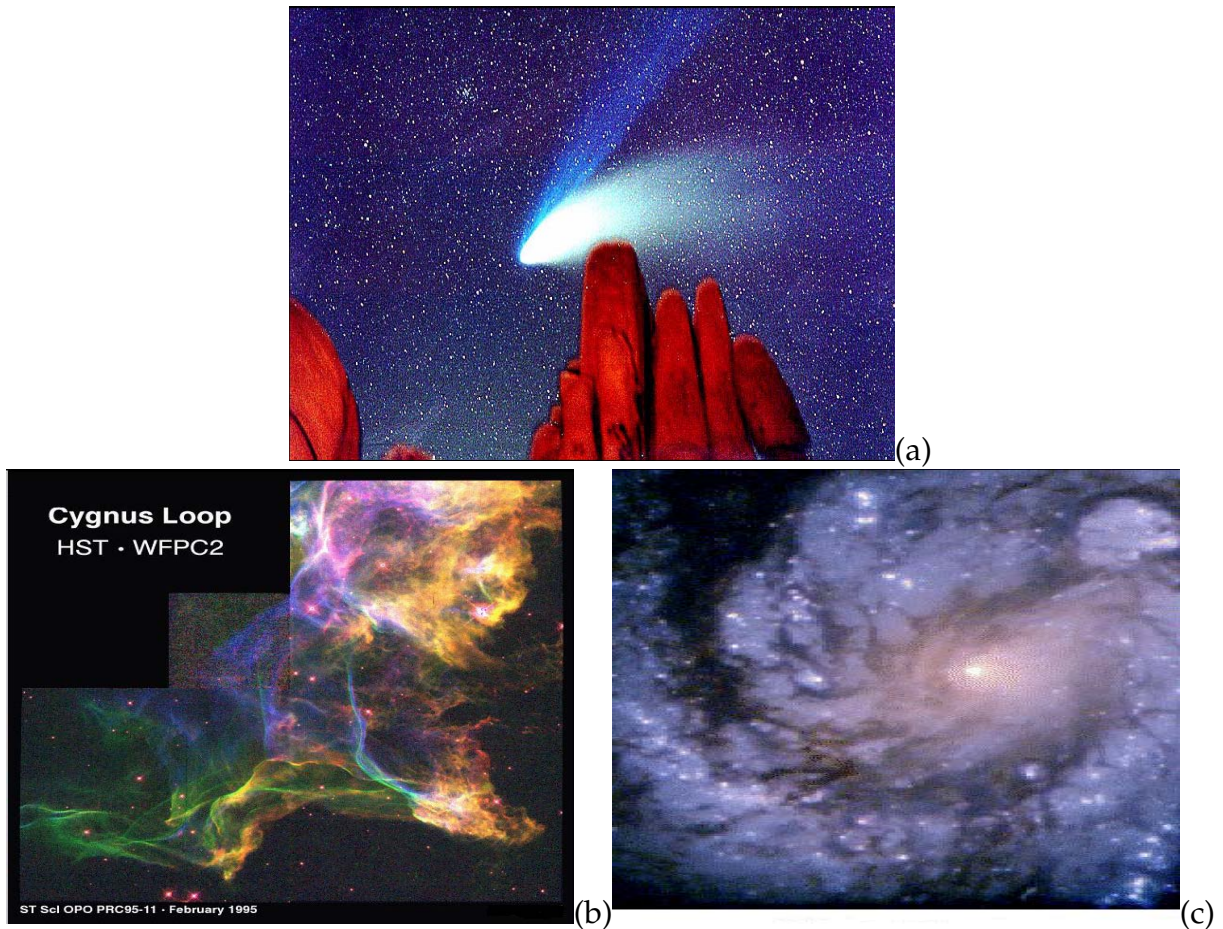


Figure 3: Examples of plasmas presents in nature: (a) A comet sketching, (b) A gaseous nebulae, (c) A galaxie. (From: Chen F. F. and Chang J. P., *Lecture Notes on principles of plasma processing*, Plenum/Kluwer Publishers, (2002), pages 1 and 2)

Here, n_e is the density, T_e is the temperature, e is the charge and m_e is the mass, all of the electrons, while k is Boltzmann's constant and ϵ_0 is the permittivity of free space. The product of λ_D and ω_p equals the electron thermal velocity.

I.1.3 Plasmas in nature and in laboratory

It is well known now that 99% of the matter in the universe is in the plasma state [45]. Plasma can be found in the interior of the stars as well as in the interstellar space and in the core of the planets. Plasma also occurs in gas discharges ("neon light", lightning) as part of our daily live. Examples include astrophysical plasmas such as in dilute interstellar gas clouds or the highly energetic and dense matter in the strongly compressed interior of stars or giant gas planets like Jupiter (see Fig.3). On earth, examples includes hot plasma ions in the magnetosphere surrounding our planet, the aurora borealis, lightning bolts, or the plasma of a candle flame. Besides these

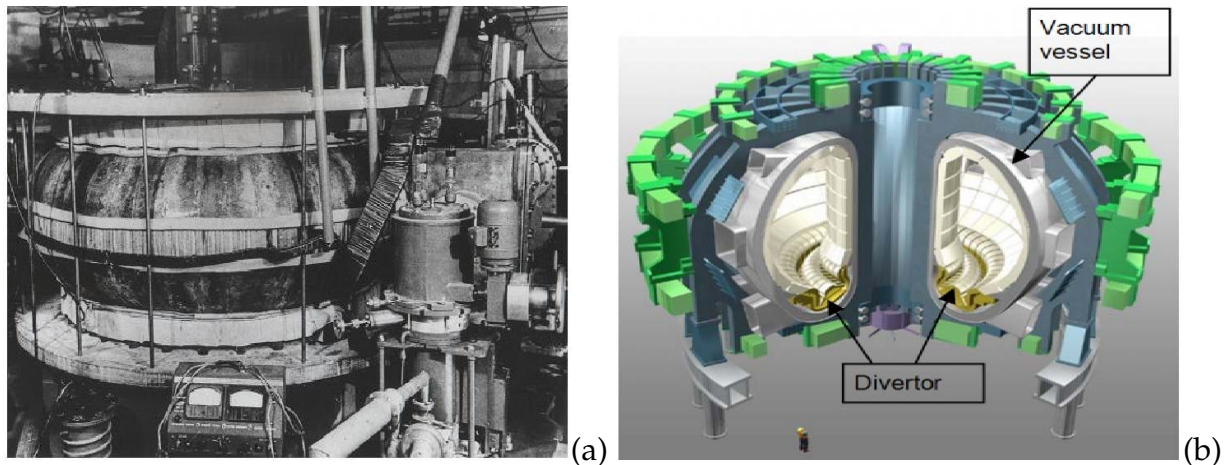


Figure 4: Tokamaks: (a) T1 the first (From: <http://alltheworldstokamaks.wordpress.com/gallery-of-external-views/>) and (b) Cut-away of ITER (From: Ariola M., Pironti A., *Magnetic Control of Tokamak Plasmas*, Springer, London, (2008), page 11), (the most recent) showing the vacuum vessel, coils and divertor region. Iter wil have a plasma volume of 840 m^3 .

natural plasmas, plasmas find technological application in many modern industrial processes, in plasma chemistry, in nanoparticle sources and a variety of surface processing technologies for the treatment of metals, optical components, and plastic materials (functionalization, sterilization, etc.).

Furthermore, they are widely used in the field of nanotechnologies which includes plasma-assisted deposition or etching in the semiconductor industry. Plasmas play a central role in the development of improved light sources, display technology, lasers, and solar cells. Also, promising medical applications on living tissues are already emerging. Other novel fields of plasma research are laser-produced plasmas, particle acceleration in plasma wake fields, the generation of ultra-dense plasmas (so-called warm dense matter) by focusing of intense laser beams on small targets, as well as energy research in large-scale nuclear fusion experiments such as ITER in France or the National Ignition Facility in the US [46].

I.2 Plasmas and particles

I.2.1 Plasma processing

After Langmuir, plasma research gradually spread in other directions, of which four are particularly significant.

Firstly, the development of radio broadcasting led to the discovery of the Earth's ionosphere,

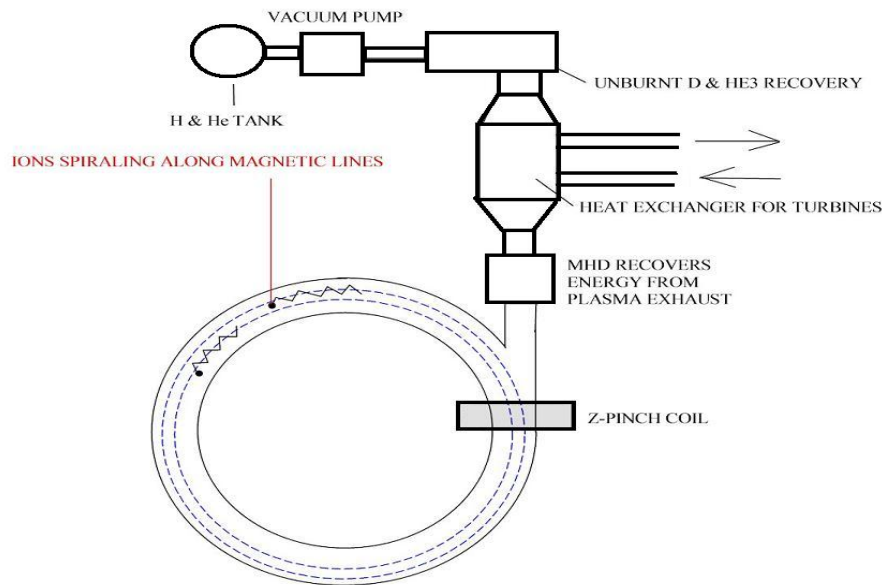


Figure 5: Use of tokamaks as energy provider.

a layer of partially ionized gas in the upper atmosphere which reflects and occasionally absorbs and distorts radio waves, and is responsible for the fact that radio signals can be received when the transmitter is over the horizon. For instance, this can give rise to "ghost signals"¹. In order to understand, and possibly correct, some of the deficiencies in radio communication, various scientists, such as E.V. Appleton and K.G. Budden, systematically developed the theory of electromagnetic wave propagation through a non-uniform, magnetized plasma.

Secondly, astrophysicists quickly recognized that much of the universe consists of plasma, and, thus, that a better understanding of astrophysical phenomena requires a better grasp of plasma physics. The pioneer in this field was Hannes Alfvén, who around 1940 developed the theory of magnetohydrodynamics, or MHD, in which plasma is treated essentially as a conducting fluid. Space scientists borrowed the theory of plasma trapping by a magnetic field from fusion research, the theory of plasma waves from ionospheric physics, and the notion of magnetic reconnection as a mechanism for energy release and particle acceleration from astrophysics. When astrophysics and nuclear physics pointed towards the conversion of nuclear binding energy into heat, the thought immediately arose that this 'latent power' could be controlled for the well-being of the human race-or for its suicide [47].

Thirdly, high-temperature plasmas have been studied for decades in connection with con-

¹i.e., signals which arrive a little before, or a little after, the main signal

trolled fusion; that is, the production of electric power by creating miniature suns on the earth. The creation of the hydrogen bomb in 1952 generated a great deal of interest in controlled thermonuclear fusion as a possible power source for the future. Before 1958 where thermonuclear fusion research was declassified, this research was carried out secretly, and independently, by the United States, the Soviet Union, and Great Britain. Theoretical plasma physics first emerged as a mathematically rigorous discipline in these years. Not surprisingly, Fusion physicists are mostly concerned with understanding how a thermonuclear plasma can be trapped, in most cases by a magnetic field, and investigating the many plasma instabilities which may allow it to escape.

Finally, the development of high powered lasers in the 1960's opened up the field of laser plasma physics. When a high powered laser beam strikes a solid target, material is immediately ablated, and a plasma forms at the boundary between the beam and the target. A major application of laser plasma physics is the approach to fusion energy known as inertial confinement fusion. In this approach, tightly focused laser beams are used to implode a small solid target until the densities and temperatures characteristic of nuclear fusion (i.e., the centre of a hydrogen bomb) are achieved. Another interesting application of laser plasma physics [48] is the use of the extremely strong electric fields generated when a high intensity laser pulse passes through a plasma to accelerate particles. High-energy physicists hope to use plasma acceleration techniques to dramatically reduce the size and cost of particle accelerators.

Why study plasma processing? Because we can't get along without computer chips and mobile phones these days. About half the steps in making a semiconductor circuit require a plasma, and plasma machines account for most of the equipment cost in a "fab". Designers, engineers, and technicians need to know how a plasma behaves [49]. These machines have to be absolutely reliable, because many millions of transistors have to be etched properly on each chip. It is amazing that this can be done at all; improvements will certainly require more plasma expertise. Chemically reactive plasma discharges are widely used to modify the surface properties of materials. Plasma processing technology is vitally important to several of the largest manufacturing industries in the world. Plasma-based surface processes are indispensable for manufacturing the very large scale integrated circuits (ICs) used by the electronics industry. Such processes are also critical for the aerospace, automotive, steel, biomedical, and toxic waste management industries [50]. The low-temperature plasmas used in manufacturing are more complicated because they are not fully ionized; there are neutral atoms and many collisions [51].

1.2.2 Particles heating

Let give more detail on the ionization process. Not all the atoms have to be ionized: the cooler plasmas used in plasma processing are only 1 – 10% ionized, with the rest of the gas remaining as neutral atoms or molecules. At higher temperatures, such as those in nuclear fusion research, plasmas become fully ionized, meaning that all the particles are charged, not that the nuclei have been stripped of all their electrons [52]. Before the atoms become ionized, the electrons could stay bound to their nuclei but in excited states. These have a higher energy than the original ground state. The electrons later decay from these excited states accompanied by the emission of radiation in the visible part of the spectrum. This happens, for example, in auroras where the atoms high up in the atmosphere become excited by electrons, which enter from the solar wind and become trapped by the Earth's magnetic field in the polar region. The decay of the excited atoms may subsequently generate beautiful luminous curtains of auroral radiation.

The next generation of large machines is being designed for auxiliary heating and current drive systems: Neutral Beam Injection (NBI), Ion Cyclotron Resonance Heating (ICRH), Electron Cyclotron Resonance Heating (ECRH) [53] and Lower Hybrid (LH). Since none of these systems can fulfil all the operational requirements one attempts to increase the flexibility by using combinations of auxiliary systems in order to study different scenarios for optimizing performance.

The use of external heating has a tendency to lead to a degradation of plasma confinement. It has been found that such effects are extremely sensitive to the plasma conditions near the plasma external boundary. Detailed studies of related phenomena led to the discovery of a new mode, the so-called H-mode (high mode) of operation, in the ASDEX machine (Garching) which was later confirmed in other machines. Experiments with the H-mode, which was associated with steep gradients near the boundary, showed that heating could be obtained without degradation of the confinement. In fact, the H-mode could typically have twice the confinement time of that with L-mode (low-mode) operation. This discovery may be seen as an example of how important improvements and new openings in science often come in steps. One reason for building larger and larger tokamaks is that the confinement time crudely depends on the tokamak minor radius, and the diffusion coefficient as a relation which applies for energy as well as for particles and indicates that larger machines should provide better confinement. For practical and economic reasons one might, however, envisage other lines of development using stronger magnetic fields leading to higher densities n in more compact machines. One might even for such

devices eliminate or reduce the external heating, using essentially ohmic heating produced by the plasma itself.

I.2.3 Plasma classification

Astrophysical and laboratory plasmas

There are a variety of astrophysical plasmas in nature. The interior of the sun and the stars consists of a very dense and very hot plasma where light atomic nuclei fuse to heavier ones and release the excess of binding energy according to Einstein's famous formula $E = MC^2$. The sun emits an extremely dilute supersonic plasma, the solar wind, into its planet system. By interaction with the electromagnetic radiation from the sun the atoms of the upper atmosphere become partly ionized. We call this plasma which expands from about $60km$ to $2000km$ altitude the ionosphere [44].

A completely other type of plasmas are the degenerate plasmas within white dwarfs or neutron stars showing extremely high densities and thus behaving differently from the typical ideal plasmas we know from the majority of the Laboratory plasmas. Since the plasma may carry an electric current, plasma discharges of various types are investigated in fundamental research and applied in industry. Low-pressure discharges like glow discharges carry small currents with cold electrodes. They serve for lightening, for gas lasers like the CO_2 laser or the $HeNe$ laser, and for the wide-spread applications of plasma etching and deposition. High-pressure discharges like arcs may carry larger currents and thereby attain higher temperature. They may also serve for lightening like the well-known high-pressure mercury lamp, for switches, and for plasma-material processing like melting, cutting, and welding. In order to gain fusion energy in laboratories, high-temperature plasma physics has been started as a classified project as mentioned before, around 1950.

The fundamental measure of a magnetic field's effect on a plasma is the magnetization parameter δ_{mag} . The fundamental measure of the inverse effect is called β , and is defined to be the ratio of the thermal energy density nT to the magnetic energy density $B^2/2\mu_0$. It is conventional to identify the plasma energy density with the pressure, and then $\beta = 2\mu_0 P/B^2$. Although scale-independence of the magneto hydro dynamic (MHD) equations permits analysis of global plasma dynamics in laboratory and astrophysical plasmas by the same techniques, the important differences of the parameters that govern overall force balance should not be neglected. For ex-

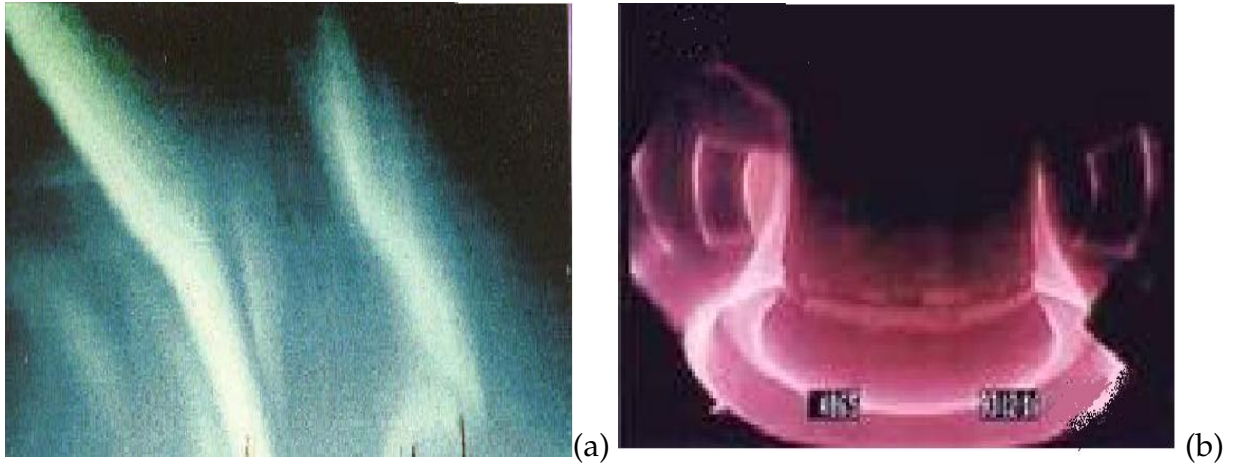


Figure 6: (a) aurora borealis ((From: Chen F. F. and Chang J. P., *Lecture Notes on principles of plasma processing*, Plenum/Kluwer Publishers, (2002), pages 1 and 2)), (b) Tokamak

ample, the parameter β ($J \wedge B = \nabla P \sim \beta \ll 1$), where J is the ion current, B the magnetic field and P the pressure, is small for tokamak plasmas and usually large for astrophysical plasmas, so that plasma dynamics in tokamaks is always dominated by magnetic fields whereas this may not be the case for astrophysical plasmas [54]. Hence, MHD instabilities occur in astrophysical plasmas under conditions that do not allow instability in laboratory plasmas.

Ideal neutral and quasi-neutral plasmas

An idealized plasma consist of an equal number of electrons, with mass m_e and charge $-e$ (here, e denotes the magnitude of the electron charge), and ions, with mass m_i and charge $+e$. Quasi-neutrality demands that $n_e \simeq n_i$.

Plasmas could be considered as charged fluids which obey Maxwell's equations, but in a complex way. One of Maxwell's equations is Poisson's equation

$$\nabla \mathbf{D} = \nabla \epsilon_0 \mathbf{E} = e(n_i - n_e) \quad (4)$$

E can be derived from a potential V by $E = -\nabla V$. We then have $\nabla^2 V = (e/\epsilon_0)(n_i - n_e)$. By replacing ∇^2 with $1/L^2$, where L is the length over which V varies, the ratio of the potential energy $|eV|$ of an electron in the electric field to its thermal energy kT_e is then approximately

$$\left| \frac{eV}{kT_e} \right| = L^2 e^2 \frac{(n_i - n_e)}{\epsilon_0 kT_e} \quad (5)$$

Then,

$$\left| \frac{eV}{kT_e} \right| = \frac{L^2}{\lambda_D^2} \left(1 - \frac{n_i}{n_e} \right) \quad (6)$$

The left-hand side of this equation cannot be much larger than 1, because if a large potential is imposed inside the plasma, such as with a wire connected to a battery, a cloud of charge will immediately build up around the wire to shield out the potential disturbance. λ_D is of order $50\mu m$ for $kT_e = 4eV$ and $n_e = 10^{17}m^{-3}$ or $10^{11}cm^{-3}$, a value on the high side for industrial plasmas and on the low side for fusion plasmas. If we take L to be of order $10cm$, an average dimension for a laboratory plasma, the factor L^2/λ_D^2 is of order 10^8 , so that n_i must be equal to n_e within one part in 10^8 to keep the left-hand side reasonably small. In the interior of a plasma, then, the charge densities must be very nearly equal, and we may define a common density, called the plasma density n , to be either n_i or n_e [45, 46]. However, there are regions, called sheaths, where L is the order of λ_D ; there, the ratio n_i/n_e does not have to be near unity (It is what happens near the walls around a plasma and near objects, such as probes, inserted into the plasma). In the preceding development we have implicitly assumed that the ions are singly charged; if the ions have a charge Z , the condition of quasineutrality is simply $n_i = Zn_e$.

Cold and hot plasmas

Space plasmas [55] vary from very hot ($T > 30000K$) and dense plasmas at the centre of stars, corona flares and sunspots, to cold and less dense plasmas such as the aurora borealis and the ionosphere within the Earth's gravitational system. In space the chance of a collision is very low, and electrons and ions travel through space at high velocities over large distances.

Kinetic plasmas are generally described as hot plasmas since the ion temperature which is approximately equal to the electron temperature ($T_e \approx T_i$), is high although the gas is not necessarily in thermal equilibrium since the neutral atoms and molecules may be at a much lower temperature. In a kinetic plasma, the mean free path of a particle is long (i.e. the time between collisions is long and the collision frequency is low), electrons and ions tend to behave separately and their behaviour can be described in terms of individual particles in both space and time.

Fusion plasma is an example of hot plasma ($T_e \approx T_i > 10^6K$). At higher pressures (such as the plasma used in atomic fusion [56]) the effects of diffusion gradients, collisions and the fluid electromagnetic properties also affect the plasma processing process, and they may also be described as magneto plasma dynamic (MPD) (although the collision processes can be described

as kinetic) [57]. Very high energy densities are possible and kinetic plasmas are the subject of areas such as fusion research.

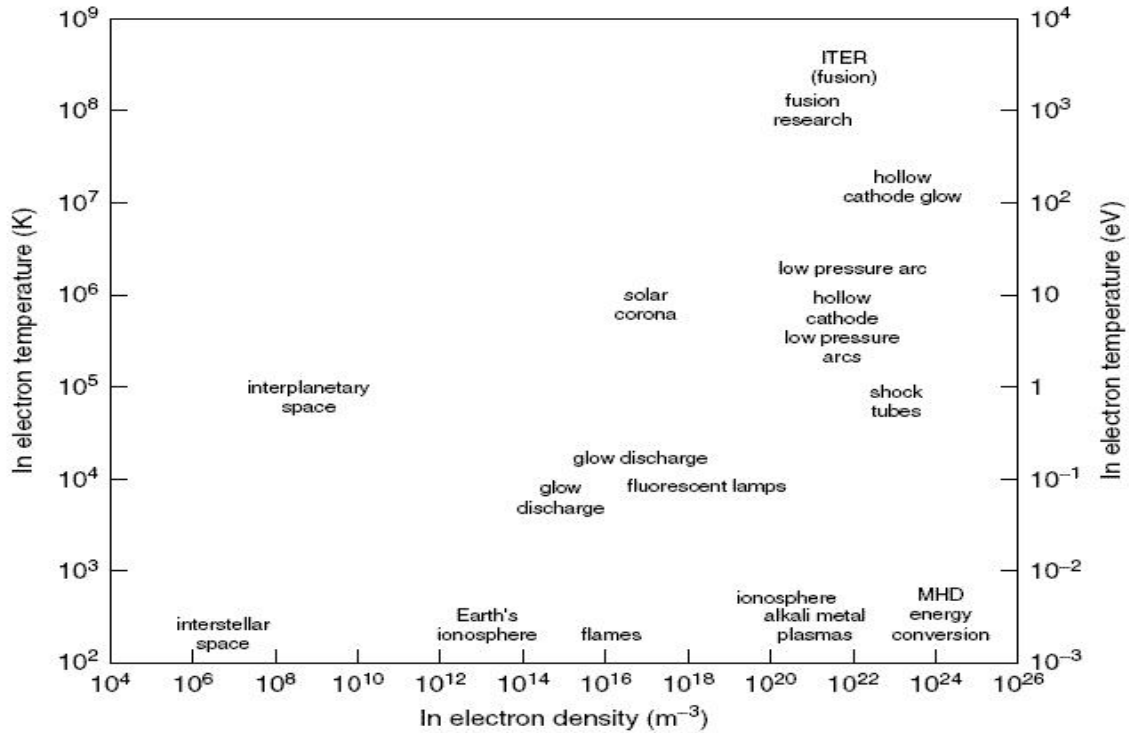


Figure 7: Plasmas as a function of temperature and density (From: Harry J. E., *Introduction to Plasma Technology Science Engineering and Applications*, Wiley-VCH, Weinheim, (2010), page 3).

Technological plasmas such as glow and arc ($T_e \approx T_i \approx 300K$, $T_i \ll T_e \ll 105K$, Low pressure $\sim 100Pa$, $1eV = 11604K$), are normally supplied with energy from electric power sources [58]. Gas pressures as low as $10^{-11}Pa$ ($7.52 \times 10^{-14}Torr$) are obtainable in the laboratory, but the use of plasmas is limited by the energy density at low pressures to about $100 \times 10^{-3}Pa$ ($0.752 \times 10^{-3}Torr$), at which the mean free path is of the order of $100mm$. Technological plasmas are often referred to as cold plasmas [59]. The behaviour is more accurately described by the behaviour of individual particles (free electrons or ions), such as those in electron and ion beams [60].

Non neutral plasmas

A nonneutral plasma is a many-body collection of charged particles in which there is not overall charge neutrality. Such systems can be characterized, depending on the charge density, by intense self electric fields. It has been known for some time that nonneutral plasmas exhibit

collective properties that are qualitatively similar to those of neutral plasmas. For example, in klystrons and traveling-wave tubes, the collective oscillations necessary for microwave generation and amplification are excited even under conditions in which the electron beams in these devices are unneutralized [61]. As is the case with neutral plasmas, the macroscopic and Vlasov descriptions of nonneutral plasmas involve the use of averaged quantities such as the mean density or the distribution function. This means that in these models the details of the motion of individual charged particles are suppressed. There is a dramatic difference between the motion of charged particles in a neutral, field-free plasma and their motion in a nonneutral plasma, which has an equilibrium electric field.

I.2.4 Principles of particle confinement

The main representatives of magnetic confinement are the mirror machine, the tokamak device and the stellarator. A short description of the technical layout and the theory of plasma confinement in these concepts will be given.

Trapping principles

The technique of using electromagnetic fields to confine and isolate atomic particles in vacuo, rather than by material walls of a container, was initially conceived by W. Paul in the form of a 3D version of the original rf quadrupole mass filter, for which he shared the 1989 Nobel Prize in physics [62]. In considering the application of electric and magnetic fields to the problem of confining charged particles in plasma, it is useful to recall some salient properties of the motion of particles in such fields, particularly inhomogeneous high frequency electric fields and crossed electric and magnetic fields. Some insight can be gained by assuming that the inhomogeneity of the electric field is so weak that the variation in the field intensity is negligible over the amplitude of the particle oscillation: the so called adiabatic condition. The motion of charged particles in crossed static electric and magnetic fields is also of interest in the trapping of particles, since a static electric field can be designed to trap particles along one axis, and a static magnetic field to trap particles in a plane perpendicular to that axis. This clearly indicates the possibility of constraining the motion of a particle in a divergent electric field by using a strong magnetic field [63].

General principles: Let consider a particle of mass m and charge q moving in a weakly inhomogeneous electric field oscillating with an angular frequency Ω . consider the motion of the particle in an electric field having a static component $E_0(x)$ and a high frequency component $E_\Omega(x, t)$ such that, although $E_\Omega(x, t)$ is not necessarily small compared with $E_0(x)$, his participation in the amplitude is assumed to be small. We then search for a solution in the form $x(t) = X(t) + \xi_p(t)$, where ξ_p is oscillatory at frequency Ω . Expanding the field in powers of ξ_b and retaining only first order terms we have for the equation of motion:

$$\frac{d^2 X}{dt^2} + \frac{d^2 \xi_p}{dt^2} = \frac{q}{m} (E_0 + \xi_p \frac{dE_0}{dx} + E_\Omega(X) \cos(\Omega t) + \xi_p \frac{dE_\Omega(X)}{dx} \cos(\Omega t)) \quad (7)$$

The solution of the oscillatory term is $\xi_p = \frac{q}{m\Omega^2} (E_\Omega(X)) \cos(\Omega t)$. Substituting this result in the equation of motion, and averaging over the oscillation period of the field, give rise to:

$$\frac{d^2 X}{dt^2} = \frac{q}{m} (E_0 - \frac{q}{m\Omega^2} \left\langle E_\Omega(X) \frac{dE_\Omega(X)}{dx} \cos(\Omega t)^2 \right\rangle) \quad (8)$$

The smooth or secular motion is then determined by an effective potential given by

$$U_{eff} = U_0 + \frac{q}{4m\Omega^2} E_\Omega(X)^2 \quad (9)$$

Clearly this can be directly generalized to three dimensions, and since the phase of the high frequency field is not involved, it is possible to establish a three dimensional effective potential well in which to trap ions. In general the required function U is a quadratic form in the cartesian coordinates x, y, z , as follows:

$$U = q\Phi_e = q \frac{\Phi_{e0}}{2d^2} (Ax^2 + By^2 + Cz^2) \quad (10)$$

where Φ_e is the electrostatic field acting on an ion of charge q . In order to satisfy Laplace's equation ($\Delta\Phi_e = 0$), we should have $A + B + C = 0$. For the interesting case of rotational symmetry around the z -axis, this could leads to $A = B = 1$ and $C = -2$, giving us the quadrupolar form

$$U = q\Phi_e = q \frac{\Phi_{e0}}{2d^2} (x^2 + y^2 - 2z^2) = q \frac{\Phi_{e0}}{2d^2} (r^2 - 2z^2) \quad (11)$$

The choice $A = B, C = -2B$ leads to the axisymmetric three-dimensional trap.

Paul traps and Penning traps: Three-dimensional confinement of charged particles requires a potential energy minimum at some region in space, in order that the corresponding force is directed toward that region in all three dimensions. From the difference in signs between the radial and axial terms In Eq.(11), the potential has a saddle point at the origin, having a minimum along one coordinate but a maximum along the other [63]. Earnshaw's theorem [64] states that it is not possible to generate a minimum of the electrostatic potential in free space. Nevertheless, it is possible to circumvent Earnshaw's theorem by superimposing a magnetic field along the z -axis to create what is called the Penning trap or to use a time-dependent electric field (an electric quadrupole field alternating at high frequency), leading to the Paul trap [65].

Magnetic and inertial confinement of plasma

Since high temperatures preclude confinement by material walls a new method of confinement was needed in fusion plasmas. The tokamak [66], sterellator and inietal confinement machines offers such a method . As discussed before, plasmas can be confined by magnetic fields, but in linear configurations the end losses are by far too large to reach the necessary energy confinement time t_c of the order of some seconds. These end losses can be completely avoided in a toroidal system, but in a simple toroidal system with purely toroidal magnetic field, the magnetic field curvature and gradient result in a vertical drift which is in opposite directions for ions and electrons. The resulting electric field causes an outward $E \wedge B$ drift of the whole plasma, and therefore render the magnetic field configuration unstable. To avoid this charge separation, it is necessary to twist the magnetic field lines by additional magnetic field components. Then, single field lines map out so-called flux surfaces. On these flux surfaces, plasma transport is fast, as it is always parallel to B , and therefore plasma parameters usually are constant on a given flux surface. Perpendicular to the flux surfaces, transport is hindered because particle motion perpendicular to B is restricted by the Lorentz force, and therefore plasma parameters can vary strongly in this direction. Two different principles for twisting the magnetic field lines have been invented in the 50s, and are under investigation worldwide.

The stellarator was invented in 1951 by Lyman Spitzer, Jr. in Princeton. In a stellarator the twist of the field lines is created by external coils [67], wound around the plasma torus, it could have different configurations [68]; an example is shown in Figs. 8(a), (b). Due to these external currents the plasma shape is not circular, but shows some indentation. In this case, with f-our

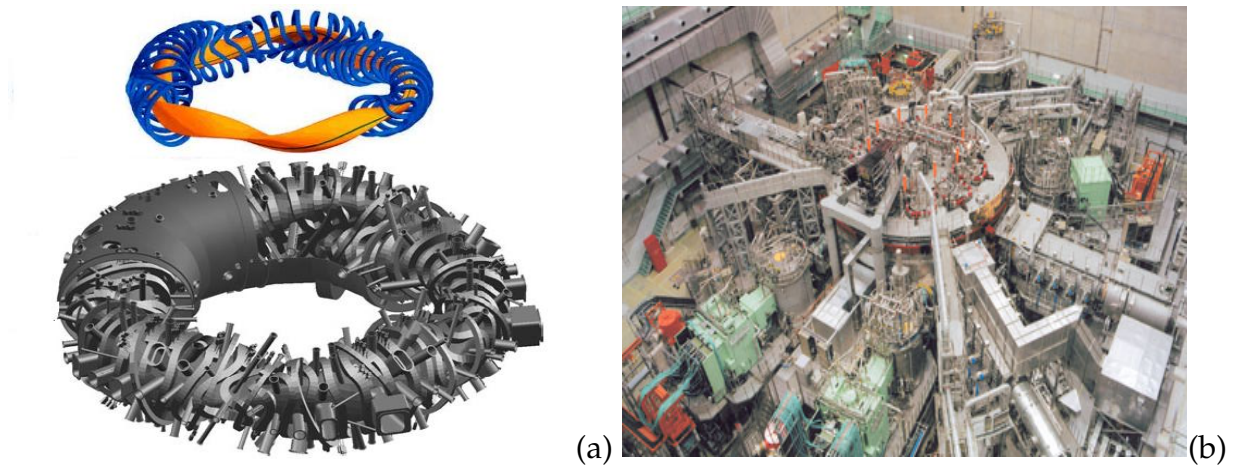


Figure 8: (a) Stellarator configuration (From: Piel A., Plasma Physics, An Introduction to Laboratory, Space, and Fusion Plasmas, Springer, New York, (2010), page 21) and (b) The Large Helical Device (LHD) at the National Institute for Fusion Science in Toki, Japan is the world's largest stellarator (from the Fusion Energy Division Oak Ridge National, TN 37831-6169).

coils (neighboring coils carry opposite current), the plasma has an oval shape. These external coils have the advantage that the current can be controlled from outside, and can flow continuously, but the configuration shown in Figure 8-(b), is very difficult from the engineering point of view. Therefore such "classical" stellarators nowadays have been replaced by "modular" stellarators, where the planar toroidal coils and the helical coils have been replaced by one complex, but modular system of non-planar coils. In stellarator, the toroidal drift of particles is compensated by external helical magnetic fields. Then, there is no induced toroidal current flowing in the plasma. Unlike a tokamak, a stellarator can therefore operate continuously. The absence of plasma current also limits the possibilities for undesired instabilities.

The basic geometry of fusion reactors will be a torus (ring) for magnetically confined plasmas. A schematic cross-section of such a reactor is shown in figure . The hot plasma is surrounded by the first wall and blanket. The latter is filled with lithium to produce the tritium, and the majority of thermal energy of the plant is delivered here by neutron moderation. A shield is provided behind the blanket to stop the neutrons not captured by the blanket in order to reduce the heat and radiation loads to the cold structures of the superconducting magnets.

In order to gain energy by fusion in a similar way as the sun, specific conditions must be fulfilled [69]. For example, in the case of a deuterium–tritium plasma the triple product nTt_c , which is the product of density, temperature and confinement time, must be larger than $3.3 \times 10^{21} \text{ m}^{-3} \text{ keVs}$ in the ideal case of a clean plasma. As a side condition the temperature must

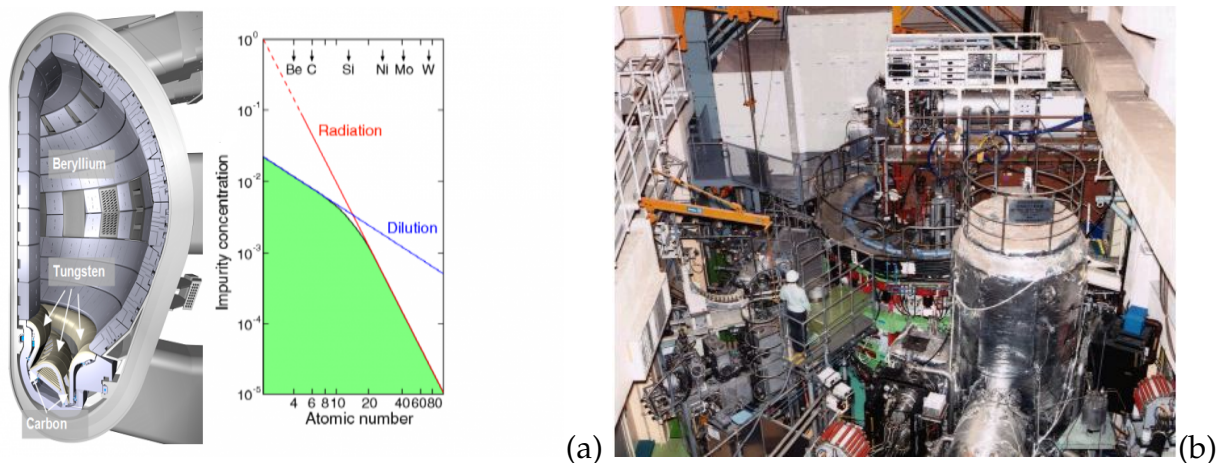


Figure 9: (a) Cut of ITER tokamak showing location of plasma facing materials and impurity concentration limit in the plasma core for different elements, and (b) JFT2M tokamak (From: <http://alltheworldstokamaks.wordpress.com/gallery-of-external-views/>).

be about $15keV$, where the maximum of the fusion output is. The goal of magnetic confinement is to reach a Lawson parameter of $nt_e > 2.2 \times 10^{20} m^{-3}s$ at a density of about $2 \times 10^{20} m^{-3}$ and a confinement time of several seconds [70].

Controlled fusion devices of Tokamaks type: importance and configuration

The second approach for confinement is the tokamak proposed by two Russian physicist, Tamm and Sakharov, in the year 1952 and realized by Artsimovich. The tokamak concept invented in the Soviet Union in the late 1950s is now the major and most promising magnetic confinement approach being pursued around the world [71]. Tokamak is an acronym developed from the Russian words TORoidalnaya KAMERA ee MAGnitaya KATUSHKA which means “toroidal chamber with magnetic coils”. As the name suggests, it is a magnetic confinement device with toroidal geometry. The largest tokamak in the world is the Joint European Torus (JET) in Culham, England. The DIII-D tokamak, is one of roughly a dozen medium-sized tokamaks around the world; other tokamak, as FTU in Italy and TCV, in Switzerland are also used. Tokamaks are nowadays the most promising devices for the development of nuclear fusion power plants. These devices could be one of the best approaches to energy generation in the long term and therefore are the subject of intensive international programmes of research, one of the most important being the ITER [72] project.

The concept of the ITER tokamak is outlined in figure(9-(a)) with

in the non-relativistic approximation.

$$m \frac{d\mathbf{v}}{dt} = q(\mathbf{E} + \mathbf{v} \wedge \mathbf{B}) \quad (14)$$

where m and q are the mass and charge of the particle, respectively, v is the particle velocity. In uniform and constant crossed fields ($\mathbf{E} \perp \mathbf{B}$), this equation is satisfied by $v = v_d$, where v_d is the drift velocity, which is independent of mass and charge. This relation reappears as the drift of a plasma in crossed electric and magnetic fields. Superimposed on this drift may be a random velocity in the form of a spiralling motion with arbitrary radius and pitch, that is with arbitrary parallel and perpendicular velocities, and with angular frequency

$$\mathbf{v}_d = \frac{(\mathbf{E} \wedge \mathbf{B})}{B^2}; \quad (15)$$

charged particle will describe a simple cyclotron gyration around the magnetic field line. When the component of the velocity parallel to the magnetic field, which is not affected by the Lorentz force, is different from zero, the trajectory of the charged particle is a helix as shown in figure (10-(b)).

In this case the particle would fall out from the ends of the magnetic field line, contrary to our desire to keep them confined. To solve this, the tokamak uses field lines bent into a torus so that there is no end. The addition of a poloidal field generated by the toroidal plasma current, produces a combined field. To initiate the discharge, hydrogen gas is puffed into the tokamak vacuum vessel and the toroidal field coil current is increased to create a steady-state magnetic field to contain the plasma when initially created. Then a large electric field is produced within the torus using the CS (ohmic heating) coils. This electric field rips apart the neutral gas atoms and produces the plasma. The plasma current in the plasma is built up by transformer action. The collisions of the ions in the plasma make the plasma resistive. It is this resistance that heats up the plasma (thus the origin of the term "ohmic heating"). When the temperature increases, the resistance decreases and the ohmic heating loses effectiveness. To significantly increase fusion reactions, the temperature must be increased to over 100 million degrees, which is six times the temperature at the centre of the sun. This heating is accomplished by particle beams (injecting energetic ions) or by radio frequency or microwaves (heating ions or electrons). Shortly after the discharge starts, additional gas is puffed into the chamber to increase the density and/or pressure

to the desired levels. In fully ionized plasmas, a homogeneous electric field causes $E \wedge B$ drift both for electrons and ions perpendicular to the electric field and no current in the direction of the electric field is generated [73].

Tokamaks which is subject to various instabilities [74] (such as magneto hydro dynamic instabilities, resistive instabilities driven by external (ideal) ballooning, electrostatic microinstabilities, some varieties of electromagnetic instabilities and others), have proved to be very successful in improving the desired fusion plasma conditions and the today's best experiments are based on the tokamak principle. A transformer can induce the plasma current only during a finite time, while, as mentioned before, a stellarator may principally run steady-state. For truly continuous tokamak operation, alternative current drive methods are being developed. Another disadvantage of the required large plasma current is the potential danger of so-called disruptions: uncontrolled very fast ($\sim 10ms$) plasma current decays which can give rise to large forces on the machine. A review on the status of tokamak research is given in [75].

I.2.5 Plasmas and technological application

Fusion for energy supply as a response to environmental problems

If man is to survive, he needs energy. Energy provides us with electricity, heat, transportation, communication, and a multitude of other things. However, most important is the fact that energy enables us to acquire food. In order to feed the vast world population of about six billion people of today and to provide for the growing number of the future, an enormous amount of energy is required. Today, we can obtain energy by burning coal and petroleum on a large scale and from the Sun, waterfalls, or windmills on a small scale. In developed countries, energy is also acquired from nuclear reactors by the burning of nuclear fuel such as uranium. But what will happen when most of the energy supplies of today become exhausted? Without an alternative solution, civilization will be destroyed (see figure 11). Moreover, the environmental damage from a coal or an oil plant is very disturbing. The pollution from these plants may also change the climate, causing irreversible damage. One coal-fired power plant produces 2000 railcars of ash per year and about 100 tons of poisonous sulfur oxides are absorbed into our atmosphere every day from this one power plant alone. Oil plants cause similar atmospheric pollution. The ocean waters of the Earth contain an effectively inexhaustible supply of deuterium. The second generation of fusion reactors will use only deuterium as the thermonuclear burning fuel. There

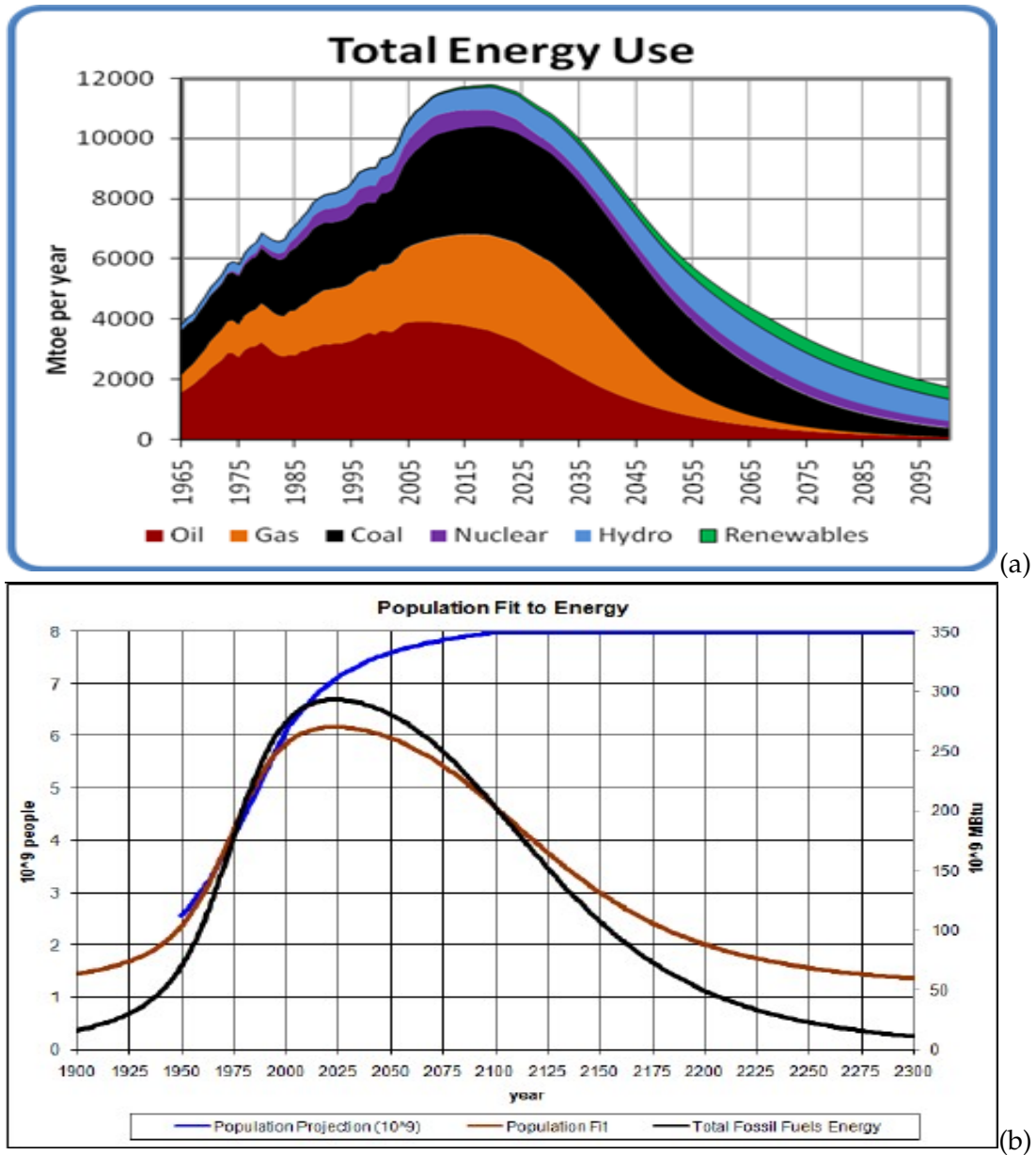


Figure 11: (a)Energy consumption (From: [http:// www.courtfool. info](http://www.courtfool.info)) and (b)population growth (From: [http:// www.roperld.com/ science/ energyfuture. htm](http://www.roperld.com/science/energyfuture.htm)) curves .

are no comparable 'ashes' and chemical pollution from either fission or fusion plants. However, whereas fission nuclear power stations have the problem of radioactive waste, fusion plants are clean reactors, both chemically and radioactively [41].

Plasmas present a new kind of matter not previously encountered and that investigation of this new field of physics is only in its first stage. Usually, most new discoveries in fundamental science have many future applications, new discoveries usually require some time to be incorporated into everyday life. But the situation with plasmas is different because the recent boom in the field not only stems from scientific discoveries but was simultaneously dictated by several problems of industry.

Material sciences

The procedure of deposition of a mono-layer complex plasma crystal on the surface of a material can be continued by depositing one surface layer after another, and each of the subsequent mono-layers can either have a different crystal structure or be composed of different types of grains. This is the way to produce a new composite material. This possibility of using complex plasma mono-layer crystals to create materials with different surface properties as well as the possibility of producing new composite materials have been discussed in literature [76]. In this context, one should notice the success of implanting in nano-tubes the fullerene molecules which can serve as valves in possible future nanohydraulic technology. All this is only provisional, and attempts have been made to initiate experiments on complex plasmas with nano-tubes or experiments for the creation of nano-hydraulics. Mono-layer magnetic crystals also await laboratory discovery and detailed investigations. Covering materials with magnetic mono-layer crystals can be of major importance for new technologies. Another possibility is related to the creation of a magnetic field by complex plasma crystals. This possibility is due to the alignment of asymmetric dust grains to the ion flow [77]. Finally, plasma phase offers an unique way for the synthesis of hard ultra materials that do not exist at the natural state as carbon nitride.

Others applications

Plasmas physics is located as upstream of a vast field of technological applications; for example, in the high technology domains like micro-electronics and spatial exploration: more of the half manufacture operations of processors and memory chips are done currently in plasmas re-

actors; and, plasmas propulsors are considered as the most applicable option for a lived mission toward Mars. Beams of electrons and ion beams at low pressures that are used in semiconductor manufacture and for welding and melting can be regarded as kinetic plasmas. Low-pressure glow discharge plasma processes are also used extensively in the manufacture of semiconductors and specifically computer memory chips.

The continuous electric discharges, found numerous applications; that it is the sparks in ignition systems, arc in steel-making industries, luminescent discharges (glow) lighting systems or the discharges so-called crowns (corona) in dépollution systems. The electric, thermal, optic and chemical properties, of these non-linear structures allowed the elaboration of reliable devices replacing the flames advantageously.

I.3 Plasma and numerical computation

The key obstacle for reaching the ignition has been the lack of fundamental understanding, and thus the limited ability to control the complex, nonlinear, and dynamical system characteristic of high temperature plasma in fusion tokamak experiments. Renewed optimism in magnetic confinement has come from recent progress marked by the strong coupling between experiment (with a construction of a data base needed for plasma processing [78]), theory, and simulation. In particular, large-scale simulations enabled by the ever increasing power of modern computers are rapidly advancing fusion energy science. Numerical simulations, in tandem with analytic theories and experimental measurements, have helped to discover fundamental physics in fusion plasmas, to understand tokamak experimental results, to guide the design and installation of advanced tokamak diagnostics, to control plasma behavior, and to optimize tokamak operation regimes [79].

Over the years, there have been numerous examples, and it is not possible to review all of them in this section. Let mention the effort to reduce the uncertainty in plasma devices; significant theoretical effort has been devoted to improve our understanding of the processes which govern the ELM [80] and $E \wedge B$ flow for example when the physics of the mean $E \wedge B$ flow becomes relatively well-established [81]. The study of turbulence driven zonal flows then become an active area of current research in both the theory and experimental communities. Codes based on the ideal magneto-hydrodynamics model of the plasma have predicted the no-wall and infinitely conducting wall β -limits for many years with some accuracy, confirmed by numerous

experiments on tokamaks. However, it is only relatively recently that we are starting to understand the full physics of the resistive wall mode. For example, theory predicts that sufficient plasma rotation can stabilize the RWM, allowing higher values of β to be achieved [82]. Experiments, notably on DIII-D confirm that provided rotation can be maintained, the RWM is indeed stabilized and values of β well above the no-wall limit can be reached [83].

I.4 Plasma instabilities

Why is it that the field of waves and instabilities has constantly attracted such great interest since the very beginning of fusion plasma research? One reason is that these phenomena may have very important consequences for the behaviour of fusion plasmas, and another is that they offer many challenging basic scientific problems.

A fusion plasma can carry a large variety of different types of wave, such as plasma waves, electromagnetic waves, ion-cyclotron waves, electron-cyclotron waves, hybrid waves, magnetoacoustic waves, magnetohydrodynamic waves (Alfvén waves) ..etc [84]. From a practical point of view certain waves are particularly important, because heating of the plasma to high temperatures by external sources can be achieved by exciting the plasma at certain frequencies which are characteristic of those particular waves. As examples low-frequency ion-cyclotron waves or high-frequency electron-cyclotron waves can be used for this purpose, the excitation frequencies being determined by the magnetic field and the masses of the particles. Instabilities of waves or other perturbations may occur as self-amplifying phenomena in plasmas. They have been investigated extensively with regard to various plasma configurations and conditions and with regard to different kinds of wave oscillation. Such instabilities show a tendency to develop when the plasma possesses some kind of free energy, which it would prefer to get rid of and transfer to wave motion. The origin of such free energy could be an inhomogeneity in the plasma density or temperature or magnetic field. Such inhomogeneities almost always exist.

Instabilities may affect the plasma configuration negatively and even spoil the confinement completely. An example of an instability which could have disastrous effects is one that could occur in a tokamak torus if the current in a plasma were to be driven by magnetic induction to such high values that the magnetic poloidal field became too strong for the plasma torus to be kept together causing it to break into wiggles. In limiting the plasma current to avoid the risk of such instabilities one also limits the heating due to plasma resistance, ohmic heating. Nonlinearities

may saturate instabilities but they can also cause or enhance instabilities [85]. Hydromagnetic instabilities of the Rayleigh–Taylor and Kelvin–Helmholtz type for example may occur in the plasma when domains of different densities meet each other. In the nonlinear regime interaction between modes may lead to turbulence, which is studied intensively using numerical simulation methods. Parametric instabilities may occur for example when a laser radiation interacts with the natural modes of oscillation of the plasma [86]. Plasma instabilities known as ELM present a significant challenge to the development of next-generation fusion reactors [87]. Flute instability, anomalous transport, and back-reaction on density profile in the Helimak can be self-consistently described by the diffusionless Lorenz-model. The model exhibits chaos and is to some extent analytically tractable. As demonstrated before chaos and turbulence are considered as troublesome features of plasma devices; a number of strategies have been developed to achieve control over this complex temporal or spatio-temporal behavior. Many of these techniques apply to plasma instabilities.

1.5 Chaos as an explanation of plasma collapse

In Plasma Physics chaos could be useful in some ways. In the laboratory of NCSR “Demokritos” the plasma chemistry method through the exploitation of chaos, has been used for the restoration and conservation of metallic archaeological objects during the last decades. The obtained experience conduct to conclude that plasma parameters and different status of treated objects are so specific, so as to become unique [88]. But chaos is generally associated with harmful behavior for confinement system.

Izrailev and Chirikov [89], discovered that the ordered motions found by Fermi, Pasta and Ulam [90] in their model [91] become chaotic above a certain stochasticity threshold. Transitions of this type were met also in the frame of plasma physics, in connection with the destruction of magnetic surfaces [92], and also with the chaoticity thus induced on single particle motions [93]. The relaxation time from order to chaos can be very long, as occurs for example with glasses and with the FPU model, and was recently pointed out also in connection with orbital magnetization [94].

Plasma in a magnetic field, conceived microscopically as a system of point charges, can exist in a magnetized state, and thus remain confined, in as much as it is in an ordered state of motion, with the charged particles performing gyrational motions transverse to the field. The

phenomenon of destruction of magnetic surfaces was considered to play a role in explaining the breakdown occurring at the density limit. However, such considerations did not prove sufficient to explain the quick collapses of plasmas. The above ordered motions induced by the external magnetic field, persist indefinitely in the unperturbed case, when one neglects the perturbation due to the so called microfield, i.e., the microscopic electric field acting on each charge and due to the Coulomb interactions with all the other ones². In microscopic terms, each electron is equivalent to a magnetic moment, just in virtue of its dynamical property of performing gyration motions transverse to the field lines, this is the kind of analogous ordered motions we are referring to. The perturbations caused by the fluctuations of the microfield³ introduce a chaoticization, until a stochasticity limit⁴ is attained, beyond which ordered motions are lost, together with magnetic pressure and confinement. Such a theoretical density limit⁵, is found to fit pretty well the empirical data for collapses of fusion machines.

Experiment exhibiting period doubling and chaos in a plasma was made by Jain et al. [97], they observed an instability occurring in rather unusual conditions. The frequency of about 10 kHz was below that of most instabilities except drift waves, but was above the argon-ion cyclotron frequency. The magnetic field was sufficient to constrain the electrons but not the ions. The dependence of the occurring of self-oscillations and its period-doubling route to chaos on many input parameters vary from system to system [98]. The self-oscillations in undriven [99] without external ac driver and driven [100] plasma systems are observed in many parallel-plate thermionic with an electron beam injected from the cathode discharges, electron-cyclotron-resonance plasma discharge [101], and rf plasmas [102]. Once excited, these self-oscillations follow one of the standard routes to chaos via period-doubling, intermittency, or quasiperiodic oscillation. As another example, a plasma-filled diode can be used as a model for the interaction space in a virtual cathode oscillator (VCO) (vircator). It is shown that depending on the separation of the electrodes, the initial ion/electron ratio, and the load, the system may exhibit a cascade of bifurcations leading to chaos. The positioning and extent of chaos can be controlled by a judicious choice of the above parameters [103]. Chaotic behavior caused by the ion-ion instability was observed by Matsukuma et al. [104]. An experimental observations of deterministic chaos in a steady-state plasma which is not driven by any extra periodic forces was made by Qin

²see [95]

³which increase as the density

⁴and so a density limit

⁵see [96]

et al. [105]. Two routes to chaos have been found, period-doubling and intermittent chaos. The fine structures in chaos such as periodic windows and bifurcations in windows have also been observed [106]. A transition scenario from stability to drift wave turbulence was experimentally investigated in a magnetized low- β plasma with cylindrical geometry. It was demonstrated that the temporal dynamics is determined by the interaction and destabilization of spatiotemporal patterns, in particular, traveling waves. The bifurcations sequence towards weakly developed turbulence follows the Ruelle-Takens scenario [107]. Some investigation have shown the role of noise on the plasma dynamics [108].

1.5.1 Motivation

To summarize the highlights of this chapter, we can say that the understanding of matter, the development of electricity, and the unveiling of the structure of the atom have led to the discovery of a new state of matter, giving rise to many challenges. Some of them could be used as motivation for this study.

(i)-When heating the plasma with a sinusoidally oscillating voltage, the sheath oscillate; the heating is enhanced when the sheaths are oscillated. There is a good quantitative agreement with a resonant particle heating theory in the measured rates [109]. In the usual resonance method, the oscillations of particles are excited by adding a low frequency voltage of small amplitude to the rf voltage. The voltage modulation can be a sine or a square wave. **This additional voltage leads to a periodic change of the sheath width which “shakes” the potential well of the particles, thus leading to the excitation of the oscillations of the entire plasma. This sheath disturbance in the width, could then give rise to an oscillation of the particles density, thus the parametrization of the density potential [110].**

When the plasma is excited by a probe wire inserted in the plasma sheath, this results in a number of horizontal and vertical type of oscillations and waves. Anharmonic effects due to distortion of the potential well by variation of the particles charge in the sheath can't be neglected if the electrode modulation voltages used in the experiment is not small. It is also found that the particles in the plasma sheath excited by a biased wire show parametric resonances, when using a simplified analysis, that is based on the reasonable assumption that the probe bias affects the sheath width, at least in the vicinity of the wire. **A change in the sheath width or in the particles charge results in a periodic modulation of the potential well and its resonance frequency;**

which show that the wire itself strongly distorts the plasma trap [111].

The sheath instability discussed below could appear also to be due to the nonlinear dependence of the total electron current in the sheath on the plasma potential. The electron current at the wall with second electron energy is

$$J_e = -e(\Gamma_1 - \Gamma_2) \quad (16)$$

where $\Gamma_{1,2}$ are the primary and the secondary electron current. **If for some reason, the secondary electron flux decreases faster than the primary flux, then the wall will continue to charge negatively and the sheath becomes unstable [112]. Based on all the above arguments we could conclude that there is a coupling between the sheath instability and a potential parametrization, with an incidence on plasma confinement [113].**

(ii)-The various dynamical regimes of collisional drift waves in a magnetized plasma column are related with strong modulations of the ion and electron density. **Using a control parameter of the dynamics, could give rise to: regular, chaotic and turbulent regimes. The obtained turbulent regime could be controlled [114].**

A dynamical scenario could reflect a situation of chaotic regime that is close to the well-developed turbulent regimes found in plasmas, where one expects a huge number of modes to become actively involved in the dynamics. Also, the intermittency phenomenon is characterized by a strong departure from noisy Gaussian behavior related to turbulence. **The serious role of turbulence in fusion-oriented plasmas creates a special interest in controlling chaos. The transition from spontaneous regular regimes to chaotic and turbulent regimes could be obtained by changing the plasma parameters.** Magnetized bounded plasmas are subjected to a class of low-frequency electrostatic instabilities, the drift waves, caused by the $E \wedge B$ motion of particles in the presence of electric field fluctuations and gradients in the background plasma parameters. **Drift waves can be responsible for anomalous transport in magnetically confined high-temperature plasmas. Therefore, controlling these instabilities is of great interest [115].**

Zonal flows could be nonlinearly generated by a finite amplitude monochromatic drift wave [116]. Zonal flows and transient dynamics of the L-H transition recent studies revealed a crucial role of self-generated zonal flows in regulating turbulence [117].

The onset of intermittent chaos leads to chaotic saddles and unstable periodic orbits. Nonattracting chaotic solutions, known as chaotic saddles, play an important role in the transition from

weak chaos to strong chaos via an interior crisis; unstable chaotic saddles can interact to produce the plasma intermittency observed in the strongly chaotic regimes [28].

Plasma has an intrinsic property: structural formation through interaction with the electromagnetic field, generally explained by bifurcation of electric field. The mutual interaction between many particles is an essential aspect of plasmas. Collective effects must be taken into account [118]. **In many magnetically confined fusion experiments, plasmas may undergo a spontaneous transition to a turbulence suppressed regime, which is known as the before mentioned L-H transition [119].** It is then possible to modify the global confinement and edge plasma parameters with limiter biasing, illustrating the direct impact of radial electric fields on confinement properties [120].

I.6 Fundamental statement of the thesis

The preceding description of various motivating phenomena occurring in plasma give rise to many theoretical challenges. In this thesis we propose some axes of investigation, in order to better understand plasma systems and theoretical insight on chaos management:

- Aim 1: Build and explore the dynamics of plasma with a minimal set of model (two fluid model) equations built in order to explain the possible density instability and achieves a reliable density confinement.
- Aim 2: Search for the consequences of change in the sheath width, and its consequences on the appearance of chaotic motion that lead to the plasma collapse.
- Aim 3: Explore the effect of physical (bounded) noise on the density state and divert resonance phenomena, using two fluid model.
- Aim 4: Analyze the relation between noise presence and plasma collapse, using a dynamical approach, using two fluid model.
- Aim 5: Explore the effect of noise on the appearance of chaos and turbulence regarded as irregular behavior in a model of L-H transition in tokamak, in order to improve confinement.

I.7 Conclusion

We addressed a brief overview of plasma science and the nonlinear processes and different applications therein. High-temperature plasmas have been studied for decades in connection with

controlled fusion; that is, the production of electric power by creating miniature suns on the earth. About half the steps in making a semiconductor circuit require a plasma, and plasma machines account for most of the equipment cost in a fab. Designers, engineers, and technicians need to know how a plasma behaves. For many years, plasma sources were developed by trial and error, there being little understanding of how these devices worked. With the vast store of knowledge built up by the fusion effort, the situation is changing. Chapter II present the different methods and modelizations we used to give our little contribution, in other to perform this changes.

METHODOLOGY: MODELLING AND MATHEMATICAL METHODS

The previous chapter has introduced five problems: the dynamics of species in plasmas and the confinement configuration, the problem of instability in plasma density, the parametrization of confinement well due to instabilities in the sheath, the problem of noise presence in plasma devices and the role of parameters such as electric field in confinement. The above problems were described literally i.e. without any mathematical details. The aim of this chapter is to highlight on the methodology through mathematical description, and details on the numerical simulation.

Plasma can not provide quasi-neutrality of the densities and the diffusion of the fluxes in the entirety of its volume. Plasmas, are joined to wall surfaces across thin positively charged layers called sheaths. The force acting on electrons is directed into the plasma; this reflects electrons traveling toward the walls back into the plasma. Conversely, ions from the plasma that enter the sheaths are accelerated into the walls.

II.1 Modelling

The wide range of time scales and space scales present in the most general mathematical description of plasmas make meaningful numerical simulations which span these scales enormously difficult. This is the motivation for deriving and solving reduced systems of equations that purport to describe plasma phenomena over restricted ranges of time and space scales, but are more amenable to numerical solution [121].

As mentioned before, a plasma is an ensemble of particles electrons e , ions i and neutrals with different positions r and velocities v which move under the influence of external forces (electromagnetic fields, gravity) and internal collision processes (ionization, Coulomb, charge exchange etc.). However, what we observe is some “average” macroscopic plasma parameters such as J -

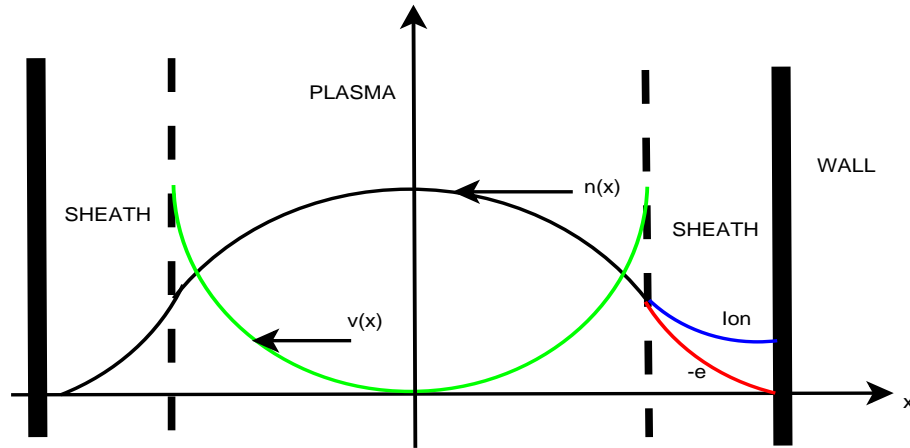


Figure 12: Plasma sheath.

current density, n_s -species density, P - pressure, T_i - ion temperature etc. These parameters are macroscopic averages over the distribution of particle velocities and/or positions. The particle velocity distribution is critical in plasma science, and can be derived from the Boltzmann transport equation. The transport properties of the electrons and the ions can be derived once their velocity distributions are determined [122]. The ultimate goal of magnetic confinement fusion research is to produce steady-state burning plasmas in a fusion power plant [123].

II.1.1 Boltzman equations for species

Let consider a single particle of species s , described by a position vector

$$\mathbf{r} = x \mathbf{i} + y \mathbf{j} + z \mathbf{k} \quad (17)$$

in the configuration space and a velocity

$$\mathbf{v} = v_x \mathbf{i} + v_y \mathbf{j} + v_z \mathbf{k} \quad (18)$$

in velocity space.

For multiple-particles systems, let introduce the distribution function $f_s(r, v, t)$ [124], which temporal evolution gives a description of the system more detailed than a fluid description, but less detailed than following the trajectory of each individual particle, for species s , defined such

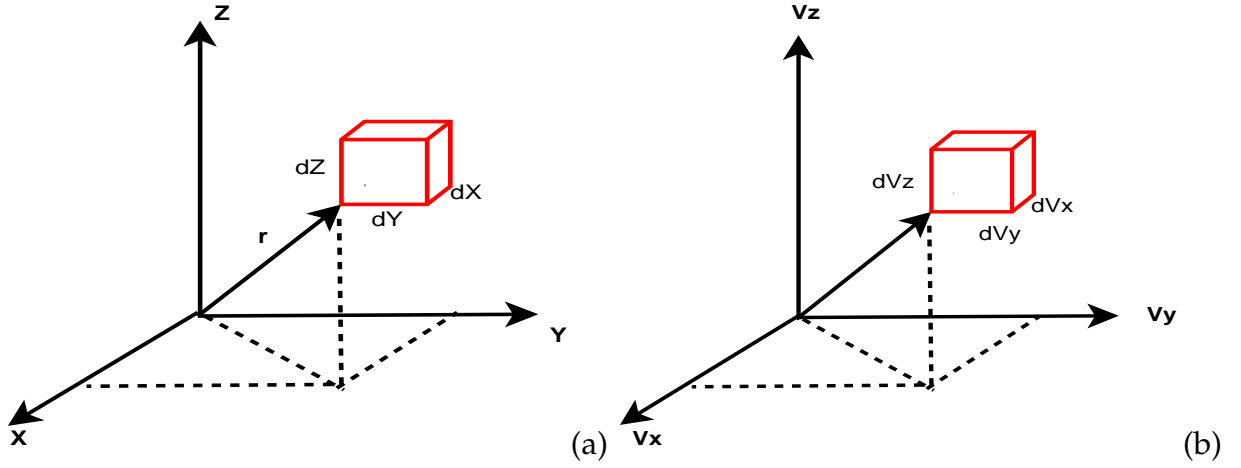


Figure 13: A configuration space volume element dr with the equivalent velocity space element. $dV = drdv$ is the volume element in (\mathbf{r}, \mathbf{v}) phase space.

that

$$f_s(\mathbf{r}, \mathbf{v}, t) drdv = dn(\mathbf{r}, \mathbf{v}, t) \quad (19)$$

is the number of particles in the element of volume $dV = drdv$ in phase space. Where $dr \equiv d^3r \equiv dx dy dz$ and $dv \equiv d^3v \equiv dv_x dv_y dv_z$. $f_s(r, v, t)$ is a positive finite function that decrease to zero as $|\mathbf{v}|$ becomes large. The element must not be so small that it doesn't contain a statistically significant number of particle, then allowing $f_s(r, v, t)$ to be approximated by a continuous function. The distribution is: (i) inhomogeneous if f_s depends on r . (ii) anisotropic if f_s depends on the direction of v . $f_s(r, v, t) drdv$ is the number of particles at time t having positions in the range between r and $r + dr$ and velocities in the range between v and $v + dv$. Using the evolution of f_s to characterize the system rather characterizes classes of particles having the same r, v .

By using the derivation given in [125], we could notice that $f_s(r, v, t)$ changes because of the flux of particles across the surface bounding the elemental volume $drdv$ in phase space. Conservation of particles requires that the rate of particle flow over the surface ds bounding the elemental volume δV_o plus those generated by collisions and source, be equal to the rate at which particle phase space density changes with time. by letting $V = (v, a)$ be the generalized velocity vector for phase space (r, v) , then the rate of flow over the surface S_v into the volume element is

$$- \int_{S_v} ds \cdot [\mathbf{V} f] \quad (20)$$

Using the divergence theorem, Eq. (20) can be rewritten as

$$- \int_{\delta V_o} d\mathbf{r} d\mathbf{v} [\nabla_{\mathbf{r}} \cdot (\mathbf{v}f) + \nabla_{\mathbf{v}} \cdot (\mathbf{a}f)] \quad (21)$$

where

$$\begin{aligned} \nabla_{\mathbf{r}} &= \mathbf{i} \frac{\partial}{\partial x} + \mathbf{j} \frac{\partial}{\partial y} + \mathbf{k} \frac{\partial}{\partial z} \\ \nabla_{\mathbf{v}} &= \mathbf{i} \frac{\partial}{\partial v_x} + \mathbf{j} \frac{\partial}{\partial v_y} + \mathbf{k} \frac{\partial}{\partial v_z} \end{aligned} \quad (22)$$

Since δV_o is an elemental volume, the integrand in Eq.(21) changes negligibly and can be removed from the integral. For plasmas, the dominant force is electromagnetic, then

$$\mathbf{a} = q_s(\mathbf{E} + \mathbf{v} \wedge \mathbf{B}) \quad (23)$$

As mentioned in [121], the most basic set of equations describing the six dimension plus time (r, v, t) phase space probability distribution function $f_s(r, v, t)$ for species s of indistinguishable charged particles (electrons or a particular species of ions) is a system of Boltzmann equations for each species:

$$\frac{\partial f_s(\mathbf{r}, \mathbf{v}, t)}{\partial t} + \mathbf{v} \cdot \nabla_{\mathbf{r}}(f_s(\mathbf{r}, \mathbf{v}, t)) + \nabla_{\mathbf{v}} \cdot \left[\frac{q_s}{m_s}(\mathbf{E} + \mathbf{v} \wedge \mathbf{B})f_s(\mathbf{r}, \mathbf{v}, t) \right] = C_s + \hat{S}_s \quad (24)$$

where m_s is the particle mass and q_s is the particle charge for species s . The collision operator $C_s = \sum_i C_{is}$ represents the effect of scattering due to collisions between particles of species s and i . External sources of particles, momentum, and energy are represented by \hat{S}_s . The electric and magnetic fields $E(r, t)$ and $B(r, t)$ are obtained by solving the free space Maxwell's equations

$$\begin{aligned} \frac{\partial \mathbf{B}}{\partial t} &= -\nabla \wedge \mathbf{E} & (a) \\ \nabla \wedge \mathbf{B} &= \frac{1}{c^2} \frac{\partial \mathbf{E}}{\partial t} + \mu_0 \mathbf{J} & (b) \\ \nabla \cdot \mathbf{E} &= \frac{1}{\epsilon_0} \rho_q & (c) \\ \nabla \cdot \mathbf{B} &= 0 & (d) \end{aligned} \quad (25)$$

here charge and current density given by the following integrals over velocity space:

$$\begin{aligned} \rho_q &= \sum_s q_s \int d^3\mathbf{v} f_s(\mathbf{r}, \mathbf{v}, t) \\ \mathbf{J} &= \sum_s q_s \int d^3\mathbf{v} \mathbf{v} f_s(\mathbf{r}, \mathbf{v}, t) \end{aligned} \quad (26)$$

where ϵ_0 and μ_0 are the permittivity and permeability of free space, and c is the speed of light.

II.1.2 Two fluid equations

In plasma fluid theory, a plasma is characterized by a few local parameters, such as the particle density, the kinetic temperature, the flow velocity, and the time evolution of which are determined by means of fluid equations. These equations are analogous to, but generally more complicated than, the equations of hydrodynamics.

We now take the moments of the entire Vlasov equation to obtain a set of partial differential equations relating the mean quantities $n_s(r, t)$, $u_s(r, t)$; where $n_s(r, t)$ is the density and $u_s(r, t)$ is the mean velocity

$$n(\mathbf{r}, \mathbf{t}) = \int f_s(\mathbf{r}, \mathbf{v}, t) d\mathbf{v} \quad ; \quad u(\mathbf{r}, \mathbf{t}) = \frac{\int \mathbf{v} f_s(\mathbf{r}, \mathbf{v}, t) d\mathbf{v}}{n(\mathbf{r}, \mathbf{t})}, \quad (27)$$

The collision-induced velocity jump occurs very fast so that if the phase-space trajectories were recorded with a “movie camera” having insufficient framing rate to catch the details of the jump the resulting movie would show particles being spontaneously created or annihilated within given volumes of phase-space. Here we really want to know is the cumulative effect of many collisions. It is therefore both efficient and sufficient to follow the trajectories on the slow time scale while accounting for the apparent “creation” or “annihilation” of particles by inserting a collision operator on the right hand side of the Vlasov equation. In the example shown here it is seen that when a particle is apparently “created” in one box, another particle must be simultaneously “annihilated” in another box at the same r coordinate but a different v coordinate. Inclusion of collisions and source term in the Vlasov equation is expressed in the form

$$\frac{\partial f_s}{\partial t} + \frac{\partial}{\partial \mathbf{r}}(\mathbf{v} f_s) + \frac{\partial}{\partial \mathbf{v}}(\mathbf{a} f_s) = \sum_k C_{sk}(f_s) + \hat{S}_s \quad (28)$$

Boltzmann’s collision operator $C_s(f_s) = \sum_k C_{sk}(f_s)$, for a neutral gas considers only binary collisions, and is, therefore, bilinear in the distribution functions of the two colliding species. C_{sk} is linear in each of its arguments. Unfortunately, such bilinearity is not strictly valid for the case of Coulomb collisions in a plasma. Because of the long range nature of the Coulomb interaction, the closest analogue to ordinary two-particle interaction is mediated by Debye shielding, an

intrinsically many-body effect. Fortunately, the departure from bilinearity is logarithmic in a weakly coupled plasma, and can, therefore, be neglected to a fairly good approximation (since a logarithm is a comparatively weakly varying function). Thus, from now on, C_{sk} is presumed to be bilinear.

We begin by integrating the Vlasov equation,

$$\int \left[\frac{\partial f_s}{\partial t} + \frac{\partial}{\partial \mathbf{r}}(\mathbf{v} f_s) + \left(\frac{q_s}{m_s} (\mathbf{E} + \mathbf{v} \wedge \mathbf{B}) \right) \cdot \frac{\partial f_s}{\partial \mathbf{v}} \right] d\mathbf{v} = \sum_k \int C_{sk}(f_s) d\mathbf{v} + S_s \quad (29)$$

Where C_{sk} is characterized by constrained sources and sinks for particles in phase-space. Because r , v , and t are independent variables, the velocity integral commutes with both the time and space derivatives on the left hand side, while the third term on the left hand side is the volume integral of a divergence in velocity space. Using Gauss's theorem ($\int_{vol} dr \nabla \cdot Q = \int_{surf} ds \cdot Q$), we obtain f_s evaluated on a surface at $v = \infty$. Because $f_s \rightarrow 0$ as $v \rightarrow \infty$, this surface integral in velocity space vanishes. For the fourth term of the left hand side of Eq. (29) we have

$$\int \left[(\mathbf{v} \wedge \mathbf{B}) \cdot \frac{\partial f_s}{\partial \mathbf{v}} \right] d\mathbf{v} = \int \frac{\partial}{\partial \mathbf{v}} \cdot (f_s \mathbf{v} \wedge \mathbf{B}) d\mathbf{v} - \int f_s \frac{\partial}{\partial \mathbf{v}} \wedge (\mathbf{v} \wedge \mathbf{B}) d\mathbf{v} = 0 \quad (30)$$

because $\left(\frac{\partial}{\partial \mathbf{v}} \right)$ is perpendicular to $(\mathbf{v} \wedge \mathbf{B})$. The first term of the right hand side of Eq. (29) vanish because collisions cannot change the number of particles (at least for warm plasmas, where recombination can be ignored). We then obtain the following species continuity equation

$$\frac{\partial n_s}{\partial t} + \nabla \cdot (n_s \mathbf{u}_s) = S_s \quad (31)$$

Where external sources of particles, momentum, and energy are represented by $S_s = \int_{vol} d^3v \hat{S}_s$. From thermodynamic arguments [126], S_i is a source term which can be due to heating of the plasma, and is, consequently, a function of density, n , electron temperature, T_e , and electric field, E , in the plasma. The species source S_i could also be caused by the pressure of large amplitude fluctuations in the plasma or by ionization. By multiplying Eq. (29) without source term by v and integrate over velocity to take the "first moment",

$$\int \mathbf{v} \left[\frac{\partial f_s}{\partial t} + \frac{\partial}{\partial \mathbf{r}}(\mathbf{v} f_s) + \frac{\partial}{\partial \mathbf{v}}(a f_s) \right] d\mathbf{v} = \sum_k \int \mathbf{v} C_{sk}(f_s) d\mathbf{v} \quad (32)$$

by letting $v = v' + u_s(r, t)$ where $v'(r, t)$ is the random part of a given velocity, $u_s(r, t)$ is the relative velocity, and using $\left(\frac{\partial \mathbf{v}}{\partial \mathbf{r}}\right)_{ij} = \delta_{ij}$, the first moment of the Vlasov equation becomes

$$n_s \frac{\partial(\mathbf{u}_s)}{\partial t} = -\frac{\partial}{\partial \mathbf{r}} \cdot \left(\int (\mathbf{v}' \mathbf{v}' + \mathbf{v}' \mathbf{u}_s + \mathbf{u}_s \mathbf{v}' + \mathbf{u}_s \mathbf{u}_s) f_s d\mathbf{v}' \right) + \frac{q_s}{m_s} \int (\mathbf{E} + \mathbf{v} \wedge \mathbf{B}) f_s d\mathbf{v}' - \frac{1}{m_s} \mathbf{R}_{sk} \quad (33)$$

where $\mathbf{u}\mathbf{u}$ is the tensor or dyadic

$$\mathbf{u}\mathbf{u} = \begin{pmatrix} u_x u_x & u_x u_y & u_x u_z \\ u_y u_x & u_y u_y & u_y u_z \\ u_z u_x & u_z u_y & u_z u_z \end{pmatrix} \quad (34)$$

and R_{sk} is the net frictional drag force due to collisions of species s with species k . Note that $R_{ss} = 0$ since a species cannot exert net drag on itself. This form for frictional drag has the following properties:

- $R_{sk} + R_{ks} = 0$ showing that the plasma cannot have a frictional drag on itself,
- Friction causes the faster species to be slowed down by the slower species,
- There is no friction between species if both have the same mean velocity.

Collisions cannot change: the total number of particles at a particular location, the total momentum of a species, or the total energy of that species.

By using $\int v' f_i dv' = 0$ we then obtain

$$m_s n_s \left[\frac{\partial u_s}{\partial t} + u_s \cdot \frac{\partial u_s}{\partial \mathbf{r}} \right] = n_s q_s (\mathbf{E} + u_s \wedge \mathbf{B}) - \frac{\partial}{\partial \mathbf{r}} \cdot \overset{\leftrightarrow}{P}_s - \mathbf{R}_{sk} \quad (35)$$

where $\overset{\leftrightarrow}{P} = m_s \int v' v' f_s dv'$ is the pressure tensor. If f is an isotropic function of v , expanding the derivatives on the left hand side of Eq. (35) and removing the embedded continuity, we then obtain following equation of motion for each species

$$m_s n_s \left[\frac{\partial u_s}{\partial t} + u_s \cdot \nabla(u_s) \right] = n_s q_s (\mathbf{E} + u_s \wedge \mathbf{B}) - \nabla P_s - \mathbf{R}_{sk} \quad (36)$$

In plasma physics, one has to deal with a model with two fluids and an additional term, the transfer of impulse between the electronic fluid and the ionic fluid $-\mathbf{R}_{sk}$, characterized by the frequency of impulse transfer ν , is more significant than the transfer due to viscosity. Indeed

$\frac{\langle v \rangle}{v} \approx \nu_s$ and $R_{sk} \approx m_s n_s \nu_s u_s$ [127]. Eq. (36) is then reduced to

$$m_s n_s \frac{du_s}{dt} = n_s q_s (\mathbf{E} + u_s \wedge \mathbf{B}) - \nabla P_s - m_s n_s \nu_s u_s \quad (37)$$

when considering the convective derivative

$$\frac{d}{dt} = \frac{\partial}{\partial t} + u_s \cdot \nabla \quad (38)$$

which characterizes the temporal rate of change seen by an observer moving with the mean fluid velocity u_s of species s .

Let us now take the second moment of Eq. (28). Here we use a more general pressure definition. Multiplying Eq. (28) equation by $m_s \frac{\mathbf{v}^2}{2}$ and integrating over velocity gives

$$\begin{aligned} \sum_k \int m_s \frac{\mathbf{v}^2}{2} C_{sk}(f_s) d^3 \mathbf{v} &= \int \left(m_s \frac{\mathbf{v}^2}{2} \frac{\partial f_s}{\partial t} \right) d\mathbf{v} + \int \left(m_s \frac{\mathbf{v}^2}{2} \frac{\partial}{\partial \mathbf{r}} (\mathbf{v} f_s) \right) d\mathbf{v} \\ &+ \int \left(q_s \frac{\mathbf{v}^2}{2} \frac{\partial}{\partial \mathbf{v}} ((\mathbf{E} + \mathbf{v} \wedge \mathbf{B}) f_s) \right) d\mathbf{v} \end{aligned} \quad (39)$$

by letting as before $v = v' + u(r, t)$ we obtain

$$\begin{aligned} - \left(\frac{\partial W}{\partial t} \right)_{sk} &= \frac{\partial}{\partial t} \left(\frac{3P_s}{2} + \frac{m_s n_s u_s^2}{2} \right) + \nabla \cdot \left(Q_s + \frac{5}{2} P_s u_s + \frac{m_s n_s u_s^2}{2} u_s \right) \\ &- q_s n_s u_s \cdot \mathbf{E} \end{aligned} \quad (40)$$

where $Q_s = \int m_s \frac{\mathbf{v}'^2}{2} (v' f_s) dv$ is the heat flux and $\left(\frac{\partial W}{\partial t} \right)_{sk}$ is the rate at which species s collisionally transfers energy to species k . By using the convective derivative and Eq. (37), we then obtain

$$\frac{3}{2} \frac{dP_s}{dt} + \frac{5}{2} P_s \nabla \cdot u_s = - \nabla \cdot Q_s + \mathbf{R}_{sk} \cdot u_s - \left(\frac{\partial W}{\partial t} \right)_{sk} \quad (41)$$

The first term on the right hand side represents the heat flux, the second term gives the frictional heating of species s due to frictional drag on species k , while the last term on the right hand side gives the rate at which species s collisionally transfers energy to other species. In the absence of transport process, or discontinuity, the scalar pressure verifies an adiabatic equation. Collisions, being randomizing, drive the distribution function towards isotropy, while competing processes simultaneously drive it towards anisotropy. Thus, each situation must be considered individually in order to determine whether there is sufficient collisionality to make f isotropic. For an

isotropic-adiabatic (based on geometry and statistical mechanics rather than on thermodynamic arguments) model, the pressure P and density n are not two independent variables and the relation translating the conservation of the entropy, i.e. the absence of heat transfer in a reversible transformation, is given by:

$$-\frac{1}{n_s} \frac{dn_s}{dt} = \nabla \cdot u_s \quad (42)$$

substituting Eq. (42) into Eq. (41) then gives

$$\frac{d(P_i n_i^{-\gamma})}{dt} = 0 \quad (43)$$

According to Eq. (37), the species- s flow accelerates along a fluid trajectory under the influence of the scalar pressure gradient, the viscous stresses, the Lorentz force, and the frictional force due to collisions with other species. Finally, according to Eq. (41), the species- s energy density changes along a fluid trajectory because of the work done in compressing the fluid, viscous heating, heat flow, and the local energy gain due to collisions with other species. The electrical contribution to plasma heating, which was explicit in Eq. (39), has now become entirely implicit.

It can seem, in first analysis, that the two-fluid models have a descriptive and predictive restricted potential with particular situations; in fact, except for the cases of wave-particles resonances and when the Knudsen numbers are great, the fluid models are often sufficient in plasma physics.

Recent studies having retained the attention of the researchers were focused on the development of two fluid models for non-equilibrium anisotropic plasma flows by using a 10-moment or Gaussian anisotropic moment closure to model ion and electron species transport [128]. A three-dimensional Hall-Magnetohydrodynamic (Hall-MHD) simulation code has been developed to study the self-organization process in a two-fluid plasma [129]. E.A. Johnson et al [130] following Loverich et al [131], has simulate magnetic reconnection in the geospace environmental modeling problem using a two-fluid model with 10-moments for the electron fluid as well as the proton fluid. They show that use of 10-moments for electrons gives good qualitative agreement with the the electron pressure tensor components in published [132] kinetic simulations. Several studies [133, 134] have focused on the simulation of two fluid plasmas models by using methods such as Runge-Kutta methos, Galerkin method..etc.

II.1.3 Reduced nonlinear model for charge density under parametric and external harmonic oscillations

Reduced nonlinear model for density perturbation

In order to deal with small amplitude waves, we consider a situation representing a uniform infinite plasma. The values of $n_s, v_s, P_s, \vec{E}, \vec{B}$, for this will be denoted by n_{0s} , etc; however, here we shall take $v_s = E = 0$ in the unperturbed state. We then have $J = 0$ and all of Eqs. (25), (37), (43) are satisfied except Eq. (25-(c)) which requires $\rho_q = 0$, hence

$$\sum n_s q_s = 0. \quad (44)$$

For our simple two-species plasma, that condition of charge neutrality becomes

$$n_{0e} = n_{0i} = n_0. \quad (45)$$

We now consider the $m_e = 0$ ion sound instability. Only spatial variations of the form $\exp(ik_z z)$ need to be considered, where k_z is the axial wave number associated with this wave. For perturbed responses, one assumes

$$\begin{aligned} n_i &= n_0 + \tilde{n}, & P_i &= P_0 + \tilde{P}, \\ v_i &= \tilde{v}, & \vec{B} &= \vec{B}_0 + \tilde{\vec{B}}, \end{aligned} \quad (46)$$

in which the zero subscript indicates equilibrium quantities and the tilde over quantities indicates perturbed variables. Electrons obey the Boltzmann equilibrium

$$n(x) = n_0 \exp(e\phi(x)/K_e T_e), \quad \tilde{n} = \frac{e\phi}{k_B T_e}, \quad (47)$$

where k_B is the Boltzmann's constant, $\phi(x)$ is the perturbed electric potential and e is a unit charge. However, for the ion equation of motion, inertial effects are important, but the non-isothermal case is considered in which the ion temperature $T_i \ll T_e$. Therefore, the pressure gradient term is ignored. Inserting the expressions (46) into Eqs. (37) and (43), and after all of

the second order perturbative terms have been discarded, we obtain the following equation

$$\frac{d^2\tilde{n}}{dt^2} - \frac{dS_i}{dt} - \nu_i(S_i - \frac{d\tilde{n}}{dt}) = -\frac{ien_0k_z}{m_i} \cdot (\tilde{v} \times \tilde{B}_0) + \frac{k_Bk_z^2}{m_i}(T_e + \gamma T_i)\tilde{n}. \quad (48)$$

The ion source term is given by

$$S_i = \alpha_1\tilde{n} - \alpha_2\tilde{n}^2 - \alpha_3\tilde{n}^3 \quad (49)$$

Where α_1 is the linear value and α_j with $j \in \{2, 3\}$ are the nonlinear saturation depending on the type of ion source in used. By substituting (49) into Eq. (48), a differential equation for the time varying portion of the density evolution in which we introduce an external excitation, is given by

$$\frac{d^2\tilde{n}}{dt^2} + (\nu_i - \alpha_1 + 2\alpha_2\tilde{n} + 3\alpha_3\tilde{n}^2)\frac{d\tilde{n}}{dt} + \omega_0^2\tilde{n} + \nu_i\alpha_2\tilde{n}^2 + \nu_i\alpha_3\tilde{n}^3 = F(t), \quad (50)$$

where $\omega_0^2 = \frac{k_z^2k_B(T_e + \gamma T_i)}{m_i} + \nu_i\alpha_1$ is the ion sound instability frequency. The external driving term (the right hands term) was assumed to be in the form $F_0 \cos(\omega t)$, with amplitude F_0 and frequency ω , Externally applied signals could be coupled to the plasma by a number of magnetic coils spaced azimuthally at equal intervals around the plasma machine. The plane of each coil is such that they produced an in-phase azimuthal oscillating magnetic field B_δ in the plasma, which the virtue of the $B_\delta \wedge E_r$ drift produce an oscillating axial velocity v_a in the plasma. By varying the drive current I_d to these coils the amplitude of the induced velocity (or density) perturbation in the plasma could be changed [135].

Depending of the type and the configuration of the plasma devices, there are several physical mechanisms that could mimic the driven force $F(t)$. For example, when describing the discharge apparatus in a plasma column experiment, as mentioned before, density perturbations could be applied to the plasma externally by a small magnetic coil wound around the glass tube. An oscillating current at the required frequency is applied to this coil that could be moved axially along the column and set in any desired position, in order to produce an oscillating axial magnetic field, in the plasma. This perturbation of the main containment field, had the effect of compressing and relaxing the plasma, thus modifying the containment pressure at this point. Consequently, this effect produced a density perturbation in the plasma, linearly proportional to the current in the coil. The effect of this perturbation on the plasma instability could then be

monitored by feeding the output from a floating or ion-biased probe into a spectrum analyser. This allowed the instability amplitude, the driven amplitude F_0 and the beat frequency to be measured simultaneously [33].

In some experiment also, the transport of dust particles into plasma is proportional to the dust charge and as well as to the coagulation of small particles into larger ones since charged particles attract or repel each other through the coulomb potential [136]. However, considering the fact that ultraviolet light can extract electrons from materials by photodetachment, such a light can be used as an external force to control the charge on a dust particle [137]. Such forcing terms could also be mimicked through an externally applied electric field that supplies the system with an external drive [138].

Entrainment and periodic pulling of an ion acoustic instability observed in the power spectra of a low-pressure high-beta plasma as in WOMBAT (waves on magnetized beams and turbulence) machine, can be modeled by using the van der Pol equation with a forcing term [139]. In this configuration, a steady axial magnetic field is maintained by a set of external solenoids surrounding the source and a large solenoid inside the diffusion chamber. A radio-frequency powers (that could be view as $F(t)$) at a driving frequency is applied to one end of a single loop antenna via a matching network, while the other end is kept grounded. External modulation of the instability is achieved by varying the amplitude of the rf drive frequency at frequencies. The rf amplitude modulation could be varied up to 100% of the rf signal, allowing for the instability observed in the plasma discharge to be investigated for nonlinear behavior.

A change in the sheath width can results in a periodic modulation of the potential well and its frequency as $\omega_0^2 = \Omega_0^2(1 + h \cos(\omega_p t))$, where h is the modulation depth, ω_p is the angular frequency of the parametric excited wave. Using the following dimensionless quantities

$$\tilde{n} = \frac{\nu_i - \alpha_1}{2\alpha_2} x, \quad \mu = \frac{\nu_i - \alpha_1}{\omega_0}, \quad \gamma = \frac{\alpha_3(\nu_i - \alpha_1)^2}{4\alpha_2^2}, \quad (51)$$

$$\tau = \omega_0 t, \quad \lambda = \frac{\nu_i \mu}{2\omega_0}, \quad \beta = \frac{\alpha_3 \mu^2}{4\alpha_2^2}, \quad f = \frac{2\alpha_2}{\omega_0^2(\nu_i - \alpha_1)} F(t).$$

The charge density fluctuation is then described by the following equation

$$\frac{d^2 x}{d\tau^2} + \mu(1 + x + \gamma x^2) \frac{dx}{d\tau} + \omega(\tau)x + \lambda x^2 + \beta x^3 = f(\tau). \quad (52)$$

It has been shown experimentally that the Van der Pol type of equation gives a good description of various non-linear phenomena occurring in some plasma instabilities as: mode locking and mode competition [140]; periodic pulling [6], frequency entrainment [4]. Further experimental evidence have been presented showing that the ion-sound instability behaves as a single mode Van der Pol oscillator for externally driven signals near the main instability frequency; and as a multi-mode Van der Pol system for applied signals near other possible mode resonances in the plasma. In the single mode state, it has been possible to measure the system's parameters by a number of indirect means [33].

In another experimental investigations carried out in a magnetized plasma column, for an inductive external circuit, the oscillations appear as sharp current disruptions giving rise to large voltage spikes over the plasma, similar to the disruptive behavior observed in fusion devices. The nonlinearity is shown to be determined by the static current-voltage characteristic of the plasma. For higher oscillation frequencies, the dynamic response of the plasma has to be taken into account and the oscillations are correctly described by a generalized form of the van der Pol equation only. By adding a periodic driver voltage in series to the external dc voltage, a rich variety of dynamical phenomena appear as predicted by many investigations on periodically driven van der Pol type oscillators. For the investigation of the periodically driven system, the input of the amplifier is connected to a signal generator with a suitable output signal offset. In this way, a proper modulated bias voltage is obtained. The modulation amplitude (driving force) and the modulation frequency (driver frequency) are the control parameters for the study of dynamical phenomena of the periodically driven discharge system [141].

II.1.4 Potential configuration

The above equation described the density perturbation in plasma motion where λ and β are constant parameters, μ and γ are respectively the damping term and the nonlinear saturation coefficient, $f(\tau) = A_0 \cos \omega\tau$ is an externally excited wave, and $\omega(\tau) = 1 + h \cos \Omega\tau$. With asymmetrical fourth-order polynomial potential

$$V(x) = \frac{1}{2}x^2 + \frac{\lambda}{3}x^3 + \frac{\beta}{4}x^4. \quad (53)$$

In fact, depending on the set of the parameters, it can be considered at last three physically in-

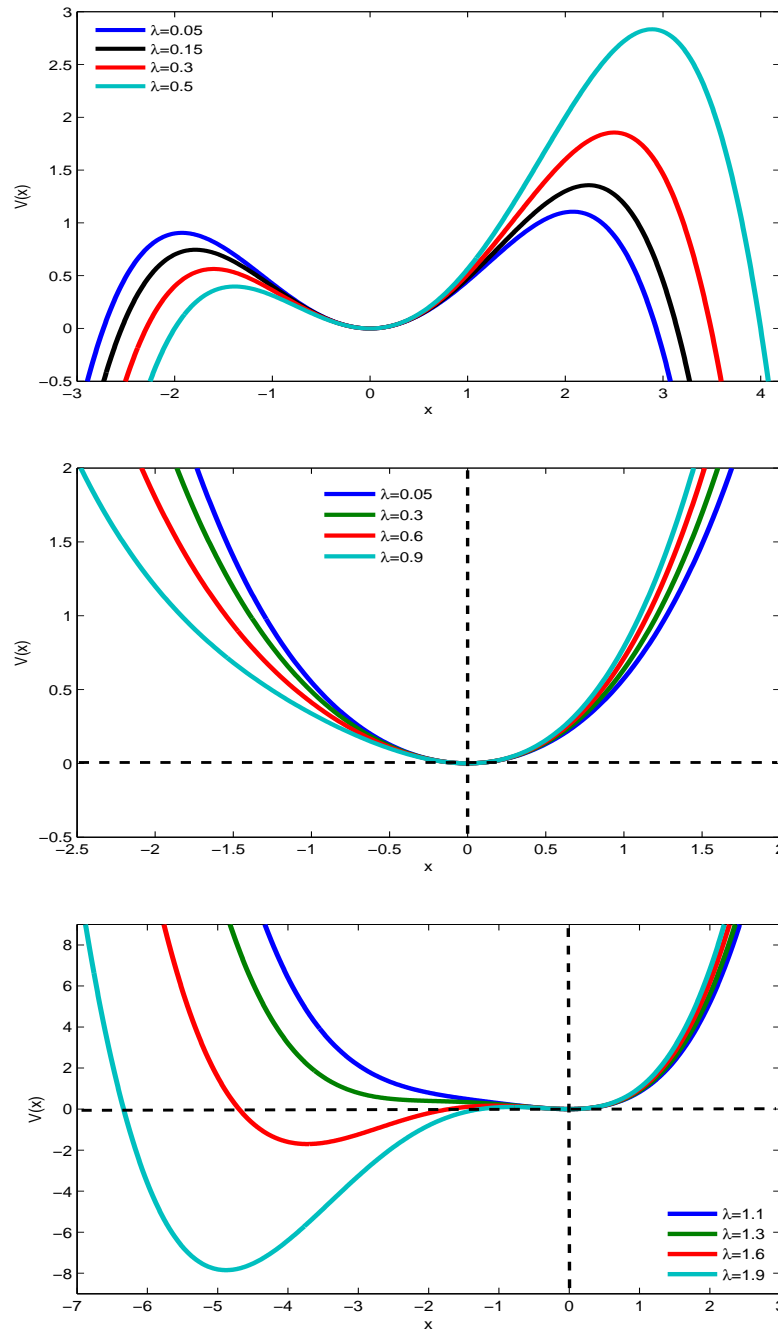


Figure 14: Potential configuration: (a) for $\beta = -0.25$ and $\lambda \in [0.05, 0.5]$, (b) for $\beta = 0.25$ and $\lambda \in [0.05, 0.9]$, (c) for $\beta = 0.25$ and $\lambda \in [1.1, 1.9]$.

interesting situations where the asymmetrical fourth-order polynomial potential is a : (i) bounded single well, (ii) unbounded single well, (iii) double well. It has been shown in [142] that the case of the unbounded single well with two unstable points can not be efficient for the confining of the density energy. It is also obvious that the case of the bounded single well potential can not be used since this type of density profile cannot be used to characterize the presence of instability in the model. Then, the only interesting case is the asymmetrical double well where the energy confining can be possible. When $h = 0$, Eq. (17) has been obtained by [33] where it has been shown the classical anharmonic resonance effects on a marginal ion sound instability, when forcing at the fundamental and the subharmonic frequencies. A family of Eq. (17) namely van der-Pol-Mathieu equation has been considered for the dynamics of dust grain charge in dusty plasma by [143], the critical stability boundaries for a particular trivial solution of the governing equation with varying parameters has been studied. The Melnikov analysis to study the homoclinic bifurcation in the model is obtained in explicit form in the next section.

II.1.5 Reduced nonlinear model for charge density under external bounded noise excitation

The ion source term[144] is given by:

$$S_i = \alpha_1 \tilde{n} - \alpha_2 \tilde{n}^2 - \alpha_3 \tilde{n}^3 \quad (54)$$

as mentioned in the preceding section we have

$$\frac{d^2 \tilde{n}}{dt^2} + \omega_0^2 \tilde{n} + \nu_i \alpha_2 \tilde{n}^2 + \nu_i \alpha_3 \tilde{n}^3 + (\nu_i - \alpha_1 + 2\alpha_2 \tilde{n} + 3\alpha_3 \tilde{n}^2) \frac{d\tilde{n}}{dt} = F(t), \quad (55)$$

where $\omega_0^2 = \frac{k_z^2 K_B (T_e + \gamma T_i)}{m_i} + \nu_i \alpha_1$ is the ion sound instability frequency. Using the following dimensionless quantities

$$\tilde{n} = \frac{\nu_i - \alpha_1}{2\alpha_2} u, \quad \tau = \omega_0 t, \quad \epsilon^2 \mu = \frac{\nu_i - \alpha_1}{\omega_0}, \quad \gamma = \frac{\alpha_3 (\nu_i - \alpha_1)^2}{4\alpha_2^2}, \quad \epsilon \lambda = \frac{\nu_i \mu_0}{2\omega_0}, \quad (56)$$

$$\epsilon^2 \beta = \frac{\alpha_3 \mu_0^2}{4\alpha_2^2}, \quad \epsilon^2 f = \frac{2\alpha_2}{\omega_0^2 (\nu_i - \alpha_1)} F(t). \quad \text{with } \nu_i - \alpha_1 \sim \epsilon; \quad \frac{1}{\omega_0} \sim \epsilon.$$

The charge density fluctuation is described by the following equation.

$$\frac{d^2u}{d\tau^2} + \epsilon^2\mu(1 + u + \gamma u^2)\frac{du}{d\tau} + u + \epsilon\lambda u^2 + \epsilon^2\beta u^3 = \epsilon^2 f(\tau), \quad (57)$$

where u is the plasma density moving along the axis in tokamak plasmas under the influence of a restoring force $u + \epsilon\lambda u^2 + \epsilon^2\beta u^3$, with the small terms proportional to λ and β quantifying its nonlinearity. μ and γ are respectively the damping term and the nonlinear saturation coefficient. We consider that $f(\tau)$ is affected by noise; then $f(\tau) = A_0\vartheta(\tau)$ is an external superimposed noise which yields a global perturbation. This stands in contrast to intrinsic noise of plasma, which is typically local in space and time. It is well known that an unperturbed ('deterministic') particle in one of the potential wells will remain in that well for infinitely long time, independent of whether the well is deep or flat. If there is a strong stochastic perturbation acting on the particle, it will randomly move forth and back between the two wells, again independently of their depth. The most interesting situation occurs when there is a moderate stochastic perturbation acting on the particle. The particle will then typically stay in the well it occupies for some time, until the random diffusion drives it over the potential barrier into the other well. To our knowledge, what is considerably less known is the effect of the bounded noise on nonlinear response of an asymmetry plasma density with nonlinear damping. In Eq. (57), the form of the bounded noise is given by

$$\vartheta(\tau) = A_0 \cos(\Omega\tau + \eta W(\tau) + \eta\psi_0) \quad (58)$$

where A_0 and η are constants, $W(\tau)$ is a unit Wiener process and $\eta\psi_0 = \psi$ is a random variable uniformly distributed in the interval $[0, 2\pi]$. It has finite power and its spectral shape can be made to fit a target spectrum, such as the Dryden and Von Karman spectra of wind turbulence, by adjusting its parameters [145]. Therefore, it can be a reasonable model for the random excitation or response in engineering systems. Here, we investigate some typical dynamical phenomena features occurring in the proposed plasma model under combined nonlinear damping, asymmetry potential [146], and external bounded noise. In order to catch the insight of the variation of system parameters, the analytical solutions are found by multiple scale method. The steady states and their stability regions are examined. Using the resulting solution, we discovered interesting dynamic responses. These responses are characterized by the presence of parameters islands that have critical implications on the global stability of the response. The statistical moments are

calculated and their stability condition established. The response of the global system is affected by bounded noise. Through numerical simulations, we show that the density perturbation may undergo hysteretic transitions induced by the bounded noise.

As mentioned before, magnetized bounded plasmas are subjected to a class of instabilities. These instabilities are generally believed to be responsible for anomalous crossfield particle transport. Drift waves are caused by pressure-driven instabilities in magnetized plasmas. Drift wave turbulence is generally believed to be responsible for anomalous cross-field particle transport and it is an appealing long-term perspective to influence systematically the turbulent transport in magnetically confined plasmas by active control of drift wave dynamics. Whereas chaos is characterized by the interplay between highly ordered structures and instability, noise and strong turbulence are both of stochastic nature owing to the large number of degrees of freedom. Indeed the turbulent regimes are seemingly accounting for anomalous transport in the magnetically confined high-temperature plasmas of tokamaks. Therefore, controlling these instabilities through the control of the turbulent (or chaotic) regime could be of a great interest for improving the performance of the magnetic fusion devices. Plasma column devices, as a approximation of tokamaks, easily exhibits nonlinear instabilities. In fact the characteristics of the unstable waves are slightly different from the instabilities observed in tokamaks. Indeed, very high mode numbers are excited in tokamaks and thus the plasma slab approximation is valid. On the contrary, the unstable wavelengths in plasma column devices are of the order of the plasma radius and global modes are excited. However, the dynamics is of great interest because the system is extended in space, leading to spatiotemporal characteristics, as in a tokamak.

Two-fluid models in plasmas are usually approximations of phenomena occurring in large machines plasmas, such as tokamaks. The observations made in the study of plasma columns, for example, can be generalized to large machines, or simply give a perspective on the physical phenomena that take place there. Using the two-fluid model, gives rise to a set of nonlinear equations, which are capable of describing the dynamics of long wavelength drift instabilities, as well as of giving a reason for the plasma turbulence rising [147], and a way for controlling them. Various destabilizing mechanisms have been identified. The electron collision rate or the existence of an axial electron beam have been extensively studied. In plasma devices [148] which exhibits easily nonlinear drift waves, the characteristics of the unstable waves are sometime indeed very different of the drift waves observed in the plasmas of the tokamaks. Indeed, very

high mode numbers are excited in tokamaks drift wave turbulence and thus this plasma slab approximation is valid.

But it is possible to model the phenomena described in large plasma machines, by making simplifications related to geometry and toroidal symmetry in tokamaks. This leads to fluids equations, which describe phenomena such as the L-H transition in tokamaks.

The edge region, or boundary layer, of a magnetically confined high-temperature plasma is observed experimentally to be complex and dynamic. Significant fluctuation levels in the plasma density and plasma potential have been related theoretically and experimentally to the anomalous transport observed in tokamak devices. Electrostatic oscillations are found to be maximum in this edge region. Core plasma density limits and improved global confinement in the H-mode have been related to the physics of the edge plasma, although the mechanisms are not well understood. Additionally, neutral particle and plasma recycling in the edge must be controlled to maintain acceptably low plasma temperatures at the walls and to minimize sputtering and erosion losses. The behavior of the edge plasma is critical in designing particle and power exhaust systems for the power levels expected in fusion reactors. The plasma sheath formed at the walls accelerates plasma ions to the sound speed, and acts as a sink for momentum in the plasma. This must be balanced by the momentum efflux from the core plasma. The interface between the core and the edge plasma region is where a boundary condition is established for the core plasma. Expressions for the sheath potential drop show a range in values depending on the analysis. Plasma fluid or kinetic model are applied to evaluate transmission coefficients, which relate the plasma density flux, electron energy flux, and ion energy flux through the plasma sheath as a function of the sheath potential drop. The core particle confinement time relates to the core fueling flux. The flux boundary condition can be a function of time to simulate plasma startup conditions and various time-dependent characteristics of the core such as a reduced flux at the L-H transition, flux pulses observed in the Edge localized modes (*ELM's*), or sawteeth propagation from the core to the edge plasma.

Void et al. [149] aim to develop a model that can be implemented computationally in a stepwise fashion while improving approximations to drift flows and nonambipolarity. They search for a fully self-consistent calculation in the edge region. An important consideration is coupling these equations with the core plasma region at the core-edge interface. A set of plasma fluid transport equations was then developed and their application to the edge plasma

region was described. They first focusing on fluid models and then develop equations for a toroidally symmetric device (Metric formulation (considering the toroidal symmetry) transport equations is used to describe the plasma in the fluid approximation, appropriate for the low beta plasma edge region of a tokamak or similar magnetic confinement device.), including plasma drifts; additional simplifications to the fluid model was discussed for numerical implementation. The simplified plasma equations was applied to a tokamak divertor plasma and the results was discussed with an emphasis on the poloidal flow, the plasma potential, and the potential gradient electric fields. Implications of the results on transport was also discussed.

The electric field appears to play a vital role in confinement and is coupled to the edge plasma physics. Consistent models of particle recycling and coupled nonambipolar flows are simultaneously required to fully resolve the edge transport physics. Analytic results supporting this assumption show that a drift wave model with a poloidally periodic forcing function (e.g., poloidal flow through a poloidally localized recycling zone) supports aperiodic or “turbulent-like” solutions. Combining nonlinear equations for the plasma density and plasma potential with the assumed flux (velocity component) terms has produced time-dependent simulations with chaotic or “turbulent” solutions [150]. A coupled plasma density and potential solver in the limit of weakly ionized plasma has proven successful in predicting experimental simulations of the steady-state edge plasma [151]. The fluctuating potential and steady-state potential profiles may be related in the H-mode improved confinement [152]. Drift waves are naturally excited in magnetized plasmas exhibiting a radial density gradient.

It is also possible to model the phenomena described in large plasma machines, using equations that model them directly, without passing through the fluid equations. This allows us to investigate the behavior of some plasma parameters, such as radial electric field, which has already been reported in fluid modeling as playing a major role in the transition to the high level of energy, that one seek to achieve in fusion plasmas. The goal here is to control the same instabilities.

II.1.6 Reduced nonlinear model of radial electric field in plasma L-H transition under external bounded noise

After the release of the first physical model showing the possible role of radial electric fields in the development of plasma bifurcations [153], initial experimental verifications of the estab-

ishment of the mean radial electric field during edge plasma bifurcations were reported [154]. From the empirical perspective, achieving the Low to High confinement transition requires exceeding a power threshold that is usually given in terms of plasma density, magnetic field and edge plasma surface. However, large uncertainties are still present in the determination of this threshold, with the consequent implications for the overall research programme of next step magnetic confinement devices, such as the International Tokamak Experimental Reactor ITER [155]. The build-up of the transport barrier, and the improvement of plasma confinement have been attributed to the generation of the radial electric field. Different scenarios of relaxation of the radial electric field toward the steady-state in response to sudden and adiabatic changes of the equilibrium temperature gradient were presented in [156] as mentioned before; this electric field, existing in the region of the sharp pressure gradients, produces the $\mathbf{E} \wedge \mathbf{B}$ flow with a shear, which in turn has a strong stabilizing influence on the plasma turbulence [157]. The reduction of the anomalous transport due to the inhomogeneous radial electric field was theoretically studied for toroidal helical plasmas (see [153]).

The plasma of our interest is restricted to the plasma boundary $-L < \tau - a < 0$, where a is the minor radius. It is also considered that plasma parameters and temperature are constant in the toroidal and poloidal directions. In the quasineutrality assumption ($n_i = n_e = n$); the one-dimensional Ginzburg-Landau type perturbed diffusion dimensionless [158] equations for the density of the plasma and the radial electric field near the plasma edge in Tokamak can be written as

$$\frac{\partial n}{\partial t} = \frac{\partial}{\partial x} \left(D(E_r) \frac{\partial n}{\partial x} \right) \quad (59)$$

The Poisson equation, combined with the equation of ion motion, is written as

$$\gamma \frac{\partial E_r}{\partial t} = \Gamma_e - \Gamma_i + \mu_1 \frac{\partial^2 E_r}{\partial x^2} \quad (60)$$

where $x = \tau - a$ is the cartesian coordinate, $\Gamma_e - \Gamma_i$ represents the bipolar component of the particle flux and derives the nonlinear relation between the particle flux and the density gradient, where, Γ_e and Γ_i are the normalized particle flux of electrons and ions, respectively. The point which holds the relation $x = 0$ represents the plasma edge and γ indicates the smallness parameter $O\left(\frac{B_p^2}{B^2}\right)$; where B_p , and B are the poloidal and toroidal magnetic field, respectively. The third term in the right hand side of Eq. (60) shows the diffusion effect of the radial electric

field E_r . The influence of the inhomogeneous electric field on the anomalous transport is governed by the parameter $H_1 \equiv (T_e/e\gamma_d l B \rho_{pi})^2$; γ_d been the decorrelation rate of turbulence which causes anomalous transport; $l = (\mu/\sigma(0))^{1/2}$, where $\sigma(0)$ is the conductivity in the absence of the radial electric field. We analyze the case where the assumption of the constant viscosity is valid i.e. for $H_1 E_r^* < 1$, where E_r^* correspond to the extremum of bipolar flux. For our analysis, Eqs. (59), (60) could be rewritten as

$$\begin{aligned} \frac{\partial n_d}{\partial t} &= \frac{\partial}{\partial x} \left[D(E_r) \frac{\partial n_d}{\partial x} \right] + f_1 \cos(\Omega_1 t) \\ \gamma \frac{\partial E_r}{\partial t} &= -N_e(E_r, g) + \mu_1 \frac{\partial^2 E_r}{\partial x^2} + f_2 \cos(\Omega_2 t) \end{aligned} \quad (61)$$

where n_d and E_r are the density of the particle near the plasma edge and the normalized radial electric field respectively, $D(E_r)$ and μ_1 are the diffusion coefficients of the density and electric field, $\Gamma_e - \Gamma_i = N_e(E_r, g)$ is the total current effect (Here we retain only local part which arise from ion orbit loss or drift wave convection), f_1 , Ω_1 , f_2 and Ω_2 are the amplitudes and frequencies of the particle perturbation and the controlling radial electric field [158]. It is known that $D(E_r)$, $N_e(E_r, g)$ and γ respectively satisfy the following equations [158]:

$$D(E_r) = \frac{D_p}{2}(1 + \tanh(E_r)) + \frac{D_m}{2}(1 - \tanh(E_r)) \quad (62)$$

$$N_e(x, t) = g(n_d) - g_0 + (\beta E_r(x, t)^3 - \alpha E_r(x, t))$$

$$g(n_d) = \frac{3}{n_d^2} \frac{dn_d}{dx} ; \quad \gamma = \left(1 + \frac{v_A^2}{c^2} \right) \frac{B_p^2}{B^2} \quad (63)$$

where D_p and D_m respectively denote the diffusion coefficients of H-mode and L-mode, the parameters v_A , c , B_p , B , α , β and g_0 are constants, and v_A , c , B_p , B respectively are the Alfvén velocity, the light velocity, the magnetic field which is parallel to the poloidal direction in tokamak, and the characteristic magnetic field. By letting [159] $n_d(x, t) = \frac{1}{V(x, t)}$; $E_r(x, t) = G(x)u(t)$; $V(x, t) = V_0 + A(x)v(t)$; in equation (61), using Eqs.62 and 63, and considering that u and v are small we obtain for u ,

$$\dot{u} = b_1 v + b_2 u + b_3 u^3 + b_4 \cos(\Omega_2 t) + b_0. \quad (64)$$

where b_i [$i = 0..4$] are given in the appendix. Using the Taylor expansion of $\frac{1}{V(x, t)}$ around with the small quantity $\frac{A(x)v(t)}{V_0}$ in which we only retain the term under the quartic term, we then obtain

$$\begin{aligned} \dot{v} = & a_0 + a_1u + a_2uv + a_3v + a_4v^2 + a_5v^3 \\ & + a_6uv^2 + (a_7v + a_8v^2 + a_9) \cos(\Omega_1 t) \end{aligned} \quad (65)$$

where the coefficients a_i [$i = 0..9$] are given in appendix. By differentiating equation (64) with respect to time and introducing equation (65) in the obtained equation, we obtain

$$\begin{aligned} \ddot{u} = & -\Omega^2u + \alpha_2u^2 + \alpha_3u^3 + \alpha_4u^4 - \alpha_5u^5 - \epsilon(\mu + \beta_3u + \beta_5u^2)\dot{u} + \epsilon(\beta_2 + \beta_4u + \beta_6\dot{u})\dot{u}^2 \\ & -\epsilon\delta_1u \cos(\Omega_1 t) + \epsilon F_2 \cos(\Omega_2 t + \Theta_0) + \epsilon\alpha_0 \end{aligned} \quad (66)$$

variable u indicates the change of the normalized radial electric field near plasma edge in Tokamak, and ϵ is a small parameter.

One of the most important physical discoveries of the past few decades is that random behavior can arise in deterministic nonlinear systems with just a few degrees of freedom. This discovery gives new hope to providing simple mathematical models for analyzing, and ultimately controlling, physiological and engineering systems. Chaos occurs widely in engineering and natural systems; historically it has usually been regarded as a nuisance and is designed out if possible. It has been noted only as irregular or unpredictable behavior, often attributed to random external influences [160]. Noise effects on nonlinear dynamical systems exhibiting chaotic behavior have been of interest to researchers in various fields in recent years, and their effect on structural instabilities in nonlinear dynamical system can't be runned out. Homoclinic bifurcations an heteroclinic bifurcations are two kinds of important sources of structural instabilities in nonlinear dynamical systems. The subsequent occurrences of scattered chaotic dynamics and fractal bassin boundaries are usually derived from the homoclinic or heteroclinic transversal intersections between the stable and unstable manifold of the hilltop saddle in the Poincaré map.

Virtually all engineering and most natural systems are subjected during operation to external forcing. This forcing will contain (and hopefully be dominated by) planned and intentional components; it will also almost invariably contain unintentional 'noise'[160]. Judicious design and control of this forcing is often able to annihilate, or shift to a harmless region of parameter space. We then consider that the controlling radial electric field is affected by noise, the external

harmonic perturbation of Eq. (66) becomes $F_2 \cos(\Omega_2 t + b(t) + \Theta_0)$, with $b(t) = \eta(W(t) + \varphi_0)$ different to intrinsic noise of plasma, typically local in space and time; here F_2 and η are constants, $W(t)$ is a unit Wiener process and φ_0 is a random variable uniformly distributed in the interval $[0, 2\pi]$. The bounded noise $\vartheta(t) = F_2 \cos(\Omega_2 t + b(t) + \Theta_0)$ has finite power and its spectral shape can be made to fit a target spectrum, such as the Dryden and Von Karman spectra of wind turbulence, by adjusting its parameters [145]. Therefore, it can be a reasonable model for the random excitation or response in engineering systems. The main assumption concerning the real noise process is that it should be uniformly bounded. This will permit to use ergodic-theoretic methods which is one of the main points in L. Arnold's program to study random dynamical systems. The power of these methods has been demonstrated by a vast number of applications [161].

K. Itoh et al [162] have found that a bifurcation from the radial-uniform structure of E_r which belong to key issues of the high confinement mode H-Mode, to the solitary structure solution of the radial electric field E_r in the tokamak plasmas occurs at a certain applied voltage, this, associated to a hysteresis. Repeated transition phenomena with abrupt reductions and jumps of the electron density were observed by Shunjiro Shinohara and Shoichiro Matsuyama [163], by voltage biasing in a cylindrical magnetized plasma. These global, self-excited, density transitions and back ones between two states were accompanied by changes of the floating potential profile and the bias current under various parameters.

A new bifurcation¹ [164] of turbulent transport caused by the change of the damping rate of the zonal flows, which governs the global confinement of toroidal plasmas was analyzed in a toroidal helical plasma.

Recent developments in plasma physics, including fusion research in a new era of ITER as well as space research and astrophysics, have focused on structural formation in turbulent plasma associated with electromagnetic field formation [165]. Progress made to date on the specially promoted research project "Structure Formation and Selection Rule in Turbulent Plasmas" was reported [166], including the control of transport by modifying the damping rate of zonal flow which could be regarded as a bifurcation control.

¹The plasma state changes from the branch of a weak negative radial electric field to the strong positive one

II.2 Mathematical methods for the control of global bifurcation

II.2.1 Chaos control using Melnikov method

Although the Melnikov method is merely approximative, it is one of a few methods allowing analytical prediction of chaos occurrence. Moreover, it can be applied to a relatively large class of dynamical systems. A generalized version of the Melnikov function for a system subjected to an excitation with multiple frequencies was introduced by Wiggins [30], and by Gruendler [167]. The Melnikov method [168, 30] is an effective approach to detect chaotic dynamics and to analyze near homoclinic or heteroclinic motion with deterministic or random perturbation. The method was first applied by Holmes [31] to study a periodically forced Duffing oscillator with negative linear stiffness, and by Adriaratnam and Xie [32] to investigate the chaotic behavior of a parametrically excited system such as the transverse vibration of a buckled column under axial periodic excitation.

The main advantages of both methods cover: (i) possibility of obtaining analytical results; (ii) possibility of applying the method in dynamical systems characterized by arbitrary but integrable characteristics (including discontinuities which occur in a finite number of points like e.g. friction characteristics); (iii) high efficiency of the verification of numerically generated results; (iv) possibility of examination of strongly nonlinear systems.

Both mentioned methods are not ideal, since they exhibit the following drawbacks: (i) they are applicable to systems characterized by a specific phaseportrait, namely homoclinic or heteroclinic orbits of one or two critical saddle points; (ii) they are not exact but approximative methods which use a small parameter; (iii) non-perturbed system should be integrable; (iv) they enable prediction of values of the parameters associated only with the so-called homoclinic or heteroclinic chaos ; (v) they are associated with rather complicated algebraic computations.

Case of external and parametric perturbation

The escape of the states of a dynamical system from a potential well is a significant problem of interest in engineering and physical sciences. Under the action of periodic forces chaotic motions will often trigger the escape. Dynamics of density perturbation in plasma is typical example of dynamical systems having the ability to escape from a potential well. In physical

terms escape may mean failure of the system in some sense. For example, in the case of the density perturbation in plasma problem escape would mean the loss of confining of the density energy. The escape of a periodically driven damped oscillator from a potential well is intimately associated with homoclinic bifurcation, fractal basins, and a variety of chaotic bifurcations [169]. We aim in this section is to give the conditions under which homoclinic bifurcation may appears. First, scaling $\mu \rightarrow \varepsilon\tilde{\mu}$, $A_0 \rightarrow \varepsilon\tilde{A}_0$ and $h \rightarrow \varepsilon\tilde{h}$, where ε is a small positive parameter, then dropping the tildes, equation (52) can be rewritten as

$$\begin{cases} \dot{x} = y, \\ \dot{y} = -x - \lambda x^2 - \beta x^3 + \varepsilon(-\mu(1+x+\gamma x^2)y + f_1(\tau)), \end{cases} \quad (67)$$

where $f_1(\tau) = -hx \cos \Omega\tau + A_0 \cos \omega\tau$. Melnikov analysis starts with the renormalisation of the potential given by Eq. (53) [170]. If we let $x = z + x_0$, where x_0 is the unstable fixed point obtained by solving Eq. (53), and $V_1(z) = V(x) - V(x_0)$, then,

$$V_1(z) = \frac{\beta}{4} z^2 (z - z_1)(z - z_2), \quad (68)$$

where

$$z_{1,2} = -\frac{6\beta x_0 + 2\lambda \pm \sqrt{-18\beta^2 x_0^2 - 12\beta x_0 \lambda + 4\lambda^2 - 18\beta}}{3\beta}. \quad (69)$$

Figs. 15(a) and (b) respectively shows the renormalized of the potential and it phase diagram.

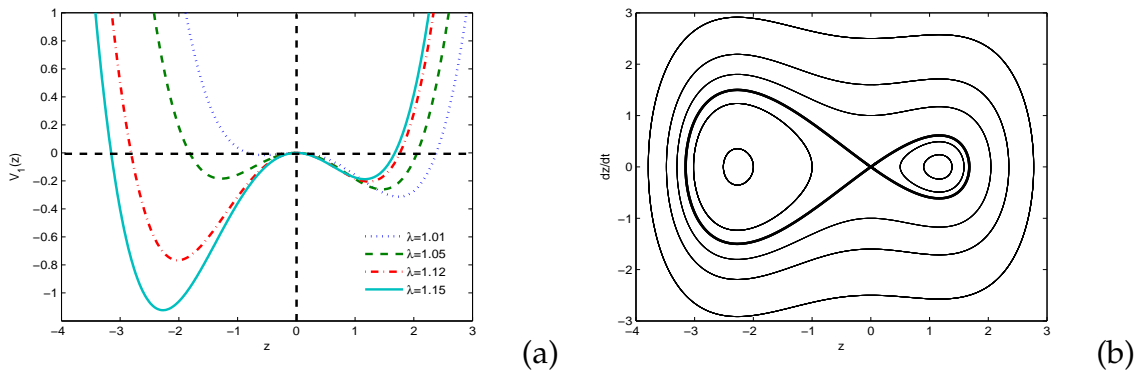


Figure 15: (a) Shape of the renormalized potential Eq. (19), (b) corresponding phase portrait for $\beta = 0.25$ and $\lambda \in [1.01, 1.2]$, with $\lambda^2 - 4\beta > 0$

While being interested in this phase diagram, we note that, it contains a homoclinic orbit. More-

over, by taking in consideration the renormalisation, the equation of the movement has the following form:

$$\ddot{z} + \varepsilon\mu((1 + x_0 + \gamma x_0^2) + (1 + 2\gamma x_0)z + \gamma z^2)\dot{z} + \beta \left\{ z^3 - \frac{3}{4}(z_1 + z_2)z^2 + \frac{1}{2}z_1 z_2 z \right\} = \varepsilon f_1(\tau). \quad (70)$$

The general one-dof nonlinear oscillator Eq. (70) is considered in the following form:

$$\begin{aligned} \dot{z} &= v, \\ \dot{v} &= -\beta \left\{ z^3 - \frac{3}{4}(z_1 + z_2)z^2 + \frac{1}{2}(z_1 z_2)z \right\} - \varepsilon(\mu((1 + x_0 + \gamma x_0^2) + (1 + 2\gamma x_0)z + \gamma z^2)v \\ &\quad + h(z + x_0) \cos \Omega\tau - A_0 \cos \omega\tau). \end{aligned} \quad (71)$$

Note that the unperturbed equations ($\varepsilon = 0$) can be obtained from the gradients of the Hamiltonian $H^0(z, v)$,

$$\dot{z} = \frac{\partial H^0}{\partial v}, \dots \dot{v} = -\frac{\partial H^0}{\partial z}, \quad (72)$$

where the Hamiltonian function is defined as

$$H^0 = \frac{1}{2}v^2 + \frac{1}{4}\beta(z - z_1)(z - z_2)z^2 = cte. \quad (73)$$

The non-symmetric potential plotted in Fig. 15(a) has a local peak at the point $(0, 0)$, existence of this point with a horizontal tangent makes homoclinic bifurcations of the system possible, i.e. potential transition from a regular to chaotic solution. By setting the unperturbed Hamiltonian equal to zero and after a simple integration of Eq. (73), the homoclinic orbits (Fig. 15(b)) is obtained as

$$\tau - \tau_0 = \sqrt{\frac{-2}{z_1 z_2 \beta}} \ln \left| \frac{-2z_1 z_2 + (z_1 + z_2)z + 2\sqrt{z_1 z_2(z - z_1)(z - z_2)}}{z} \right|, \quad (74)$$

where τ_0 is a constant of integration. Through evaluation of above Eq. (26) after some lengthly algebra, the following homoclinic trajectories are obtained:

$$z_r^* = \frac{4z_1 z_2 \kappa_1}{-(z_1 - z_2)^2 - \kappa_2 + 2(z_1 + z_2)\kappa_1}, \quad (75)$$

$$v_r^* = \frac{-4z_1z_2\sqrt{\frac{-\beta z_1z_2}{2}}\kappa_1((z_1 - z_2)^2 - \kappa_2)}{(-(z_1 - z_2)^2 - \kappa_2 + 2(z_1 + z_2)\kappa_1)^2}, \quad (76)$$

$$z_l^* = \frac{4z_1z_2\kappa_1}{(z_1 - z_2)^2 + \kappa_2 + 2(z_1 + z_2)\kappa_1}, \quad (77)$$

$$v_l^* = \frac{-4z_1z_2\sqrt{\frac{-\beta z_1z_2}{2}}\kappa_1(\kappa_2 - (z_1 - z_2)^2)}{((z_1 - z_2)^2 + \kappa_2 + 2(z_1 + z_2)\kappa_1)^2}, \quad (78)$$

where the index "r" corresponds to the right-hand side well, and the index "l" to the left one;

with

$$\kappa_1 = \exp\left((\tau - \tau_0)\sqrt{\frac{-\beta z_1z_2}{2}}\right), \quad (79)$$

and

$$\kappa_2 = \exp\left(2(\tau - \tau_0)\sqrt{\frac{-\beta z_1z_2}{2}}\right). \quad (80)$$

Now suppose that

$$\tau_0 = \tau_{01} + \tau_{02}, \quad (81)$$

where

$$\tau_{01} = -\left(\frac{\ln(z_2 - z_1)}{\sqrt{\frac{2}{-\beta z_1z_2}}}\right), \quad (82)$$

τ_{01} has been fixed to guarantee the proper parity (under the time transformation $\tau \rightarrow -\tau$), and

hence

$$z_{r,l}(-\tau) = z_{r,l}(\tau), \text{ and } v_{r,l}(-\tau) = -v_{r,l}(\tau), \quad (83)$$

τ_{02} is an arbitrary constant to be determined later in the minimization of the Melnikov integral $M(\tau_{02})$. The distance between perturbed stable and unstable manifolds and their possible cross-sections may be examined by means of the integral $M(\tau_{02})$ given by

$$M(\tau_{02}) = \int_{-\infty}^{+\infty} \mathbf{H}(z^*(\tau - \tau_{01} - \tau_{02}), v^*(\tau - \tau_{01} - \tau_{02})) \wedge \mathbf{G}(z^*(\tau - \tau_{01} - \tau_{02}), v^*(\tau - \tau_{01} - \tau_{02})) d\tau. \quad (84)$$

Where the wedge product for two dimensional vectors is defined as

$$\mathbf{H} \wedge \mathbf{G} = h_1g_2 - h_2g_1.$$

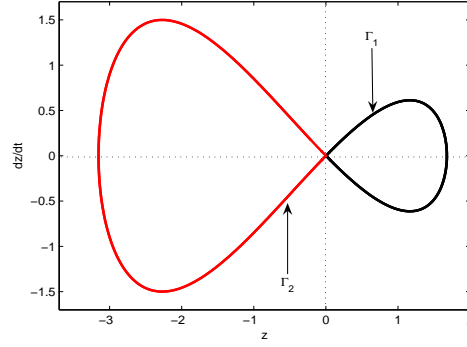


Figure 16: Homoclinic orbits Γ_1 , and Γ_2 for the renormalized bounded double well potential.

The corresponding vector H is the gradient of unperturbed Hamiltonian (73),

$$\mathbf{H} = \left[\beta(-z^{*3} + \frac{3}{4}(z_1 + z_2)z^{*2} - \frac{1}{2}z_1 z_2 z^*), v^* \right], \quad (85)$$

while the vector G consists of the perturbation terms to the same Hamiltonian,

$$\mathbf{G} = [-\mu((1 + x_0 + \gamma x_0^2) + (1 + 2\gamma x_0)z + \gamma z^2)v^* - h(z + x_0) \cos \Omega\tau + A_0 \cos \omega\tau, 0]. \quad (86)$$

Thus, shifting the time coordinate $\tau \rightarrow \tau + \tau_{02}$ under the integral (84), gives

$$\begin{aligned} M(\tau_{02}) &= \int_{-\infty}^{+\infty} v^*(\tau - \tau_{01}) (-\mu((1 + x_0 + \gamma x_0^2) + (1 + 2\gamma x_0)z^*(\tau - \tau_{01}) \\ &\quad + \gamma z^{*2}(\tau - \tau_{01}))v^*(\tau - \tau_{01}) - h(z^*(\tau - \tau_{01}) + x_0) \cos(\Omega(\tau + \tau_{02})) \\ &\quad + A_0 \cos(\omega(\tau + \tau_{02})))d\tau. \end{aligned} \quad (87)$$

The above Melnikov function can be written after some algebraic manipulations as

$$M_r(\tau_{02}) = \mu I_{1r} - A_0 I_{3r}(\omega) \sin \omega\tau_{02} + h[I_{2r}(\Omega) + x_0 I_{3r}(\Omega)] \sin \Omega\tau_{02}, \quad (88)$$

$$M_l(\tau_{02}) = \mu I_{1l} - A_0 I_{3l}(\omega) \sin \omega\tau_{02} + h[I_{2l}(\Omega) + x_0 I_{3l}(\Omega)] \sin \Omega\tau_{02}, \quad (89)$$

where

$$I_{1(r,l)} = - \int_{-\infty}^{+\infty} (1 + x_0 + \gamma x_0^2 + (1 + 2\gamma x_0)z_{r,l}^*(\tau - \tau_{01}) + \gamma z_{r,l}^{*2}(\tau - \tau_{01}))v_{r,l}^{*2}(\tau - \tau_{01})d\tau, \quad (90)$$

$$I_{2(r,l)}(\Omega) = \int_{-\infty}^{+\infty} v_{r,l}^*(\tau - \tau_{01})z_{r,l}^*(\tau - \tau_{01}) \sin \Omega\tau d\tau, \quad (91)$$

and

$$I_{3(r,l)}(\omega) = \int_{-\infty}^{+\infty} v_{r,l}^*(\tau - \tau_{01}) \sin \omega \tau d\tau. \quad (92)$$

If $M(\tau_{02})$ has a simple zero then a homoclinic bifurcation occurs. In the case where the amplitude of the parametrical excitation is equal to zero ($h = 0$), the transverse crossings of stable and unstable manifolds exist if the Melnikov function (87) has simple zeros, i.e.,

$$A_{0,r} > \left| \frac{\mu I_{1r}}{I_{3r}(\omega)} \right|, \quad (93)$$

$$A_{0,l} > \left| \frac{\mu I_{1l}}{I_{3l}(\omega)} \right|. \quad (94)$$

From these relations, the threshold values of the parameters can be plotted. The plane (A_0, ω) can be divided in into three domains. We first have the zone where homoclinic intersection do not occur; secondly we have the region where only transverse intersection of Γ_1^s and Γ_1^u (u =unstable, s =stable; Γ_1 for the unperturbed system (71) is depicted in Fig. 16) occur, and thirdly a region where transverse intersection of Γ_1^s and Γ_1^u and Γ_2^s and Γ_2^u (Γ_2 for the unperturbed system (71) is depicted in Fig. 16) occur. If one notes A_c , the smallest value between the values $A_{0,r}$ for the right well and between the values $A_{0,l}$ for the left one; then, as mentioned above, one will have no intersection for values of A_0 lower than A_c . If we now let the amplitude of the parametrical excitation acts on the system ($h \neq 0$), we are interested in parameters h and A_0 for which $M(\tau_{02})$ has simple zero for some value of τ_{02} ; i.e. the condition of homoclinic transition to chaos corresponding to a horseshoe type of cross-section and written as:

$$\forall \tau_{02}, M(\tau_{02}) = 0, : \frac{\partial M(\tau_{02})}{\partial \tau_{02}} \neq 0. \quad (95)$$

These conditions imply transverse intersections of stable and unstable manifolds. Hence, by using a technique proposed by [171] and [172], the Melnikov distance corresponding to the unperturbed system (23), changes sign at some τ_0 . In this case, the condition to be satisfied is

$$A_0 I_{3i}(\omega) - \mu I_{1i} > 0, \quad (96)$$

where $i = r, l$. Moreover, as it is clear from (40) and (41), if

$$h | I_{2i}(\Omega) + x_0 I_{3i}(\Omega) | < A_0 I_{3i}(\omega) - \mu I_{1i}, \quad (97)$$

i.e.,

$$h \leq \frac{| I_{2i}(\Omega) + x_0 I_{3i}(\Omega) |}{A_0 I_{3i}(\omega) - \mu I_{1i}} = h_{cr}, \quad (98)$$

where h_{cr} is the critical parametric amplitude. It is easy to see from Eqs. (88) and (89), that for some τ_o , the Melnikov function will change sign and the situation remains unchanged.

Case of radial electric field in L-H transition under bounded noise excitation: Random Melnikov method

In any real physical system, the presence of external noise cause transitions between previously stable attractors as well as diverse noise-induced phenomena such as multistability, stochastic resonance, multimodality, and stochastic ratchets, to quote a few. Noise comes from great diverse sources: quantum fluctuations in lasers, random switching of ion channels and quasi-random release of neurotransmitter by the synapses in neurons, and finite-size effects in chemical reactions are well-known examples. It is a common practice to apply noise externally in experiments as well as to include external noise sources in theoretical models in order to systematically investigate the role of noise by controlling its features. It is well known that noise-induced transitions are characterized by a qualitative change of the system's state as the intensity of noise acting upon it increases. This change can manifest itself in diverse forms or mechanisms such as either stabilization or destabilization of system equilibrium states (noise-induced multistability) and excitation of oscillations [173]. For a mathematical modelization, the noise function $\vartheta(t)$ could be writted as

$$\vartheta(t) = A_1 \int_{-\infty}^{\infty} S_p(\omega) \exp(i\omega t) d\omega \quad (99)$$

$\vartheta(t)$ has zero mean and oscillate within $[-A_1, A_1]$ with a even fourier spectrum $S_p(\omega)$. Instances of this generic type of noise are: gaussian noise

$$S_p(\omega) \equiv \exp\left(\frac{-\omega^2}{A_2}\right), \quad (100)$$

fractal noise

$$S_p(\omega) \equiv \frac{1}{|\omega|^{A_3}}, \quad 0 < A_3 < \frac{3}{2}, \quad (101)$$

or band-limited noise

$$S_p(\omega) \equiv |\omega| \exp\left(\frac{-|\omega|}{A_4}\right) \quad (102)$$

$\vartheta(t)$ could also be writted as a bounded noise

$$\vartheta(t) = A_5 \cos(\Omega_2 t + \eta(W(t) + \varphi_o)) \quad (103)$$

with

$$S_p(\omega) \equiv \left(\frac{A_5^2 \eta^2}{4\pi}\right) \left(\frac{\omega^2 + \Omega_2^2 + \frac{\eta^4}{4}}{(\omega^2 - \Omega_2^2 - \frac{\eta^4}{4})^2 + \omega^2 \eta^4}\right). \quad (104)$$

Melnikov method has shown to be an easy and effective method to detect chaotic dynamics in nonlinear systems. As mentioned in the preceeding section, the starting point is an autonomous system having one or more hyperbolic fixed points and a non-degenerate homoclinic $(u_{ho}(t), p_{ho}(t))$ and/or heteroclinic $(u_{he}(t), p_{he}(t))$ orbits. Then associated to a given smooth perturbation $\epsilon F(t, u, \dot{u})$ sufficiently small, there is the so called Melnikov function

$$M(t_0) = \int_{-\infty}^{\infty} p_h(t) F(t + t_0, u, p) dt \quad (105)$$

II.2.2 Random Melnikov process

To examine the noisy nonlinear behavior of the system in a stochastic sense, generalized stochastic Melnikov process is developed to analytically demonstrate noise-induced transitions.

Consider as in [174] an one degree-of-freedom Hamiltonian system with light nonlinear damping under both external bounded noise and parametric perturbation.

Let us consider our nonlinear Eq.66 with $u = Q, \dot{u} = P$; and

$$H(Q, P) = \frac{1}{2}P^2 + \frac{1}{2}\omega^2 Q^2 - \frac{1}{4}\alpha_3 Q^4 + \frac{1}{6}\alpha_5 Q^6 \quad (106)$$

with,

$$\begin{aligned} -c(Q, P) &= -\mu - \beta_2 P - \beta_3 Q - \beta_4 QP - \beta_5 Q^2 - \beta_6 P^2 \\ \vartheta(t) &= \cos(\Omega_2 t + \eta W(t) + \eta \varphi_0 + \Theta_0) \end{aligned} \quad (107)$$

and

$$g(Q, P) = -\delta_1 Q ; f_1(t) = \cos(\Omega_1 t) \quad f_2(Q, P) = F_2 \quad (108)$$

It is known that the unperturbed ($\epsilon = 0$) Hamiltonian system possesses two hyperbolic fixed point

$$u_1^\pm = \pm \frac{\sqrt{2\alpha_5 (\alpha_3 - \sqrt{\alpha_3^2 - 4\alpha_5\omega^2})}}{2\alpha_5} \quad (109)$$

, and three other equilibrium points

$$u_2^\pm = \pm \frac{\sqrt{2\alpha_5 (\alpha_3 + \sqrt{\alpha_3^2 - 4\alpha_5\omega^2})}}{2\alpha_5}, u_0 = 0; \quad (110)$$

u_1^\pm are connected themselves by two homoclinic orbits,

$$\begin{aligned} u_{ho}(t) &= \pm \frac{\sqrt{2}u_1 \cosh\left(\frac{T_1 t}{2}\right)}{\sqrt{\xi + \cosh(T_1 t)}} \\ p_{ho}(t) &= \pm \frac{1}{2} \frac{\sqrt{2}u_1 (1 - \xi) T_1 \sinh\left(\frac{T_1 t}{2}\right)}{(\xi + \cosh(T_1 t))^{3/2}} \end{aligned} \quad (111)$$

Also, u_1^+ is connected to u_1^- by a heteroclinic orbit

$$\begin{aligned} u_{he}(t) &= \pm \frac{\sqrt{2}u_1 \sinh\left(\frac{T_1 t}{2}\right)}{\sqrt{-\xi + \cosh(T_1 t)}} \\ p_{he}(t) &= \pm \frac{1}{2} \frac{\sqrt{2}u_1 (1 - \xi) T_1 \cosh\left(\frac{T_1 t}{2}\right)}{(-\xi + \cosh(T_1 t))^{3/2}} \end{aligned} \quad (112)$$

The mean value of random Melnikov process for Eq. (66) can be obtained as follows:

$$M_d = - \int_{-\infty}^{\infty} [P^2 \mu + \beta_2 P^3 + \beta_3 P^2 Q + \beta_4 QP^3 + \beta_5 P^2 Q^2 + \beta_6 P^4 + \delta_1 PQ \cos(\Omega_1 (t + t_0))] dt \quad (113)$$

where, $P(t) = p_{ho}(t)$ or $p_{he}(t)$ and $Q(t) = u_{ho}(t)$ or $u_{he}(t)$; and then, for homoclinic orbits the criterion for possible chaotic phenomenon based on the mean-square method for the stochastic

Melnikov process [175] is

$$-\langle \mu I_1 + I \rangle^2 + \langle \delta_1 I_7 \sin(\Omega_1 t_0) \rangle^2 + \sigma_{zho}^2 = 0 \quad (114)$$

and for heteroclinic orbits the criterion for possible chaotic phenomenon based on the mean-square method is

$$-\langle \mu J_1 + J \rangle^2 + \langle \delta_1 J_7 \sin(\Omega_1 t_0) \rangle^2 + \sigma_{zhe}^2 = 0 \quad (115)$$

where $I = I_3 + I_5 + I_6$ and $J = J_2 + J_5 + J_6$; I_j ($j = 1, 3, 5, 6, 7$); J_i ($i = 1, 2, 5, 6, 7$) are given by in appendix. The above conditions could be simplified into

$$\langle \mu I_1 + I \rangle^2 = \delta_1^2 \langle I_7 \rangle^2 + \sigma_{zho}^2 \quad (116)$$

for homoclinic orbits $(\pm u_{ho}(t), \pm p_{ho}(t))$, and

$$\langle \mu J_1 + J \rangle^2 = \delta_1^2 \langle J_7 \rangle^2 + \sigma_{zhe}^2 \quad (117)$$

for heteroclinic orbits $(\pm u_{he}(t), \pm p_{he}(t))$. Now, let us compute the random part of random Melnikov process with mean square criterion, and evaluate the distance measured along the *homoclinic/heteroclinic* loop between the stable and unstable manifolds of the hyperbolic fixed points of the associated Poincaré map.

Homoclinic orbits

For homoclinic trajectories we have:

$$H_1(\omega) = -j \frac{2 u_1}{T_1} \sin\left(\frac{2 \omega}{T_1}\right) \quad (118)$$

Hence, the random Melnikov process has simple zeros in mean-square sense if

$$\sigma_{zho}^2 = \int_{-\infty}^{\infty} H_1(\omega) \left(\frac{\eta^2}{4\pi}\right) \left(\frac{\omega^2 + \Omega_2^2 + \frac{\eta^4}{4}}{(\omega^2 - \Omega_2^2 - \frac{\eta^4}{4})^2 + \omega^2 \eta^4}\right) d\omega. \quad (119)$$

If the amplitude of linear damping and the amplitude of density perturbation are fixed

$$F_2 \geq \sqrt{\frac{\langle \mu I_1 + I \rangle^2 - \delta_1^2 \langle I_7 \rangle^2}{\sigma_{z0}^2}} \quad (120)$$

with

$$\sigma_{z0}^2 = \int_{-\infty}^{\infty} H_1(\omega) \left(\frac{\eta^2}{4\pi} \right) \left(\frac{\omega^2 + \Omega_2^2 + \frac{\eta^4}{4}}{(\omega^2 - \Omega_2^2 - \frac{\eta^4}{4})^2 + \omega^2 \eta^4} \right) d\omega. \quad (121)$$

Where the parameters I_i are given in the appendix. If the amplitude of bounded noise, the amplitude of density perturbation and the amplitude of linear damping are fixed, we have to resolve numerically the Eq. 116 to have η .

More precisely, this condition provides a domain on the parameter plane (F_2, η) of the controlling radial electric field (which can be viewed as external perturbation) on which the chaotic behavior may be suppressed from the normalized electric field change.

Heteroclinic orbits

For heteroclinic trajectories we have:

$$H_1(\omega) = -j \frac{2\pi u_1 F_2}{T_1} \frac{\omega}{\sinh\left(\frac{\pi \omega}{T_1}\right)} \quad (122)$$

the random Melnikov process has simple zeros in mean-square sense if

$$\sigma_{zhe}^2 = \int_{-\infty}^{\infty} H_1(\omega) \left(\frac{\eta^2}{4\pi} \right) \left(\frac{\omega^2 + \Omega_2^2 + \frac{\eta^4}{4}}{(\omega^2 - \Omega_2^2 - \frac{\eta^4}{4})^2 + \omega^2 \eta^4} \right) d\omega. \quad (123)$$

If the amplitude of linear damping and the amplitude of density perturbation are fixed

$$F_2 \geq \sqrt{\frac{\langle \mu J_1 + J \rangle^2 - \delta_1^2 \langle J_7 \rangle^2}{\sigma_{z1}^2}} \quad (124)$$

with

$$\sigma_{z1}^2 = \int_{-\infty}^{\infty} H_1(\omega) \left(\frac{\eta^2}{4\pi} \right) \left(\frac{\omega^2 + \Omega_2^2 + \frac{\eta^4}{4}}{(\omega^2 - \Omega_2^2 - \frac{\eta^4}{4})^2 + \omega^2 \eta^4} \right) d\omega. \quad (125)$$

Where the parameters J_i are given in the appendix. If the amplitude of bounded noise, the amplitude of density perturbation and the amplitude of linear damping are fixed, we have to resolve numerically the Eq. (117) to have η .

Associated to the general melnikov method that analytically characterise chaos, there are several other numerical method that could be used. Bifurcation diagrams, Lyapunov exponent, correlation dimension, etc., derived on the basis of chaos theory, have been used through numerical simulations, to characterize chaos and its different routes [176].

II.2.3 Response of charge density using multiple scales method

Multiple scale method have been widely used in plasma physics; Das [177] investigated nonlinear oscillations in a hot electron plasma. Davidson [178] treated nonlinear oscillations in a Vlasov-Maxwell plasma. Butler and Gribben [179] discussed nonlinear waves in a nonuniform plasma. Maroli and Pozzoli [180] studied the penetration of high-frequency electromagnetic waves into a slightly ionized plasma. Chen and Lewak [181], Chen [182], and Prasad [183] studied parametric excitation in a plasma. In plasma stability, Frieman and Rutherford [184] developed a kinetic theory for weakly unstable plasmas, while Albright [185] analyzed the stabilization of transverse plasma instability.

Stochastic averaging: Itô-type equation and statistic moment method

Let (Ω, B, P) denote a probability space; i.e., the set Ω is the space of "elementary" outcomes, B is a σ -algebra of subsets of Ω , and P is a probability measure on B [186]. Let $\{W(t), \infty > t \geq 0\}$ denote a family of real-valued random variables defined on the space. Generally, the generic variable ω of the set Ω will not be explicitly written. However, when there is a greater possibility of ambiguity, the ω will be included. Also, $W(\omega, t)$ will denote the value of the random variable $W(t)$ at ω , and $W(\omega, \cdot)$ will denote the path corresponding to ω . The entire process $\{W(t), \infty > t \geq 0\}$ will be denoted by $W(\cdot)$. The process $W(\cdot)$ is said to be a standard Wiener process if it satisfies (a), (b) and (c):

(a) it is a gaussian process;

(b) it has independent, stationary, and normally distributed increments with zero mean value ($E[W(t)] = 0$) and $W(0) = 0$.

(c) $E[W_1(t)W_2(t)] = \sigma^2 t_1, t_1 < t_2$; $E[W_1(t)W_2(t)] = \sigma^2 t_2, t_2 < t_1$, where σ^2 is a positive constant.

$W(t)$ is continuous in L_2 , and could be written

$$\begin{aligned} B(t) &= \int_0^t dB(\tau) \\ B_1(t_1) B_2(t_2) &= \int_0^{t_1} dB(\tau_1) \int_0^{t_2} dB(\tau_2) \end{aligned} \quad (126)$$

Quantities of interest in this subsection are given by the moments $E[X^n]$ since these are often easily calculated. However, probability densities must always vanish as $x \rightarrow \infty$, so, higher moments tell us only about the properties of unlikely large values of X . In practice we find that the most important quantities are related to the first and second moments. In particular, for a single variable X , the variance defined by [187]

$$\mathbf{var}(X) \equiv (\sigma[X])^2 \equiv E[(X - E[X])^2] \quad (127)$$

and as is well known, the variance $\mathbf{var}(X)$ or its square root the standard deviation $\sigma[X]$, is a measure of the degree to which the values of X deviate from the mean value $E[X]$.

It is possible to obtain an approximate solution for multidimensional stochastic nonlinear system. The most frequently used approximation scheme is the equivalent linearization procedure [188]. In the special case of gaussian white noise, this procedure is equivalent to the gaussian closure [189]. Following [190], another generalization of the gaussian closure focuses on the properties of cumulants. Since the third and higher order cumulants of gaussian random variable are zero, gaussian closure is equivalent to neglecting those cumulants above the second order. A more general scheme, the cumulant neglect closure, is based on the premise that successive improvements can be achieved by retaining additionally the third, fourth, and higher order cumulants.

The complexity of directly estimating the probability distribution of nonlinear stochastic systems with Markov transitions rapidly increases toward intractability with the magnitude of the assumed state space. This increase in complexity is magnified in a network setting when there are multiple nodes (compartments) and numerous intensities. The formulation of a partial differential equation that describes the moment-generating function of such systems is immediate, yet the solution to this is often intractable for even the simplest systems, thereby leaving the direct estimation of the moments unattained. Moment-closure methods, however, may be used to specify a functional relationship between the moments of the system, which thereby allows

for the approximation of only a few moments through a closed set of approximating differential equations. These functional relationships are achieved either through the imposition of a known parametric probability distribution on the state space of the system or through the neglect of the high-order cumulants [191].

The n^{th} cumulant of a set of random variables X_1, X_2, \dots, X_n is defined as [192],

$$\kappa_n [X_1, X_2, \dots, X_n] = \frac{1}{i^n} \left[\frac{\partial^n}{\partial \theta_1 \partial \theta_2 \dots \partial \theta_n} \ln [M_{X_1, X_2, \dots, X_n} (\theta_1, \theta_2, \dots, \theta_n)] \right]_{\theta_1 = \theta_2 = \dots = \theta_n = 0} \quad (128)$$

where $i = \sqrt{-1}$, and $M_{X_1, X_2, \dots, X_n} (\theta_1, \theta_2, \dots, \theta_n)$ is the joint characteristic function of random variables X_1, X_2, \dots, X_n given by

$$\begin{aligned} M_{X_1, X_2, \dots, X_n} (\theta_1, \theta_2, \dots, \theta_n) &= E \{ \exp [i (\theta_1 X_1 + \theta_2 X_2 \dots + \theta_n X_n)] \} \\ &= \int_{-\infty}^{\infty} \dots \int_{-\infty}^{\infty} P_{X_1, X_2, \dots, X_n} (x_1, x_2, \dots, x_n) \\ &\quad \times \exp [i (\theta_1 x_1 + \theta_2 x_2 \dots + \theta_n x_n)] dx_1 dx_2 \dots dx_n \end{aligned} \quad (129)$$

and where the logarithm of the complex variable is taken to be the principal value. Eq.(129) implying that the natural logarithm of a characteristic function has a series expansion

$$\begin{aligned} \ln [M_{X_1, X_2, \dots, X_n} (\theta_1, \theta_2, \dots, \theta_n)] &= i\theta_j \kappa_1 [X_j] + \frac{1}{2} (i\theta_j) (i\theta_k) \kappa_2 [X_j, X_k] \\ &\quad + \frac{1}{2} (i\theta_j) (i\theta_k) (i\theta_l) \kappa_3 [X_j, X_k, X_l] + \dots \end{aligned} \quad (130)$$

that all the cumulants involved exist, and that the series converges. The cumulants are related to the statistical moments by [193]

$$\begin{aligned} E [X_j] &= \kappa_1 [X_j] \\ E [X_j, X_k] &= \kappa_2 [X_j, X_k] + \kappa_1 [X_j] \kappa_1 [X_k] \\ E [X_j, X_k, X_l] &= \kappa_3 [X_j, X_k, X_l] + 3 \{ \kappa_1 [X_j] \kappa_2 [X_k, X_l] \}_s + \kappa_1 [X_j] \kappa_1 [X_k] \kappa_1 [X_l] \end{aligned} \quad (131)$$

where $\{ \cdot \}_s$ denotes a symmetrizing operation with respect to all its arguments; that is, an operation that takes the arithmetic mean of different permuted terms similar to the one within braces. By letting $X(t_j) = X_j$, Eq.(130) is then a series expansion of the n^{th} -order log-characteristic function of $X(t)$. Therefore, a random process can also be described by a complete set of cumulants which are functions of various times. Since a cumulant function of an order higher than one represents a measure of correlation of the random process at different times, its value tends to

zero as the t values are separated further from each other. It is then expected that the physical significance of a cumulant decreases as the order increases, and the most important properties of a random process are revealed in the lower order cumulants.

If we consider a nonlinear system

$$\frac{dX_i}{dt} = f_i(\mathbf{X}) + g_{ij}(\mathbf{X}) W_j(t) \quad i = 1, 2, \dots, n \quad j = 1, 2, \dots, m \quad (132)$$

where $W_j(t)$ are gaussian process. Eq. (132) is equivalent to the following set of Itô-type stochastic differential equations:

$$dX_i = \left(f_i + \pi K_{ls} g_{rs} \frac{\partial g_{il}}{\partial X_r} \right) dt + \sqrt{2\pi K_{ls} g_{il} g_{js}} dB_j(t) \quad (133)$$

where $B_j(t)$ are independent unit Wiener processes, and K_{ls} are the cross-spectral density of $W_l(t)$ and $W_s(t)$. Let write $M(X) = X_1^{k_1} X_2^{k_2} \dots X_n^{k_n}$ where the superscripts k_1, k_2, \dots, k_n are non-negative integers. According to the Itô differential rule,

$$dM = \left[\left(f_i + \pi K_{ls} g_{rs} \frac{\partial g_{il}}{\partial X_r} \right) \frac{\partial M}{\partial X_i} + \pi K_{ls} g_{il} g_{js} \frac{\partial^2 M}{\partial X_i \partial X_j} \right] dt + \sqrt{2\pi K_{ls} g_{il} g_{js}} \frac{\partial M}{\partial X_i} dB_j(t) \quad (134)$$

It follows upon taking the ensemble average of Eq.(133) that,

$$\frac{dE[M]}{dt} = E \left[\left(f_i + \pi K_{ls} g_{rs} \frac{\partial g_{il}}{\partial X_r} \right) \frac{\partial M}{\partial X_i} \right] + \pi K_{ls} E \left[g_{il} g_{js} \frac{\partial^2 M}{\partial X_i \partial X_j} \right] \quad (135)$$

The left hand side of Eq. (135) is the time derivative of a statistical moment of order N , where $N = k_1 + k_2 + \dots + k_n$, whereas the right-hand side depends on the functional forms of f_i and g_{jk} .

Questions concerning the meaning of probability and its applications in physics are notoriously subtle. Further, although each of the interpretations of the notion of probability is usually intended to be adequate throughout, independently of context, the various applications of the theory of probability pull in different interpretative directions: some applications, say in decision theory, are amenable to a subjective interpretation of probability as representing an agent's degree of belief, while others, say in genetics, call upon an objective notion of probability that characterizes certain biological phenomena [194].

II.2.4 Response of density perturbation and resonances

Using the method of multiple scales, we then have a second-order nonlinear solution in the form

$$u(T_0, T_1, T_2) = u_0(T_0, T_1, T_2) = A(T_1, T_2) e^{iT_0} + \bar{A}(T_1, T_2) e^{-iT_0} + \epsilon u_1(T_0, T_1, T_2) + \epsilon^2 u_2(T_0, T_1, T_2) \quad (136)$$

where $T_n = \epsilon^n \tau$ and ϵ is a small bookkeeping parameter. We express the nearness of the excitation frequency Ω to the natural frequency by introducing a detuning parameter σ and letting $\Omega = 1 + \epsilon^2 \sigma$. Substituting Eqs. (136) into Eq. (57) and equating coefficients of like powers of ϵ , yield:

$$D_0^2 u_1 + u_1 = -\lambda \left(A^2 (e^{iT_0})^2 + A\bar{A} \right) + cc., \quad (137)$$

where $D_n = \frac{\partial}{\partial T_n}$ and "cc" represents the conjugate complex of the previous terms. Thus, the order ϵ^1 solution can be rewritten in the form

$$u_1(T_0, T_1, T_2) = \frac{1}{3} \lambda A^2 (e^{iT_0})^2 - 2 \lambda A\bar{A} + \frac{1}{3} \lambda \bar{A}^2 (e^{-iT_0})^2 \quad (138)$$

The order ϵ^2 equation becomes

$$D_0^2 u_2 + u_2 = A^3 \left(-\beta - \frac{2}{3} \lambda^2 - i\mu \gamma \right) (e^{iT_0})^3 - (i\mu A + (3\beta + i\mu \gamma) A^2 \bar{A} - \frac{10}{3} \lambda^2 A^2 \bar{A} + 2i \frac{\partial A}{\partial T_2} - \frac{1}{2} A_0 e^{i(\sigma T_2 + \eta W(T_2) + \psi)}) e^{iT_0} - i\mu A^2 (e^{iT_0})^2 + cc., \quad (139)$$

where A and \bar{A} are undetermined complex function. They can be determined by imposing the solvability conditions at the next approximation by eliminating the secular and small-divisor terms. The terms under a bar represent the conjugate complex functions. We want to solve Eq. (57) of the original manuscript, using perturbation theory, treating all the terms multiplied by ϵ as the perturbation. However, the simple iterative method, taking the first order solution plus perturbation terms, fails: secular terms appear and cause the perturbative corrections to grow linearly in time, this violates the assumption that the perturbation terms give small corrections. In the method of multiple scales, the amplitude is allowed to vary slowly, which makes it possible to eliminate the secular terms that cause unbounded perturbations. $A(T_2)$ is a function of slow time T_2 , it is treated as constant with respect to the fast oscillations, on the time scale

τ ; ϵ^2 is the parameter measuring the proximity to the bifurcation. By deriving equations on the slow T_2 scale for the amplitude u or envelope described by $A(T_2)$, one gets an asymptotic approximation for the process near the bifurcation, that is for $\epsilon^2 \ll 1$. Depending on the function $A(T_2)$, every particular solution of Eq. (139) contains term proportional to $T_0 e^{iT_0}$, the so called secular term. Thus $\epsilon^2 u_2$ can dominate u_0 for large τ , resulting in abnormal expansion. Notice that the right side of Eq. (139) contains a term proportional to e^{iT_0} which acts like a forcing at the resonant frequency of the oscillator. We choose the function A , so that secular terms are eliminated from u_0 and thereby obtain a uniformly valid expansion, by eliminating resonant forcing of Eq. (139). Eliminating the terms that produce secular terms in the solution yields

$$i\mu A + (3\beta + i\mu\gamma - \frac{10}{3}\lambda^2)A^2\bar{A} + 2i\frac{\partial A}{\partial T_2} - \frac{1}{2}A_0 e^{i(\sigma T_2 + \eta W(T_2) + \psi)} = 0 \quad (140)$$

To construct the modulation equations, we introduce the polar transformation $A(T_2) = a(T_2) e^{i\varphi(T_2)}$, $\bar{A}(T_2) = a(T_2) e^{-i\varphi(T_2)}$ and substitute it into Eq. (140), then we separate the real and imaginary parts of the outcome to obtain

$$\begin{aligned} 2\frac{da}{dT_2} + \mu a + \mu\gamma a^3 - \frac{1}{2}A_0 \sin(\theta) &= 0 \\ -2a\frac{d\varphi}{dT_2} + (3\beta - \frac{10}{3}\lambda^2)a^3 - \frac{1}{2}A_0 \cos(\theta) &= 0 \end{aligned} \quad (141)$$

where $\theta = \sigma T_2 + \eta W(T_2) + \psi - \varphi$.

Noise-free case

In the noise-free case, we have $\eta = 0$; $\psi = 0$; then the following system is obtained

$$\begin{aligned} 2\frac{da}{dT_2} + \mu a + \mu\gamma a^3 + \frac{1}{2}A_0 \sin(-\sigma T_2 + \varphi) &= 0 \\ -2a\frac{d\varphi}{dT_2} + 3\beta a^3 - \frac{10}{3}a^3\lambda^2 - \frac{1}{2}A_0 \cos(\sigma T_2 - \varphi) &= 0 \end{aligned} \quad (142)$$

By letting $\varphi(T_2) = \sigma T_2 - \chi(T_2)$, we obtain

$$\begin{aligned} 2\frac{da}{dT_2} + \mu a + \mu\gamma a^3 &= \frac{1}{2}A_0 \sin(\chi) \\ 2a\left(\frac{d\chi}{dT_2} - \sigma\right) + 3\beta a^3 - \frac{10}{3}a^3\lambda^2 &= \frac{1}{2}A_0 \cos(\chi) \end{aligned} \quad (143)$$

For the steady-state response, $\frac{da}{dT_2} = 0$, $\frac{d\varphi}{dT_2} = 0$. It follows from Eq. (143) that

$$n_1 a_0^6 + n_2 a_0^4 + n_3 a_0^2 + \frac{1}{4} A_0^2 = 0 \quad (144)$$

where a_0 is the steady-state amplitude and phase of the response and,

$$-\mu^2 \gamma^2 + (3\beta - \frac{10}{3} \lambda^2)^2 = n_1; \quad -2\mu^2 \gamma - 4\sigma(3\beta - \frac{10}{3} \lambda^2) = n_2; \quad -\mu^2 + 4\sigma^2 = n_3 \quad (145)$$

Thus, the approximation periodic solution can be rewritten in the form

$$\begin{aligned} u(T_0, T_2) = & a e^{i(\sigma T_2 - \chi)} e^{iT_0} + \frac{1}{3} \lambda a^2 \left(e^{i(\sigma T_2 - \chi)} \right)^2 (e^{iT_0})^2 + \frac{1}{12} a^3 \left(e^{i(\sigma T_2 - \chi)} \right)^3 \lambda^2 \\ & + \frac{1}{3} \lambda a^2 \left(e^{-i(\sigma T_2 - \chi)} \right)^2 (e^{-iT_0})^2 + \left(\frac{1}{8} \beta a^3 \left(e^{i(\sigma T_2 - \chi)} \right)^3 - 2\lambda a^2 \right. \\ & \left. + \frac{1}{8} i\mu\gamma a^3 \left(e^{i(\sigma T_2 - \chi)} \right)^3 \right) (e^{iT_0})^3 + \frac{1}{3} i\mu a^2 \left(e^{i(\sigma T_2 - \chi)} \right)^2 (e^{iT_0})^2 + cc. \end{aligned} \quad (146)$$

Noisy case

In the noisy case, we have $\eta \neq 0$; $\psi \neq 0$. By letting

$$\varphi(T_2) = \eta W(T_2) + \psi + \sigma T_2 - \chi(T_2) \quad (147)$$

we obtain [145] the following equations

$$\begin{aligned} 2da &= (-\mu a - \mu\gamma a^3 + \frac{1}{2} A_0 \sin(\chi)) dT_2 \\ 2ad\chi &= \left(\frac{10}{3} a^3 \lambda^2 + 2a\sigma - 3\beta a^3 + \frac{1}{2} A_0 \cos(\chi) \right) dT_2 + 2a\eta dW \end{aligned} \quad (148)$$

To study the process stability, we assume that each equilibrium state is submitted to a small perturbation as follows: $a(T_2) = a_0 + a_1(T_2)$ and $\chi(T_2) = \chi_0 + \chi_1(T_2)$, then, the following set of Ito-type stochastic differential equations:

$$\begin{aligned} da_1 &= \left(\left(-a_0 \sigma + \frac{3}{2} \beta a_0^3 - \frac{5}{3} a_0^3 \lambda^2 \right) \chi_1 + \left(-\frac{3}{2} \mu \gamma a_0^2 - \frac{1}{2} \mu \right) a_1 \right) dT_2 \\ d\chi_1 &= \left(\left(-\frac{1}{2} \mu \gamma a_0^2 - \frac{1}{2} \mu \right) \chi_1 + \left(\frac{\sigma}{a_0} + 5 a_0 \lambda^2 - \frac{9}{2} a_0 \beta \right) a_1 \right) dT_2 + \eta dW. \end{aligned} \quad (149)$$

Assuming $a_1 = X_1$; $\chi_1 = X_2$, Eq. (149) becomes

$$\begin{aligned} dX_1 &= \left(\left(-a_0 \sigma + \frac{3}{2} \beta a_0^3 - \frac{5}{3} a_0^3 \lambda^2 \right) X_1 + \left(-\frac{3}{2} \mu \gamma a_0^2 - \frac{1}{2} \mu \right) X_2 \right) dT_2 \\ dX_2 &= \left(\left(-\frac{1}{2} \mu \gamma a_0^2 - \frac{1}{2} \mu \right) X_1 + \left(\frac{\sigma}{a_0} - \frac{9}{2} a_0 \beta + 5 a_0 \lambda^2 \right) X_2 \right) dT_2 + \eta dW \end{aligned} \quad (150)$$

The first order and second order moments can be obtained by moment method [145]. Let $\rho_{\zeta\tau} = E(X_1^\zeta X_2^\tau)$ where the superscripts ζ, τ are nonnegative integers; according to Ito differential rule, it follows upon taking the ensemble average.

$$\begin{aligned} \frac{d\rho_{\zeta\tau}(T_2)}{dT_2} &= E \left(\left(\left(-a_0 \sigma + \frac{3}{2} \beta a_0^3 - \frac{5}{3} a_0^3 \lambda^2 \right) X_1 + \left(-\frac{3}{2} \mu \gamma a_0^2 - \frac{1}{2} \mu \right) X_2 \right) X_1^{\zeta-1} X_2^\tau \right) \\ &\quad + E \left(\left(\left(-\frac{1}{2} \mu \gamma a_0^2 - \frac{1}{2} \mu \right) X_1 + \left(\frac{\sigma}{a_0} - \frac{9}{2} a_0 \beta + 5 a_0 \lambda^2 \right) X_2 \right) X_1^\zeta X_2^{\tau-1} \right) \end{aligned} \quad (151)$$

The left-hand side of (151) is the time derivative of the statistical moment of order ϑ , $\vartheta = \zeta + \tau$, whereas the right-hand side depends on the functional form of f_1, f_2, g , given by

$$\begin{aligned} f_1 &= \left(-a_0 \sigma + \frac{3}{2} \beta a_0^3 - \frac{5}{3} a_0^3 \lambda^2 \right) X_1 + \left(-\frac{3}{2} \mu \gamma a_0^2 - \frac{1}{2} \mu \right) X_2; \\ f_2 &= \left(-\frac{1}{2} \mu \gamma a_0^2 - \frac{1}{2} \mu \right) X_1 + \left(\frac{\sigma}{a_0} - \frac{9}{2} a_0 \beta + 5 a_0 \lambda^2 \right) X_2; \quad g = \eta \end{aligned} \quad (152)$$

As f_1, f_2, g are linear the right-hand side of Eq. (151) contains only the ϑ th and lower order statistical moments. We then obtain the following differential equations for the statistical moments:

$$\begin{aligned} \frac{d\rho_{10}}{dT_2} &= \left(-a_0 \sigma + \frac{3}{2} \beta a_0^3 - \frac{5}{3} a_0^3 \lambda^2 \right) \rho_{01} + \left(-\frac{3}{2} \mu \gamma a_0^2 - \frac{1}{2} \mu \right) \rho_{10} \\ \frac{d\rho_{01}}{dT_2} &= \left(-\frac{1}{2} \mu \gamma a_0^2 - \frac{1}{2} \mu \right) \rho_{01} + \left(\frac{\sigma}{a_0} - \frac{9}{2} a_0 \beta + 5 a_0 \lambda^2 \right) \rho_{10} \end{aligned} \quad (153)$$

the second order steady state moments ρ_{20}, ρ_{11} and ρ_{02} satisfy the following equations

$$\begin{aligned} \frac{d\rho_{20}}{dT_2} &= 2\Gamma_1 \rho_{11} + 2\Gamma_2 \rho_{20} \\ \frac{d\rho_{11}}{dT_2} &= \Gamma_3 \rho_{02} + \Gamma_4 \rho_{11} + \Gamma_5 \rho_{20} \\ \frac{d\rho_{02}}{dT_2} &= \Gamma_6 \rho_{02} + \Gamma_7 \rho_{11} + 2\pi K_{22} \eta^2 \end{aligned} \quad (154)$$

where,

$$\Gamma_1 = -a_0 \sigma + \frac{3}{2} \beta a_0^3 - \frac{5}{3} a_0^3 \lambda^2; \quad \Gamma_2 = -\frac{3}{2} \mu \gamma a_0^2 - \frac{1}{2} \mu; \quad \Gamma_3 = -a_0 \sigma + \frac{3}{2} \beta a_0^3 - \frac{5}{3} a_0^3 \lambda^2 \quad (155)$$

$$\begin{aligned}\Gamma_4 &= -2\mu\gamma a_0^2 - \mu; \quad \Gamma_5 = \frac{\sigma}{a_0} - \frac{9}{2}a_0\beta + 5a_0\lambda^2 \\ \Gamma_6 &= 2 - \frac{1}{2}\mu\gamma a_0^2 - \frac{1}{2}\mu; \quad \Gamma_7 = 2\frac{\sigma}{a_0} - \frac{9}{2}a_0\beta + 5a_0\lambda^2\end{aligned}\quad (156)$$

and K_{22} is the cross-spectral density of W and itself. For stationary solutions, the statistical moments are constant, and their time derivatives are equal to zero. Eqs. (153), (154) then reduce to algebraic equations. Furthermore, it is obvious that $\rho_{10} = 0$. We then have by substitution the following results

$$\rho_{11} = -2\frac{\pi K_{22}\eta^2\Gamma_2\Gamma_3}{-\Gamma_6\Gamma_4\Gamma_2 + \Gamma_6\Gamma_5\Gamma_1 + \Gamma_7\Gamma_2\Gamma_3}\quad (157)$$

$$\rho_{02} = -2\frac{\pi K_{22}\eta^2(-\Gamma_4\Gamma_2 + \Gamma_5\Gamma_1)}{-\Gamma_6\Gamma_4\Gamma_2 + \Gamma_6\Gamma_5\Gamma_1 + \Gamma_7\Gamma_2\Gamma_3}\quad (158)$$

$$\rho_{20} = 2\frac{\pi K_{22}\eta^2\Gamma_3\Gamma_1}{-\Gamma_6\Gamma_4\Gamma_2 + \Gamma_6\Gamma_5\Gamma_1 + \Gamma_7\Gamma_2\Gamma_3}\quad (159)$$

The necessary conditions for the existence of the second order moments of the response are $\rho_{02} \geq 0$ and $\rho_{20} \geq 0$.

II.2.5 Stability of equilibrium states and statistic moments

To assess the stability of the resulting solutions, we sketch $a(T_2) = a_0 + a_1(T_2)$ and $\chi(T_2) = \chi_0 + \chi_1(T_2)$ where $a_1(T_2)$ and $\chi_1(T_2)$ are slight variations. Inserting these equations into Eq. (143), and canceling nonlinear terms enables us to obtain

$$\frac{da_1}{dT_2} + \frac{\mu}{2}a_1 + \frac{3}{2}\mu\gamma a_1 a_0^2 - \frac{3}{2}a_0^3\chi_1\beta + \frac{5}{3}a_0^3\chi_1\lambda^2 + a_0\chi_1\sigma = 0\quad (160)$$

$$2a_0\frac{d\chi_1}{dT_2} + 9\beta a_1 a_0^2 - 10\lambda^2 a_1 a_0^2 - 2a_1\sigma + \mu a_0\chi_1 + \mu a_0^3\chi_1\gamma = 0$$

Using $a_1(T_2) = c_1 e^{\xi T_2}$ and $\chi_1(T_2) = c_2 e^{\xi T_2}$ we obtain the following system

$$a_0\left(\frac{10}{3}a_0^2\lambda^2 + 2\sigma - 3\beta a_0^2\right)c_2 + (2\xi + \mu + 3\mu\gamma a_0^2)c_1 = 0\quad (161)$$

$$a_0(\mu + \mu\gamma a_0^2 + 2\xi)c_2 + (-2\sigma + 9\beta a_0^2 - 10\lambda^2 a_0^2)c_1 = 0$$

The stability process depends on the sign of eigenvalues of Eq. (160), which are given through the following characteristic equation:

$$\begin{aligned} & \xi^2 + \mu (1 + 2\gamma a_0^2) \xi + \frac{\mu^2}{4} (1 + \gamma a_0^2) (1 + 3\gamma a_0) \\ & - \left(\left(\frac{10}{3} \lambda^2 - 3\beta \right) a_0^2 + 2\sigma \right) \left(-\frac{\sigma}{2} + \left(\frac{9}{4} \beta - \frac{5}{2} \lambda^2 \right) a_0^2 \right) = 0 \end{aligned} \quad (162)$$

Solving this equation might not be difficult, but for the stability, we only need the sign of the eigenvalues. We know that a steady point is stable if the real part of ξ is < 0 for all ξ . Important criteria that gives necessary and sufficient conditions for all the roots of the characteristic polynomial (162) (with real coefficients) to lie in the left half of the complex plane are known as the Routh-Hurwitz criteria. The stability condition could then be established by these criteria. Applying it, the necessary conditions for the steady states of the response to be stable are:

$$\mu (1 + 2\gamma a_0^2) > 0 \quad (163)$$

$$-\frac{1}{4} \left(\frac{10}{3} a_0^2 \lambda^2 + 2\sigma - 3\beta a_0^2 \right) (-2\sigma + 9\beta a_0^2 - 10\lambda^2 a_0^2) + \frac{\mu^2}{4} (1 + \gamma a_0^2) (1 + 3\gamma a_0) > 0 \quad (164)$$

The preceding discussion aims at demonstrating that the systems can exhibit primary resonances at a large number of frequencies. Depending on parameters values, these resonances may occur at frequencies that are near the natural frequency. To study the stability of equilibrium state, we let $\rho_{20}(T_2) = c_1 e^{\xi T_2}$, $\rho_{11}(T_2) = c_2 e^{\xi T_2}$, $\rho_{02}(T_2) = c_3 e^{\xi T_2}$; we then obtain,

$$M \begin{pmatrix} c_1 \\ c_2 \\ c_3 \end{pmatrix} = \begin{pmatrix} 0 \\ 0 \\ 0 \end{pmatrix} \quad (165)$$

where

$$M = \begin{pmatrix} 2\Gamma_2 - \xi & 2\Gamma_1 & 0 \\ \Gamma_5 & \Gamma_4 - \xi & \Gamma_3 \\ 0 & \Gamma_7 & \Gamma_6 - \xi \end{pmatrix}$$

The characteristic equation for our system, can be easily obtained:

$$\begin{aligned} \Delta(\xi) = & \xi^3 + (-2 \Gamma_2 - \Gamma_4 - \Gamma_6) \xi^2 + (2 \Gamma_4 \Gamma_2 - 2 \Gamma_5 \Gamma_1 + \Gamma_4 \Gamma_6 + 2 \Gamma_2 \Gamma_6 - \Gamma_3 \Gamma_7) \xi \\ & - 2 \Gamma_6 \Gamma_4 \Gamma_2 + 2 \Gamma_6 \Gamma_5 \Gamma_1 + 2 \Gamma_7 \Gamma_2 \Gamma_3 \end{aligned} \quad (166)$$

The necessary and sufficient condition for the second order moments of the response to be stable is that the coefficient matrix M must be negative definite. Applying Routh-Hurwitz criterion, the necessary conditions for the second order moments of the response to be stable are:

$$-2 \Gamma_2 - \Gamma_4 - \Gamma_6 > 0; \quad 2 \Gamma_4 \Gamma_2 - 2 \Gamma_5 \Gamma_1 + \Gamma_4 \Gamma_6 + 2 \Gamma_2 \Gamma_6 - \Gamma_3 \Gamma_7 > 0 \quad (167)$$

$$-2 \Gamma_6 \Gamma_4 \Gamma_2 + 2 \Gamma_6 \Gamma_5 \Gamma_1 + 2 \Gamma_7 \Gamma_2 \Gamma_3 > 0 \quad (168)$$

$$\begin{aligned} -2 \Gamma_6 \Gamma_4 \Gamma_2 + 2 \Gamma_6 \Gamma_5 \Gamma_1 + 2 \Gamma_7 \Gamma_2 \Gamma_3 < & (-2 \Gamma_2 - \Gamma_4 - \Gamma_6)(2 \Gamma_4 \Gamma_2 - 2 \Gamma_5 \Gamma_1 \\ & + \Gamma_4 \Gamma_6 + 2 \Gamma_2 \Gamma_6 - \Gamma_3 \Gamma_7) \end{aligned} \quad (169)$$

We then obtain the total statistic moments by combining the steady state of the statistical moments given by Eqs. (153) with Eq.(159) as follows

$$\rho_a = a_0^2 + \frac{\eta^2 \Gamma_3 \Gamma_1}{-\Gamma_6 \Gamma_4 \Gamma_2 + \Gamma_6 \Gamma_5 \Gamma_1 + \Gamma_7 \Gamma_2 \Gamma_3} \quad (170)$$

Probabilistic analysis has many major benefits in understanding the practical behavior of a structure, the influence of parameters on the structure behavior, and the estimation of the structural reliability [195]. There is a plethora evidence from simulation and experiment that plasma turbulence is highly intermittent, and that turbulent transport has a fundamentally "bursty" character. it is thus necessary to develop a probabilistic theory of plasma transport [196, 197]. Probabilistic theory have already been employed for data analysis in steady-state fusion devices, such as Wendelstein 7-X [198]. A statistical theory of Vlasov turbulence was constructed by Diamond et al. in [199].

A numerical package (following others algorithms [200]), "Moment Closure" was proposed [201] to provide an efficient mechanism to generate the closure differential equations and closure approximations of the cumulants of a stochastic Markov system, by neglecting those cumulants that exceed a user-defined level.

Sanae-I. Itoh et al. [202] have analyzed a statistical model for the bifurcation of the radial

electric field E_r in view of describing L-H transitions of tokamak plasmas. Noise in microfluctuations was shown to lead to random changes of E_r if a deterministic approach allows for more than one solution. They also obtain the probability density function for and the ensemble average of E_r . The L-to-H and the H-to-L transition probabilities were calculated, and the effective phase limit which deviate from Maxwell's rule was derived.

If system (135) is asymptotically stable, then the motion tends to statistical stationarity. At the same stationary state, the statistical moment are independent of time, and Eq. (135) reduces to an algebraic equation.

For numerical simulation, we use the pseudorandom signal given by Shinozuka [203]. The essential feature of Shinozuka's approach is that a random process can be simulated by a series of cosine functions with random frequency. The density function (or joint density function) of the random frequency is derived from the specified cross-spectral density matrix for multivariate process or from the specified spectral density function for multidimensional process [204]. Each physical realization of noise represented by $W(\tau) + \psi = \vartheta_b(\tau)$ can be approximated by

$$\vartheta_b(\tau) = A \sum_{k=1}^N \cos(\omega_k \tau + \varphi_k) \quad (171)$$

where $A = \sqrt{\frac{4\omega_0 S_0}{N}}$, ω_k ($k = 1, 2, \dots, N$) are independent and nonnegative random variables over the interval $[\omega_l, \omega_r]$, $\Delta\omega = 2/N$ is the frequency increment, φ_k ($k = 1, 2, \dots, N$) are identically uniformly distributed over the interval $[0, 2\pi)$ and N is a fixed positive integer. For a large positive integer N , the physical realization generated by Eq. (171) is almost ergodic, and numerical results show that the influence of this large integer can be neglected [204]. The duration of time is not concerned with the sum in Eq. (171)

II.3 Conclusion

In this chapter, we have described the mathematical modeling of the dynamics of plasma density and electric field in L-H transition, based on the Vlasov formulation and quasineutrality. We have also sketched some analytical and numerical methods used. These methods are used to obtain the results presented in chapter III.

RESULTS AND DISCUSSION

In this chapter we present and discuss the main results of our work, using numerical simulations. The first section deals with transition to chaos in plasma density with asymmetric double-well potential for parametric and external harmonic oscillations, the second section deals with the effect of external bounded noise on nonlinear dynamics of plasma density and the third section is reserved to the global bifurcation of mean electric field in plasma L-H transition under external bounded noise excitation.

III.1 Transition to chaos in plasma density with asymmetric double-well potential for parametric and external harmonic oscillations

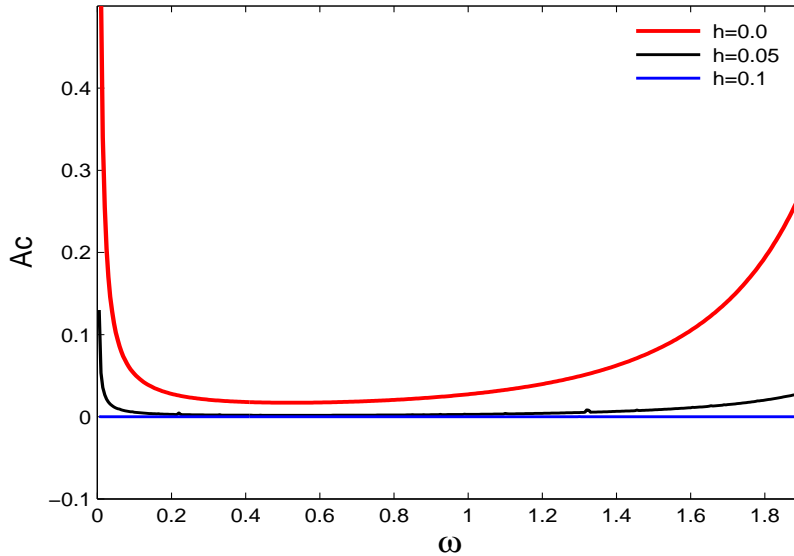


Figure 17: Critical amplitude versus the frequency ω of the right well for $\mu = 1.0$, $\gamma = 5.0$, $\beta = 0.25$, $\lambda = 1.15$, $\Omega = 0.66114$; and $h = 0.0$ (red); $h = 0.05$ (black); $h = 0.1$ (blue).

The results of Eq. (98) indicate that the system dynamics undergo an homoclinic bifurcation at $h = h_{cr}$, resulting in the loss of energy density confining in plasma device. In order to see

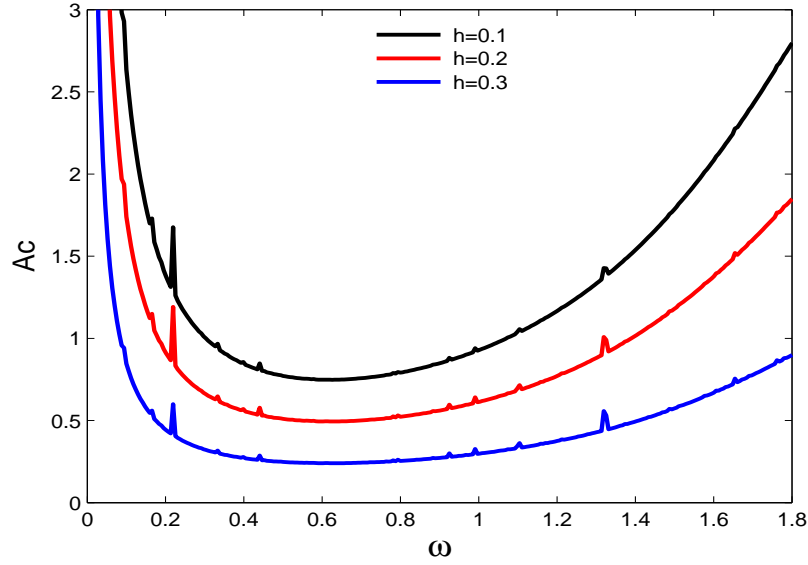


Figure 18: Critical amplitude versus the frequency ω the left well for $\mu = 1.0$, $\gamma = 5.0$, $\beta = 0.25$, $\lambda = 1.15$, $\Omega = 0.66114$; and $h = 0.1$ (black), $h = 0.2$ (red), $h = 0.3$ (blue).

clearly the dependence of the chaotic regions on the system parameters, starting from Eq. (98), we plot the semi-analytically critical force A_c versus the frequency ω for the right well in Fig. 17, and for the left well in Fig. 18. As shown in Fig. 17, when the modulation depth h is very low, the system could exhibit a chaotic behavior for very low values of A_0 . If h is increased the critical value A_c of A_0 also increase. From Fig. 18, the system will have a chaotic set, which may or may not be an attractor for low value of A_0 . In Fig. 18, if we select a value of h , the areas above the curves correspond to Melnikov chaotic regions in which the evolution of the density has the properties of Smale-horseshoe chaos; those below denote regions of regular motion. From Fig. 18, we observe that for low modulation depth $h = 0.1$, the threshold value of the external force intensity is approximately obtained as $A_c \approx 1.181$ when $\mu = 1.0$; this implies that, for low modulation depth the criterion (98) can indeed be satisfied. If the modulation depth is increased to about 0.2 or 0.3, from Eq. (98), the critical value becomes $A_c \approx 0.958$ or $A_c \approx 0.5315$ respectively. If γ becomes too large, the threshold may become very large and so, the perturbational treatment becomes invalid. On the other hand, from Fig. 18, we find that a larger h value is associated with a lower A_c value, but not linearly.

Bifurcations diagram and maximum lyapounov exponent

We now use the numerical simulations including bifurcation diagrams and Lyapunov exponents to examine the consistence with the theoretical analysis and finding new complicated behaviors of Eq. (71). As mentioned before, the maximum Lyapunov exponents characterize quantitatively the dynamics of a system representing the asymptotic rate of exponential convergence or divergence of nearby orbits in phase space. Exponential divergence of nearby orbits implies that the dynamical behavior is sensitive to initial conditions. A positive maximum Lyapunov exponent for certain situations can be considered as a sign of chaos [205]. In fact, positive largest Lyapunov exponent doesn't, in general, indicate chaos [206]. The fourth order Runge-Kutta algorithm is used to check the threshold of harmonic excitation amplitude for onset of possible chaos obtained for system (71). Results have been made and are displayed in Figs. 19 and 20. Meanwhile, the thresholds of excitation amplitude for onset of chaos are obtained by letting the maximum Lyapunov exponents vanish. It is important to determine what type of chaos occurs. Transient (temporary) chaos, attracting (sustained) chaos, or both could exist. Both attracting and transient chaos are found; but due to its impact in practical experimental design and applications, sustained chaos is the main interest.

Holding $\omega = 1.33$, a series of bifurcation diagrams with their corresponding maximum Lyapunov exponent are displayed in Figs. 19 and 20, showing the dependance of chaos occurrence on A_0 , for $0.1 \leq h \leq 0.4$. With $\omega = 1.332$, a series of bifurcation diagrams and corresponding lyapunov exponent (see Fig. 21), with initial conditions taken in the right well, are depicted to examine the influence of the modulation depth h . We wish to find other bifurcation structures of the system (71). With parameter chosen as above and initial conditions taken in the right well, for $h = 0.0$, numerical bifurcation analysis with ω treated as the bifurcation parameter reveals transitions between periodic and chaotic states. When increasing ω for a sufficient amount of time up to transients, Fig. 23 is depicted. Due to the initial conditions ($A_0 = 0.0 - 2.0$), there is no coexisting attractors when there is a very large difference between the external force amplitude values.

Poincaré maps

The poincaré bifurcation is a common non linear process through which a system changes from a fixed point to a limit cycle state. Equation (70) is integrated numerically under the initial

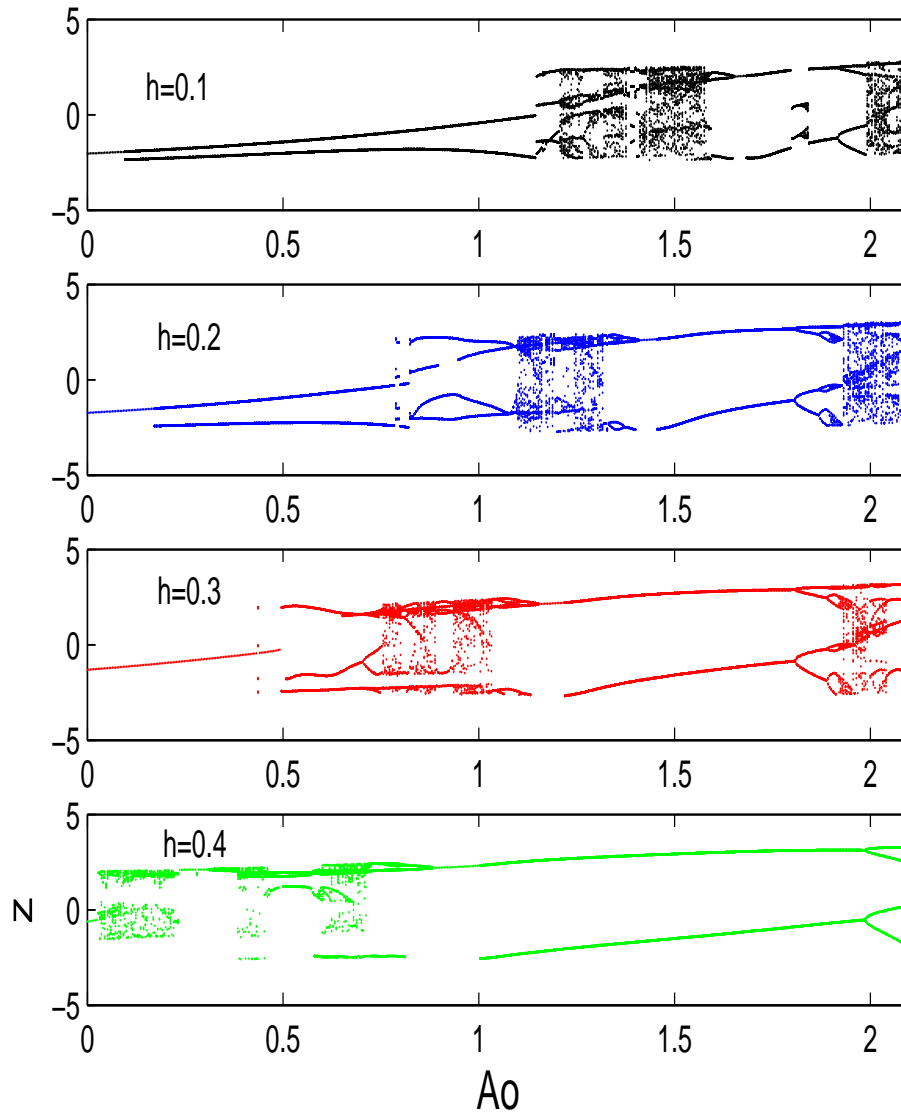


Figure 19: Bifurcation diagrams of the system (71) for different values of h , with initial condition taken in the left well; $\omega = 1.33$ and $\Omega = 0.66114$. Other parameters are those of Fig. 4.

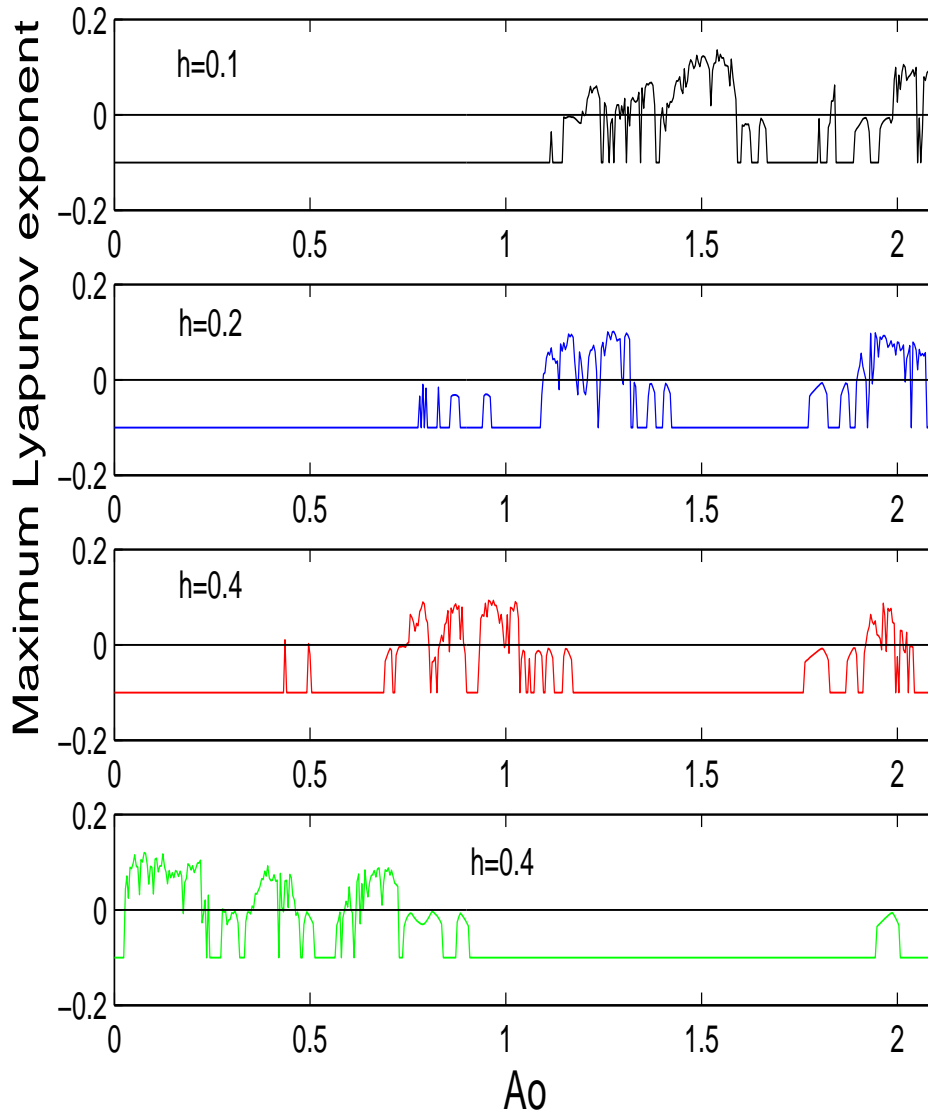


Figure 20: Corresponding maximum Lyapunov curves of the bifurcation diagrams (Fig.(19)). Other parameters are those of Fig. 4.

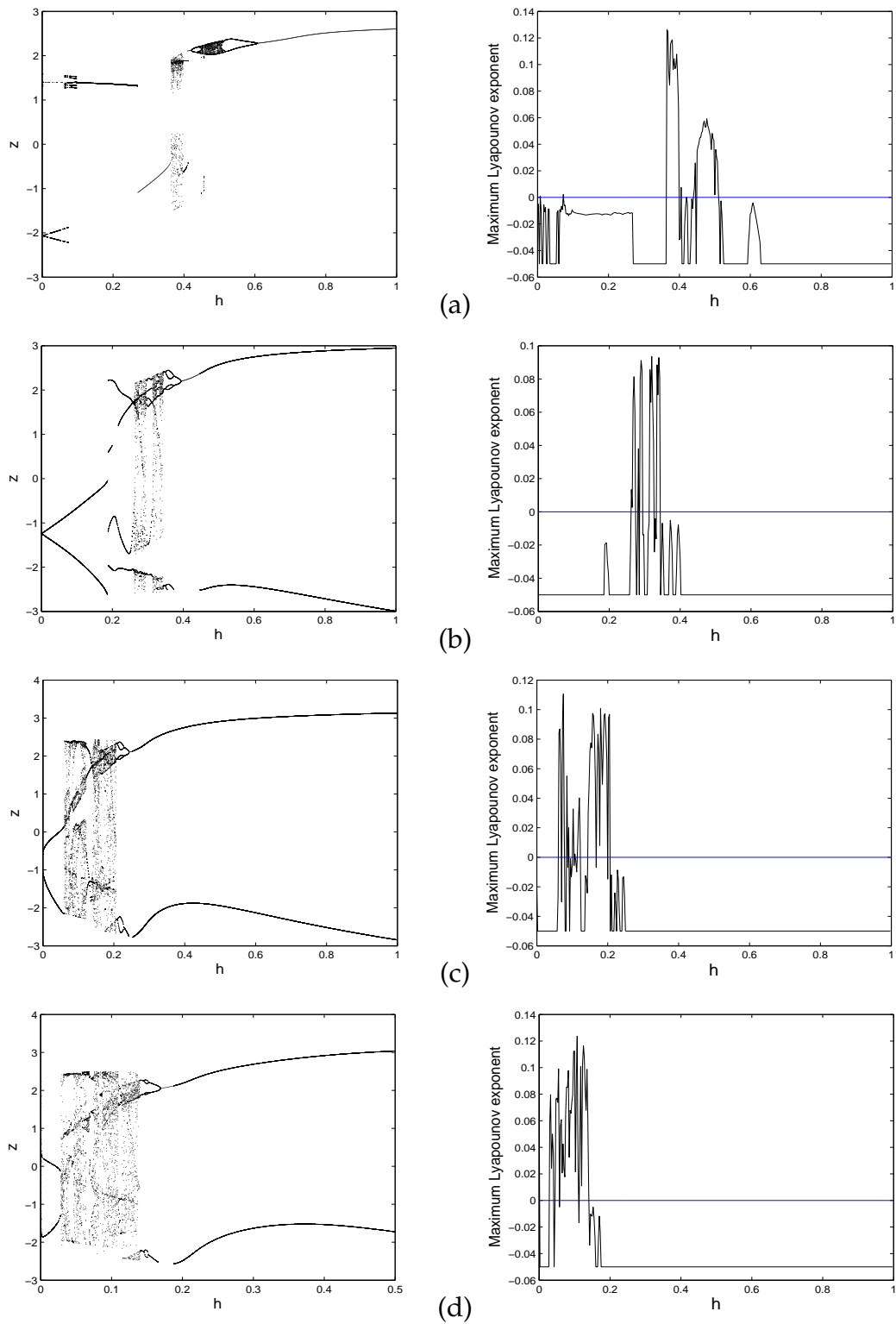


Figure 21: Bifurcation diagrams of the system (71) and the corresponding maximum Lyapunov exponent calculate for h varying, with initial condition taken in the right well, $\Omega = 0.66114$ and $\omega = 1.33$ for (a) $A_0 = 0.224$, (b) $A_0 = 0.9$, (c) $A_0 = 1.3$ and (d) $A_0 = 1.485$. Other parameters are those of Fig. 4.

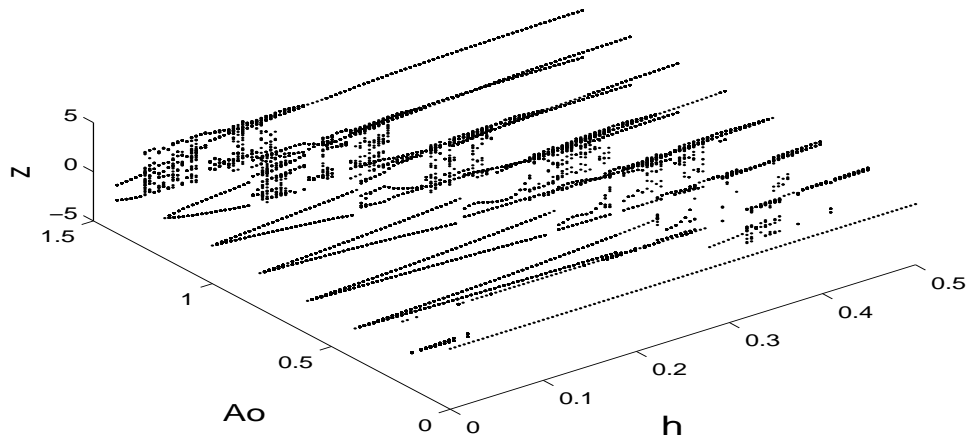


Figure 22: Bifurcation diagrams of the nonlinear system (71) with initial condition taken in the right well for $\Omega = 0.66114, \omega = 1.33$. System parameters as for Figure 4.

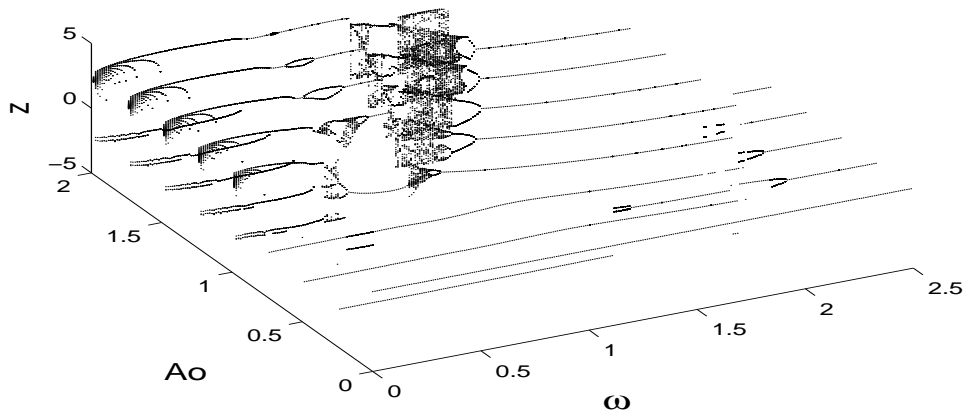


Figure 23: Bifurcation diagrams of the nonlinear system (71) with initial condition taken in the right well for $\Omega = 0.66114, h = 0.0, \omega = 1.33$. System parameters as for Figure 4.

condition taken in the right well by using four-order-fixed step Runge-Kutta method. In order to gain better insights into chaos features, various kinds of attractors and strange attractors which are generated by sampling the system stroboscopically with a period $T = 2\pi/\omega$ are depicted. The Poincaré maps for different values of the external excitation amplitude in (z, v) plane for

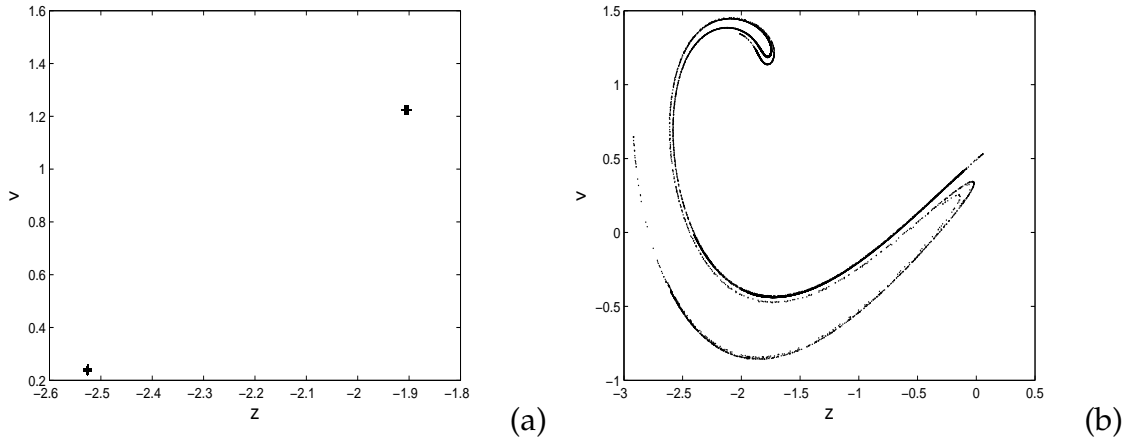


Figure 24: Influence of the external amplitude on the Poincaré maps of the system (a) a non chaotic states for $A_0 = 1.40$ (b) chaotic attractor for $A_0 = 1.480$. System parameters as for Figure 4.

initial condition taken in the right well are depicted in Fig. 24.

Bassin of attraction

A basin of attraction is defined as initial conditions, which are attracted to a fixed point or an given set. We want to study the effect of the modulation depth, and how the basins of attraction are affected as the amplitude of excitation A_0 is increased. To numerically generate basins we take initial conditions in a plane element $(z, v) = (-6.4 \times -4.4)$. We first consider the damping oscillation $\mu = 1.0$ with the focused set chosen in the left well, when time increases from the initial conditions z_0 and v_0 . If the trajectory is attracted out of that well, the lattice element of the initial condition is drawn in white, otherwise in blue(online) for Fig. 25. The boundary of the color specified the boundary of the attractor.

III.1.1 Discussion

From Fig. 19, when $h = 0.1$, with initials conditions taken in the left well, for values of $A_0 \leq 1.208$ one observes a period doubling bifurcation as A_0 is increased from zero with a disruption followed by an period multiplication. It is also shown that the transition to chaotic state occurs

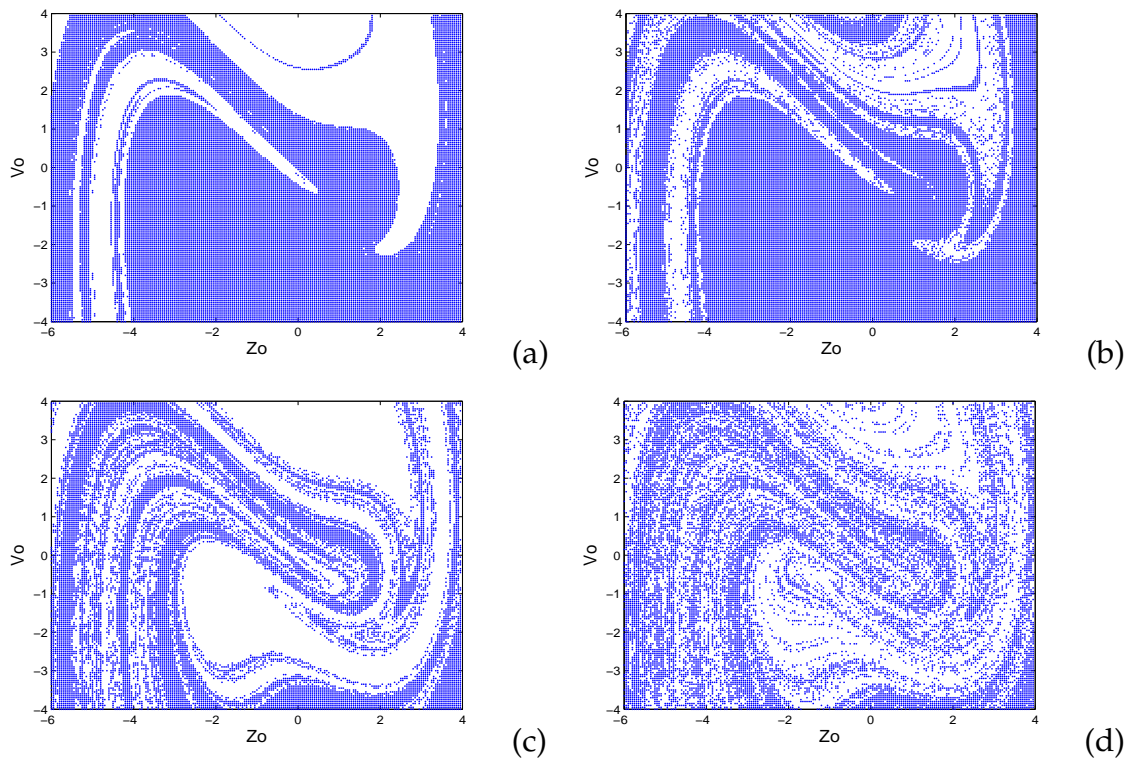


Figure 25: Basin of attraction for strong external forcing. $\ddot{z} = -0.25 \left\{ z^3 - \frac{3}{4}(z_1 + z_2)z^2 + \frac{1}{2}(z_1 z_2)z \right\} + 0.015 \left(-(1 + x_0 + 5.0x_0^2) + (1 + 2 \times 5.0 \times x_0)z + (5.0)z^2 \right) v - h(z + x_0) \cos \Omega\tau + A_0 \cos(1.33\tau)$, for $A_0 = 1.30$: (a) $h = 0.1$ (b) $h = 0.115$, (c) $h = 0.29695$, (d) $h = 0.2980$ with $\Omega = 0.66114$.

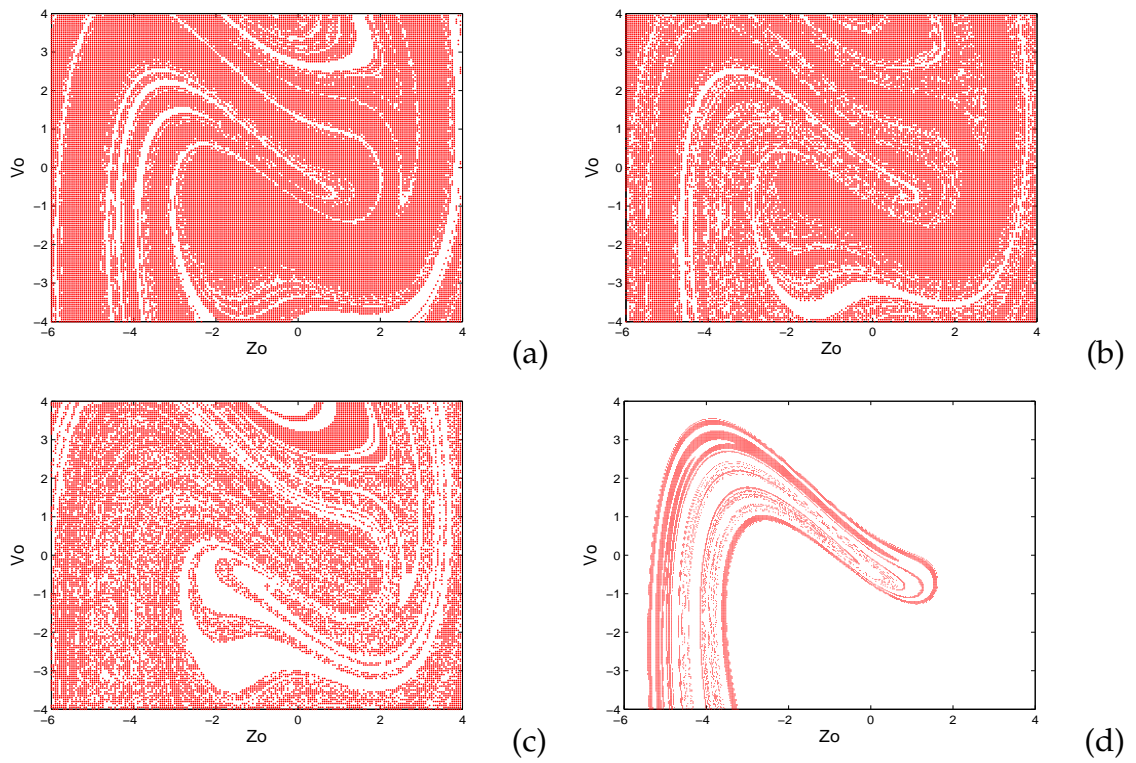


Figure 26: Basin of attraction for strong external forcing. $\ddot{z} = -0.25 \left\{ z^3 - \frac{3}{4}(z_1 + z_2)z^2 + \frac{1}{2}(z_1 z_2)z \right\} + 0.015 \left(-(1 + x_0 + 5.0x_0^2) + (1 + 2 \times 5.0 \times x_0)z + (5.0)z^2 \right) v - 0.3(z + x_0) \cos \Omega \tau + A_0 \cos(1.33\tau)$, with $\Omega = 0.66114$: (a) $A_0 = 0.81$; (b) $A_0 = 0.9$; (c) $A_0 = 1.0$; (d) $A_0 = 1.1$.

around $A_0 \approx 1.208$. The corresponding maximum Lyapunov exponent confirms the existence of the chaotic regions and periodic orbits. When $h = 0.2$, as shown in Fig. 19 we observe that the first periodic band is reduced, with a slight increasing of the width of the first period $4T$ window; as shown in Fig. 20 transition to chaotic state occurs around $A_0 \approx 1.092$. For $h = 0.3$ a very thick banded chaotic domain resides for $A_0 \approx 0.444$. It can also be observed that the system does not enter chaotic motions sometimes through a sequence of period doubling bifurcations, but with a jump. For low A_0 ($A_0 = 0.224$), as shown in Fig. 21(a) there is a transient chaos for very low h . For $A_0 = 0.9$ (see Fig. 21(b)) there is a period-one orbit for h closed to zero, and a period doubling bifurcation of period-one. In Fig. 21(c), plotted for $A_0 = 1.3$ there is a sudden jump in the size of the chaotic attractor after a period two orbit as in Fig. 21(d). But in Fig. 21(d), plotted for $A_0 = 1.485$, the period two comes from a chaotic attractor, which exists for h closed to zero. The existence of this attractor is associated with the transverse intersection of the stable and unstable manifold of the perturbed saddle. As shown in Fig. 22 the high values of h are associated with low values of the threshold A_0 . Fig. 23 shows that there is a transient chaos at around $\omega \approx 1.33$ for A_0 up to ≈ 1.40 . For $\omega \geq 2.4$ there are periodic attractors with roughly the same period as that of the forcing. There is an abrupt transition to a chaotic state for $A_0 \geq 1.25$ when increasing ω from around $\omega \approx 0.8$. Within this chaotic region lie $\omega \approx 1.332$, which is consistent with the other above observations. The value of ω for which we have chaotic behavior globally increases when increasing A_0 ; then if an experimental study is conducted, chaotic behavior should be relatively easy to avoid by adjusting the system's parameters. For $A_0 = 1.40$ (See Fig. 24(a)) the portrait on the Poincaré map is a set of points (two-point represented by two crosses in the figure) and the corresponding maximum Lyapunov exponent is negative. The system motion is quasi-periodic. When A_0 is around 1.480, the portrait on the Poincaré map is no longer a countable number of points, the quasi-periodic ring is broken-up; the Poincaré section is a strange attractor. The chaotic attractors in the Poincaré map of system (70), are shown in Fig. 24(b). The variation of the basin of attraction is depicted in Fig. 25. Taking the parameters specified in the specified equation of motion, the basin of attraction subjected to the action of the strong external forcing exhibits a complicated behavior. From Fig. 25(c), the boundary of the targeted area is not regular when $A_0 = 1.0$ and $h = 0.29695$. At the same time, the escaping phenomenon of the targeted domain occurs. The relative number of initial conditions, belonging to these boxes, are uncertain in the sense that a small deviation in the boundaries would render the evolution to

be towards a different attractor from the original initial condition. Holding the external forcing, when slightly increasing h to $h = 0.2980$, the fractal boundaries of the basin of attraction as shown in Fig. 25(d) is modified, the boundaries become more fractal. See from Fig. 25(a), if the external forcing is again increased to $A_0 = 1.30$ with $h = 0.1$ the smoothness of the basin boundaries tend to be reconstructed. But, if the modulation depth amplitude is slightly increased to $h = 0.115$, the smoothness of the boundaries tend to vanish, the boundaries become more fractal (see Fig. 25(b)). Holding the modulation depth at $h = 0.3$, the basin of attraction is depicted in Figs. 26(a) and (b) for. If the trajectory is attracted out of the left well, the lattice element of the initial condition is drawn in white, otherwise in red (online). For $A_0 = 0.81$, the basin of attraction exhibit light fractal boundaries (see Fig. 26(a)), the escaping phenomenon of the targeted domain also occurs. When increasing A_0 at $A_0 = 0.9$, Fig. 26(b) shows that the safe area inside the well is more destructed, and the erosion of the basin increase notably. When $A_0 = 1.0$ the smoothness of the boundaries tend to vanish completely as shown in Fig. 26(c). If the external forcing is again increased to $A_0 = 1.1$ the escaping phenomenon is strongly increased.

A series of experiments on temporal control of plasma instabilities have already been carried out [207, 208]. Control of chaos is a first approach, where unstable periodic states are stabilized by tiny adjustments of one or more accessible parameters.

Experiments have been carried out in the linear section of the low plasma device (MIRABELLE) [207]. In this experiment, plasma is produced by a thermoionic discharge in one of the two source chambers; the other one staying unoperated in the experiments. Confinement is ensured in the central section by 24 coils, which create a uniform magnetic field whose strength can be varied up to $120mT$. Compensation coils, installed on each source chamber, allow null axial \mathbf{B} field in front of the cathodes, which avoids filamentary plasma. The base pressure inside the device is of the order of $5 - 10 mbar$ and the working pressure in argon is typically $1 - 2, 4 - 10mbar$. A high transparency grid is located at the entrance of the column. Its biasing influences the axial drift of the particles and the radial profiles of density and potential, allowing a dynamic control of the plasma regime. Discharge current, magnetic field strength, pressure, and biasing of an internal tube inside the central section determine the plasma regime as well. Without any limiter, only drift waves due to the radial density gradient can be excited in the plasma column. Thus, in order to increase transverse gradients, a metallic diaphragm is inserted at the entrance of the col-

umn. The plasma rotation due to the increased radial electric field can then trigger flute modes, especially at low B field, when the drift dispersion scale is large, or of the same order as the transverse length scale spatiotemporal control is achieved with an eight-plates exciter located in the first part of the column.

In another experiment [208], nonlinear drift waves are experimentally studied in a cylindrical magnetized laboratory plasma. The transition from spontaneous regular regimes to chaotic and turbulent regimes is obtained by changing the plasma parameters. The scenario starts with a state where the density fluctuations are periodic in time. Then, changing the control parameter (azimuthal velocity of the plasma column), a bifurcation occurs leading to a mode-locked state. Next, increasing the control parameter lead to the gradual dissolution of the mode locked state. The periodic regime disappears and a chaotic regime is obtained. The spontaneous excitation of drift waves is obtained by applying a potential difference between the anode and the grid. For the study of the transition from a regular regime to a turbulent one, the bias of the tube is taken as the control parameter determining the dynamical state of the plasma. Biased Langmuir probes located at the radial position of the maximum density gradient are used for the measurement of density fluctuations in order to investigate experimentally the temporal and the spatio-temporal drift wave dynamics.

III.2 Effect of external bounded noise on nonlinear dynamics of plasma density

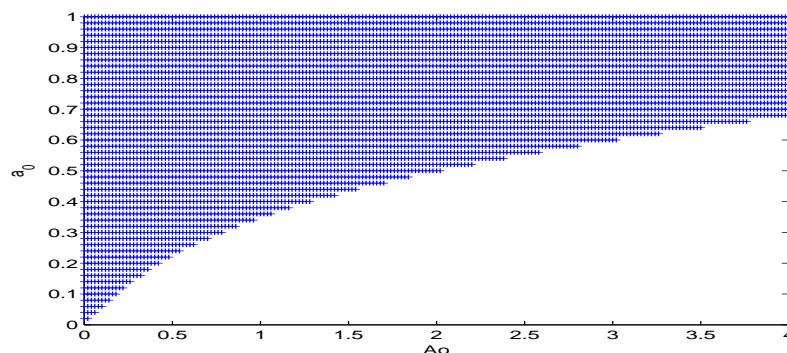


Figure 27: Stability map of the equilibrium solutions of equation (143) for $\gamma = 5.0$, $\mu = 0.9$. Shaded regions represent asymptotically stable equilibria.

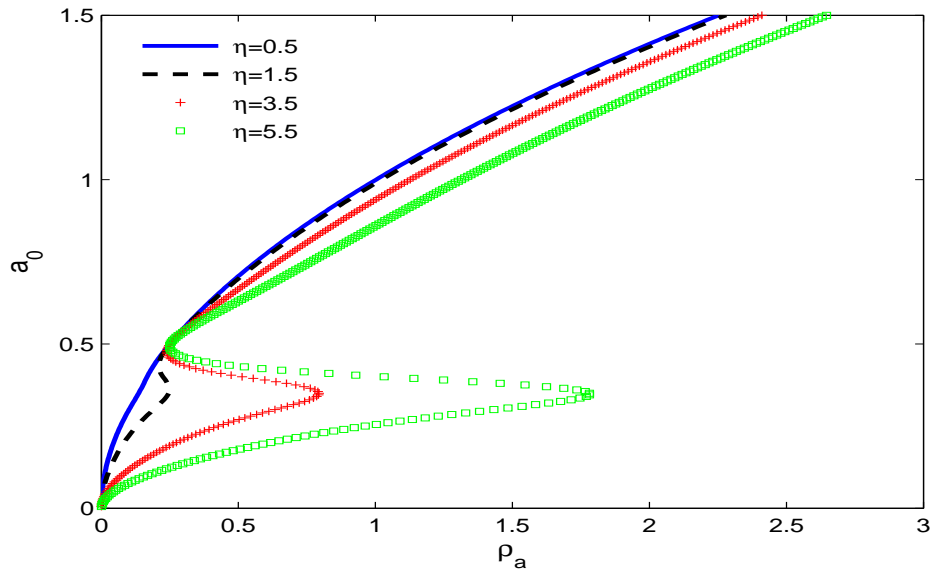


Figure 28: Frequency response of system (57) in the (ρ_a, a_0) –plane, for $\mu = 1.1$, $\gamma = 5.0$, $\sigma = -1.5$; and $\eta = 0.5$ (blue), $\eta = 1.5$ (black), $\eta = 3.5$ (red), $\eta = 5.5$ (green).

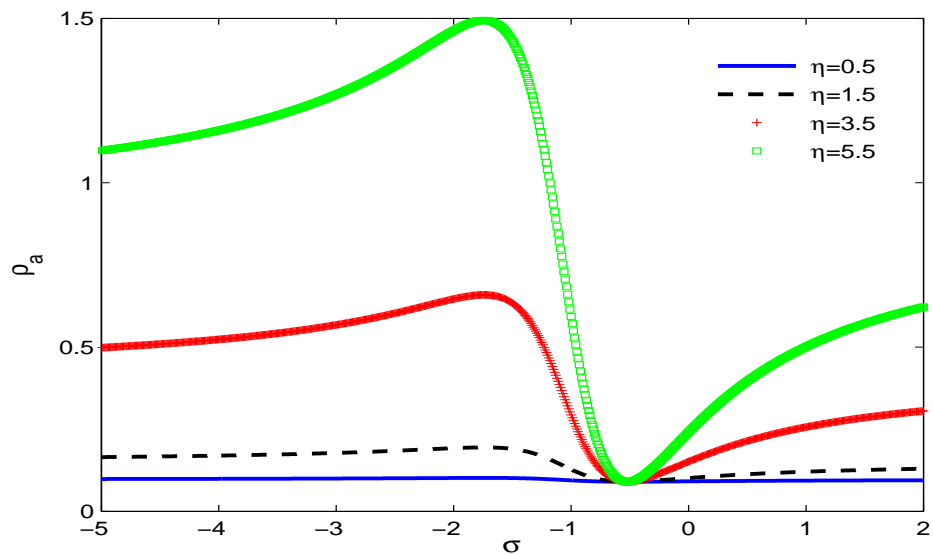


Figure 29: Frequency response of system (57) in the (σ, ρ_a) –plane, for $\mu = 1.1$, $\gamma = 5.0$, $a_0 = 0.3$; and $\eta = 0.5$ (blue), $\eta = 1.5$ (black), $\eta = 3.5$ (red), $\eta = 5.5$ (green).

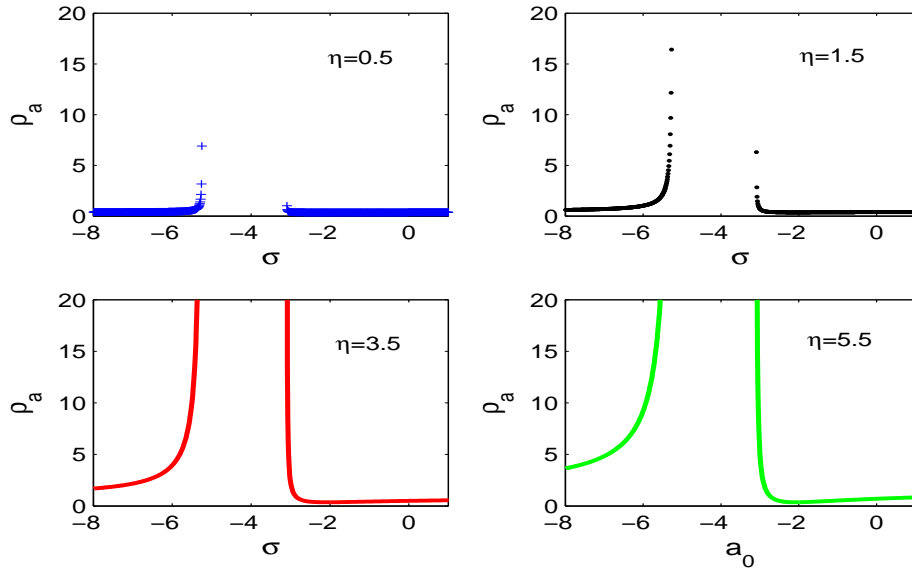


Figure 30: Frequency response of system (57) in the (σ, ρ_a) –plane, for $\mu = 1.1$, $\gamma = 5.0$, $a_0 = 0.6$; and $\eta = 0.5$ (blue), $\eta = 1.5$ (black), $\eta = 3.5$ (red), $\eta = 5.5$ (green).

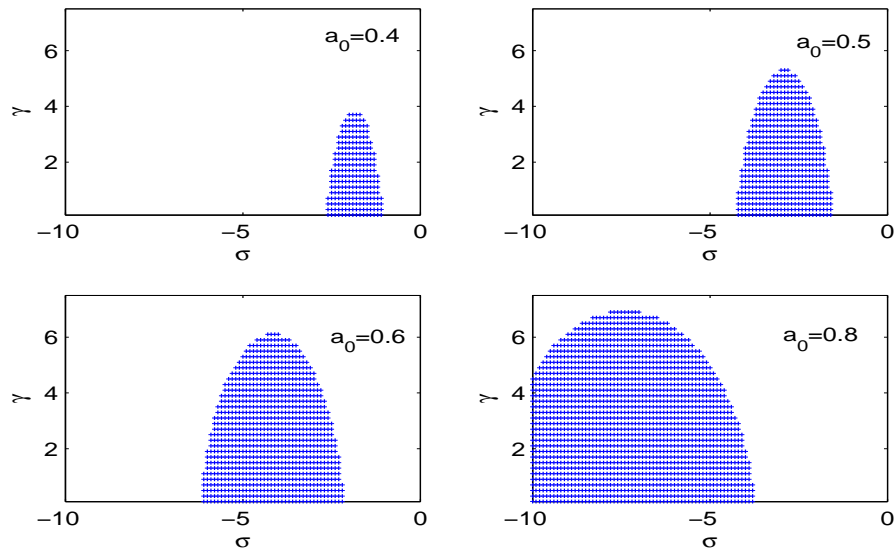


Figure 31: Regions of the existence of the statistic moment ρ_{20} in the (σ, γ) – plane, for $a_0 = 0.8$; $\mu = 1.1$; $A_0 = 0.2$. There is no solution in the white region.

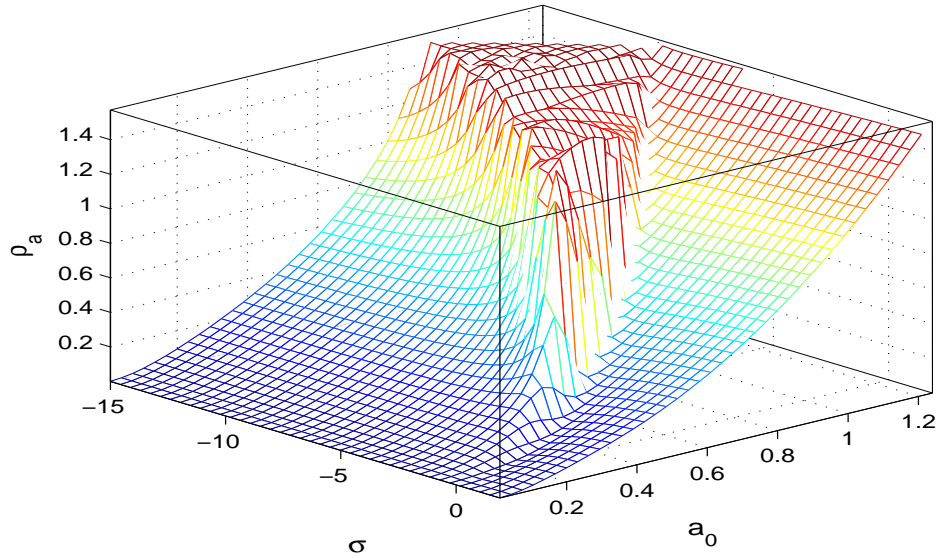


Figure 32: 3-D resonance region plotted in the space (a_0, σ, ρ_a) , for $\mu = 1.1, \gamma = 5.0, \eta = 1.8$.

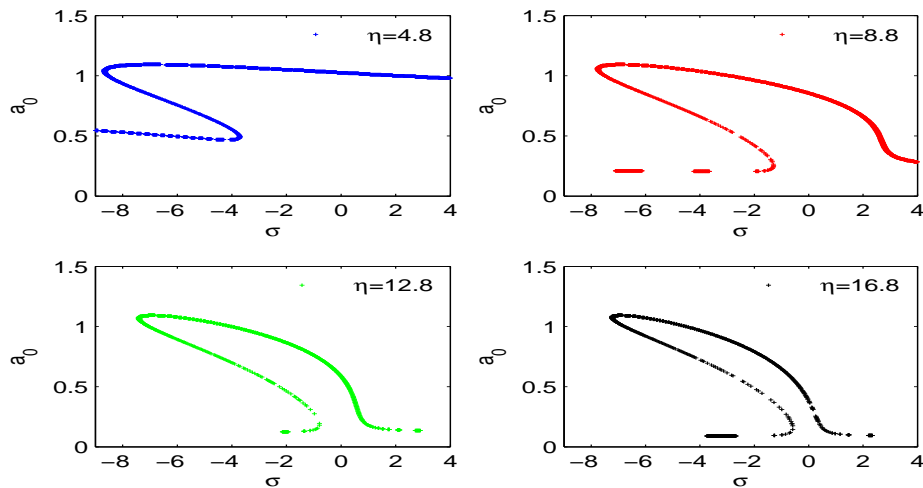
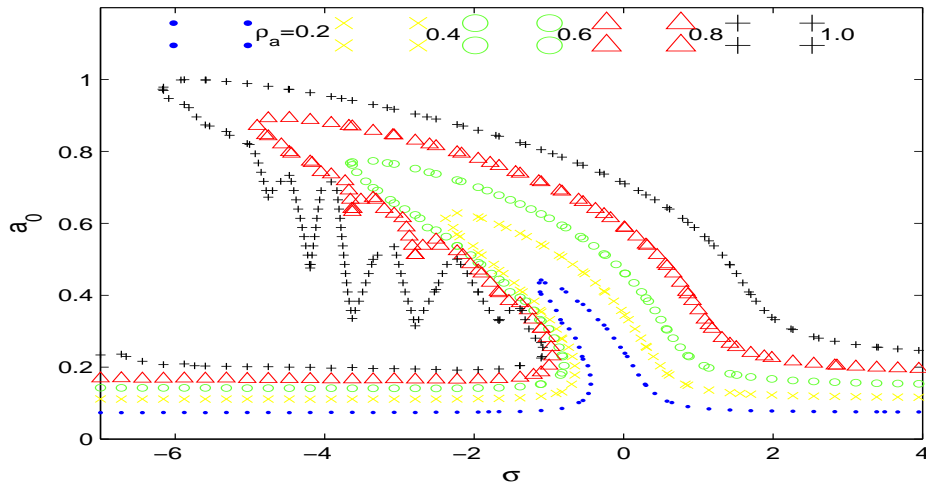
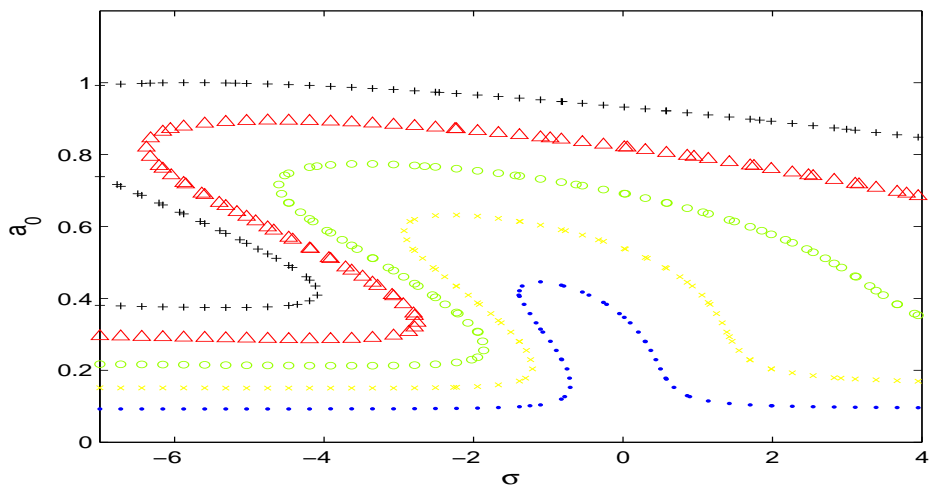


Figure 33: Frequency response of system (57) in the (σ, a_0) –plane, for different values of gaussian noise intensity η , for $\mu = 1.1, \gamma = 6.0, A_0 = 0.2, \rho_a = 1.2$; and $\eta = 4.8$ (blue), $\eta = 8.8$ (red), $\eta = 12.8$ (green), $\eta = 16.8$ (black).



(a)



(b)

Figure 34: Resonance curves measured at successively values of complete statistic moment ρ_a , with: (a) $\eta = 6.8$, (b) $\eta = 5.8$; $\rho_a = 0.2$ (blue), $\rho_a = 0.4$ (yellow), $\rho_a = 0.6$ (green), $\rho_a = 0.8$ (red), $\rho_a = 1.0$ (black). Arrows on the highest pair of curves indicate sweep direction. All lower curves are not similar. Note sharp peak and reinforcement of asymmetry and hysteresis phenomena at the highest moment.

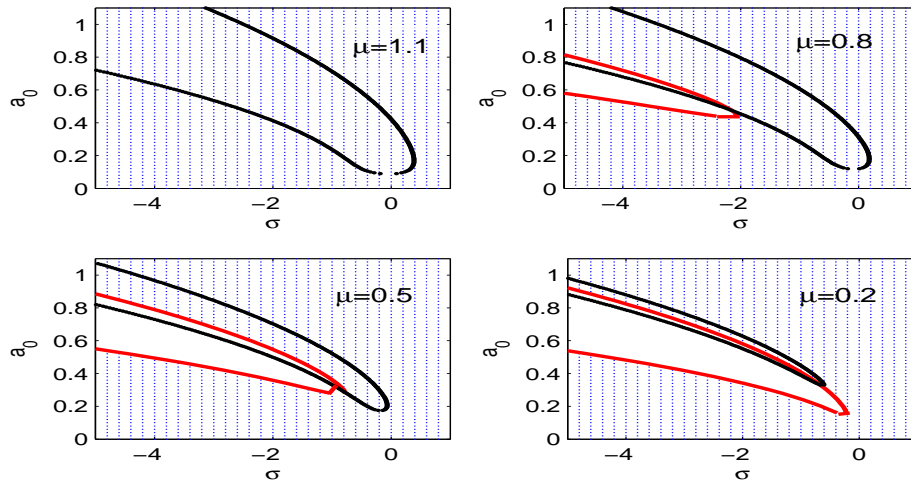


Figure 35: Effect of varying parameter μ on the frequency response curves and on the stability of solutions; for $A_0 = 1.2$, $\gamma = 5.0$.

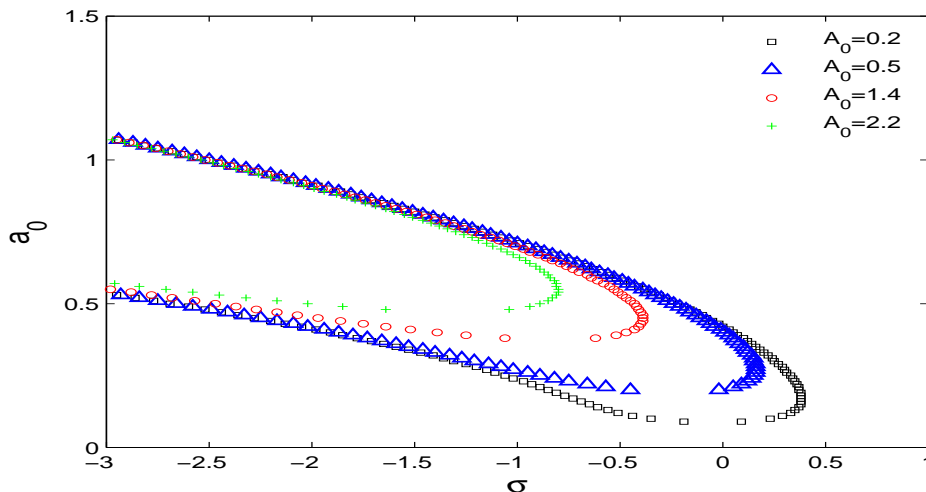


Figure 36: Effect of varying the external excitation magnitude A_0 on the frequency response curves; for $\mu = 1.1$, $\gamma = 5.0$; and $A_0 = 0.2$ (black), $A_0 = 0.5$ (blue), $A_0 = 1.4$ (red), $A_0 = 2.2$ (green).

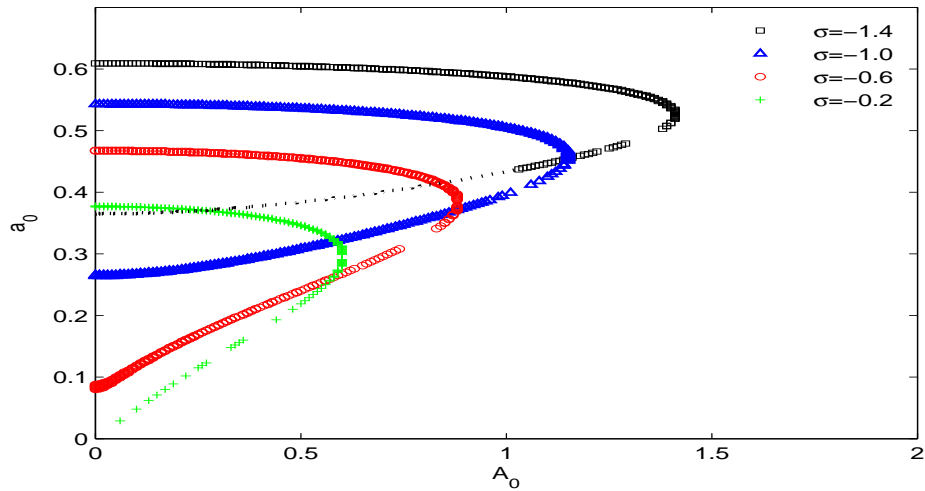


Figure 37: Forced response of density perturbation in the case of the fundamental parametric resonance, for different values of detuning frequency σ ; $\mu = 1.1$, $\gamma = 5.0$; and $\sigma = -1.4$ (black), $\sigma = -1.0$ (blue), $\sigma = -0.6$ (red), $\sigma = -0.2$ (green).

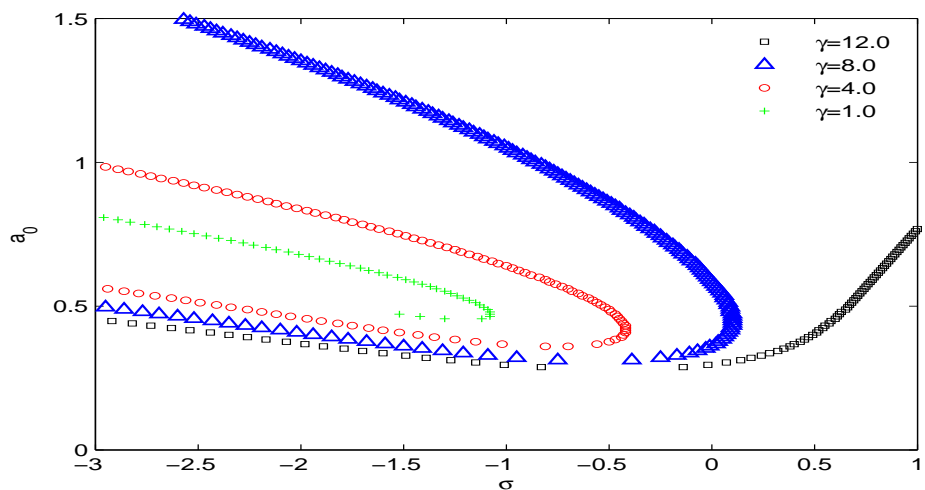


Figure 38: Effect of varying parameter γ on the frequency response curves; for $\mu = 1.1$, $A_0 = 1.2$; and $\gamma = 12.0$ (black), $\gamma = 8.0$ (blue), $\gamma = 4.0$ (red), $\gamma = 1.0$ (green).

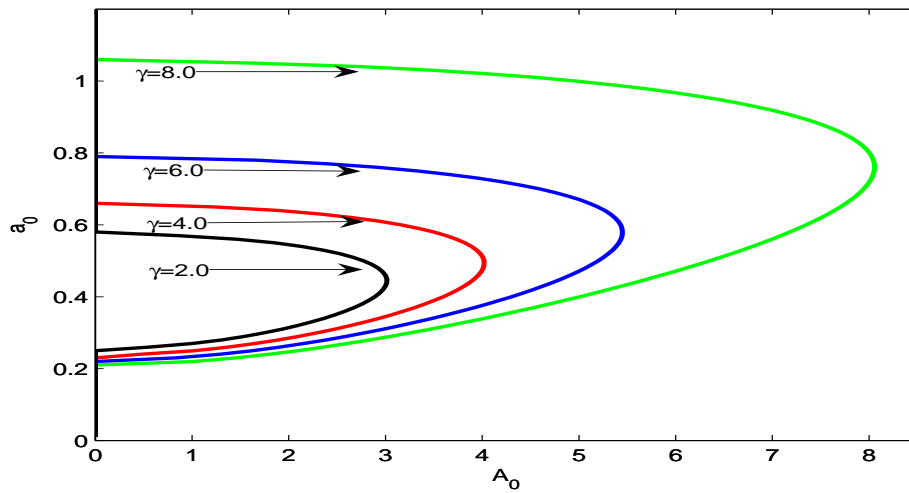


Figure 39: Forced response of density perturbation in the case of the fundamental parametric resonance, for different values of parameter γ ; $\mu = 1.1$, $\sigma = -1.0$; and $\gamma = 8.0$ (green), $\gamma = 6.0$ (blue), $\gamma = 4.0$ (red), $\gamma = 2.0$ (black).

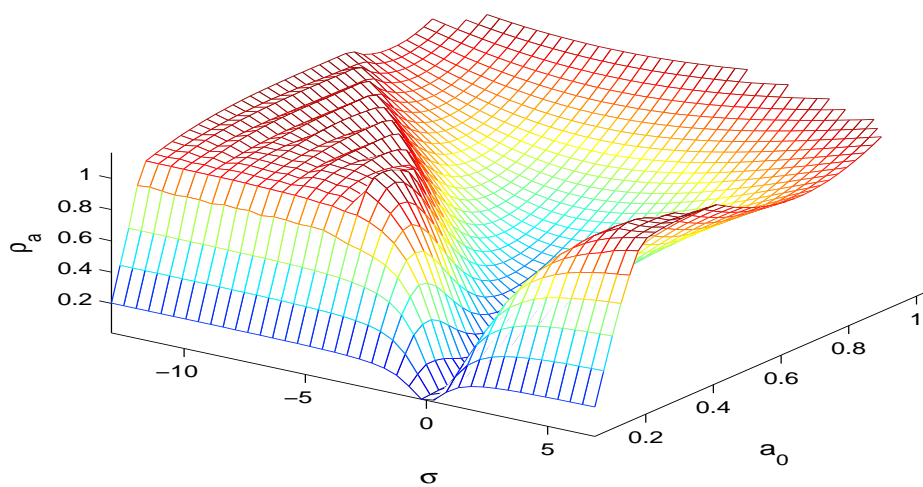


Figure 40: 3-D resonance basin plotted in the space (a_0, σ, ρ_a) , for $\mu = 2.1$, $\gamma = 20.0$, $\eta = 16.8$.

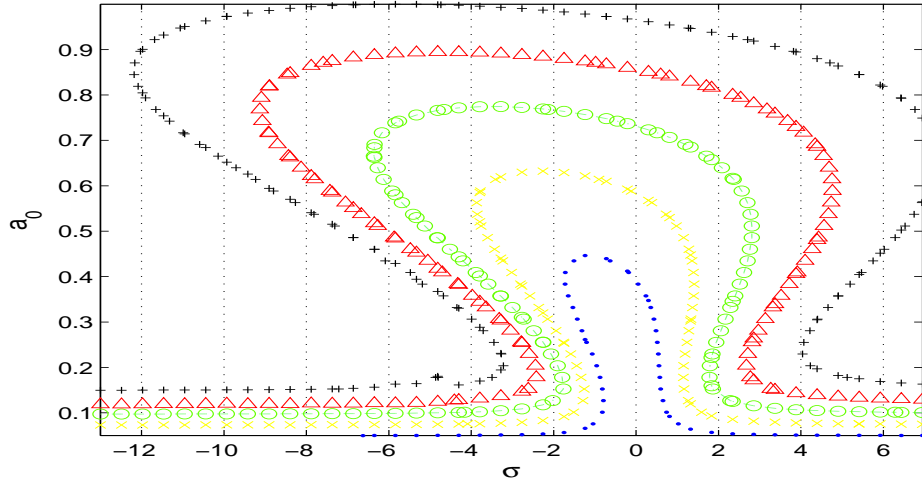


Figure 41: Resonance curves measured at successively values of complete statistic moment ρ_a . All curves are not similar as in (34). As in (34), we have: $\rho_a = 0.2$ (blue curve); 0.4 (yellow curve); 0.6 (green curve); 0.8 (red curve); 1.0 (black curve). Note right hand and left hand hysteresis phenomena at the highest moment.

III.2.1 Numerical simulation of nonlinear response

Case $\eta = 0$

In this section, the frequency response curves of density perturbation in plasma are obtained by solving Eq. (144), a nonlinear algebraic equation, which is solved numerically using Newton-Raphson's method. The numerical results are shown in Figs. 35, 36, 38 as the amplitude a_0 against the detuning parameter σ ; in Figs. 37, 39 as the amplitude a_0 against the external excitation magnitude A_0 , for different values of parameters. In Fig. 35 the frequency response is combined with the stability region plotted by using Eqs. (163)-(164). Fig. 35 shows the response intensity of density perturbation as a function of the frequency σ for fixed values of μ . The instability tongue widened when μ decreases. The greatest value of σ for which one has solutions decreases when μ decreases. The largest amplitude required for having an instability decrease when μ decreases. From Fig. 36 we see that when A_0 increases the lowest value of the amplitude decreases when A_0 increases. Fig. 37 shows that when σ decreases, the largest amplitude of solutions also decreases. As shown in Fig. 38, the minimal values of the amplitude concentrate around $a_0 = 0.5$, and there is a value of $\gamma \in]8.0, 12.0[$ from which one has only one value of

a_0 for a value of σ . For γ varying (see Fig. 39), the steady state amplitudes increases when γ increases for the upper branch, and decreases when γ increases for the lower branch, For a fixed

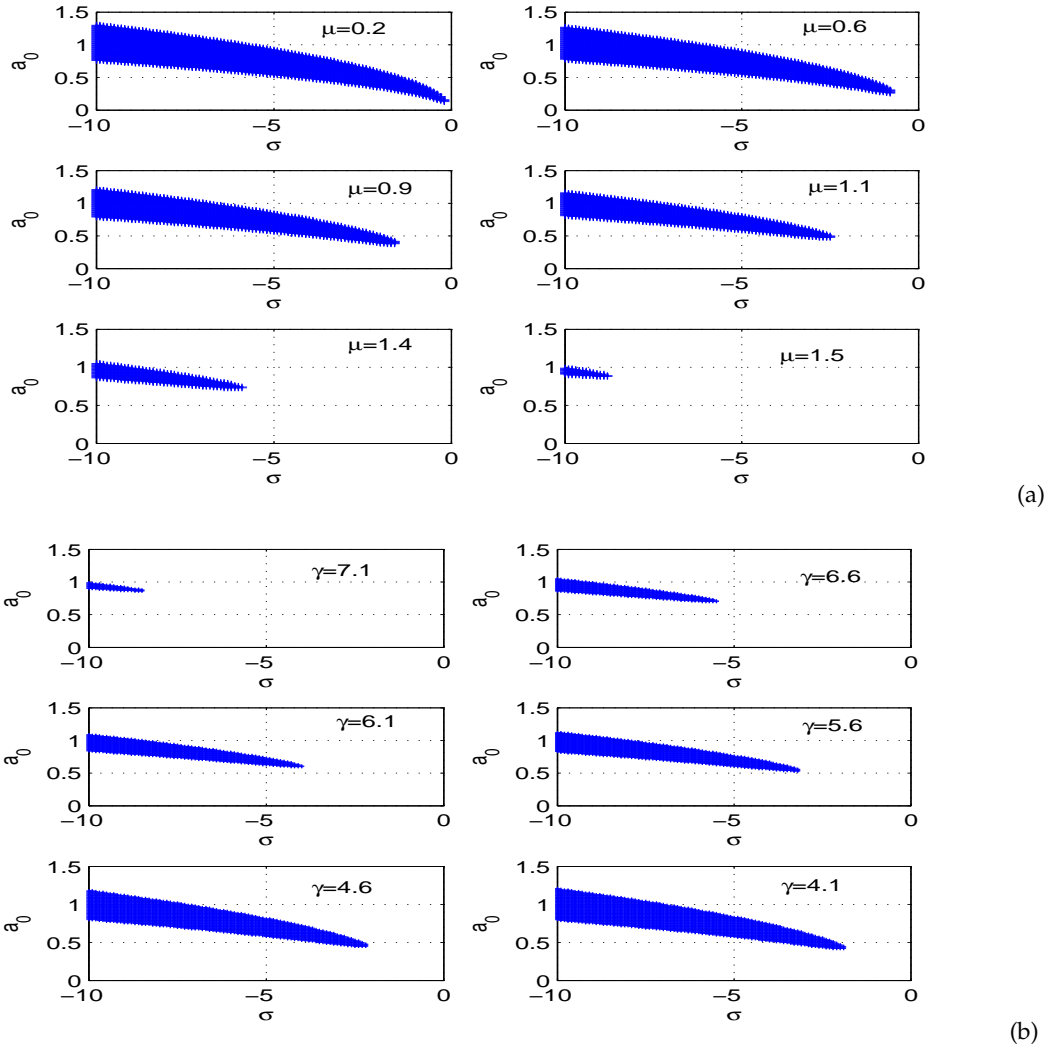


Figure 42: Regions of stability of the statistic moment ρ_{20} in the (σ, a_0) – plane, from Eqs. (167)-(170), for different values of parameter: (a)- μ for $\gamma = 4.1$; $A_0 = 0.2$,(b)- γ for $\mu = 1.1$; $A_0 = 0.2$. The solutions are stable in the white region.

detuning parameter, the stability region is plotted for $\mu = 0.9$ and $\gamma = 5.0$. The crossed area corresponds to stable solutions.

Case $\eta \neq 0$

As a function of a_0 , Eq. (170) is a nonlinear equation; it is solved numerically as shown in Figs. 28 - 41. From Fig. 28, the results are presented as steady-state amplitudes a_0 against statistic

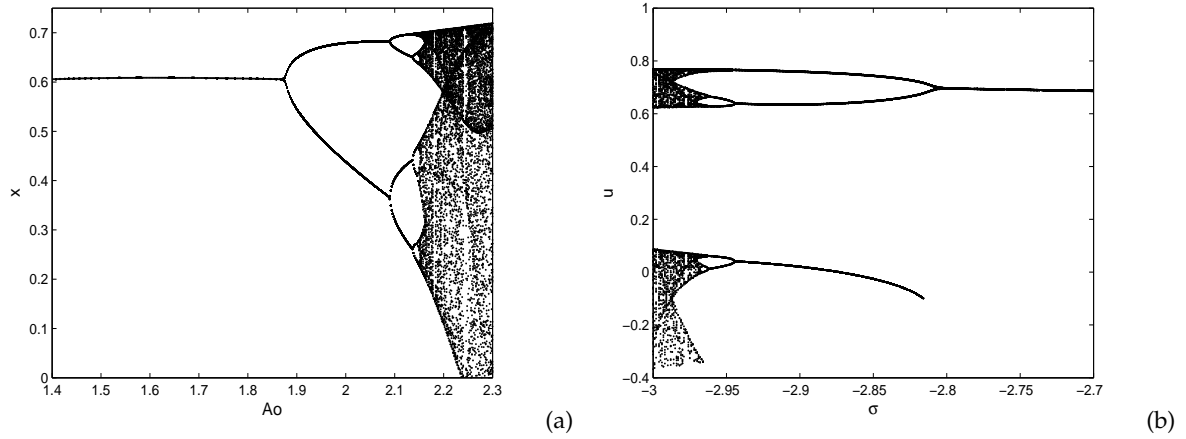


Figure 43: Bifurcation diagrams obtained from (57) for $\eta = 0$ and : (a)- $\sigma = -1.1; \gamma = 5.0; \epsilon = 0.4$; (b)- $A_0 = 2.0; \gamma = 5.0; \epsilon = 0.44$.

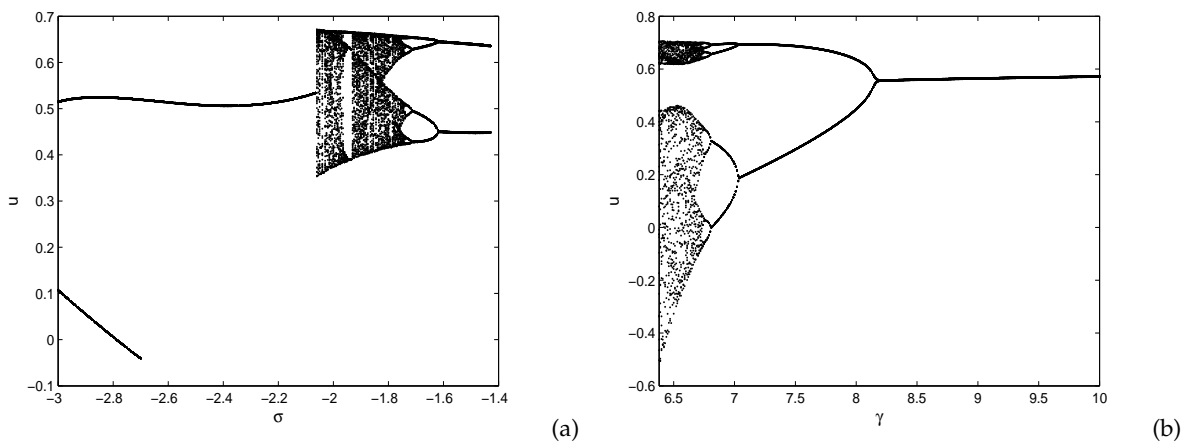


Figure 44: Bifurcation diagrams obtained from (57) for $\eta = 0$ and : (a)- $A_0 = 2.0; \gamma = 7.0; \epsilon = 0.44$.(b)- $A_0 = 2.2; \sigma = -1.1; \epsilon = 0.44$.

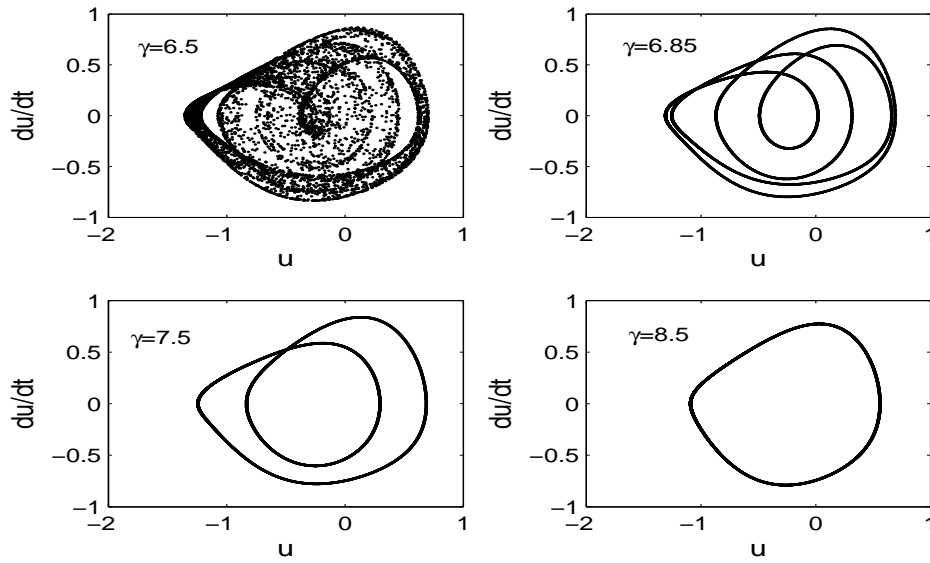


Figure 45: Influence of parameter γ on the Poincaré maps of (57) for $\eta = 0$ and $\mu = 1.1$; $\beta = 0.15$; $\lambda = 1.9$; $A_0 = 2.2$.

moment ρ_a for primary resonance, and different values of noise intensity η . From Fig. 28, it is observed that the steady-state amplitudes increase when η decreases. But the steady-state amplitudes have multivalued solutions where the jump phenomenon exists due to hysteresis phenomena. The phenomenon of hysteresis disappears for a value of $\eta \in]0.5, 1.5[$. As shown in Fig. 9, the smaller η is, the more the curve flattened; like what, η induces a form of multiplication of solutions. The value of the statistic moment ρ_a (see Fig. 30) for the smallest value of σ increases when η increases. The regions of the existence of statistic moment are shown in Fig. 31 in the (σ, γ) plane. From Fig. 31 we see that the existence zone (the colored one) enlarges when the resonant amplitude a_0 increases. The steady-state amplitude a_0 is depicted in Fig. 33 for σ varying. Increasing η shrinks the basis of the curve. The 3-D resonance map is shown in Fig. 32 and a contour plot in Fig. 34 for (a) $\eta = 6.8$, (b) $\eta = 5.8$ and $\gamma = 7.0$. From these figures, the frequency response curves in the plane (σ, a_0) are bent to the left and they have multivalued solutions where the jump phenomenon exists, see Figs. 34(a) and (b). We also see that as ρ increases the summit of the peak is destroyed, and the hysteretic behavior is comforted. When η decreases the region of σ where we observe hysteretic phenomena shrink. This shows the influence of Gaussian noise amplitude on the resonant frequency response curves. The response curves possess a softening-spring-type. In Fig. 34(a) and (b), the bending of the curves indicates softening-type nonlinearity; it also illustrates the influence of the stochastic moment on the resonant frequency

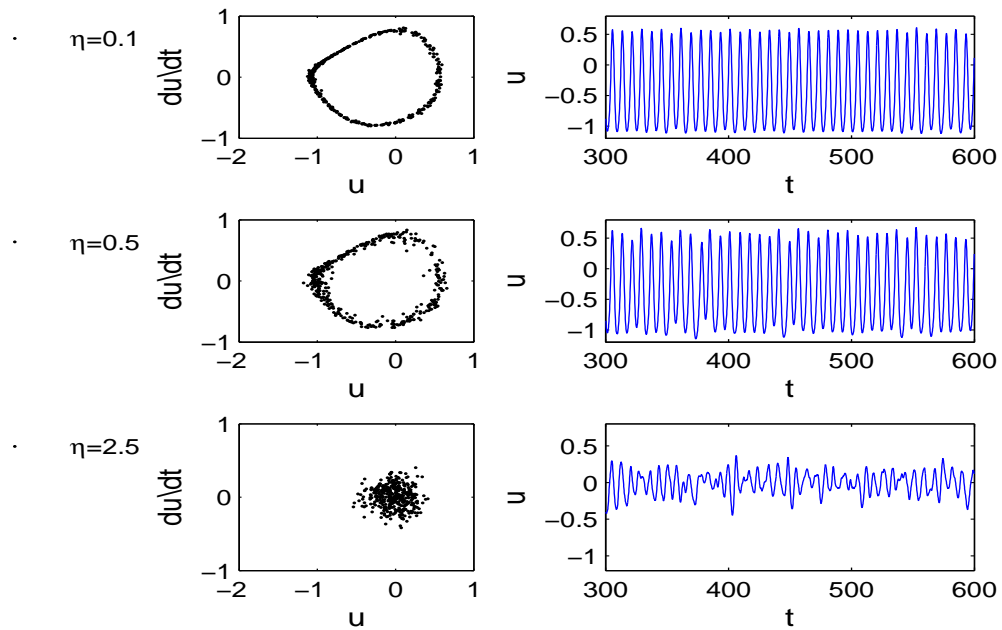


Figure 46: Influence of the gaussian noise intensity η on the limit cycles maps of (57) for $\mu = 1.1$; $\beta = 0.15$; $\lambda = 1.9$; $A_0 = 2.2$; $\gamma = 8.5$.

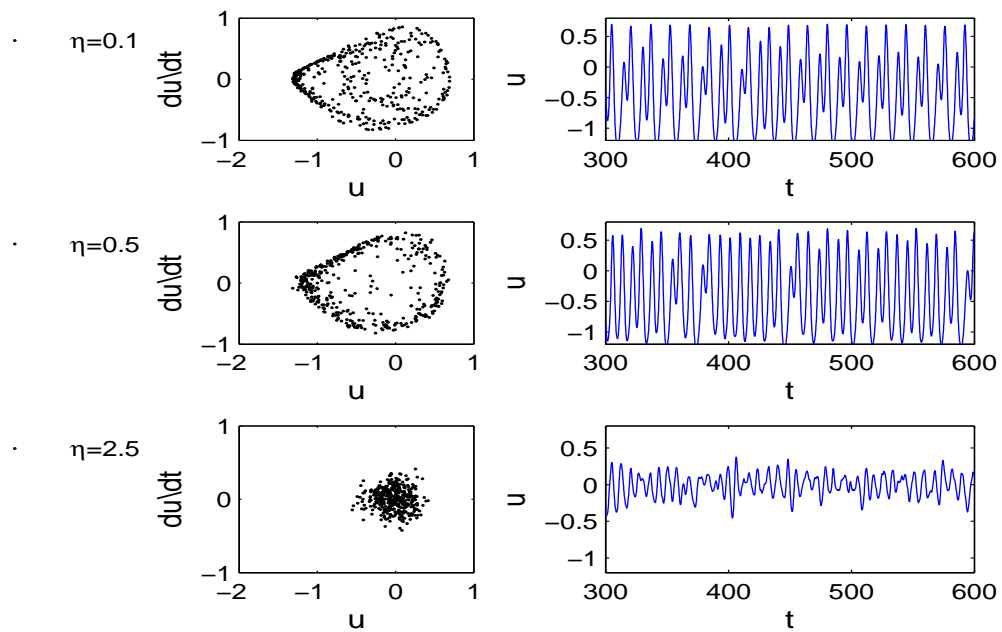


Figure 47: Influence of the gaussian noise intensity η on the limit cycles maps of (57) for $\mu = 1.1$; $\beta = 0.15$; $\lambda = 1.9$; $A_0 = 2.2$; $\gamma = 6.85$.

response curves. The 3-D basin of resonance map is depicted in Fig. 40 and a contour plot in Fig. 41. Here, the peaks are not really sharp. When the stochastic moment increases, the peaks are enlarged. These figures indicate that there are multiple solutions and, that jumping phenomena are also multiplied when the stochastic moment takes a value $\rho_{as} =]0.2, 0.4[$. The response curve possesses both softening-spring type and hardening-spring type when $\rho_a > \rho_{as}$. The curves are bent to the right and left, which indicates a hardening and softening-type nonlinearity. Increasing the stochastic moment ρ_a also increases the amplitude of the resonant response a_0 . The stability regions of the statistical moment are shown in Fig. 42 for μ and γ varying. From Fig. 42 we see that the stability zone (the colored one) becomes narrow when μ increases and enlarges when γ increases.

III.2.2 Numerical simulations

Simulation of bounded noise

As mentioned in the preceding chapter, for numerical simulation, we use the pseudorandom signal given by Shinozuka [203]. Since the duration of time is not concerned with the sum in the noise approximation, a specific Poincaré map can then be set up as in [209].

Noise effect on limit cycle

Bifurcation diagram for A_0 varying is depicted in Fig. 43(a). We see that for A_0 less than a value ≈ 1.86 , we have only period one oscillation, we can observe clearly chaotic regions with a few number of complex period windows. It can also be observed that the system enters chaotic motions usually through a sequence of period-doubling bifurcations, while period-doubling is at present the most commonly known route to chaos. As A_0 increases from 1.4 the system starts entering period-2 and period-4 bifurcations and is brought into chaos via a period doubling cascade. In the largest period window of Fig. 43(a) bifurcations occur at, $A_0 \approx 1.867; 2.10; 2.15$ (approximately), etc., until just beyond 2.172, where the system is chaotic. However, the system is not chaotic for all values of A_0 lower than ≈ 2.17 . The behavior of a non-autonomous two-dimensional system such as system (57) can be depicted by using Poincaré map, which is defined as

$$P : \Sigma \rightarrow \Sigma$$

$$\Sigma = \{u, du/dt | \theta = 2\pi n/\Omega \quad n = 1, 2, 3, \dots\} \in \mathbf{R}^2$$

Considering the primary resonance; The Poincaré maps for system (57) with externally excitation $f(\tau)$ with $\eta = 0$ are depicted. Equation (57) is integrated numerically under the initial condition $(u, \dot{u}) = (1.41, 0.1)$ by using four-order fixed step Runge-Kutta method. The results are presented on Poincaré maps, which are generated by sampling the system stroboscopically with a fixed period as mentioned before (the effect of transitional course is renowned). The Poincaré maps for different value of parameter γ are shown in Fig. 45. It is seen from these figures that the motion of the system is periodic when $\gamma = 8.5$ and chaotic when $\gamma = 6.5$.

III.2.3 Discussion

The bifurcation diagram depicted in Fig. 43(b) nicely shows the reverse forking of the possible periods of stable orbits from chaotic to 5 to 3 to 1. All the bifurcation points are not period-doubling bifurcation. If the system as shown in Fig. 43(b) is subject to slowly varying frequency (by varying σ), jump phenomena can be observed. As σ is decreased Let us fix the amplitude A_0 , the detuning parameter σ and change only the varying parameter to γ . Increasing the parameter γ leads to the increase of damping. As a result, when γ is varying, the sequential stabilization of orbits of the period-doubling cascade occurs in the reverse order (see Fig. 44(b)). Around $\gamma \approx 8.1$, the coexisting orbits, multiple of period 2 appear. They can be eliminated by slow modulation either μ or γ . Similar effect of the reverse period-doubling is reached at decreasing γ . However, suppressing the oscillation (when the trajectory remains in small vicinity of 1 or -1) occurs only at low γ ; hereupon, system dynamics becomes. In addition, the perturbations with $A_0 = 1.53$ effectively suppress the oscillations when γ remains relatively small ($\gamma = 5.0$) (see Fig. 44(a)). Note, the jump around $\sigma \approx -2.7$ (see Fig.44(a)), the system trajectory suddenly evolves from period-2 to period-1 bifurcation. Notice that at several values of σ greater than -2.07 , a small number of σ values is visited. These regions produce the 'white space' in the diagram. Look closely at $\sigma \approx -1.92$ there is a three-point attractor. In fact, between $\sigma \approx -2.07$ and $\sigma \approx -1.70$ there is a rich interleaving of chaos and order. A small change in σ can make a stable system chaotic, and vice versa. Explicitly it may be seen from Fig. 45 that: (1) When $\gamma = 8.5$, the portrait on Poincaré map is closed curved and as shown in Fig. 44, the system's motion is quasi-periodic. (2) When $\gamma = 7.5$, the portrait on Poincaré map is still a closed curve, but the curve twists itself into a circle, and as shown in Fig. 44, the system shows a two-frequency quasi-periodic motion.

(3) When $\gamma = 6.85$, the portrait on Poincaré map is also closed curved, but its shape is much more complicated and twisty, and as shown in Fig. 44, a four-frequency quasi-periodic motion occurred in the system. (4) When $\gamma = 6.5$, relatively to Fig. 44, the portrait on Poincaré map is a strange attractor, and the chaotic motion takes place in the system. Next is to determine the noise effect on the response of system (57). When $S_0 = 1.0$, for the initial values $(u, \dot{u}) = (1.41, 0.1)$. Figs. 46, 47 show that in some parameter area of η , the stationary variances of the displacement response of system (57) may be different for different values of γ . The random noise $\vartheta_b(t)$ will change the steady-state response of system (57) from a limit cycle to a diffused limit cycle. With the same initial values, As in [210], further numerical simulation shows that when the random noise intensity η increases, the width of the diffused limit cycle also increases also. From Figs. 46 and 47, when the noise is present in the system, one can see that for larger noise intensity, the Poincaré maps diffuse larger in phase plane. And then increasing the noise amplitude η , the Poincaré maps diffuse to a large area. In short, the chaotic attractors diffuse by increasing the bounded noise. All these figures show how the motion of system (57) goes from random to random chaos as η increases. It should be noted that the transition of the motion of the system from random to random chaos is gradual. These parameters, depending on the physical mechanism of the species instabilities could be used to sketch an appropriate control strategy, that should be applied to the plasma device to reduce the effect of chaotic motion resulting from noise [211] or stabilize the chaotic state. Our results indicate that the density perturbation in the plasma, is stable (see Fig.35) in some parameters ranges. In this case, the particle density perturbation cannot cause the catastrophe of the amplitude for the normalized density perturbation in plasma device. Since a pre-condition for the realization of high-performance plasma regimes with superior energy confinement is its operation in a stable quasi-steady state [212]; parameters A_0 , μ and γ (see Figs. 35 - 39), could be used to realize a specific stable state, that is helpful [213, 214] for confinement in plasma devices. From the aforementioned analysis, it is shown for example that (see Figs.44(b) and 45) when tuning the parameter γ a limit cycle could arise, it corresponds to a stable controlled density in plasma device. We also show that when the noise intensity is increased, the density perturbation become more chaotic, which results in the increase of instability that is harmful for plasma device. Monitoring the parameter γ (see Figs.45 - 47) could slightly reduce the noise effect. It is illustrated that in the case of choosing suitable parameters the density perturbation in the plasma device is stable. Using the physical correspondents of these parameters,

it is possible to establish periodic operation of plasma devices in regimes where usually chaotic oscillations occur.

In many plasma experiments chaotic dynamics and turbulence are considered as an undesired situation and there is a particular interest to influence the plasma system in order to achieve a stationary state (fixed point in the phase space) or a state of regular motion (limit cycle in the phase space). The most straightforward approach would be to change the set of discharge parameters to establish a new non-chaotic state. This, of course, may be cumbersome or even impossible. Recent results have demonstrated the efficiency of chaos control in laboratory plasmas. Moreover, recent computational studies of chaos control strategies offer the possibility of applications in fusion plasmas. In a third experiment [215], the change of chaotic dynamics into periodic dynamics induced by random noise in a system of two coupled perturbed van der Pol oscillators and comparison with the experimentally observed behavior of a double discharge plasma that it models have been presented. Methods specific to nonlinear analysis such as phase portraits, Lyapunov exponents, and Fourier spectra was used to demonstrate the changeover from chaotic to regular dynamics induced by random noise. The experimental setup consists of a system allowing simultaneous functioning of two electrical discharges sustained by separate voltage sources. They are running in the same discharge tube filled with argon at low pressure. The anodes of the two discharges are situated facing each other at a distance of a few centimeters. They are biased one against the other by a continuous voltage source whose voltage is considered as the experimental control parameter. An additional coupling is possible by connecting in series with the biasing source a sinusoidal voltage. Without this forcing the discharge shows periodic dynamics that slowly changes with changing of the control parameter. Chaos in the system described by a one-dimensional nonlinear drift-wave equation is controlled by directly adding a periodic force with appropriately chosen frequencies [150].

As mentioned in the preceding chapter, there is a possibility to model the phenomena described in large plasma machines, using equations that model them directly, without passing through the fluid equations; allowing the investigation of the behavior of some plasma parameters, such as radial electric field, which has already been reported in fluid modeling as playing a major role in the transition to the high level of energy, that one seek to achieve in fusion plasmas. In the following section, we sketch the obtained result with an incidence on the instabilities control.

III.3 Global bifurcation of mean electric field in plasma L-H transition under external bounded noise excitation

Result for homoclinic orbits

For homoclinic trajectories we have: More precisely, this condition provides a domain on the

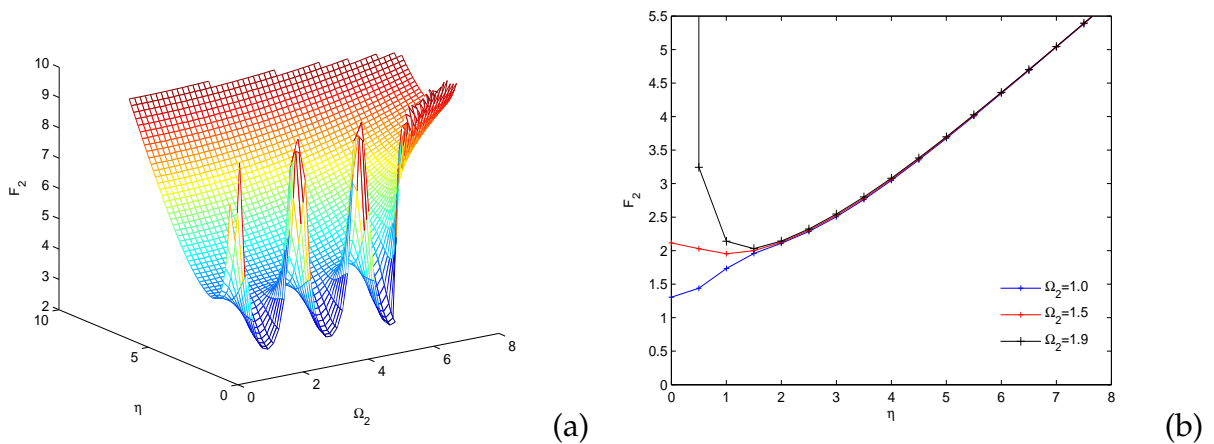


Figure 48: 3D upper threshold bound in (Ω_2, η) plane with the associated threshold amplitude F_2 versus noise intensity η for homoclinic bifurcation; analytic results for different values of Ω_2 .

parameter plane (F_2, η) of the controlling radial electric field (which can be viewed as external perturbation) on which the chaotic behavior may be suppressed from the normalized electric field change. In Fig. 48(a) we illustrate the 3 – D regions in the space (F_2, η, Ω_2) of suppression of chaos. The region under the surface corresponds to a regular motion for which the condition (120) is not satisfied and in the region over the surface will exhibit chaotic behavior. From Fig. 48(b) we observe that for low noise intensity η , the threshold value of the external forcing intensity is approximately obtained as $F_2 \approx 1.3$ when $\eta \approx 0.18$; this implies for low modulation depth the criterion (120) can indeed be satisfied. If the noise intensity becomes extremely large, the threshold may become very large and so the perturbational treatment becomes invalid. From Fig. 48(a), for low value of Ω_2 we observe a small quasi-periodicity.

Result for heteroclinic orbits

For heteroclinic trajectories we have: If one notes $F_{2(critical)}$, the value of F_2 corresponding to η

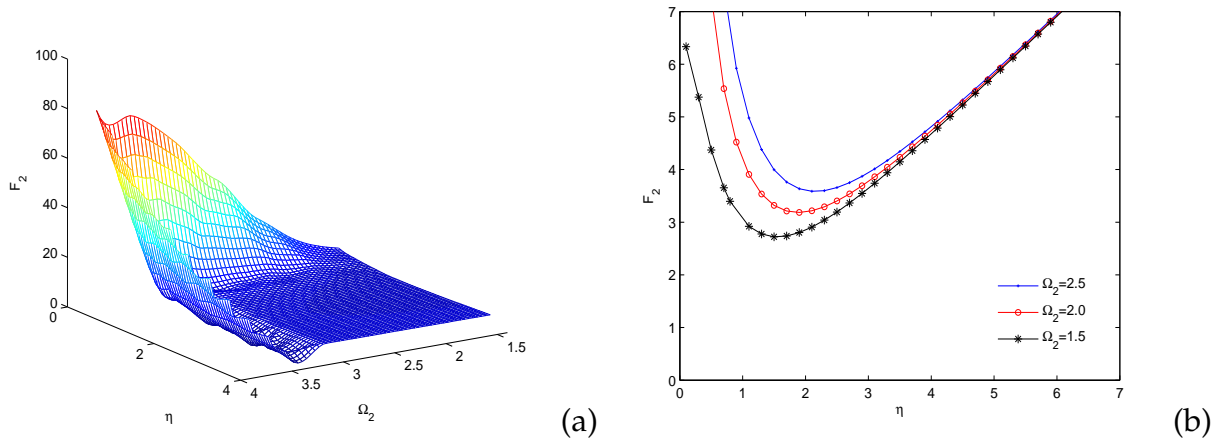


Figure 49: 3D inverse upper threshold bound in (Ω_2, η) plane with the associated threshold amplitude F_2 versus noise intensity η for homoclinic bifurcation; analytic results for different values of Ω_2 .

depicted as shown in Fig. 49(b), when the noise intensity is very low ($F_{2(critical)} \approx 6.1, \eta = 0.1$), the mean electric field change could exhibit a chaotic behavior for $\Omega_2 = 1.5$. If η is increased the critical value $F_{2(critical)}$ of F_2 in contrary decrease until reached $\eta \approx 1.5$, and begin to increase. From Fig. 49(b), the system will have a chaotic set, which may or may not be an attractor for low value of η . In Fig. 49(a), the areas above the surface correspond to Melnikov chaotic regions in which the evolution of the mean electric field has the properties of Smale-horseshoe chaos; those below denote regions of regular motion. In particular, Fig. (49) demonstrated that, in general, a controlling excitation can reliably play an enhancer or inhibitor role solely from adjusting its initial phase or intensity. Here also, if the noise intensity become extremely large, the threshold may become very large and so the perturbational treatment becomes invalid.

III.3.1 Numerical simulations

0-1 test for chaos

The final value of K_c is obtained by searching the median value of all the values obtained from different values of c . The median rather than the mean is used, since the median gives less weight to the strong outliers stemming from resonances. In Figs. 51-53, 55-56, we show the mean square displacement with the corresponding asymptotic growth rate for homoclinic and heteroclinic orbits respectively, clearly showing bounded behavior for regular dynamics, and linear growth for chaotic dynamics. In practice, to ensure $n \ll N$ we take $n \leq N_1, N_1 = \frac{N}{10}$

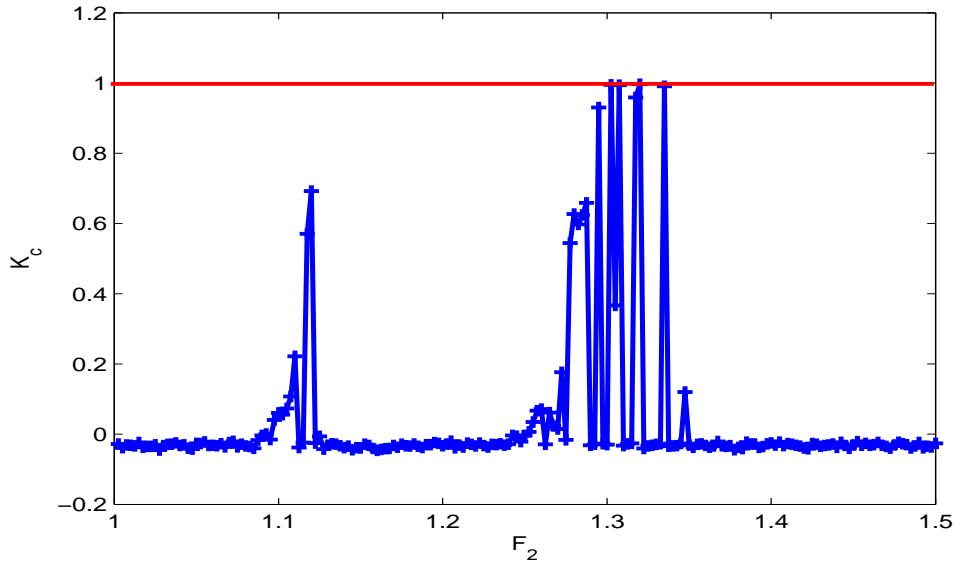


Figure 50: Asymptotic growth rate K_c versus F_2 for Eq. (66); homoclinic orbits.

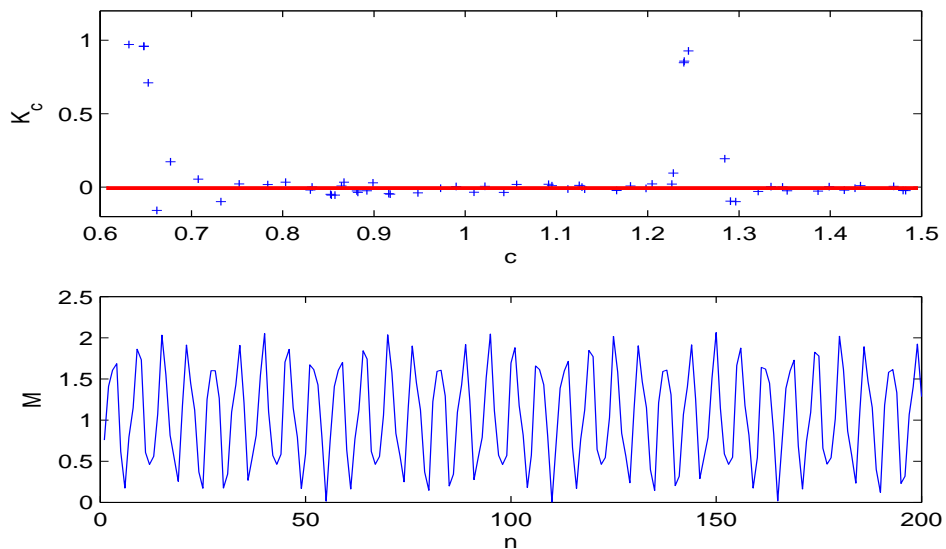


Figure 51: Plot of asymptotic growth rate K_c versus c for system (66) with the associated mean square displacement $M(n)$ as a function of n . We used here $N = 20000$ data points, and 100 equally spaced values for c . $F_2 \approx 1.2$; $\eta = 0.0$ corresponding to regular dynamics.

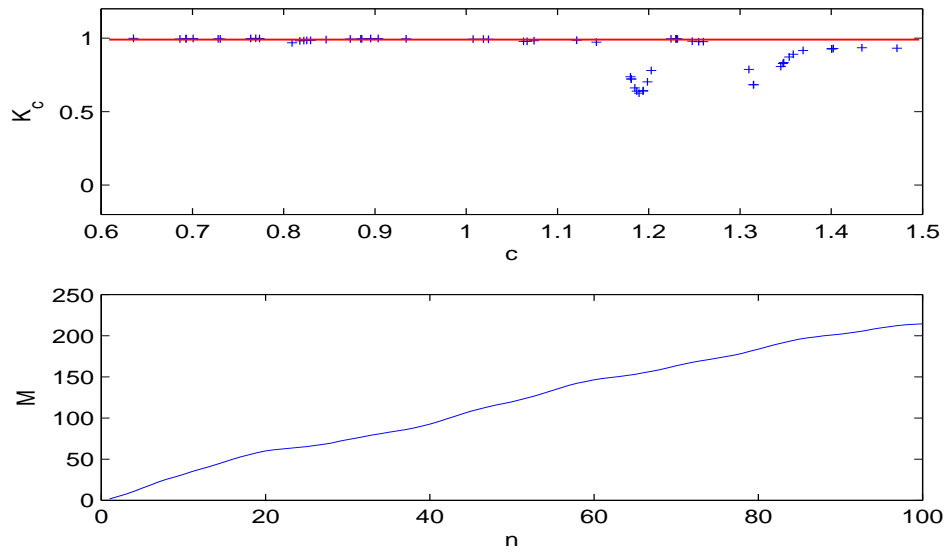


Figure 52: Plot of asymptotic growth rate K_c versus c for system (66) with the associated mean square displacement $M(n)$ as a function of n . We used here $N = 2000$ data points, and 100 equally spaced values for c . $F_2 \approx 1.31$; $\eta = 0.18$ corresponding to chaotic dynamics.

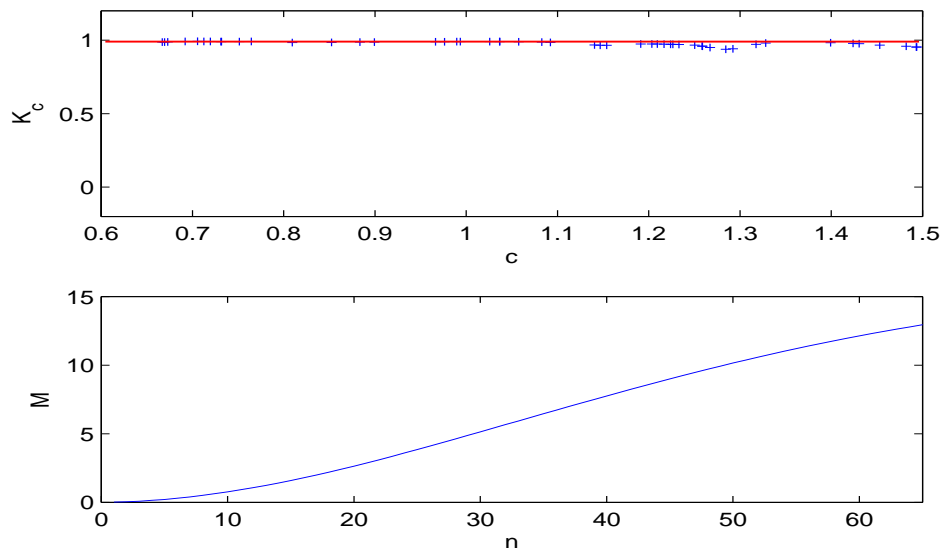


Figure 53: Plot of asymptotic growth rate K_c versus c for system (66) with the associated mean square displacement $M(n)$ as a function of n . We used here $N = 20000$ data points, and 100 equally spaced values for c . $F_2 \approx 1.31$; $\eta = 10.0$ corresponding to noise induced chaotic dynamic dynamics.

in the definition of $M(n)$. The asymptotic growth rate K_c of the mean square displacement is determined by the before mentioned formula. This has the advantage compared to a least square fit that outliers are weighted less [216] which is desirable as the linear behavior of $M(n)$ is only valid for $n \gg 1$ and can deviate strongly for small n . In Figs. 51-53, 55-56, we also plot K_c as a function of c where c is sampled uniformly as mentioned before. The figure shows that the test is essentially independent of the specific choice of c and that we are justified in taking randomly chosen values of c . Only exceptional resonant values of c yield values of K_c which do not fit the picture of $K_c = 0$ for regular dynamics and $K_c = 1$ for chaotic dynamics. Resonances with a corresponding value of $K_c \neq 0$ or 1 occur if the frequency c is commensurate with a nonlinear frequency of the dynamical equation (66). To partially avoid that these resonances distort the “true” value of K_c , we take the median value of K_c .

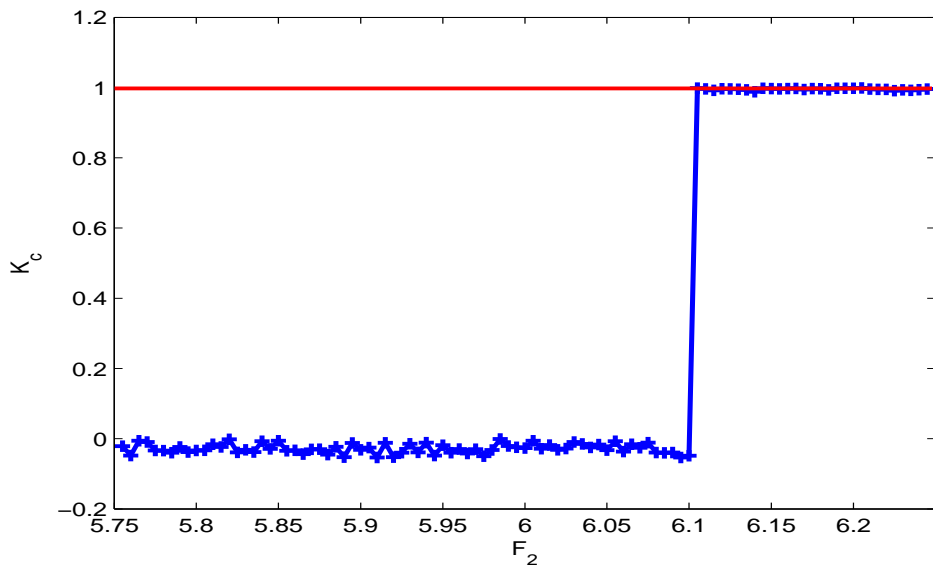


Figure 54: Asymptotic growth rate K_c versus F_2 for Eq.(66); heteroclinic orbits.

K_c is estimated in the interval $c = [\frac{\pi}{5}, \frac{3\pi}{5}]$. Predictions of F_2 from Eq. (66) through K_c could be used for comparison with the one obtain from Eqs. (120), (124). From Figs. 51-53, we observe a smooth variation of K_c when switching from $F_2 = 1.31, \eta = 0.18$ to $F_2 = 1.31, \eta = 1.0$, allowing a suspected reduction of the attractor size by noise. The before mentioned method was

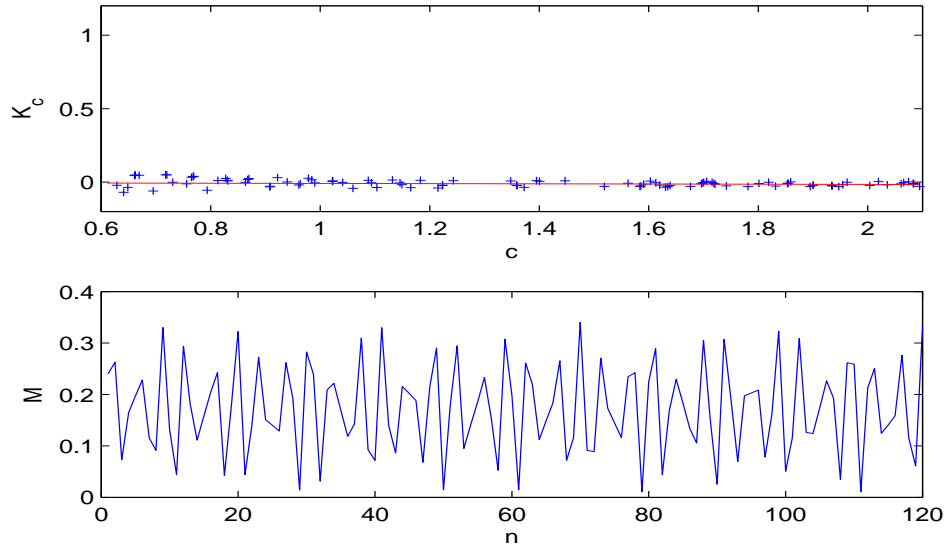


Figure 55: Plot of asymptotic growth rate K_c versus c for system (66) with the associated mean square displacement $M(n)$ as a function of n . We used here $N = 20000$ data points, and 100 equally spaced values for c . $F_2 \approx 5.0$; $\eta = 1.0$ corresponding to noisy regular dynamics.

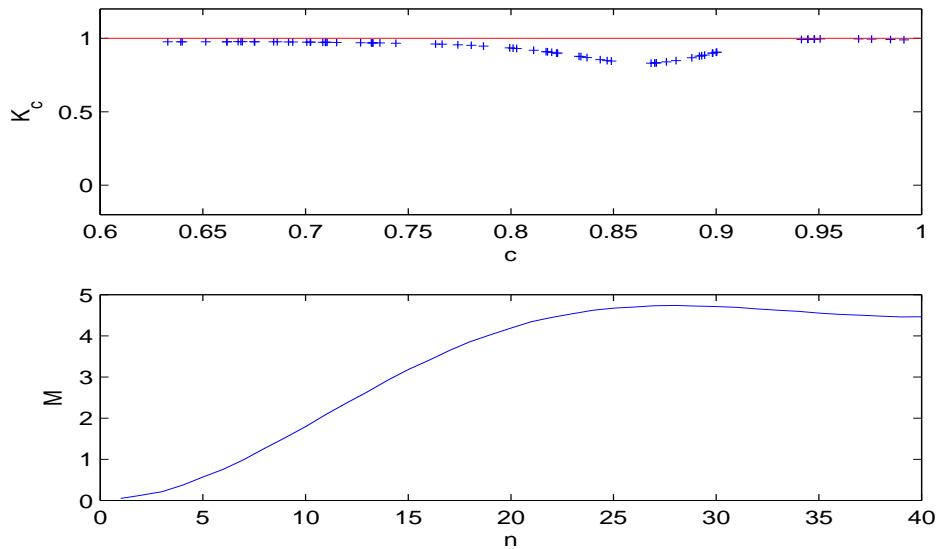


Figure 56: Plot of asymptotic growth rate K_c versus c for system (66) with the associated mean square displacement $M(n)$ as a function of n . We used here $N = 20000$ data points, and 100 equally spaced values for c . $F_2 \approx 6.1$; $\eta = 10.0$ corresponding to noise induced chaotic dynamics.

used to determine the threshold results shown in tables (172, 173)

F_2	η	$Median - K_c$	
1.2	0.0	0.0012	
1.2	1.0	0.0531	
1.2	5.0	0.9126	
1.31	0.18	0.9781	(172)
1.31	1.0	0.7902	
1.31	10.0	0.9719	

homoclinic orbits

F_2	η	$Median - K_c$	
5.0	1.0	-0.0079	
5.0	5.0	0.0899	
6.1	0.1	0.9405	
6.1	5.0	0.7642	(173)
6.1	10.0	0.97	
6.2	0.0	0.99	

heteroclinic orbit

for low noise range the numerical results are found to be in agreement (as shown in Figs. 50 and 54) with predictions from Eqs. (120), (124), instead of the variation of K_c for large noise intensity when dealing with homoclinic orbits.

Autocorrelation function and fast fourrier transform

For the homoclinic orbits the autocorrelation function are plotted in Figs. 57-58. The autocorrelation function (ACF) for Eq. 66 time series, shown in Fig. 57, with a lag time of about $l \in [0..N-1]$, reveal that when the noise intensity is increased from zero, the ACF become irregular. However, it is important to underline that absence of an initial abrupt fall of the ACF may be an indication of a non-complex behavior.

We now analyze the case of heteroclinic orbit (see Figs. 59- 62). Under the threshold F_2 , when the noise intensity is increased to $\eta = 5.0$ (see Fig. 59), the discrepancy of frequency growth up

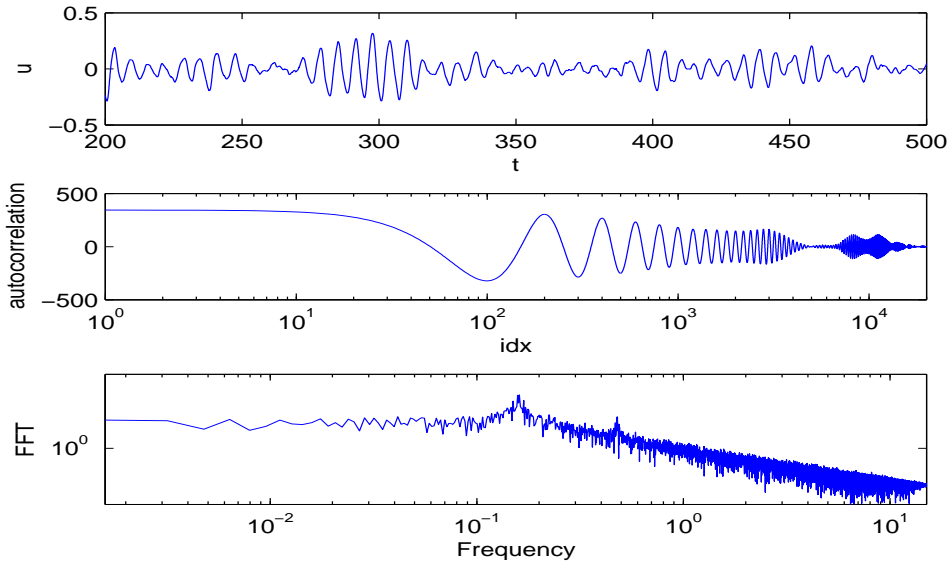


Figure 57: Time history with the associated autocorrelation functions and fast Fourier transform for time series data from system (66): $F_2 \approx 1.0$; $\eta = 5.0$ corresponding to noisy motion.

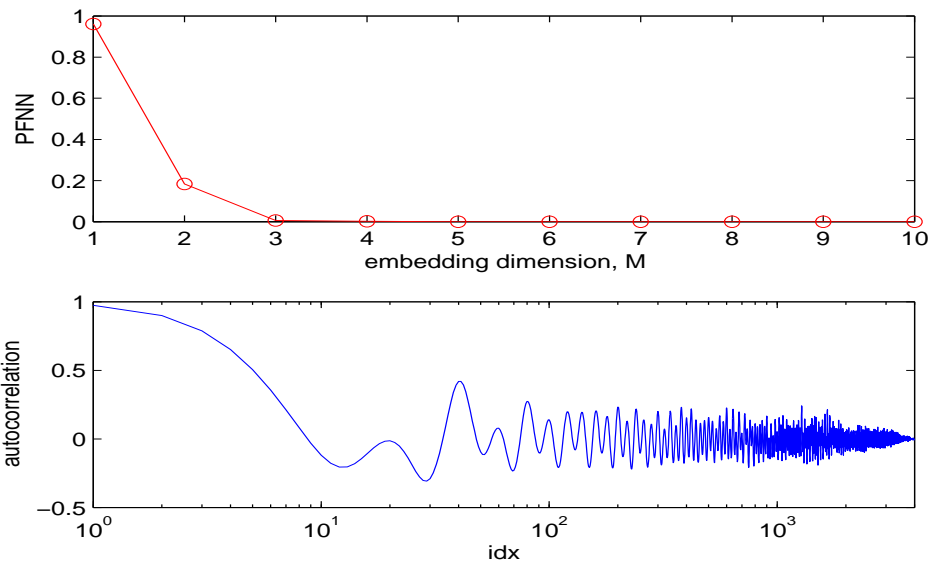


Figure 58: Percentage of false nearest neighbor for time series data from system (66), with embedding dimension m in $[0..10]$: $F_2 \approx 1.31$; $\eta = 0.18$ corresponding to chaotic motion.

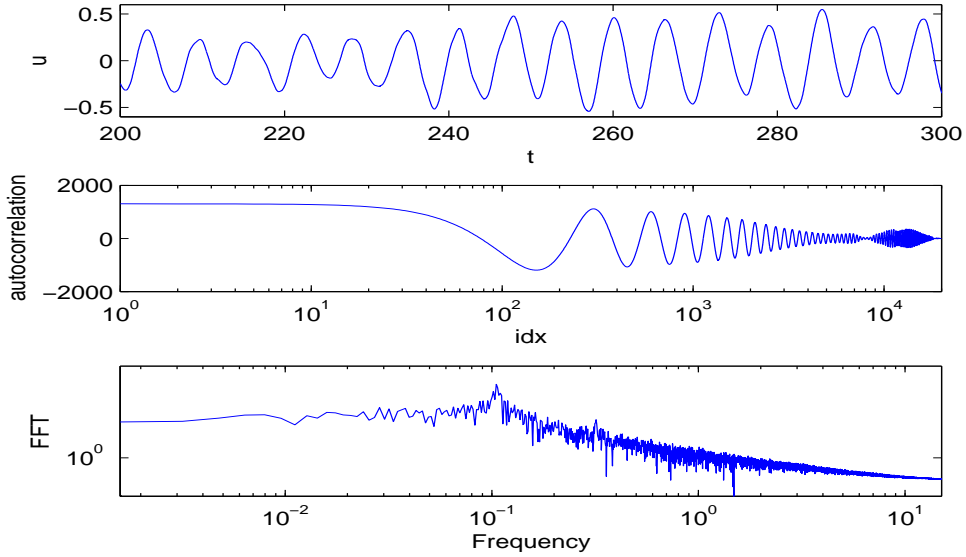


Figure 59: Time history with the associated autocorrelation functions and fast Fourier transform for time series data from system (66)-(heteroclinic orbit): $F_2 \approx 5.0$; $\eta = 5.0$ corresponding to noise-induced chaotic motion.

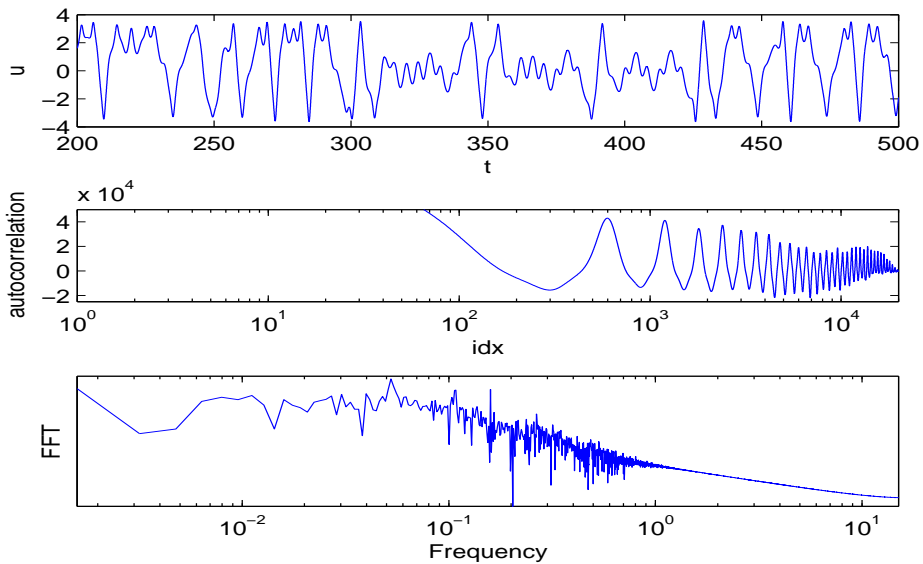


Figure 60: Time history with the associated autocorrelation functions and fast Fourier transform for time series data from system (66)-(heteroclinic orbit): $F_2 \approx 6.1$; $\eta = 0.1$ corresponding to chaotic motion.

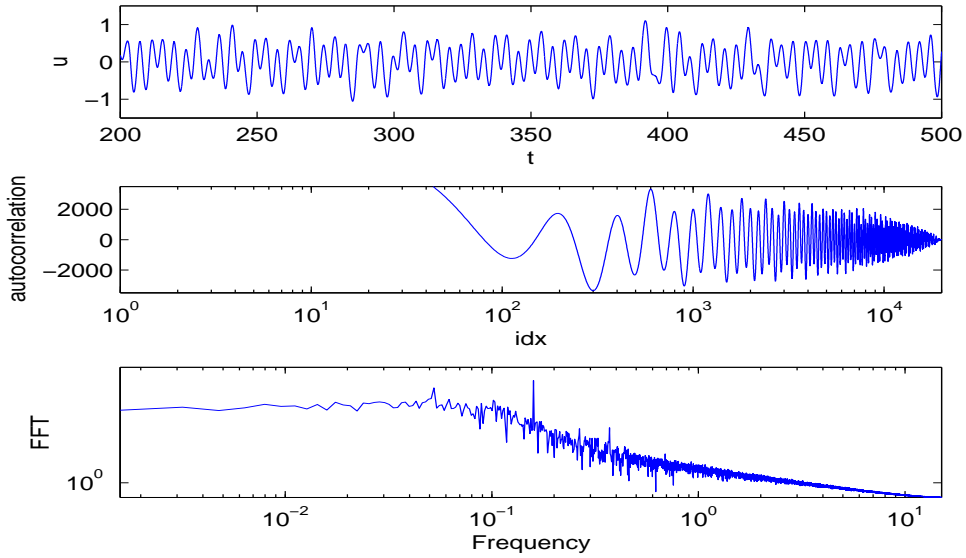


Figure 61: Time history with the associated autocorrelation functions and fast Fourier transform for time series data from system (66)-(heteroclinic orbit): $F_2 \approx 6.1$; $\eta = 1.0$.

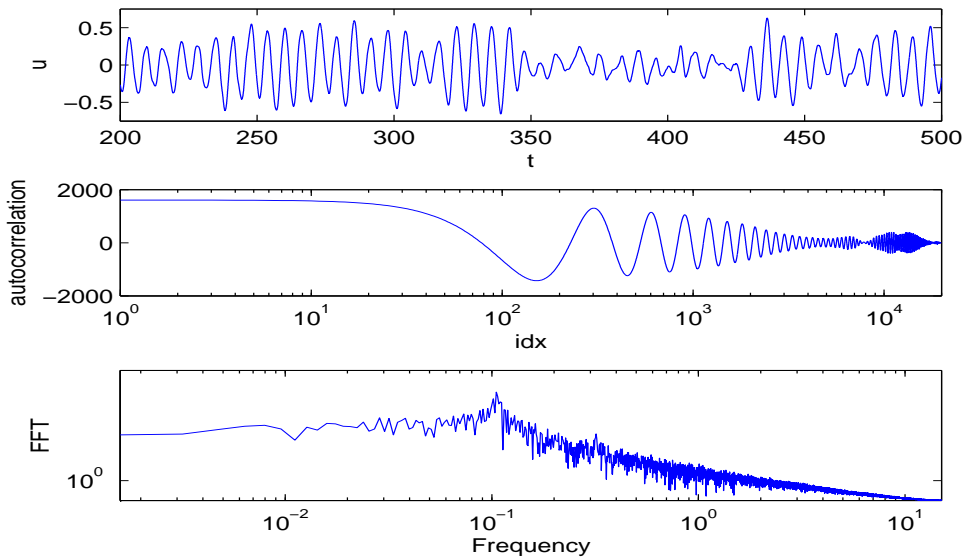


Figure 62: Time history with the associated autocorrelation functions and fast Fourier transform for time series data from system (66)-(heteroclinic orbit): $F_2 \approx 6.1$; $\eta = 5.0$.

and the apparent 3 – period of the ACF give place to irregular motion associated to high rate of decay, indicating a medium noise-induced chaotic motion.

Poincaré maps

We use the same modelization of noise as in the preceding section for numerical simulations.

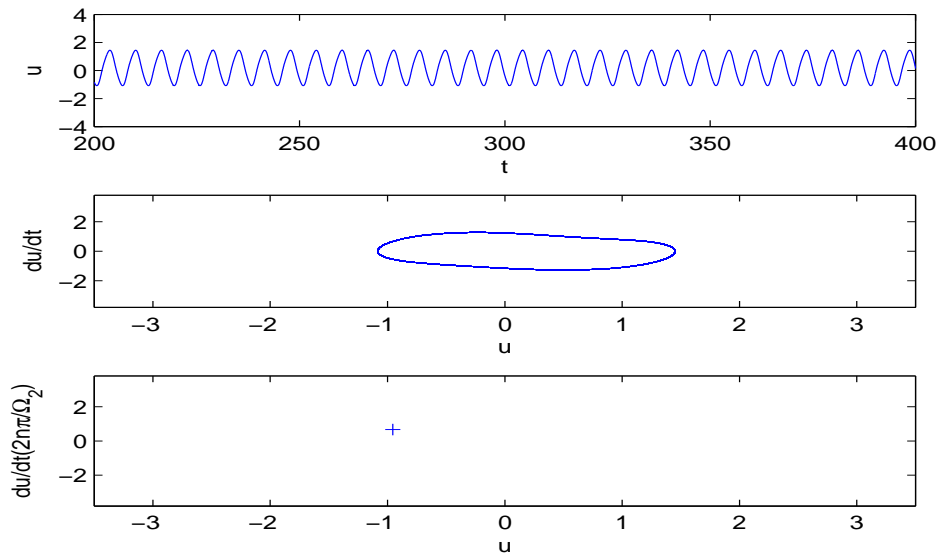


Figure 63: Poincaré map for homoclinic orbits with the associated phase portrait and time history (noise-free system, under the critical threshold): $F_2 = 1.1$; $\eta = 0.0$.

Noise can indeed induce chaos. However, this is not associated with the main 2^k cascade (see Fig. 65). One could identify three basic conditions for noise to induce chaos: (1) the noise level has to fall within a certain narrow range, below this range it would not be sufficient to induce chaos, whereas noise above this range would destroy the induced chaos, if chaos can indeed be induced. (2) when subject to a noise source of strength within this range, the adjacent chaotic states should still behave chaotically on certain finite scales. (3) and most important, the periodic state itself, when subject to weak noise, should undergo a process that is much more diffusive than the Brownian motion [217]. When noise induces chaos the complete period-doubling cascade is inhibited, otherwise the cascade is simply masked by noise. In a continuous-time dynamical system, a nonchaotic attractor coexists with a nonattracting chaotic saddle. Under the influence of noise, chaos can arise. The topology of the flow is fundamentally disturbed after the onset of noisy chaos; such a disturbance is due to changes in the number of unstable eigendirections along a continuous trajectory under the influence of noise.

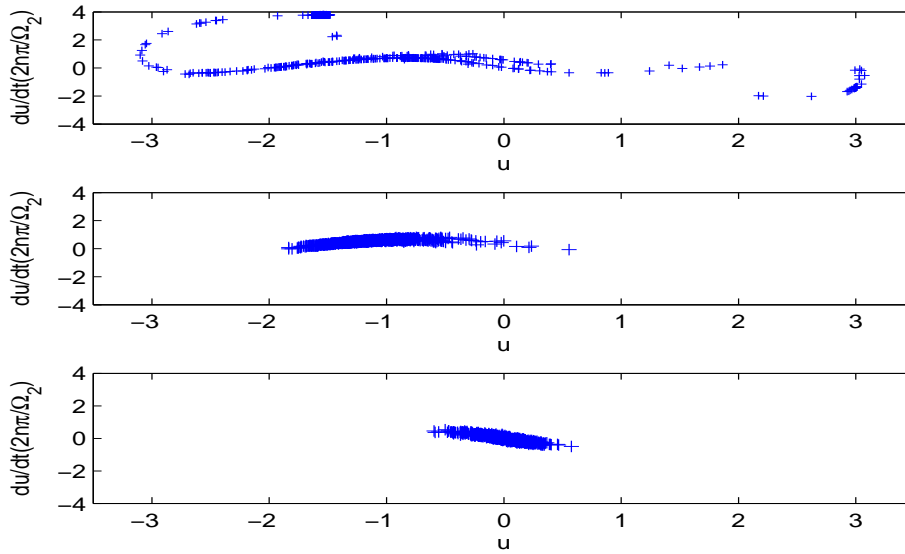


Figure 64: Poincaré map for homoclinic orbits with different noise amplitude: $F_2 \approx 1.3$ (first row) $\eta = 0.18$; (second row) $\eta = 1.0$; (third row) $\eta = 5.0$.

The Poincaré maps for Eq. 66 for heteroclinic orbits, subject to external bounded noise are shown in Figs. 66-68.

Scaled power spectrum densities

Again we postpone a detailed description of the influence of noise. Since the structure of the periodic orbit must acquire finer structure, it is clear that even very small noise will eventually play a role. The power spectrum (Figs. 70-72) for Eq. 66, with different value of noise level and F_2 ; computed using a standard algorithm along an orbit of 20000 iterates are depicted for homoclinic orbit.

The heteroclinic orbit seem to be more sensitive to noise than the homoclinic ones. The power spectrum of the bounded noise excited system (Eq. (66)) for different value of F_2 are plotted in Figs. 71-72. Results are plotted in Fig. 71 for noise-free system with $F_2 \approx 5.9$, $\eta \approx 0.0$.

III.3.2 Discussion

The ACF for Eq. (66) time series, shown in Fig. 58, indicates an exponential decay. Such an exponential decay of the ACF may be an indication of the chaotic behavior of the process. On the other hand, the irregular behavior of the ACF may be an indication that one is dealing with a process, which is not completely deterministic but has a very low stochasticity. The above

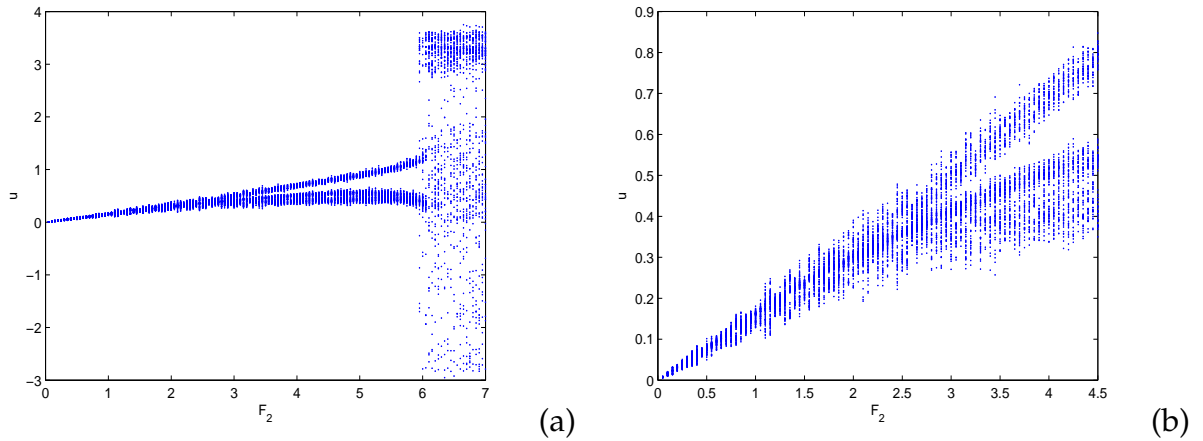


Figure 65: Noisy bifurcation diagram for heteroclinic orbits with the associated zoom for $F_2 \in [0.4, 5]$ (noisy system, under the critical threshold): $\eta = 0.18$.

observation is confirmed by the rapid decay to zero [218], of the associated percentage of false nearest neighbor.

When the critical threshold ($F_2 \approx 6.1$; $\eta \approx 0.18$) is reached as shown in Fig. 60, the ACF for the same sets of data is depicted. The "grassy appearance" of the Fourier transform(FFT) in Fig. 60 and the aperiodicity and complexity of the autocorrelation function are characteristic of a chaotic signal, the exponential decay shows a loss of memory and confirms the presence of chaotic dynamics. We integrate Eq. (66), with different noise amplitudes. From the threshold, when the noise amplitude is increased (see Figs. 61, 62) the complex behavior of ACF give place to: apparent regular motion for $\eta \approx 1.0$ and irregular motion for $\eta \approx 5.0$. Therefore, hyperbolic coherent chaos exhibits some properties of nonhyperbolic chaos; "dynamical stochasticity" proves to be stronger than the "chaoticity". Then, noise has a great effect on the ACF of the quasihyperbolic attractor. However, in the regime of the nonhyperbolic attractor, the FFT has less peaks with the presence of same level of noise (see the curves in Fig. 59). Noise also reduce the amplitude of oscillations. The results reported in Figs. 61, 62 show that for both small and large noise amplitudes, the noise-excited oscillations appear to be rather irregular, while for low noise relatively coherent oscillations are observed. This phenomenon, which is call coherence resonance [219], resembles the well-known stochastic resonance. The stochastic resonance appears if both periodic and noisy forces drive a nonlinear system, with the periodic response having a maximum at some noise amplitude. One can see that the correlations decay rate is indeed much more pronounced for the large noise. The dynamical regimes appearing in this bounded noise-driven

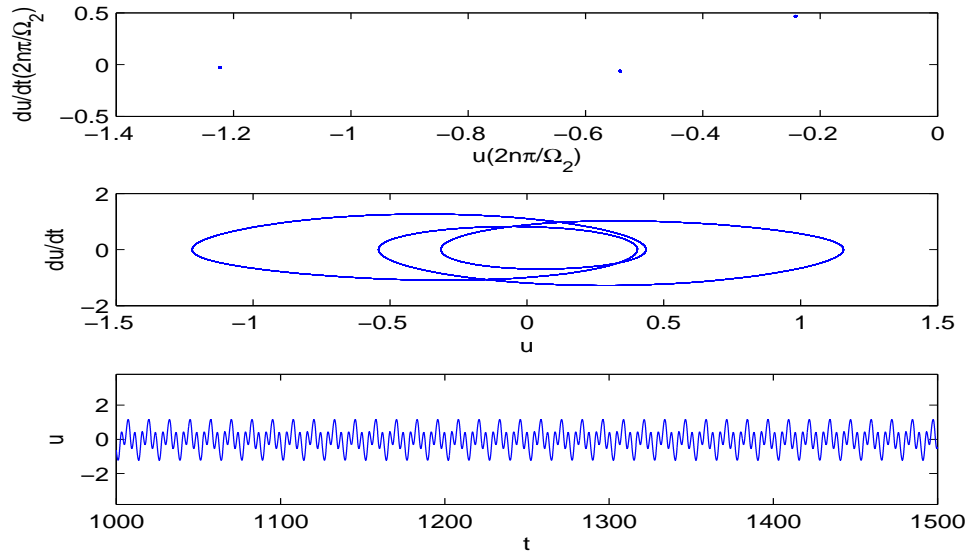


Figure 66: Poincaré map for heteroclinic orbits with the associated phase portrait and time history (noise-free system, under the critical threshold): $F_2 = 5.9; \eta = 0.0$.

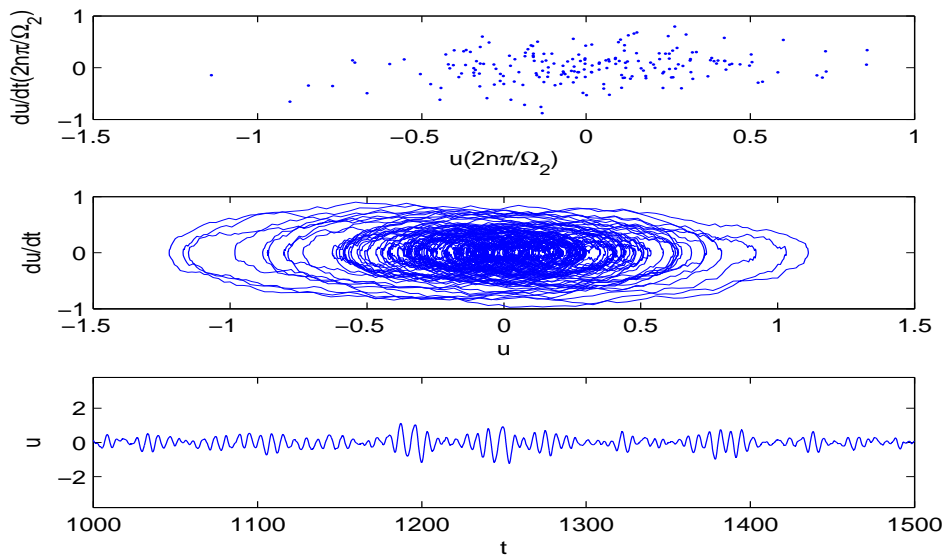


Figure 67: Poincaré map for heteroclinic orbits with the associated phase portrait and time history (noisy system, F_2 under the critical threshold): $F_2 = 5.9; \eta = 5.0$.

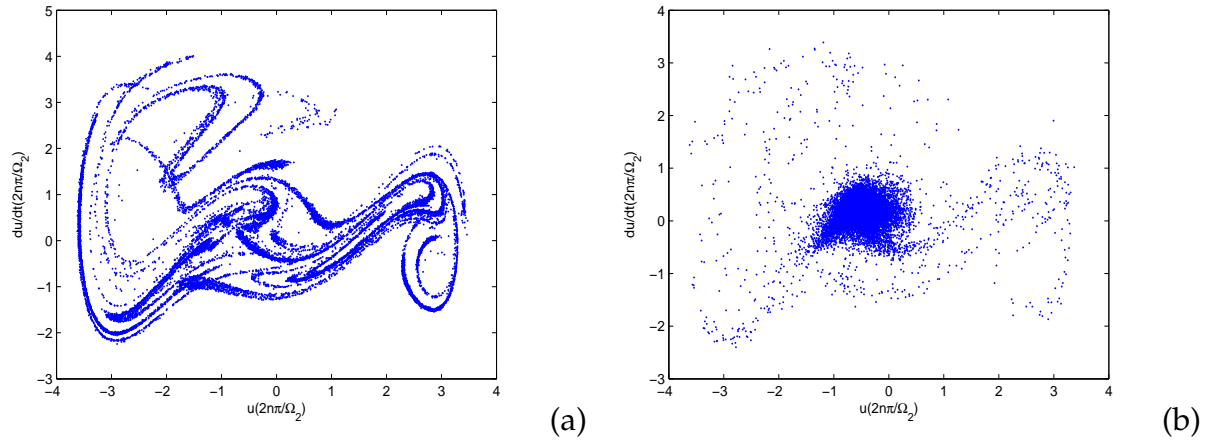


Figure 68: (a)-Poincaré map for heteroclinic orbits (noisy system, F_2 at the critical threshold): $F_2 = 6.1; \eta = 0.1$; (b)-Poincaré map for heteroclinic orbits (noisy system, F_2 at the critical threshold): $F_2 = 6.1; \eta = 1.0$.

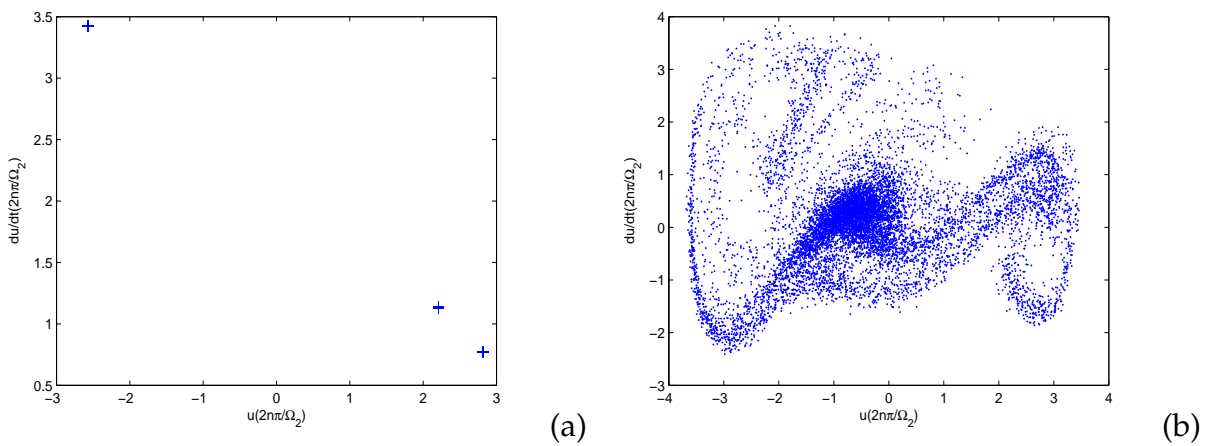


Figure 69: (a)-Poincaré map for heteroclinic orbits: $F_2 = 8.0; \eta = 0.0$. ; (b)-Poincaré map for heteroclinic orbits: $F_2 = 8.0; \eta = 1.0$.

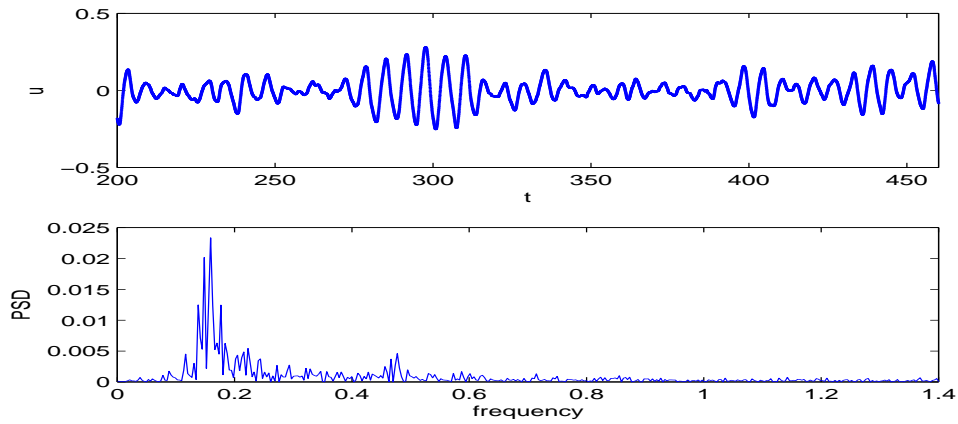


Figure 70: Scaled power spectrum of $u(t)$ oscillations in system (66) -(homoclinic orbits) for: $F_2 = 1.0$ and noise intensity $\eta = 5.0$.

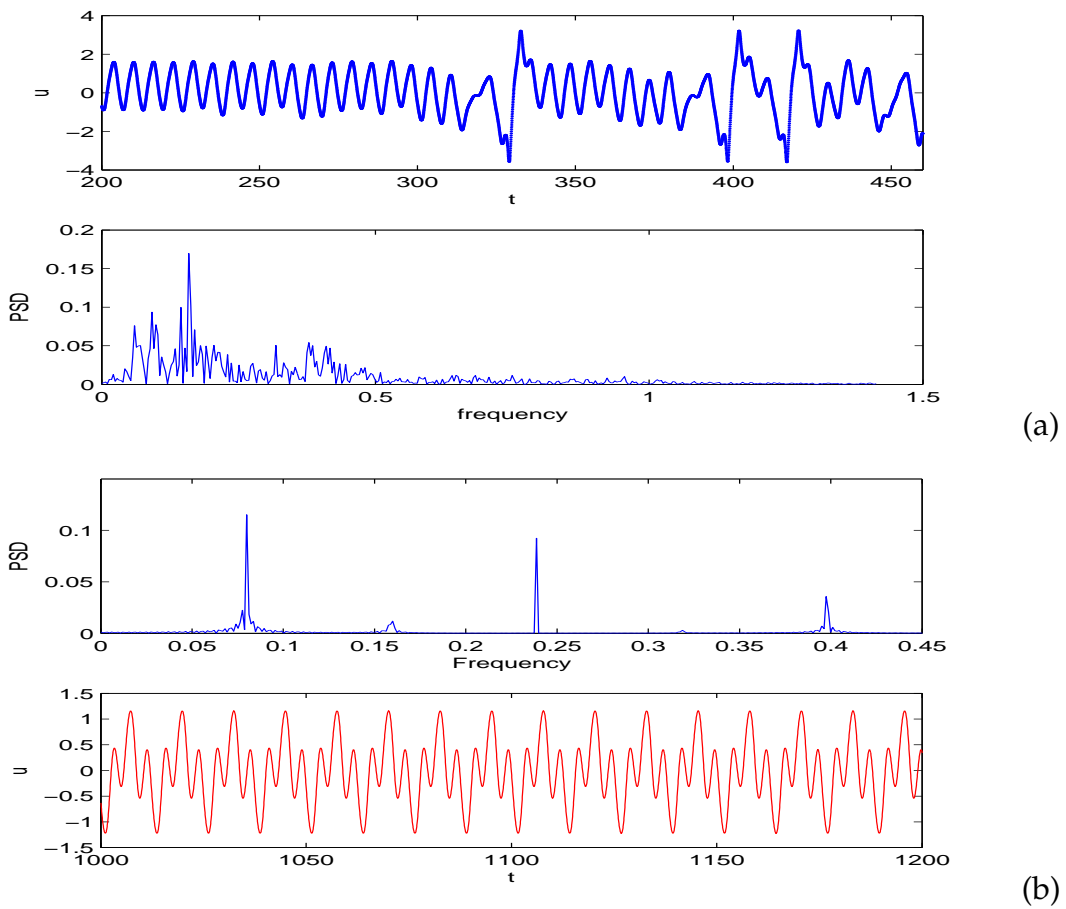


Figure 71: (a)-Scaled power spectrum of $u(t)$ oscillations in system(66) -(homoclinic orbits) for: $F_2 \approx 1.3$ and noise intensity $\eta = 0.18$. ; (b)-Scaled power spectrum of $u(t)$ oscillations in system(66) -(heteroclinic orbits) for: $F_2 = 5.9$ and noise intensity $\eta = 0.0$.

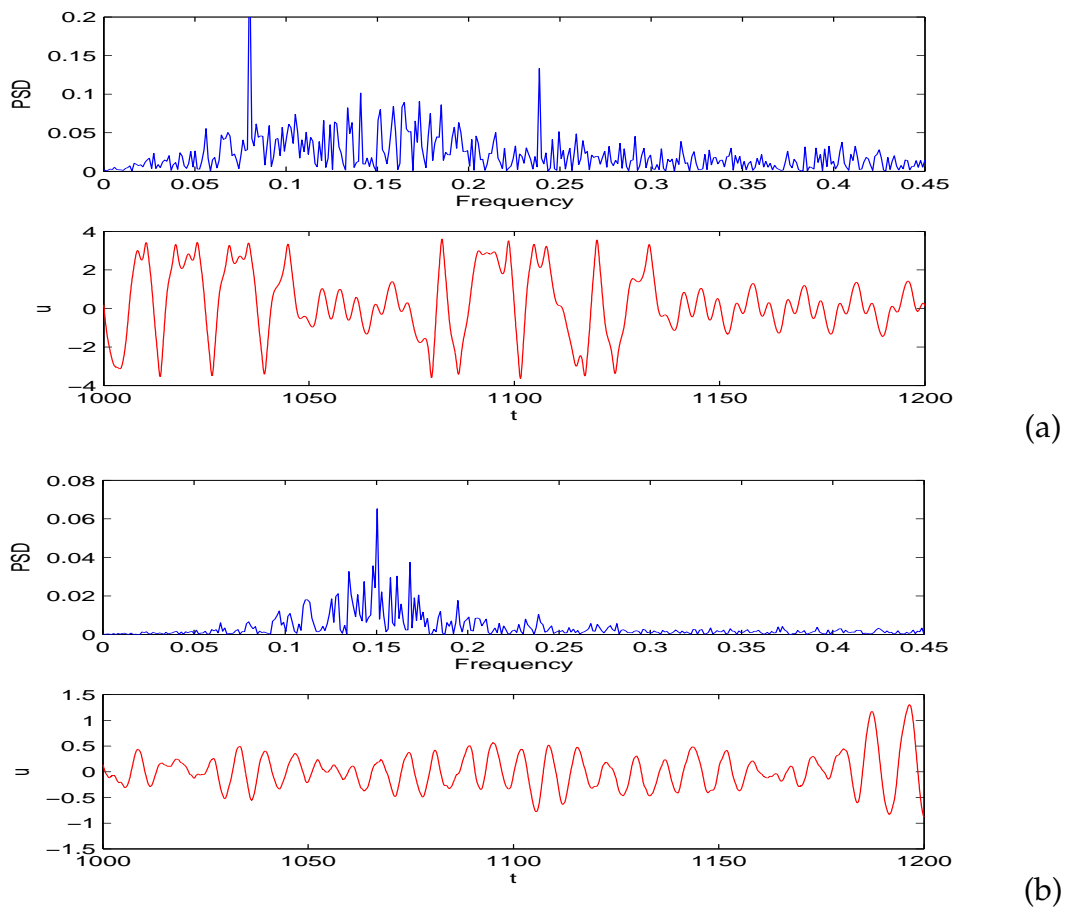


Figure 72: (a)-Scaled power spectrum of $u(t)$ oscillations in system(66) -(heteroclinic orbits) for: $F_2 = 6.1$ and noise intensity $\eta = 0.1$. ; (b)-Scaled power spectrum of $u(t)$ oscillations in system(66) -(heteroclinic orbits) for: $F_2 = 6.1$ and noise intensity $\eta = 5.0$.

excitable system can be rather nontrivial. For the selected values of parameters mentioned before and on figures captions, the oscillator exhibit a chaotic motion developing onto an attractor which does not display a unique center of rotation (see Fig. 64). It is seen from Fig. 64 that for larger noise intensity the map occupies small area in phase plane. Without noise, under the threshold, the steady-state Poincaré map of periodic motion is one points (see Fig. 63). When bounded noise is present in the system, the Poincaré maps are not diffused but reduced into one smaller area in phase plane. It can be observed from Figs. 66-67 that under the threshold, the motion of Eq. (66) goes from periodic to random as η increases from zero and diffuses in a smaller and smaller domain of phase plane as η further increases. From Fig. 68 we can see that the strange attractors for two different noise level are different when reached the threshold. One can see that as noise increase, the Poincaré map diffuse in the phase plane; for larger noise intensity, the Poincaré maps diffuse and accumulate around the point $(x, y) \approx (-0.782, 0.272)$ in phase plane. All these figures show how the motion of Eq. (66) goes:- from periodic to random chaos as η increases,-from noise induced chaos to completely random chaos, and confirm both the threshold amplitudes obtained by the Melnikov and $0 - 1test$ methods. It should be noted that the transition of the motion of the system from noise induced chaos to random chaos is gradual and the threshold amplitude F_2 for the onset of chaos should be in a range $F_2 \pm \delta F_2$. Thus, it can be concluded that over some range of η both the random Melnikov process with meansquare criterion and $0 - 1test$ can correctly predict the threshold amplitude for the onset of chaos for Eq. (66) under external bounded noise excitation. For $F_2 \approx 8.0$, the Poincaré section consists of three points (see Fig. 69(a), the motion is periodic with the period $3T$; for $F_2 \approx 7.5$, the Poincaré section does not consist of identifiable finite number of discrete points, the motion is aperiodic, it may be chaotic as shown by the attractor obtained. Similarly, when we are over the critical threshold F_2 , the motion of Eq.66 goes from: - chaos to random chaos as η increases from zero to $\eta = 1.0$ and becomes more random and less chaotic for $F_2 \approx 7.5$; - $3 - period$ limit cycle to random chaos suddenly (see Figs. 69(a,b)) for $F_2 \approx 8.0$. It should then be noted that the random chaos obtained at the threshold is transient. The difference in threshold amplitude obtained by random Melnikov process with meansquare criterion and by the $0 - 1test$ is larger for large noise intensity. For small η the PSD has only one maximum. With the increase of η as shown in Fig. 70 however, there appears a second low maximum at a different frequency ≈ 0.47 , and many other low amplitudes around them, which corresponds to the diffusion of the

trajectory on a diffused limit cycle. Fig. 71(a) shows, the power spectrum of the same signal at the threshold amplitude $F_2 \approx 1.31$. Although in the presence of a chaotic attractor all trajectories converge toward a subset of the phase space, inside the attractor, two neighboring trajectories may diverge (see the before explained corresponding Poincaré map). This fact reflects the extreme sensitivity of chaotic dynamics to the initial conditions. In this case the power spectrum has a continuous broadband character. The broadness of the peaks in Fig. 71(a) together with the time domain behavior displayed within show that the processes are not deterministic limit cycles. The broad-band nature of the power spectrum is another aspect of chaotic systems. Spectral analysis confirms the visual impression from the time history that the processes represent a nonlinear oscillation that is strictly chaotic. There exist estimates on the relation between the noise level and the maximal period which can be observed. This result, which is somewhat counterintuitive, will be explained. This is of course related to the power spectrum described above. In effect, as demonstrated in the above paragraphs the chaos of the scenario is not so strong, order can be accidentally established by small noise terms, much like a very attracting fixed point could be locally and dramatically altered by noise, and globally there is at most a great probability to change stochastically from one basin of attraction to another. It is seen from Fig. 71(b) that the spectrum of periodic motion consists of three discrete peaks; there are spikes at the frequencies which are multiples of the excitation frequency and/or inverse multiple of the excitation frequency. as the noise intensity becomes larger, the power spectrum is not only composed of discrete peaks, but also of continuous, broadband nature. Also, as the noise intensity becomes larger, there are several harmonic peaks that appear, and the system becomes more chaotic. Figs. 72(a,b) shows, respectively, the power spectrum of the same signal, but at the critical threshold. The broadband nature of the power spectrum is another aspect of chaotic systems. A transition from multifrequency regular oscillations to complex oscillations with a continuous spectrum are observed in the medium at any spatial point. It should be noted the band into which the power spread is reduced when increasing the noise intensity. The analysis of the local slopes of the correlation function, Poincaré sections and power spectral density give evidence for deterministic dynamics, chaos slightly affected by noise; and noise induced chaos, for some parameters ranges. Some times the analysis of the local divergence of nearby trajectories suggests a stochastic dynamics.

Tokamaks as high order, distributed parameter, nonlinear systems with a large number of

instabilities, give rise to many extremely challenging mathematical modelling and control problems, that need to be solved; this is especially true for a fusion power reactor. The tokamak control problems can be separated into two major classes: electromagnetic control and plasma kinetic control.

Plasma kinetic control refers to controlling particle feed rates and heating to modify the plasma density, temperature, pressure, and current density. Due to the distributed parameter nature of tokamaks, it is important to control not only spatially averaged values of these physical variables but also their spatial profiles. Energy confinement, stability properties, and the fraction of noninductive current, which is fundamental for steady-state operation, can be improved through control of internal pressure and current profiles. In addition, electromagnetic and kinetic control, including internal profile control, must be well coordinated with control action to avoid or stabilize instabilities. Optimization of the plasma shape and internal profiles can reduce the strength of these instabilities, or in some cases prevent them.

A approximation of plasma behavior in tokamaks have been made by Schröder and Klinger [220], where the magnetized plasma column is immersed in a stainless-steel tube, which is positively biased to predefine the potential at the azimuthal boundary. Drift waves propagate azimuthally in the magnetized plasma column due to fluctuation-induced $\mathbf{E} \wedge \mathbf{B}$ drift in the presence of a radial density gradient. Control parameters for drift wave dynamics are the grid bias and the tube bias V . Both biases superimpose a radial electric field across the plasma column and thereby an $\mathbf{E} \wedge \mathbf{B}$ rotation, which destabilize drift waves. Increasing either grid bias or tube bias leads to a transition scenario from a stable plasma state to drift wave turbulence. The spatiotemporal drift wave dynamics is observed using a circular array of 32 equally spaced cylindrical Langmuir probes, operated in the electron saturation current regime to measure density fluctuations.

Tokamak reactors are pulsed machines [221], in each pulse the plasma is created (“start-up” phase), then its current is ramped up to a reference constant value, called the “flat-top” current, which is maintained in a burning state along the main phase of the discharge, and eventually the current is ramped down and the plasma is terminated. The time trajectories of the poloidal field (PF) and toroidal field (TF) coil currents and of the main plasma parameters that guarantee this sequence define a “scenario”. To initiate the discharge, hydrogen gas is puffed into the tokamak vacuum vessel and the toroidal field coil current is increased to create a steady-state magnetic

field to contain the plasma when initially created. Then a large electric field is produced within the torus using the CS (*ohmic heating*) coils. This electric field rips apart the neutral gas atoms and produces the plasma. The plasma current in the plasma is built up by transformer action. The collisions of the ions in the plasma make the plasma resistive. It is this resistance that heats up the plasma (thus the origin of the term “ohmic heating”). When the temperature increases, the resistance decreases and the ohmic heating loses effectiveness. To significantly increase fusion reactions, the temperature must be increased to over 100 million degrees, which is six times the temperature at the centre of the sun. This heating is accomplished by particle beams (injecting energetic ions) or by radio frequency or microwaves (heating ions or electrons). Shortly after the discharge starts, additional gas is puffed into the chamber to increase the density and/or pressure to the desired levels.

Electromagnetic control refers to controlling the magnetic and electric fields, which maintain or change the plasma position, shape and current. As was previously explained, this task is performed by the poloidal coils distributed around the vessel that contains the plasma. Voltages are applied to these coils, which drive currents that generate the magnetic fields [222]. The magnetic fields, regulated by feedback control, induce plasma current, change the plasma shape, and stabilize the intrinsically unstable plasma vertical position. AT plasma regimes require production and regulation of extreme plasma shapes that allow operation at high plasma pressure.

The plasma magnetic control action varies the current in the PF coils [223]; these currents generate magnetic fields which interact with the plasma, modifying its current (plasma current control), position, and shape (plasma shape control). The PF coil currents are then decomposed into the sum of two terms: a preprogrammed nominal (feedforward) part, that is decided before the discharge in order to have the desired plasma parameters along the prescribed trajectories corresponding to given scenarios, plus a component used for feedback control, that is needed to counteract the effect of disturbances, model inaccuracies, etc.

In many magnetically confined fusion experiments, plasmas may undergo a spontaneous transition to a turbulence suppressed regime, which is known as the before mentioned L-H transition [119]. Chaos and turbulence are often considered as troublesome features of plasma devices, but they can also lead to other desirable phenomena as the generation of global structures, such as dynamo magnetic field, zonal flows, transport barriers, enhanced transport and quenching transport [117]. In the general framework of nonlinear dynamical systems, a number

of strategies applied to plasma instabilities have been developed to achieve active control over complex temporal or spatio-temporal behavior [107]. In the presence of electric field fluctuations and gradients, a class of low-frequency electrostatic instabilities, the drift waves caused by the $\mathbf{E} \wedge \mathbf{B}$ motion of particles, arise in magnetized confined plasmas; this drift waves can be responsible for anomalous transport in magnetically confined high-temperature plasmas [114]. Zonal flows, that play a crucial role in regulating turbulence could be nonlinearly generated by a finite amplitude monochromatic drift wave [116]. In 2008 Yamada et al. [117] have made the first experimental identification of a streamer (state of bunching of drift waves) that should degrade the quality of plasmas for magnetic confinement fusion.

The modeling of the H -mode have been developed focusing on the role of radial electric field which either give rise to bifurcations in confinement state [118] or suppresses instabilities thus reducing the anomalous transport. Therefore, controlling the electric field dynamics is of great interest. Maximizing the fusion power production in toroidally symmetric magnetic confinement devices (tokamaks [224]) requires high-confinement (H -mode) plasma conditions that have high edge plasma pressures. One of the critical issue for fusion plasma research is the erosion of the first wall of the experimental device due to impulsive heating from repetitive edge magneto-hydrodynamic instabilities known as “edge-localized modes”. This repetitive instabilities (ELMs) release a significant fraction of the thermal energy of the plasma to the first wall of the device. Burning plasmas require high electron pedestal temperatures at relatively high electron pedestal densities to achieve significant fusion power gain factors. If allowed to reach plasma-facing wall components, energy impulses of the required magnitude will cause increased erosion of plasma facing components and significantly reduce their lifetime [225]. Thus, controlling ELMs by replacing the energy impulses with an equivalent but more continuous transport process is a high priority issue for tokamak fusion research [226]. It had been showed that the addition of small resonant magnetic field perturbations (A particularly appealing ELM control approach in low beta plasmas is based on the concept of using an edge stochastic magnetic field to increase the electron thermal diffusivity [227]) completely eliminates ELMs while maintaining a steady-state high confinement (H -mode) plasma. Stochastic layers are created by adding small resonant magnetic perturbations ($RMPs$) to the equilibrium magnetic field using external coils. These perturbations induce a chaotic behaviour in the magnetic field lines, which reduces the edge pressure gradient below the ELM instability threshold. The pressure gradient reduction

results from a reduction in particle content of the plasma, rather than an increase in the electron thermal transport. These results provide a first experimental test of stochastic transport theory in a highly rotating, hot, plasma and demonstrate a promising solution to the critical issue of controlling edge instabilities in fusion plasma devices [228].

The various dynamical regimes of collisional drift waves that are related with strong modulations of the ion and electron density in a magnetized plasma have been experimentally studied [208], with the rotating plasma column as the control parameter of the dynamics; regular, chaotic and turbulent regimes were obtained. A transition to a quiescent H -mode is related to the completely damped out of drift waves [229], that could then be related to a coherent or regular behavior of the electric field E_r . As showed in the previous section, it is possible to control the irregular fluctuations of the radial electric field that leads to the generation of drift waves, by looking for $F_2 \equiv F(b_4, \Omega_2) \equiv F(f_2, \Omega_2)$ that depend to the controlling external electric field. This amplitude can be used to minimize the effects of noise in the system.

The dynamical scenario described in our work, could reflect a situation of chaotic regime that is close to the well-developed turbulent regimes found in plasmas, where one expects a huge number of modes to become actively involved in the dynamics. Nevertheless, we believe the dynamical systems approach discussed in this work may be helpful to understand more complex cases.

As a matter of fact, in the control of plasma position, current and shape, the use of feedback control is mandatory, not just a choice. Indeed, in order to maximize performance-to-cost ratio, it is necessary to use plasmas with vertically elongated (i.e., egg-shaped) cross-sections; unfortunately this elongation, leads to instability of the plasma vertical movements [230]. As a consequence, at least for vertical position stabilization, feedback control needs to be adopted for vertically elongated plasmas. In addition, a strong motivation for improving plasma control in next generation tokamaks is that the plasma boundary must be maintained as close as possible to nearby components. This objective guarantees the best use of the available volume. Currents in the neighboring metallic structures; these currents, generate a magnetic field that opposes plasma movement and therefore ensures a sort of passive stabilization. Hence the ability to control the shape of the plasma, while ensuring good clearance, is an essential feature of plasma control systems.

General Conclusion

Main results

We have studied different bifurcation phenomena, resonance and chaos in two models of plasma: Two fluid model of plasma, firstly without noise and secondly with an associated bounded noise; the nonlinear model of radial electric field dynamics in plasma L-H transition observed in tokamaks.

- We have derived a modified nonlinear forced van der-Pol-Duffing-Mathieu evolution equation (57) with asymmetric potential for density perturbation in plasma, by considering an appropriate source term in the two fluid model equation. The model has been analyzed under chaotic and regular considerations. Note, chaotic vibrations have a noise-like frequency spectrum of a wide range which are very harmful for surface plasma confinements. Introducing a parametric excitation in the internal frequency of the system, we use the analytical Melnikov theory and predict the lowest critical amplitude where the system may transit to a chaotic motion. This prediction has been confirmed numerically. It must be underlined that for fixed value of the external force amplitude, an increase of the parametric excitation amplitude decreases the threshold of the appearance of chaotic motion. The prediction is also valid for fixed value of the parametric force amplitude and varying external perturbation amplitude. Numerical calculation of the maximum Lyapunov exponents of the original system also validates that the threshold amplitude A_0 for onset of chaos will globally decrease as the parametric excitation intensity increases. However, for very low values of the external excitation, large parametric excitation intensity, and high values of γ , further investigation is needed to clarify the inconsistency between the two kinds of thresholds given by the Melnikov method, and by the Poincaré maps or the numerical simulation of the maximum

Lyapunov exponents. These results provide some insight into the dynamics and control of instabilities occurring in double plasma device, that could be helpful for experimental studies design.

- We addressed analytically and numerically the effect of bounded noise excitation on the dynamic response of density perturbation in plasma. Analytically solutions are obtained firstly by multiple scale method. In order to have an approximate solution for our nonlinear system with noise, the cumulant-neglect closure is applied to bounded noise excited density perturbation. We use it to compute the statistical moments of the stationary response to noise excitation for which the moment equations to be solved are algebraic. The result shows the effect of variations induced by different system parameters such as damping component and bounded noise parameters on the amplitude response of the system when it undergoes a principal parametric resonance condition. It was found that the steady-state response is a monotonic increasing function in the nonlinear terms γ , and detuning parameter σ . For the steady- state response with noise, it is a monotonic increasing function in the statistical moments which multiplies the jump phenomena and increases the hysteresis one. The bounded noise through η also affects the behavior of the system. Numerically simulated results showed the influence of bounded noise on the time evolution, and on the poincaré map of the system. Generally speaking, good qualitative agreement between analytical and numerically simulated result was achieved in terms of noise effect on the system. Our work could be helpfull to establish periodic operation of plasma devices in regimes where usually chaotic oscillations occur. Our future studies could be focused on the calculation of the joint probability density for the same or different kind of noise excitation considered in our system.
- After discussing mean electric field change modeling in which we introduce a noise component which was absent in previous treatments [159], Melnikov's method was used to analytically predict the existence of chaos in the normalized radial electric field change, near plasma edge in Tokamak L-H transition; which is governed by a nonlinear Vander Pol ϕ^6 -equation perturbed by a bounded noise. The

criteria resulting from this analysis are inequalities that are useful for designing an oscillator's parameters so that chaos either occurs or does not occur as desired. The results indicate that the presence of larger noise enhances the threshold amplitude F_2 and reduces the possible chaotic domain in parameter space. For numerical calculation test for chaos, we use the asymptotic growth rate. The results also validates for some cases that the threshold amplitude F_2 for onset of chaos will move upwards as the noise intensity increases for smaller noise intensity. It must be underlined that, for larger noise intensity, further investigation is needed to clarify the inconsistency between the two kinds of thresholds given by the random Melnikov method with the associated mean-square criterion and by the numerical simulation of the asymptotic growth rate. The effect of bounded noise on the system response is also investigated through its Poincaré maps and the results reveal that for smaller noise intensity, the chaotic attractor is slightly diffused by bounded noise, and larger noise intensity results in the reduction of the attractor size. In this paper we have also obtained results on the analytic and nonvanishing nature of broadband power spectra characteristic of deterministic chaos. The criterion from Melnikov's method could be a valid tool for predicting harmful parameters values involved in experiment. Using the before mentioned criteria, experiment could be set up to find non chaotic or chaotic radial electric field change, that could be helpful in Tokamak L-H transition understanding or confinement projects.

Perspectives

The further works that could be based on this thesis are:

- Experimental applications in order to verify some theoretical results obtained in this work.
- Large Fusion devices are too expensive to the point that new research programs (as ITER) are international, these don't let any place for African countries who are limited by the modesty of their financial resources. As Africans, our gain could therefore to orient ourselves toward uses of small scale plasma; new models could be constructed, being based on small size plasma device, as those used in the computer industry. Taking in account the new parameters related to this field, we will be able to sketch more sophisticated models, but directly feasible.

Appendix

Appendix1

$$b_0 = \frac{1}{\gamma G(x)} \left(3 \frac{dV_o(x)}{dx} + g_o \right) \quad (174)$$

$$b_1 = \frac{3}{\gamma G(x)} \left(\frac{dA(x)}{dx} \right) \quad (175)$$

$$b_2 = \frac{1}{\gamma G(x)} \left(\alpha G(x) + \mu_1 \frac{d^2 G(x)}{dx^2} \right) \quad (176)$$

$$b_3 = -\frac{(G(x))^2 \beta}{\gamma} \quad (177)$$

$$b_4 = \frac{f_2}{\gamma G(x)}$$

$$a_0 = -\frac{D_p \left(\frac{dV_o(x)}{dx} \right)^2}{V_o(x) A(x)} + \frac{D_p \frac{d^2 V_o(x)}{dx^2}}{2A(x)} \quad (178)$$

$$a_1 = \frac{D_m \left(\frac{dG(x)}{dx} \right) \frac{dV_o(x)}{dx}}{2A(x)} - \frac{D_m G(x) \left(\frac{dV_o(x)}{dx} \right)^2}{V_o(x) A(x)} \quad (179)$$

$$+ \frac{D_m G(x) \frac{d^2 V_o(x)}{dx^2}}{2A(x)}$$

$$a_2 = \frac{D_m \left(\frac{d}{dx} G(x) \right) \frac{dA(x)}{dx}}{2A(x)} + \frac{D_m G(x) \left(\frac{dV_o(x)}{dx} \right)^2}{(V_o(x))^2} \quad (180)$$

$$- \frac{2D_m G(x) \left(\frac{dV_o(x)}{dx} \right) \frac{dA(x)}{dx}}{V_o(x) A(x)} + \frac{D_m G(x) \frac{d^2 A(x)}{dx^2}}{2A(x)}$$

$$a_3 = \frac{D_p \left(\frac{dV_o(x)}{dx} \right)^2}{(V_o(x))^2} - \frac{2D_p \left(\frac{dV_o(x)}{dx} \right) \frac{dA(x)}{dx}}{V_o(x) A(x)} + \frac{D_p \frac{d^2 A(x)}{dx^2}}{2A(x)} \quad (181)$$

$$a_4 = \frac{2D_p \left(\frac{dV_o(x)}{dx} \right) \frac{dA(x)}{dx}}{(V_o(x))^2} - \frac{D_p \left(\frac{dA(x)}{dx} \right)^2}{V_o(x) A(x)} \quad (182)$$

$$a_5 = \frac{D_p \left(\frac{dA(x)}{dx} \right)^2}{(V_o(x))^2} \quad (183)$$

$$a_6 = \frac{2D_m G(x) \left(\frac{dV_o(x)}{dx} \right) \frac{dA(x)}{dx}}{(V_o(x))^2} - \frac{D_m G(x) \left(\frac{dA(x)}{dx} \right)^2}{V_o(x) A(x)} \quad (184)$$

$$\begin{aligned} a_7 &= (V_o(x))^2 f_1 \\ a_8 &= (A(x))^2 f_1 \\ a_9 &= 2V_o(x) A(x) f_1 \end{aligned} \quad (185)$$

$$\mu = -\frac{2a_4 b_0}{b_1} + \frac{3a_5 b_0^2}{b_1^2} + a_3 + b_2 \quad (186)$$

$$\beta_6 = \frac{a_5}{b_1^2} \quad (187)$$

$$\beta_2 = -\frac{3a_5 b_0}{b_1^2} + \frac{a_4}{b_1} \quad (188)$$

$$\beta_4 = \frac{a_6}{b_1} - \frac{3a_5 b_2}{b_1^2} \quad (189)$$

$$\beta_3 = \frac{2a_4 b_2}{b_1} + \frac{6a_5 b_2 b_0}{b_1^2} - \frac{2a_6 b_0}{b_1} + a_2 \quad (190)$$

$$\beta_5 = -\frac{2a_6 b_2}{b_1} + \frac{3a_5 b_2^2}{b_1^2} + 3b_3 \quad (191)$$

$$\Omega^2 = \frac{-2a_4 b_2 b_0}{b_1} - \frac{a_6 b_0^2}{b_1} + a_3 b_2 - b_1 a_1 + a_2 b_0 + \frac{3a_5 b_2 b_0^2}{b_1^2} \quad (192)$$

$$\alpha_2 = \frac{a_4 b_2^2}{b_1} - \frac{3a_5 b_2^2 b_0}{b_1^2} + \frac{2a_6 b_2 b_0}{b_1} - a_2 b_2 \quad (193)$$

$$\alpha_3 = -a_3 b_3 - \frac{3a_5 b_3 b_0^2}{b_1^2} + \frac{a_6 b_2^2}{b_1} + \frac{2a_4 b_3 b_0}{b_1} - \frac{a_5 b_3^3}{b_1^2} \quad (194)$$

$$\alpha_4 = \frac{2a_6 b_3 b_0}{b_1} + \frac{2a_4 b_2 b_3}{b_1} - a_2 b_3 - \frac{6a_5 b_2 b_3 b_0}{b_1^2} \quad (195)$$

$$\alpha_5 = \frac{2a_6 b_2 b_3}{b_1} - \frac{3a_5 b_2^2 b_3}{b_1^2} \quad (196)$$

$$\alpha_0 = -\frac{a_5 b_0^3}{b_1^2} + b_1 a_0 - a_3 b_0 + \frac{a_4 b_0^2}{b_1} \quad (197)$$

$$\delta_1 = 2 \frac{a_8 b_0 b_2}{b_1} - a_7 b_2 \quad (198)$$

$$F_2 = \sqrt{\left(-a_3 b_4 - \frac{3a_5 b_0^2 b_4}{b_1^2} + \frac{2a_4 b_0 b_4}{b_1}\right)^2 + b_4^2 \Omega_2^2} \quad (199)$$

$$\Theta_o = \arctan \left(\frac{b_4 \Omega_2}{-a_3 b_4 - \frac{3a_5 b_0^2 b_4}{b_1^2} + \frac{2a_4 b_0 b_4}{b_1}} \right) \quad (200)$$

Appendix2

$$I_1 = \frac{u_1^2 T_1}{1+\xi} \left(-\frac{(1+2\xi)}{2} \arctan \left(\sqrt{\frac{1-\xi}{1+\xi}} \right) \frac{1}{\sqrt{1-\xi^2}} + \frac{2+\xi}{4} \right) \quad (201)$$

$$I_3 = \beta_3 T_1^3 u_1 \left(-\frac{\sqrt{2}(1-\xi)^2}{10(1+\xi)} + \frac{\sqrt{1-\xi^2}(3\xi+7)(1-\xi)^{3/2}}{30(1+\xi)^{5/2}} \right) \quad (202)$$

$$I_5 = \beta_5 T_1^3 u_1^4 \left(\frac{1}{48(1+\xi)^3} \left(6 \sqrt{1-\xi^2} \arctan \left(\sqrt{\frac{1-\xi}{1+\xi}} \right) + \sqrt{\frac{1-\xi}{1+\xi}} (-2\xi^3 - 5\xi^2 - \xi + 2) \right) - \left(6 \arctan \left(\sqrt{\frac{1-\xi}{1+\xi}} \right) + \sqrt{\frac{1-\xi}{1+\xi}} (-2\xi^3 - \xi^2 - 5\xi - 2) \right) \frac{1}{48(1+\xi)^{3/2}(1-\xi)^{1/2}} \right) \quad (203)$$

$$I_6 = \frac{\beta_6 T_1^3 u_1^4}{320(1+\xi)^3(\xi-1)\sqrt{1-\xi^2}} \left(\sqrt{1-\xi^2} (2\xi^4 - 20\xi^3 - 119\xi^2 - 130\xi - 48) - 30 \arctan \left(\sqrt{\frac{1-\xi}{1+\xi}} \right) (4\xi^3 + 8\xi^2 + 7\xi + 2) \right) \quad (204)$$

$$I_7 = \frac{\pi u_1^2 \Omega_1}{T_1} \frac{\sinh \left(\frac{\Omega_1 \arccos(\xi)}{T_1} \right)}{\sqrt{1-\xi^2} \left(\sinh \left(\frac{\pi \Omega_1}{T_1} \right) \right)} \quad (205)$$

$$J_1 = \frac{u_1^2 T_1}{(1+\xi)} \left(\arctan \left(\sqrt{\frac{1+\xi}{1-\xi}} \right) \frac{(1+2\xi)}{2\sqrt{1-\xi^2}} + \frac{2+\xi}{4} \right) \quad (206)$$

$$J_2 = 4 \frac{\beta_2 T_1^2 u_1^3 (13-\xi)}{105(1-\xi)} \quad (207)$$

$$J_5 = \frac{\beta_5 T_1 u_1^4}{12} \left(\sqrt{1-\xi^2} (\xi^2 + 2) + 6 \arctan \left(\sqrt{\frac{1+\xi}{1-\xi}} \right) \right) \quad (208)$$

$$J_6 = \frac{\beta_6 T_1^3 u_1^4}{320(\xi-1)\sqrt{1-\xi^2}} \left(\sqrt{1-\xi^2} (2\xi^4 - 20\xi^3 - 119\xi^2 - 130\xi - 48) - 10 \arctan \left(\sqrt{\frac{1+\xi}{1-\xi}} \right) (12\xi^3 + 6 + 20\xi^2 + 21\xi) \right) \quad (209)$$

$$J_7 = \frac{2\pi u_1^2 \Omega_1^2}{T_1^2} \left(\sinh \left(\frac{\pi \Omega_1}{T_1} \right) \right)^{-1} \quad (210)$$

List of Publications in international refereed journals

Publications of the thesis

1- **Nono D. B. C.**, Siewe Siewe M., Tchawoua C. and Kofane T. C., *Transition to chaos in plasma density with asymmetry double-well potential for parametric and external harmonic oscillations*, International Journal of Bifurcation and Chaos 21, 7, 1879-1893, (2011).

2-**Nono D. B. C.**, Siewe Siewe M., Tchawoua C. and Kofane T. C., *Effects of external bounded noise on nonlinear dynamics of plasma density*, Physica Scripta 84, 065012(1-13), (2011).

3-**Nono D. B. C.**, Siewe Siewe M., Tchawoua C. and Kofane T. C., *Global bifurcations of mean electric field in plasma L-H transition under external bounded noise excitation*, Submitted and accepted for publication in ASME Journal of Computational and Nonlinear Dynamics, (2013).

Other publications

1-**Nono D. B. C.**, Siewe Siewe M., Tchawoua C. and Kofane T. C., *Synchronization of chaotic and nonchaotic oscillators: Application to bipolar disorder*, Physics Letters A 374, 3646-3655, (2010).

Bibliography

- [1] Steven, H. S. *Nonlinear dynamics and Chaos, with application to physics, biology, chemistry, and Engineering*, Perseus Books,(2001).
- [2] Wolf A., Swift J. B., Swinney H. L., Vastano J. A., *Determining Lyapunov exponents from a time series*, Physica D **16**, 285-317, (1985).
- [3] Michael T. Rosenstein, James J. Collins, and carlo J. De Luca, *A practical method for calculating largest Lyapunov exponents from small data sets*, Physica D **65**, 117-134, (1993).
- [4] Keen B. E. and Fletcher W. H. W, *Suppression and enhancement of an ion-sound instability by nonlinear resonance effects in a plasma*, Phys. Rev. Lett. **23**, 760-763, (1969).
- [5] Peter D. and Herbert L., *Van der-Pol model for unstable waves on a beam-plasma system*, Phys. Rev. Lett. **31**, 1039-1041, (1973).
- [6] Abrams, R. H., Yadlowsky, E. J. and Lashinsky, H., *Periodic Pulling and Turbulence in a Bounded Plasma*, Phys. Rev. Lett. **22**, 275-278, (1969).
- [7] Cheungn, P. Y. and Wong, A. Y., *Chaotic behavior and period doubling in plasmas*, Phys. Rev.Lett. **59**, 551-554, (1987).
- [8] Thompson J. M. T., Bishop S. R. & Leung L. M., *Fractal basins and chaotic bifurcation's prior to escape from a potential well*, Phys. Lett. A **121**, 116-120, (1987).
- [9] Ding J.W., HuangW.,Wang X. & Yu C. X., *Quasiperiodic transition to chaos in a plasma*, Phys. Rev. Lett. **70**, 170-173, (1993).
- [10] Qin J., Wang L., Yuan D. P., Gao P. & Zang B. Z., *Chaos and bifurcations in periodic window-observed in plasmas*, Phys. Rev. Lett. **63**, 163-166, (1989).
- [11] Thomas, B., Jorge A. L. & Jason, A. C. G., *Evidence of homoclinic chaos in the plasma of a glow discharge*, Phys. Rev. Lett. **68**, 2770-2773, (1992)

- [12] Sharma B. K., Buragohain A. & Chutia J., *Periodic window and period subtracting in ion-beam plasma system*, *Inter. J. Bifur. and Chaos* **3**, 455-458, (1993).
- [13] Atipo A., Bonhomme G. & Pierre, T., *Ionization waves: from stability to chaos and turbulence*, *Eur. Phys. J. D* **19**, 79-87, (2002).
- [14] Benzit R., Sutera A. and Vulpiani A., *The mechanism of stochastic resonance*, *J. Phys. A: Math Gen.* **14** 453-457, (1981).
- [15] Gammaitoni L., Hanggi P., Jung P. and Marchesoni F., *Stochastic Resonance*, *Rev. Mod. Phys.* **70** 223-288, (1998).
- [16] Parmananda P., Gerardo Escalera Santos J., Rivera M. and Showalter K., *Stochastic resonance of electrochemical aperiodic spike trains*, *Phys. Rev. E* **71** 031110-031116, (2005) .
- [17] Horsthemke W. and Lefever R., *Noise-Induced Transitions*, Springer, Berlin, (1984).
- [18] Neiman A., Saporin P. I. and Stone L., *Coherence resonance at noisy precursors of bifurcations in nonlinear dynamical systems*, *Phys. Rev. E* **56**, 270-273, (1997). (doi: 10.1103/PhysRevE.56.270)
- [19] Shats M. G., Rudakov D. L., Blackwell B. D., Borg G. G., Dewar R. L., Hamberger S. M., Howard J. and Sharp L. E., *Improved Particle Confinement Mode in the H-1 Helic Plasma*, *Phys. Rev. Lett.* **77**, 20, 4190-4193, (1996).
- [20] Ida K., Hidekuma S., Miura Y., Fujita T., Mori M., Hoshino K., Suzuki N., Yamauchi T., and JFT-2M Group, *Edge electric-field profiles of H-mode plasmas in the JFT-2M tokamak*, *Phys. Rev. Lett.* **65**, 1364-1367, (1990).
- [21] Cao H., Chen G., *Global and local control of homoclinic and heteroclinic bifurcations*, *Int. Journ. of Bifurcation and Chaos*, **15**, 8, 2411-2432, (2005).
- [22] Siewe M. S., Moukam Kakmeni F.M., Tchawoua C., Wofo P., *Bifurcations and chaos in periodically and externally driven ϕ^6 -Van der Pol oscillators*, *Physica A*, **357**, 383-, (2005).
- [23] Siewe M. S., Moukam Kakmeni F.M., Tchawoua C., *Resonance oscillations and homoclinic bifurcation in a ϕ^6 -Van der Pol oscillators*, *Chaos, Solitons & Fractals* **21**, 841-, (2004).

- [24] Siewe M. S., Cao H., Sanjuan M. A. F., *On the occurrence of chaos in a parametrically driven extended Rayleigh oscillator with three-well potential*, *Chaos, Solitons & Fractals* 39, 1092-, (2009).
- [25] Yang X. L., Xu W., Sun Z. K. and Fang T., *Effect of bounded noise on chaotic motion of a triple-well potential system*, *Chaos Solitons & Fractals* 25, 415-424, (2005).
- [26] Sun Z. K., Xu W. and Yang X. L., *Effect of random noise on chaotic motion of a particle in a ϕ^6 potential*, *Chaos Solitons & Fractals* 27, 127-138, (2006).
- [27] Yang X. L., Xu W. and Sun Z. K., *Effect of bounded noise on the chaotic motion of a Duffing Van der pol oscillator in a ϕ^6 potential*, *Chaos, Solitons & Fractals* 27, 778-788, (2006).
- [28] Rempel E. L., Chian A. C.-L., Preto A. J., Stephany S., *Nonlinear Processes in Geophysics*, 11 (5/6), 691- 700, (2004).
- [29] Melnikov V. K., *On the stability of the center for time-periodic perturbations*, *Trans. Moscow Math. Soc.* 12, 1-57, (1963).
- [30] Wiggins S., *Global bifurcations and chaos, analytical methods*, *Applied Mathematical Sciences* Springer-Verlag, New York, Vol73, (1988).
- [31] Holmes P. J. A., *Nonlinear oscillator with a strange attractor*, *Phylos. Trans. R. Soc. A* 292: 419-448, (1979).
- [32] Adriaratnam S. T., Xie W. C. & Vrscay E. R., *Chaotic motion under parametric excitation*, *Dyn Stability Syst.* 4(2), 111-130, (1989).
- [33] Keen, B. E. and Fletcher, W. H., *Measurement of growth rate, non-linear saturation coefficients, and mode-mode coupling coefficients of a Van der Pol plasma instability*, *J. Phys. D: Appl. Phys.* 3, 1868-1885, (1970).
- [34] Rauscher H., Perucca M., and Buyle G., *Plasma Technology for Hyperfunctional Surfaces, Food, Biomedical and Textile Applications*, Wiley-VCH Verlag GmbH & Co. KGaA, Weinheim, 428p, (2010).
- [35] Chabert P., Braithwaite N., *Physics of radio-frequency plasmas*, Cambridge University Press, Cambridge, 395p (p13), (2011).

- [36] Bellan P.M., *Fundamentals of plasma physics*, Cambridge University Press, Cambridge, 547p, (2005).
- [37] Delcroix J.-L., Bers A., *Physique des plasmas 1*, InterEditions et CNRS Editions, Paris, 408p, (1994).
- [38] Chabert P., Braithwaite N., *Physics of radio-frequency plasmas*, Cambridge University Press, Cambridge, 395p (p11), (2011).
- [39] Fitzpatrick R., *Introduction to Plasma Physics, graduate level lecture course*, University of Texas, Austin, Spring, 247p, (1998).
- [40] Knapek C. A., *Phase Transitions in Two-Dimensional Complex Plasmas*, Doctoral Thesis accepted by Ludwig-Maximilians-Universität, München, Germany, Springer-Verlag, Berlin Heidelberg, 171p (p20), (2011).
- [41] Eliezer S., Eliezer Y., *The Fourth State of Matter, An Introduction to Plasma Science, Second Edition*, Institute of Physics Publishing, Bristol and Philadelphia, 233p, (2001).
- [42] Haas F., *Quantum Plasmas, An Hydrodynamic Approach*, Springer Science+Business Media, New York, 221p, (2011).
- [43] Anderson T., *Plasma Antennas*, Artech House, Boston/London, 227p, (2011).
- [44] Koenies A., Krieger K. (eds.), *Proceeding of the Munich Summer university for plasma physics*, Max-Planck-Institut für Plasmaphysik, Munich, 287p, (2004).
- [45] Rax J.-M., *Physique des plasmas, Cours et applications*, Dunod, Paris, 438p, (2005).
- [46] Bonitz M., Horing N., Ludwig P., *Introduction to Complex Plasmas*, Springer-Verlag, Berlin Heidelberg, 450p, (2010).
- [47] Braams C. M. and Stott P. E., *Nuclear Fusion, Half a Century of Magnetic Confinement Fusion Research*, Institute of Physics Publishing, Bristol and Philadelphia, 341p, (2002).
- [48] Mendonça J. T., *Series in Plasma Physics: Theory of Photon Acceleration*, Institute of Physics Publishing, Bristol and Philadelphia, 232p, (2001).
- [49] Shafranov V. D. (Editor), *Reviews of Plasma Physics Volume 23*, Kluwer Academic / Plenum Publishers, New York, 292p, (2003).

- [50] Lieberman M.A., Lichtenberg A. J., *Principles of Plasma Discharges and Materials Processing*, John Wiley & Sons Inc., New York, 299p, (1994).
- [51] Chen F. F. and Chang J. P., *Lecture Notes on principles of plasma processing*, Plenum/Kluwer Publishers, 249p, (2002).
- [52] Inan U., Golkowski M., *Principles of Plasma Physics for Engineers and Scientists*, Cambridge University Press, Cambridge, 286p, (2011).
- [53] Guest G., *Electron Cyclotron Heating of Plasmas*, Wiley-VCH Verlag GmbH & Co. KGaA, Weinheim, 265p, (2009).
- [54] Goedbloed J. P., Keppens R., Poedts S., *Advanced Magnetohydrodynamics With Applications to Laboratory and Astrophysical Plasmas*, Cambridge University Press, Cambridge, 651p, (2010).
- [55] Das A. C., *Space Plasmas: an Introduction*, Narosa Publishing House, New Delhi., 350p, (2004).
- [56] Chen F. F., *Introduction to Plasma Physics and Controlled Fusion, Volume 1, Plasma physics, 2nd ed*, Springer, New York., 436p, (1984).
- [57] Woods L. C., *Principles of magneto plasma dynamics*, Oxford university Press, Oxford, 544p, (1987).
- [58] Roth J. R., *Industrial Plasma Engineering, Vol. 1, Principles*, Institute of Physics, Bristol Philadelphia, 538p, (1995).
- [59] Melrose D. B., *Quantum plasmadynamics Magnetized plasmas*, Springer-Verlag, Berlin, 438p, (2010).
- [60] Harry J. E., *Introduction to Plasma Technology: Science, Engineering and Applications*, Wiley-VCH Verlag GmbH & Co. KGaA, Weinheim, 231p, (2010).
- [61] R. C. Davidson, *Theory of Nonneutral Plasmas*, W. A. Benjamin inc., Advanced book program, Reading-Massachusetts, London, 214p, (1974).
- [62] Paul W., *Electromagnetic traps for charged and neutral particles, Nobel Lecture*, Rev. Mod. Phys. **62**, 531-541, (1990).

- [63] Werth G., Gheorghe V.N., Major F.G., *Charged Particle Traps II, Applications*, Springer-Verlag, Berlin Heidelberg, 275p, (2009).
- [64] Jackson J.D., *Classical Electrodynamics 2nd ed*, Wiley, New York , p 132, (1975).
- [65] Major F., Gheorghe V.N., Werth G., *Charged Particle Traps, Physics and Techniques of Charged Particle Field Confinement*, Springer-Verlag, Berlin Heidelberg, 346p, (2005).
- [66] Wesson J., *Tokamaks*, Clarendon Press, Oxford, 755p, (2004).
- [67] Sturrock P. A., *Plasma Physics, An introduction to the theory of astrophysical geophysical and laboratory plasmas*, Cambridge University Press, New York, 347p, (1994).
- [68] Kadomtsev B. B., *Tokamak Plasma: a Complex Physical System*, Institute of Physics Publishing, Bristol Philadelphia, (1992).
- [69] Zweben S. J. , Arunasalam V., Batha S. H., Budny R. V., Bush C. E., Cauffman S., Chang C.S., Chang Z., Cheng C. Z., Darrow D. S., Dendy R. O., Duong H. H., Fisch N. J., Fredrickson E. D., Fishel R. K., Fonck R. J., Fu G. Y., Goloborod'ko V., Gorelenkov N., Hawryluk R. J., Heeter R., Heidbrink W. W., Herrmann H. W., Herrman M., Johnson D. W., Machuzak J., Majeski R., McGuire K. M., McKee G., Medley S. S., Mynick H. E., Nazikian R., Petrov M. P., Redi M. H., Reznik S., Rogers J., Schilling G., Spong D. A., Strachan J. D., Stratton B. C., Synakowski E., Taylor G., Wang S., White R. B. , Wong K. L., Yavorski V. and the TFTR Group, *Alpha particle physics in the tokamak fusion test reactor DT experiment*, Plasma Phys. Control. Fusion **39**, A275- A283, , (1997).
- [70] Dinklage A., Klinger T., Marx G., Schweikhard L., (Editors), *Plasma Physics Confinement, Transport and Collective Effects*, Springer-Verlag, Berlin Heidelberg, 483p, (2005).
- [71] Ariola M., Pironti A., *Advances in Industrial Control, Magnetic Control of Tokamak Plasmas*, Springer-Verlag, London, 181p, (2008).
- [72] Colestock P. L., and the committee to Review the U.S. ITER Science Participation Planning Process, *A Review of the DOE Plan for U.S. Fusion Community Participation in the ITER Program*, The National Academies Press, Washington, 56p, (2009).
- [73] Shafranov V. D., Rozhansky V., Bakunin O. G., *Reviews of Plasma Physics Volume 24*, Springer-Verlag, Berlin Heidelberg, 213p, (2008).

- [74] Mikhailovskii A. B., *Instabilities in a Confined Plasma*, Institute of Physics Publishing, Bristol and Philadelphia, 507p, (1998).
- [75] Cordey J. G., Goldston R. J., Parker R. R., *Progress toward a Tokamak Fusion Reactor*, Physics Today, January, p. 22-42, (1992).
- [76] Moisan M. et Pelletier J., *Physique des plasmas collisionnels, application aux décharges haute fréquence*, EDP Sciences, Grenoble, 429p, (2006).
- [77] Tsytovich V. N., Morfill G. E., Vladimirov S. V., Thomas H. M., *Elementary Physics of Complex Plasmas*, Springer-Verlag, Berlin Heidelberg, 377p, (2008).
- [78] Panel on Database Needs in Plasma Processing, *Database Needs for Modeling and Simulation of Plasma Processing*, National Academy Press, Washington D.C., 73p, (1996); Ono M., Bell R., Choe W., Chang C. S., Forest C. B., Goldston R., Hwang Y. S., Jardin S. C., Kaita R., Kaye S., Kessel C. E., Kugel H., LeBlanc B., Manickam J., Menard J. E., Munsat T., Okabayashi M., Peng M., Sesnic S. and Tighe W., *Plasma transport control and self-sustaining fusion reactor*, Plasma Phys. Control. Fusion 39(5A), A361-A369, (1997).
- [79] Batchelor D.A., Beck M., Becoulet A., Budny R.V., Chang C.S., Diamond P.H., Dong J.Q., Fu G.Y., Fukuyama A., Hahn T.S., Keyes D.E., Kishimoto Y., Klasky S., Lao L.L., Li K., Lin Z., Ludaescher B., Manickam J., Nakajima N., Ozeki T., Podhorszki N., Tang W.M., Vouk M.A., Waltz R.E., Wang S.J., Wilson H.R., Xu X.Q., Yagi M., Zonca F., *Simulation of Fusion Plasmas: Current Status and Future Direction*, Plasma Science and Technology, **9(3)**, 312-387, (2007).
- [80] Huysmans G. T. A., *ELMs: MHD instabilities at the transport barrier*, Plasma Phys. Control. Fusion, **47**, B165-B178, (2005). Wilson H. R., Cowley S. C., Kirk A. and Snyder P. B., *Magneto-hydrodynamic stability of the H-mode transport barrier as a model for edge localized modes: an overview*, Plasma Phys. Control. Fusion, **48**: A71-A84, (2006).
- [81] Terry P. W., *Suppression of turbulence and transport by sheared flow*, Rev. Mod. Phys. **72**, 109-165, (2000).
- [82] Bondeson A., Ward D. J., *Stabilization of external modes in tokamaks by resistive walls and plasma rotation*, Phys. Rev. Lett., **72**, 2709-2712, (1994). Betti R., Freidberg J. P., *Stability Analysis of Resistive Wall Kink Modes in Rotating Plasmas*, Phys. Rev. Lett. **74**, 2949-2952, (1995).

- Finn J. M., *Resistive wall stabilization of kink and tearing modes*, Phys. Plasmas, 2, 198(1-7), (1995). Fitzpatrick R., Aydemir A. Y., *Stabilization of the resistive shell mode in tokamaks*, Nucl.Fusion, 36, 11-38, (1996). Chu M. S., Bondeson A., Chance M. S., Liu Y. Q., Garofalo A. M., Glasse A. H., Jackson G. L., La Haye R. J., Lao L. L., Navratil G. A., Okabayashi M., Reimerdes H., Scoville J. T., and Strait E. J., *Modeling of feedback and rotation stabilization of the resistive wall mode in tokamaks*, Phys. Plasmas, 11, 2497(1-8), (2004).
- [83] Strait E. J., Bialek J., Bogatu N., Chance M., Chu M.S., Edgell D., Garofalo A.M., Jackson G.L., Jensen T.H., Johnson L.C., Kim J.S., La Haye R.J., Navratil G., Okabayashi M., Reimerdes H., Scoville J.T., Turnbull A.D., Walker M.L. and the DIII-D Team, *Resistive wall stabilization of high-beta plasmas in DIII-D*, Nucl. Fusion, 43(6), 430-440, (2003).
- [84] Stix T. H., *Waves in Plasmas*, Springer, New York, 566p, (1992).
- [85] Sagdeev R. Z. and Galeev A. A., *Nonlinear Plasma Theory*, W.A. Benjamin Inc., Amsterdam-New York, 122p, (1969). Tsytovich V. N., *Nonlinear Effects in Plasmas*, Plenum Press, New York, 332p, (1970). Davidson R. C., *Methods in Nonlinear Plasma Theory*, Academic Press, New York, 356p, (1972). Weiland J. and Wilhelmsson H., *Coherent Nonlinear Interaction of Waves in Plasmas*, Pergamon press, Oxford, 353p, (1977).
- [86] Hans Wilhelmsson, *Fusion, A Voyage Through the Plasma Universe*, Institute of Physics Publishing, Bristol and Philadelphia, 180p, (2000).
- [87] Alberto Loarte, *Fusion plasmas: Chaos cuts ELMs down to size*, Nature Physics 2, 369- 370, (2006).
- [88] Xaplanteris C. L. and Filippaki E., *Chaotic behavior of plasma surface interaction. A table of plasma treatment parameters useful to the restoration of metallic archaeological objects*, 2nd Chaotic Modeling and Simulation International Conference, 1-5 June, Chania Crete Greece, (2009).
- [89] Izrailev F.M., Chirikov B.V., *Statistical properties of a non-linear string*, Dokl. Acad. Nauk. 166, 57-59, (1966). (Sov. Phys. Dokl. 11(1), 30-32, (1966).)
- [90] Carati A., Galgani L., Giorgilli A., *The Fermi-Pasta-Ulam problem as a challenge for the foundations of physics*, Chaos 15, 015105(1-8), (2005)., Benettin G., Carati A., Galgani L., Giorgilli

- A., *The Fermi-Pasta-Ulam problem and the metastability perspective in The Fermi-Pasta-Ulam Problem: A Status Report*, G. Gallavotti (editor), Series: Lecture Notes in Physics, Vol. 728, Springer Verlag, Berlin, 151-189, (2007).
- [91] E. Fermi, J. Pasta, S. Ulam, in *E. Fermi: Note e Memorie (Collected Papers)*, Vol. II, N. 266: 977, Accademia Nazionale dei Lincei, Roma, and The University of Chicago Press, Chicago (1965).
- [92] Rosenbluth M.N., Sagdeev R.Z., Taylor J.B., Zaslavsky G.M., *Destruction of magnetic surfaces by magnetic field irregularities*, Nucl. Fusion **6**, 297 (1966).doi: 10.1088/0029-5515/6/4/008. Filonenko N.N., Sagdeev R.Z., Zaslavsky G.M., *Destruction of magnetic surfaces by magnetic field irregularities: Part II*, Nucl. Fusion **7**, 253, (1967). doi:10.1088/0029-5515/7/4/009
- [93] Vasiliev A., Neishtadt A., Artemyev A., *Resonant particle acceleration in an oblique electromagnetic wave*, Phys. Lett. A **375**, 3075-3079, (2011).
- [94] Carati A., Benfenati F., Galgani L., *Relaxation properties in classical diamagnetism*, Chaos **21**, 023134 (2011). doi:10.1063/1.3594580
- [95] Demura A.V., *Physical Models of Plasma Microfield*, Intl. J. Spectroscopy, **671073** (1-42), (2010). doi:10.1155/2010/671073
- [96] Greenwald M., *Review: Density limits in toroidal plasmas*, Plasma Phys. Contr. Fusion **44**, R27- R80, (2002).
- [97] Jain V.K., Sakawa Y., and Joshi C., *Period doubling and eventual Chaos in an Electron Beam-Plasma System*, Bull. Amer. Phys. Soc. **33(9)**, 1877 (1988).
- [98] Lee H. J., Lee J. K., Hur M. S., and Yang Y., *A universal characterization of nonlinear self-oscillation and chaos in various particle-wave-wall interactions*, Applied Physics Letters **72(12)**, 1445-1447, (1998).
- [99] Qin J., Wang L., Yuan D. P., Gao P., and Zhang B. Z., *Chaos and bifurcations in periodic windows observed in plasmas*, Phys. Rev. Lett.**63**, 163-166, (1989).
- [100] Cheung P. Y. and Wong A. Y., *Chaotic behavior and period doubling in plasmas*, Phys. Rev. Lett. **59**, 551-554, (1987).

- [101] Lee P. W., Lee S. W., and Chang H. Y., *Undriven periodic plasma oscillation in electron cyclotron resonance Ar plasma*, Appl. Phys. Lett. **69**, 2024(1-3), (1996).
- [102] Kwon N., Yoog S.-H., Yun Y.-H., and Jhe W., *Observation of oscillations of the optogalvanic signal in an electrodeless discharge*, Phys. Rev. A **54(2)**, 1459-1462, (1996). Du J., Chiang C., and Lin I., *Spatiotemporal patterning of a transverse ionization instability in annular rf discharges*, Phys. Rev. E **54**, 1829-1832, (1996).
- [103] Chen X., Lindsay P.A., Zhang J., *Chaos and oscillations in a loaded plasma-filled diode*, IEEE Transactions on Plasma Science **28**, 3, 462-471, (2000).
- [104] Matsukuma M., Kaimoto K., Kawai Y., *Observation of chaotic behavior caused by ion-ion instability*, Journal of the Physical Society of Japan, **69(2)**, 303-305, (2000).
- [105] Qin J., Wang L., Yuan D. P., Gao P., and Zhang B. Z., *Chaos and bifurcations in periodic windows observed in plasmas*, Phys. Rev. Lett. **63**, 163-166, (1989).
- [106] Fan S.H., Yang S.Z., Dai J.H., Zheng S.B., Yuan D.P., Tsai S.T., *Chaos in plasmas*, Physics Letters A **164(3-4)**, 295-298, (1992).
- [107] Klinger T., Latten A., Piel A., Bonhomme G., Pierre T., and Dudok de Wit T., *Route to Drift Wave Chaos and Turbulence in a Bounded Low- β Plasma Experiment*, Phys. Rev. Lett. **79**, 3913-3916, (1997).
- [108] Cheung P. Y., Donovan S. and Wong A. Y., *Observations of Intermittent Chaos in Plasmas*, Phys. Rev. Lett. **61**, 1360-1363, (1988).
- [109] Cluggish B. P., Danielson J. R. and Driscoll C. F., *Resonant Particle Heating of an Electron Plasma by Oscillating Sheaths*, Phys. Rev. Lett. **81(2)**, 353-356, (1998).
- [110] Homann A., Melzer A. and Piel A., *Measuring the charge on single particles by laser-excited resonances in plasma crystals*, Phys. Rev. E **59(4)**, R3835-R3838, (1999).
- [111] Schollmeyer H., Melzer A., Homann A. and Piel A., *Dust-dust and dust-plasma interactions of monolayer plasma crystals*, Phys. Plasmas **6(7)** (1-6), (1999).
- [112] Sydorenko D., Smolyakov A., Kaganovich I. and Raitse Y., *Plasma-Sheath Instability in Hall Thrusters Due to Periodic Modulation of the Energy of Secondary Electrons in Cyclotron Motion*, Princeton Plasma Physics Laboratory Report, **PPPL-4310**, 1-8, (2008).

- [113] Rohde A., Piel A. and Klostermann H., *Simulation of the nonlinear dynamics of grid sheath oscillations in double plasma devices*, Phys. Plasmas **4 (11)**, 3933-3942, (1997).
- [114] Gravier E., Brochard F., Bonhomme G., Pierre T., Briançon J.-L., *Low frequency instabilities of a laboratory magnetized plasma column*, Physics of Plasmas **11**, 529-537, (2004).
- [115] Ott E., Grebogi C., and Yorke J. A., *Controlling chaos*, Phys. Rev. Lett. **64**, 1196-1199, (1990). Pyragas K., *Continuous control of chaos by self- controlling feedback*, Phys. Lett. A **170(6)**, 421-418, (1992). Pierre Th., Bonhomme G., and Atipo A., *Controlling the Chaotic Regime of Non-linear Ionization Waves using the Time-Delay Autosynchronization Method*, Phys. Rev. Lett. **76**, 2290-2293, (1996). Gravier E., Caron X., Bonhomme G. and Pierre Th., *Control of the chaotic regimes of nonlinear drift-waves in a magnetized laboratory plasma*, Phys. Plasmas **6(5)**, 1670(1-4), (1999).
- [116] Jovanovic D., Shukla P.K., *Nonlinear generation of zonal flows by drift waves*, Physics Letters A **289**, 219-224, (2001).
- [117] Yamada T., Itoh S.-I., Uta T. M., Kasuya N., Nagashima Y., Shinohara S., Terasaka K., Yagi M., Inagaki S. U., Kawai Y., Fujisawa A. and Itoh K., *Anatomy of plasma turbulence*, Nature physics (Letters) **4**, 721-725, (2008).
- [118] Itoh K., Itoh S.-I., A Fukuyama, *Transport and Structural Formation in Plasmas*, Institute of Physics Publishing, Bristol and Philadelphia, 341 Pages, (1999).
- [119] Numata R., Ball R., Dewar R.L., Stals L., *Bifurcation in Resistive Drift Wave Turbulence*, presented at the 8th Asia-Pacific Complex Systems Conference (2-5 July Complex07), The Australian National University, 1-13, (2007).
- [120] L. Krupnik, A. Alonso, E. Ascasibar, T. Estrada, C. Hidalgo, B. van Milligen, M. Ochando, M. Pedrosa, J. L. de Pablos, V. Tribaldos, A. Chmyga, N. Dreval, G. Deshko, S. Khrebtov, A. Komarov, A. Kozachok, V. Tereshin, L. Eliseev, a. Melnikov, C. Silva., *Radial electric fields and confinement in the TJ-II stellarator*, Czechoslovak Journal of Physics **55(3)**, 317-339, (2005). DOI: 10.1007/s10582-005-0044-8
- [121] Jardin S., *Computational Methods in Plasma Physics*, CRC Press Taylor and Francis Group, 364p, (2010).

- [122] Chen F.F., Chang J.P., *Lecture notes on Principles of plasma processing*, Plenum/Kluwer Publishers, 249p, (2002).
- [123] Chapman I.T., Akers R.J., Cooper W.A., Field A.R., Graves J.P., Gryaznevich M.P., Hastie R.J., Hender T.C., Howell D.F., Hua M.-D., Huysmans G.T.A., Liu Y.Q., Meyer H.F., Michael C.A., Naylor G., Pinches S.D., Saarelma S., Scannell R., Sabbagh S.A., and the MAST Team, *Macroscopic Stability of High β_N MAST plasmas*, Physics of plasma, 23rd IAEA Fusion Energy Conference, Daejeon, Republic of Korea, 11-16 October 2010, **EXS/P5-04** (IAEA), (2010).
- [124] Bellan P.M., *Fundamentals of plasma physics*, Cambridge University Press, New York, 547p, (2005).
- [125] Rose D. J. and Clark M., *Plasma and Controlled Fusion*, John Willey and Sons, New York, ,(1998).
- [126] Hsuan H. C. S., Ajmera R. C., and Lonngrekn K. E., *The Nonlinear Effect of Altering the Zeroth Order Density Distribution of a Plasma*, Appl. Phys. Lett., 11, 277-279, (1967) .DOI: 10.1063/1.1755133
- [127] Rax J.-M., *Physique des plasmas, Cours et applications*, Dunod, Paris, 438p, (2005).
- [128] Miura K. and Groth C. P. T., *Development of Two-Fluid Magnetohydrodynamics Model for Non-Equilibrium Anisotropic Plasma Flows*, 38th AIAA Plasmadynamics and Lasers Conference 25 - 28 June, Miami, FL, **AIAA 2007-4373**, 1-23, (2007).
- [129] Numata R., Yoshida Z. and Hayashi T., *Two-Fluid Nonlinear Simulation of Self-Organization of Plasmas with Flows*, Journal of Plasma and Fusion Research **6**, 130-141 (2004).
- [130] Johnson E.A. and Rossmannith J.A., *Ten-moment two-fluid plasma model agrees well with PIC/Vlasov in GEM problem*, In Proceedings of the 13th International Conference on Hyperbolic Problems, November, 1-8, (2010).
- [131] Loverich J., Hakim A., Shumlak. U., *A Discontinuous Galerkin Method for Ideal Two- Fluid Plasma Equations*. Submitted to Communications in Computational Physics, 9, 240-268 (2011).

- [132] Birn J., Drake J.F., Shay M.A., Rogers B.N., Denton R.E., Hesse M., Kuznetsova M., Ma Z.W., Bhattacharjee A., Otto A., and Pritchett P.L., *Geospace environmental modeling (GEM) magnetic reconnection challenge*, Journal of Geophysical Research: Space Physics **106**, 3715-3719, (2001).
- [133] Cockburn B. and Shu C.-W., *Runge-Kutta discontinuous Galerkin methods for convection-dominated problems*, Journal of Scientific Computing **16**, 173–261, (2001).
- [134] Shumlak U. and Loverich J., *Approximate Riemann solver for the two-fluid plasma model*, Journal of Computational Physics **187**, 620–638, (2003).
- [135] Keen B. E. and Fletcher W. H. W., *Suppression and enhancement of an ion-sound instability by nonlinear resonance effects in a plasma*, Phys. Rev. Lett. **23**, 760-763, (1969).
- [136] Enjieu Kadji H. G., Nana Nbandjo B. R., Chabi Orou J. B. and Talla P. K., *Nonlinear dynamics of plasma oscillations modeled by an anharmonic oscillator*, Phys. Plasmas, **15** (032308), 1-13, (2008).
- [137] Land V. and Goedheer W. J., *Manipulating Dust Charge Using Ultraviolet Light in a Complex Plasma*, IEEE Trans. Plasma Sci. **35** (2), 280-285, (2007).
- [138] Bhattacharyya R. and Janaki M. S., *Two-fluid stationary states with dissipation and external drive*, Phys. Plasmas **13**, (044508), 1-4, (2006).
- [139] Corr C. S. and Boswell R. W., *Nonlinear instability dynamics in a high-density, high-beta plasma*, Phys. Plasmas **16**, (022308), 1-5, (2009).
- [140] Lashinsky H., *Proc. Conf. Plasma Physics and Controlled Thermonuclear Fusion Research, Culham, England (Vienna: IAEA)*, 499-514, (1965).
- [141] Klinger T. and Piel A., *The bifurcation structure of periodically forced current disruptions*, Physica Scripta, **56**, 70-85, (1997).
- [142] Philippe M., *Développement d'un réflectomètre micro-onde hétérodyne à balayage ultra rapide. Etude de l'influence de la turbulence du plasma sur la mesure des profils de densité électronique*, Ph.D thesis, Université Aix-Marseille I, (1997).

- [143] Momeni M., Kourakis I., Moslehi F. P. & Shukla K., *A van der-Pol-Mathieu equation for the dynamics of dust grain charge in dusty plasmas*, J. Phys. A: Math. Theor. **40**, F473-F481, (2007).
- [144] Keen B. E. and Fletcher W. H., *Measurement of growth rate, non-linear saturation coefficients, and mode-mode coupling coefficients of a van der Pol plasma instability*, J. Phys. D: Appl. Phys. **3**, 1868-1885, (1970).
- [145] Lin Y. K. and Cai C. Q., *Probabilistic Structural Dynamics, Advanced Theory and Applications*, McGraw-Hill Book Co. Singapore, (1995).
- [146] Nono D. B. C., Siewe Siewe M., Tchawoua C. and Kofane T. C., *Transition to chaos in plasma density with asymmetry double-well potential for parametric and external harmonic oscillations*, International Journal of Bifurcation and Chaos, **21**, 7, 1879-1893, (2011).
- [147] Xaplanteris C.L., Filippaki E. and Mistakidis I.S., *Collision Frequency leads the Plasma into a Chaotic State. Influence on the Conductivity*, Chaotic Mod. and Sim. **1**, 157-168, (2012).
- [148] Gravier E., Caron X., Bonhomme G., Pierre T., and Briançon J.L., *Dynamical study and control of drift waves in a magnetized laboratory plasma*, Eur. Phys. J. D **8**, 451-457, (2000).
- [149] Void E. L., Najmabadi F., and Conn R. W., *Fluid model equations for the tokamak plasma edge*, Phys. Fluids B **3**, (11), 3132-3152, (1991).
- [150] Kaifen H. and Salat A., *Hysteresis and onset of chaos in periodically driven nonlinear drift waves*, Plasma Phys. Controlled Fusion **31**, 123-141, (1989).
- [151] LaBombard B., Grossman A., and Corm R. W., *A phenomenological model for cross-field plasma transport in non-ambipolar scrape-off layers*, J. Nucl. Mater., **548**, 176-177, (1990).
- [152] Shaing K. C., Phys. Fluids B **2**, 764-, (1990).
- [153] Itoh S. I. and Itoh K., *Model of L to H-Mode Transition in Tokamak*, Phys. Rev. Lett **60**, 2276-2279, (1988).
- [154] Groebner R. J., Burrell K. H. and Seraydarian R. P., *Role of edge electric field and poloidal rotation in the L-H transition*, Phys. Rev. Lett. **64**, 3015-3018, (1990).
- [155] Doyle E. et al. , *Plasma confinement and transport in : Progress in the ITER physics basis*, Nuclear Fusion **47**(2), 18, (2007). doi:10.1088/0029-5515/47/6/S02

- [156] Novakovskii S. V., Liu C. S., Sagdeev R. Z. and Rosenbluth M. N., *The radial electric field dynamics in the neoclassical plasmas*, Phys. Plasmas, 4 (12),4272-4282, (1997).
- [157] Burrell K. H., *Effects of $E \times B$ velocity shear and magnetic shear on turbulence and transport in magnetic confinement devices*, Phys. Plasmas 4(5), 1499-1518, (1997).
- [158] Itoh S. I., Itoh K. and Fukuyama A., *in: IAEA proceedings of the fourteenth international conference on plasma physics and controlled nuclear fusion research, Vienna, Volume 2 (IAEA-CN-56/D-4-19)*, 359-365, (1993).
- [159] Zhang W., Cao D., *Chaos, Local and global bifurcations of L-mode to H-mode transition near plasma edge in Tokamak*, Solitons & Fractals 29(1), 223-232, (2006).
- [160] Kapitaniak T., *Controlling Chaos, Theoretical and Practical Methods in Nonlinear Dynamics*, Academic Press, (1996).
- [161] Crauel H., Gundlach M., *Stochastic Dynamics*, Springer-Verlag, New York, inc.(1999).
- [162] K. Itoh, S.-I. Itoh, M. Yagi, and A. Fukuyama, *Solitary radial electric field structure in tokamak plasmas*, Physics of plasmas 5(12),4121-4123, (1998).
- [163] Shunjiro Shinohara and Shoichiro Matsuyama, *Observation of bistable density transitions in magnetized plasma by voltage-biased electrode*, Physics of plasmas **9(11)**, 4540-4550, (2002).
- [164] K. Itoh, S. Toda, A. Fujisawa, S.-I. Itoh, M. Yagi, A. Fukuyama, P. H. Diamond, K. Ida, *Physics of internal transport barrier of toroidal helical plasmas*, Physics of plasmas **14(2)**, 020702(1-4), (2007).
- [165] S.-I. Itoh, *Project Review: Research on Structural Formation and Selection Rules in Turbulent Plasmas*, J. Plasma Fusion Res. **83(3)**, 241, (2007).
- [166] Sanae-I. ITOH, *Structure Formation in Turbulent Plasmas*, Plasma and Fusion Research: Review Articles, Volume 4, 038(1-12), (2009).
- [167] Gruendler J., *The existence of homoclinic orbits and the method of Melnikov for systems in R^n* , SIAM J. Math. Anal. **16**, 907-931, (1985).
- [168] Melnikov V. K., *On the stability of the center for time-periodic perturbations*, Trans. Moscow Math. Soc. **12**, 1-57, (1963).

- [169] Thomas, B., Jorge, A. L., Ricardo, E. F. & Jason, A. C. G., *Observation of deterministic chaos in electrical discharges in gases*, Phys. Rev. Lett. **59**, 613-616, (1987).
- [170] Litak G., Borowiec M., Friswell, M. I. & Przystupa W., *Chaotic response of a quarter car model forced by a road profile with a stochastic component*, Chaos, Solitons and Fractals **39**, 2448-2456, (2009).
- [171] Chacón R., Balibrea F. & López M. A., *Role of nonlinear dissipation in the Suppression of Chaotic escape from potential well*, Physical Letters A **279**, 38-46, (2001).
- [172] Lima R. & Pettini M., *Suppression of chaos by resonant parametric perturbations*, Phys. Rev. A **41**, 726-733, (1990).
- [173] Ricardo Chacon, *Control of homoclinic chaos by weak periodic perturbations*, World Scientific Publishing Co. Re. Ltd., Singapore, (2005).
- [174] Liu W. Y., Zhu W. Q., Huang Z. L., *Effect of bounded noise on the chaotic motion of Duffing oscillator under parametric excitation*, Chaos Solitons and Fractals **12**, 527-537, (2001).
- [175] Frey M., Simiu E., *Noise-induced chaos and phase space flux*, Physica D **63**, 321-340, (1993).
- [176] Grassberger P. and Procaccia I., *Characterization of Strange Attractors*, Phys. Rev. Lett. **50(5)**, 346-349, (1983).
- [177] Das, K. P., *Interaction among three extraordinary waves in a hot electron plasma* Phys Fluids **14**, 124-128, (1971).
- [178] Davidson R. C., *The evolution of wave correlations in uniformly turbulent, weakly nonlinear systems*, Plasma Phys. **1**, 341-359, (1967).
- [179] Butler, D. S., and Gribben R. J., *Relativistic formulation for non-linear waves in a non-uniform plasma*, Plasma Phys **2**, 257-281, (1968).
- [180] Maroli, C, and R. Pozzou, *Penetration of high-frequency electromagnetic waves into a slightly ionized plasma*, Nuovo Cimento **B61**, 277-289, (1969).
- [181] Chen, C. S., and G. J. Lewak, *Parametric excitation of a plasma*, Plasma Phys **4**, 357-369, (1970).

- [182] Chen, C. S, *Parametric excitation in an inhomogeneous plasma*, Plasma Phys. **5**, 107-113, (1971).
- [183] Prasad, R, *Effect of ion motion on parametric oscillations of a cold plasma in a magnetic field*, Plasma Phys. **5**, 291-302, (1971).
- [184] Frieman, E. A., and P. Rutherford, *Kinetic theory of a weakly unstable plasma*, Ann. Phys. **28**, 134-177, (1964).
- [185] Albright, N. W., *Quasilinear stabilization of the transverse instability*, Phys. Fluids, **13** 1021-1030, (1970).
- [186] Kushner H. J., *Probability Methods for Approximations in Stochastic Control and for Elliptic Equations*, Academic Press, New York, 256p, (1977).
- [187] Gardiner C.W., *Handbook of Stochastic Methods for Physics, Chemistry and the Natural Sciences*, Springer-Verlag, Berlin Heidelberg, 438p, (2004).
- [188] Robert J. B., and Spanos P. D., *Random vibration and statistical Linearization*, Wiley, New York, 407p, (1990).
- [189] Crandall S. H., *Heuristic and Equivalent Linearization Techniques for Random Vibration of non-linear oscillators*, In proceedings of the 8th international conference on Non-Linear Oscillation Volume1, Academia, Prague, 211-226, (1978).
- [190] Lin Y. K. and Cai C.Q., *Probabilistic Structural Dynamics, Advance Theory and applications*, McGraw-Hill inc., Singapore, 486p, (1995).
- [191] J. H. Matis, Q. Zheng, and T. Kiffe, *Describing the Spread of Biological Populations Using Stochastic Compartmental Models with Births*, Mathematical Biosciences **126(2)**, 215-247, (1995).
- [192] Lin Y. K., *Probabilistic Theory of Structural Dynamics*, McGraw-Hill, New York, 368p, (1967).
- [193] Stratonovich R. L., *Topics in the Theory of Random Noise Volume I: General Theory of Random Processes, Nonlinear Transformations of Signals and Noise*, Gordon and Breach Science Publishers, New York, 292P, (1963).

- [194] Yemima Ben-Menahem, Meir Hemmo, *Probability in Physics*, Springer-Verlag, Berlin Heidelberg, 334 p, (2012).
- [195] Giora Maymon, *Structural Dynamics and Probabilistic Analyses for Engineers*, Elsevier Inc., New York, 488p, (2008).
- [196] Benford, G. and Thomson, J. J., *Probabilistic model of plasma turbulence*, Phys. Fluids **15**, 1496-1503, (1972).
- [197] Biskamp, D., Camargo, S. J., and Scott, B. D., *Spectral properties and statistics of resistive drift-wave turbulence*, Phys. Lett. A **186**, 239-244, (1994).
- [198] Dinklage A., Fischer R., Svensson J., *Topics and methods for data validation by means of bayesian probability theory*, Fusion Science and Technology, **46**, 355-364, (2004).
- [199] P. H. Diamond, S.-I. Itoh, K. Itoh, *Modern plasma physics Volume 1: Physical Kinetics of Turbulent Plasmas*, Cambridge University Press, New York, (2010).
- [200] S. F. Wojtkiewicz, B. F. Spencer Jr and L. A. Bergman, *On the cumulant-neglect closure method in stochastic dynamics*, Int. j. of Non-Linear Mechanics, **31(5)**, 657-684, (1996).
- [201] T. Matis and I. G. Guardiola, *Achieving Moment Closure through Cumulant Neglect*, The Mathematica Journal, **12**, 1-18, (2010). [dx.doi.org/doi:10.3888/tmj.12-2](https://doi.org/10.3888/tmj.12-2).
- [202] Sanae-I. Itoh, Kimitaka Itoh, and Shinichiro Toda, *Probability of Statistical L-H Transition in Tokamaks*, Phys. Rev. Lett. **89(21)**, 215001(1-4) , (2002).
- [203] Shinosuka M., *Simulation of multivariate and multi-variational processes*, Journal of the acoustic society of America **49**, 357-367, (1971).
- [204] Shinozuka M. and Jan C.-M., *Digital simulation of random processes and its applications*, J. Sound Vib. **25(1)**, 111-128, (1972).
- [205] Perron O., *Die stabilitatsfrage bei differentialgleichungen,* Mathematische Zeitschrift bd. 32, 702-728, (1930).
- [206] Leonov G. A. & Kuznetsov N. V., *Time-varying linearization and the Perron effects*, International Journal of Bifurcation and Chaos **17**, 1079-1107, (2007).

- [207] Brochard F., Bonhomme G., Gravier E., Oldenbürger S., and Philipp M., *Spatiotemporal control and synchronization of flute modes and drift waves in a magnetized plasma column*, Phys. Plasmas **13**, 052509 (1-9), (2006).
- [208] Gravier E., Caron X., Bonhomme G. and Pierre Th., *Control of the chaotic regimes of nonlinear drift-waves in a magnetized laboratory plasma*, Phys. Plasmas **6(5)**, 1670(1-4), (1999).
- [209] Makarov D. and Uleysky M., *Specific Poincaré map for a randomly-perturbed nonlinear oscillator*, J. Phys.A: Math. Gen. **39** 489-497, (2006).
- [210] Haiwu R., Wei X., Guang M. and Tong F., *Response of a Duffing oscillator to combined deterministic harmonic and random excitation*, J. Sound Vib. **242** 362-368, (2001).
- [211] Pécseli H, *Fluctuations in Physical Systems*, Cambridge University Press, Cambridge (2000).
- [212] Petit J. P. and Geffray J., *Acta physica polonica A 115, 6, Non-Equilibrium Plasma Instabilities*, 1170-1172. (2009)
- [213] Casaregola C. and Gherardesca V. A., *Periodic Report – second period –november, project: high power electric propulsion: a roadmap for the future, grant agreement number: 218859*, (2010).
- [214] Witrant E, Olofsson E and Niculescu S-I, *A time-delay approach for the modeling and control of plasma instabilities in thermonuclear fusion*, E-Delay Systems letter. Invited contribution, (2009).
- [215] Cristescu C. P., Stan C., and Alexandroaei D., *Control of chaos by random noise in a system of two coupled perturbed van der Pol oscillators modeling an electrical discharge plasma*, Phys. Rev. E **66**, 016602(1-5), (2002).
- [216] Gottwald G. A. and Melbourne I., *Testing for chaos in deterministic systems with noise*, Physica D **212**, 100-110, (2005); G.A. Gottwald and I. Melbourne, *On the implementation of the 0-1 test for chaos*, SIAM Journal on Applied Dynamical Systems **8**, 129-145, (2009).
- [217] Gao J. B., Hwang S. K. and Liu J. M., *When Can Noise Induce Chaos?*, Phys. Rev. Lett. **82** 6, 1132-1135, (1999).

- [218] Gidea M., Quaid D., *On Wesner's method of searching for chaos on low frequency*, Economics Bulletin **3** 42, 1-8, (2005).
- [219] Pikovsky A. S., Kurths J., *Coherence Resonance in a Noise-Driven Excitable System*, Phys. Rev. Lett. **78** 5, 775-778, (1997).
- [220] Schröder C. and Klinger T., *Mode Selective Control of Drift Wave Turbulence*, Phys. Rev. Lett. **86** 25, 5711-5714, (2001).
- [221] Wesson J., *Tokamaks, third edition*, Clarendon press-Oxford, (2004).
- [222] Hazeltine R. D., Meiss J. D., *Plasma confinement*, Addison-Wesley publishing group, (2003).
- [223] Weston M. S., *Fusion, An Introduction to the Physics and Technology of Magnetic Confinement Fusion Second, Completely Revised and Enlarged edition*, Wiley-Vch Verlag GmbH Co. KGaA, Weinheim, (2010).
- [224] Callen J. D., Carreras B. A., and Stambaugh R. D., *Stability and transport processes in tokamak plasmas*, Phys. Today **45**, 34-42, (1992).
- [225] Loarte A., Saibene G., Sartori R., Campbell D., Becoulet M., Horton L., Eich T., Herrmann A., Matthews G., Asakura N., Chankin A., Leonard A., Porter G., Federici G., Janeschitz G., Shimada M., Sugihara M., *Characteristics of type I ELM energy and particle losses in existing devices and their extrapolation to ITER*, Plasma Phys. Control. Fusion **45** 9, 1549-1569, (2003).
- [226] Evans T. E., Moyer R.A., Watkins J.G., Thomas P.R., Osborne T.H., Boedo J.A., Fenstermacher M.E., Finken K.H., Groebner R.J., Groth M., Harris J., Jackson G.L., Haye R.J., Lasnier C.J., Schaffer M.J., Wang G., Zeng L., *Suppression of large edge localized modes in high confinement DIII-D plasmas with a stochastic magnetic boundary*, J. Nucl. Mater. **337-339**, 691-696, (2005).
- [227] Evans T. E., Moyer R.A., Watkins J.G., Thomas P.R., Osborne T.H., Boedo J.A., Fenstermacher M.E., Finken K.H., Groebner R.J., Groth M., Harris J., Jackson G.L., Haye R.J., Lasnier C.J., Schaffer M.J., Wang G., Zeng L., *Suppression of Large edge-localized modes in high-confinement DIII-D plasmas with a stochastic magnetic boundary*, Phys. Rev. Lett. **92**, 235003(1-4), (2004).

-
- [228] Moyer R. A., Evans T. E., Osborne T. H., Thomas P. R., Becoulet M., Harris J., Finken K.-H., Boedo J. A., et al. *Edge localized mode control with an edge resonant magnetic perturbation*, Phys. Plasmas **12** 5, 056119(1-11), (2005).
- [229] Kim E.-J. and Diamond P. H., *Dynamics of zonal flow saturation in strong collisionless drift wave turbulence*, Phys. Plasmas **9**(11), 4530(1-10), (2002).
- [230] Ariola M. and Pironti A., *Advances in Industrial Control series: Magnetic Control of Tokamak Plasmas*, Springer-Verlag London Limited, (2008).